INTERACTION OF ANTICANCEROUS DRUGS WITH SPECIFIC OLIGONUCLEOTIDES

A THESIS

submitted in fulfilment of the
requirements for the award of the degree
of
DOCTOR OF PHILOSOPHY

By

NANDANA SRIVASTAVA

DEPARTMENT OF BIOSCIENCES AND BIOTECHNOLOGY
UNIVERSITY OF ROORKEE
ROORKEE-247 667 (INDIA)

FEBRUARY, 1996

Gratis

CANDIDATE'S DECLARATION

I hereby certify that the work which is being presented in this thesis entitled **"INTERACTION OF ANTICANCEROUS DRUGS WITH SPECIFIC OLIGONUCLEOTIDES"** in fulfilment of the requirements for the award of the Degree of **DOCTOR OF PHILOSOPHY**, submitted in the Department of Biosciences and Biotechnology of the University is an authentic record of my work carried out during a period from December, 1990 to February, 1996 under the supervision of Dr. (Mrs.) Ritu Barthwal, Head and Reader, Department of Biosciences and Biotechnology, University of Roorkee, Roorkee.

The matter presented in this thesis has not been submitted by me for the award of any other degree of this or any other University.

Nandana Srivastava

Date : 26.02.96 **(NANDANA SRIVASTAVA)**

This is to certify that the above statement made by the candidate is correct to the best of my knowledge.

Rtu Barthwal

(RITU BARTHWAL) 26.02.96

Head & Reader, Deptt.
of Biosciences & Biotechnology

The Ph.D. Viva-Voce examination of **NANDANA SRIVASTAVA,** Research Scholar, has been held on Nov. 16, 1996.

Rtu Barthwal

Signature of Supervisor

Professor & Head
Deptt. of Biosciences and
Biotechnology
University of Roorkee
Roorkee

Signature of Head of the Department

16.11.96

Signature of External Examiner
(KUNAL B. ROY)
Professor & Head
Centre for Biotechnology
JNU New Delhi

ABSTRACT

Intra-cellular DNA represents the target for a wide variety of clinically important antibiotics and synthetic compounds that exhibit antitumour activities. It acts as a 'flexible receptor' capable of expanding its minor groove to accommodate bulky ligand dimers or distorting the sugar-phosphate backbone to allow architecturally complex intercalators to thread chains of sugar residues between the DNA base pairs. These diverse set of antibiotics binding to DNA in a variety of ways have a common ability to act as inhibitors of DNA transcription and replication. As a result these antibiotics are of great interest as potential anticancer agents. An understanding of structure and details of dynamics of drug-DNA interactions at molecular level is important in rationale designing of new families of antitumour agents.

Adriamycin, an anthracycline antibiotic is isolated from *Streptomyces peucetius*. It is active against a number of solid tumours and has a wide spectrum of antitumour activity.

The present study has been undertaken to study the conformational features of adriamycin in D_2O by using 1D and 2D NMR techniques. The three-dimensional conformation of adriamycin specified by spin-spin coupling constants and interproton distances has been compared with X-ray crystal structure of daunomycin (the X-ray crystal structure of adriamycin is not available in literature). The conformation of deoxyhexanucleotide d-$(CGATCG)_2$ has been investigated in D_2O. Geometry of deoxyribose

sugar of each residue is obtained on the basis of double-quantum filter COSY cross peak patterns, spin-spin coupling constants and sums of couplings obtained from 1D/2D NMR spectra. This is supplemented with interproton distances obtained from NOESY spectra recorded at various mixing times (τ_m). The intra-residue base-sugar proton NOEs are used to derive information about glycosidic bond rotation (χ).

The complex of adriamycin with d-$(CGATCG)_2$ is prepared by titrating the hexamer with drug and monitoring the same by 1D NMR at every step. The 2:1 adriamycin to d-$(CGATCG)_2$ concentration ratio complex finally obtained, is studied by 1D NMR and 2D NOESY in detail. The changes in chemical shifts of various protons in 2:1 complex are attributed to stacking interactions and alteration in relative base-base overlap. The data of 2D NOESY spectra is used to assign all proton NMR signals unambiguously. The sugar puckering, helix sense, glycosidic bond rotation, etc. are estimated in complexed form. Several intramolecular NOE connectivities, within adriamycin and DNA molecule, reflect the changes in conformation of DNA and drug on complexation.

The intermolecular NOEs between ring D protons of adriamycin and base protons of 5′-3′ d-CpG step give direct evidence of intercalation of adriamycin chromophore between d-CpG base pairs. Intermolecular NOEs between daunosamine sugar and A3.T4 base pair indicate the proximity of daunosamine sugar to the third base pair in the hexamer sequence. The results are discussed with a view to understand implications of binding of the drug adriamycin to DNA.

ACKNOWLEDGEMENTS

I wish to express my sincere thanks and gratitude for Dr. Ritu Barthwal, Head and Reader, Department of Biosciences and Biotechnology, University of Roorkee, Roorkee for providing her supervision, valuable criticism, expert guidance and constant encouragement throughout the completion of this work.

I take this oppurtunity to express my gratitude to my senior, Dr. Anwer Mujeeb, who has contributed much in making this tedious task, a success.

I thank all the members of FT-NMR National facility at TIFR, Bombay for their help and cooperation during my stay. Mamta, Devidas and Mr. Ranpura specially deserve citation for their efforts, time and willingness to help.

I thank Prof. V.S. Chauhan, ICGEB New Delhi and Prof. K.B. Roy, J.N.U., New Delhi for providing all research facilities for synthesis and purification of DNA samples.

Financial assistance rendered by Council of Scientific and Industrial Research, Government of India, is gratefully acknowledged.

"Friends in need are the friends indeed" they say and I find that this saying is very true. Today I remember all my friends who have helped me in more ways than I recount. I thank Dr.

Ujjwala, Neerja, shoma and Dr. Neeti who have helped me tide over most difficult times. I don't find words to express my feelings for Uma, who has given generously of her time and support which helped to bring this dissertation to fruition. I will always remember her assistance and silent support when the going was tough for me. I enjoyed working with my labmates Sadhna, Rashmi, Ritu, Ramesh, Jignesh and Shalini.

My parents and in-laws have contributed much to this thesis. Their efforts are reflected on every page of this thesis. They provided love and affection, support and encouragement which helped me to a great extent. Here, I put on records my admiration and sentiments for my husband, Ambuj. His love, understanding nature and those few words of encouragement made it a smooth sailing for me.

I acknowledge Mr. Sewa Ram for carefully typing this thesis.

(NANDANA SRIVASTAVA)

LIST OF PUBLICATIONS

1. Barthwal R., Srivastava N., Sharma U. and Govil G. A 500 MHz proton NMR study of the conformation of adriamycin. J. Mol. Struc., 1994, 327, 201.

2. Barthwal R., Mujeeb A., Srivastava N. and Sharma U. A proton nuclear magnetic resonance investigation of the conformation of daunomycin. Chemico-Biol. Interact., 1996, (in press).

CONTENTS

Page No.

CANDIDATE'S DECLARATION

ABSTRACT

ACKNOWLEDGEMENTS

LIST OF PUBLICATION

CHAPTER - I

INTRODUCTION 1-20

... General

... Structure of anthracycline drugs

... Structure of nucleic acids

... Elements of drug-nucleic acid interaction

... Application of NMR in studying
Drug-DNA interactions

CHAPTER - II

LITERATURE REVIEW 21-63

... Adriamycin and its complexes

... Related antitumour drugs

... Scope of thesis

CHAPTER - III

MATERIALS AND METHODS 64-94

... Materials

... Sample preparation

... NMR methods

... Experimental parameters

... Conformation of nucleic acids by NMR

CHAPTER - IV

ANTHRACYCLINE ANTIBIOTIC ADRIAMYCIN 95-134

... Spectral assignments

... Spin-Spin coupling and torsional angles

... NOE connectivities and interproton distances

... Exchangeable protons and their connectivities

... Conformation of adriamycin

CHAPTER - V

CONFORMATION OF DEOXYHEXANUCLEOTIDE

d-$(CGATCG)_2$ 135-255

... Sequential assignments

... Sugar geometry of d-$(CGATCG)_2$

... Glycosidic bond rotation

CHAPTER - VI

INTERACTION OF ADRIAMYCIN WITH

DEOXYHEXANUCLEOTIDE d-$(CGATCG)_2$ 256-319

... Spectral assignment of d-$(CGATCG)_2$

... Spectral assignment of adriamycin

... Titration studies

... Changes with temperature

... Interaction of drug with DNA

CONCLUSIONS 320-321

REFERENCES 322-344

CHAPTER - I

INTRODUCTION

GENERAL

DNA, the genetic material in living cells, can interact with certain classes of drugs, carcinogens, mutagens and dyes, all of which are characterized by extended heterocyclic aromatic chromophore. A variety of biochemical evidence suggests that DNA is the principal cell target for many antitumour agents. Owing to DNA's central role in biological replication and protein synthesis, modification by such interactions greatly alters the cell metabolism, diminishing and in some cases terminating the cell growth.

The cancer chemotherapy relies on inhibition of nucleic acid synthesis or interference with mitosis as a means of discriminating selectively against fast growing tumour cells. Many of these antitumour agents are a subject of extensive study these days due to the fact that most of them have clinically useful chemotherapeutic properties; they act as probes for nucleic acid structure and function; and wide range of derivatives of these antitumour drugs can be designed with an understanding of the key features responsible for their relative cytotoxicity.

There are many types of naturally occurring and synthetic chemical agents employed in treatment of cancer. These drugs and antibiotics may interfere with the synthesis of nucleic acids in

several different ways. There are three levels at which inhibitors may exert their primary effect, and these antitumour drugs can be divided into three groups accordingly. First group comprises of drugs inhibiting nucleic acid synthesis at the level of nucleotide metabolism. Second class includes agents which act at the level of polymerization reactions. Third group includes those agents which inhibit nucleic acid synthesis via direct interference with polymerases or other enzymatic processes involved in the replication and transcription of DNA.

Agents which interfere with nucleotide metabolism

A large number of agents inhibit nucleic acid synthesis at the level of nucleotide metabolism, including many antibiotics as well as semi-synthetic derivatives of antibiotics and wholly synthetic drugs. Most of these agents act by inhibiting well - characterized enzymes. Typically they act by inhibiting de novo purine and pyrimidine synthesis, by inhibition of interconversion of nucleotides, inhibition of utilization of nucleotides and by incorporation of nucleotide analogues into polynucleotides. It is obvious that many of the drugs are structural analogues of the naturally occurring bases and nucleosides which enter into reaction sequences of nucleotide metabolism by acting as substrates for various enzymes, e.g. azaserine and DON (6-diazo-5-oxo-L-norleucine) are related antitumour antibiotics which inhibit purine synthesis at phosphoribosyl-formyl-glycine amide synthetase step. The interconversion between pyrimidine nucleotides is inhibited by 5-fluorouracil and 5-fluoro-

deoxyuridine antitumour drugs at thymidylate synthetase reaction. The two arabinose containing nucleoside analogues; cytosine arabinoside (ara-C) and arabinosyl adenine (ara-A) are examples of inhibitors of nucleotide utilization. The former is a synthetic antitumour drug while latter occurs naturally as a metabolite of Streptomyces antibioticus.

Agents which impair the template function of DNA

A drug may interfere with the role of DNA as a template in replication and transcription (a) directly by reacting with it to form a complex, or (b) indirectly by causing structural alterations such as strand breakage, removal of bases or, formation of cross links. Some of the drugs react with DNA covalently to form an irreversible complex and some form reversible non-covalent complex with DNA. There are certain drugs which interact by intercalation between base pairs of DNA. The best known antibiotics used for the treatment of cancer are anthracyclines, falling under the class, quinone antibiotics. Adriamycin and daunomycin are best known representatives of this group of antibiotics which also includes nogalamycin, carminomycin, aclacinomycin, etc. These drugs intercalate between base pairs of DNA, hence cause alteration in DNA structure. X-ray investigations and various other biochemical techniques have proved the intercalative mode of binding of these drugs. In intact cells they inhibit both DNA and RNA synthesis. The possibility of chemotherapy of these drugs has been suggested through lysosome - mediated release of drug after administration

of a adriamycin - DNA complex. The example of a drug which binds covalently to DNA and causes strand breaks is mitomycin C. It is an antitumour antibiotic which can both alkylate and form inter-strand cross links in DNA. It also generates semiquinone, H_2O_2 and $OH^{\cdot}$ which causes single-strand breaks in DNA. Carzinophilin A, produced by Streptomyces sahachiroi has been used clinically in treatment of human skin cancer, cancer of jejunum, reticulosarcoma, etc. It reversibly binds to DNA by bisintercalation and forms covalent cross links. Alkylating agents like sulphur mustard and nitrogen mustard are basically electrophiles. They attack electron rich sites in DNA, adding alkyl groups to nitrogen, sulphur or, oxygen atom and cross links to DNA.

Agents which inhibit enzymatic processes in nucleic acid synthesis

These agents do not exert their action via binding to DNA but rather by interfering directly with the enzymes involved in polymerization reactions. Rifamycin and streptovaricin drugs are similar in structure and mode of action. These drugs act specifically by binding to RNA polymerase and inhibit nucleic acid synthesis. Streptolydigin, another antitumour drug inhibits the chain-polymerization reaction. It slows the rate of phosphodiester bond formation without affecting the fidelity of the transcription process. At high concentrations, the formation of all phosphodiester bonds are inhibited.

STRUCTURE OF ANTHRACYCLINE DRUGS

Anthracycline drugs are characterized by a tetrahydro-tetracene quinone chromophore which contains three flat, coplanar six-membered rings. Adriamycin has one additional non-planar six membered ring and a daunosamine sugar moiety (Fig. 1.1). Ring A of adriamycin differs from that of daunomycin, another anthracycline drug. The $COCH_3$ group at position nine in daunomycin is replaced by the $COCH_2OH$ group in adriamycin. The daunosamine sugar moiety is attached to ring A at C1′ position through a glycosyl linkage. The torsion angles ϕ, ψ defined as H1′-C1′-O7-C7 and C1′-O7-C7-H7, respectively describe the orientation of sugar moiety with respect to non-planar ring A. These angles play an important role in three-dimensional conformation of adriamycin. Ring A conformation is ascertained by torsion angles θ = H(7)-C(7)-C(8)-H(8eq) and θ' = H(7)-C(7)-C(8)-H(8ax). The C14-OH group of adriamycin forms additional hydrogen bond to DNA which stabilizes the complex. 4′-epiadriamycin an analogue of adriamycin differs from it only by an inversion of the stereochemistry at the 4′ position of the sugar.

The analogue of daunomycin, N-acetyl daunomycin, has N-acetyl group at 3′ position of daunosamine sugar moiety. Carminomycin differs from daunomycin in having hydroxyl group at fourth position of ring D.

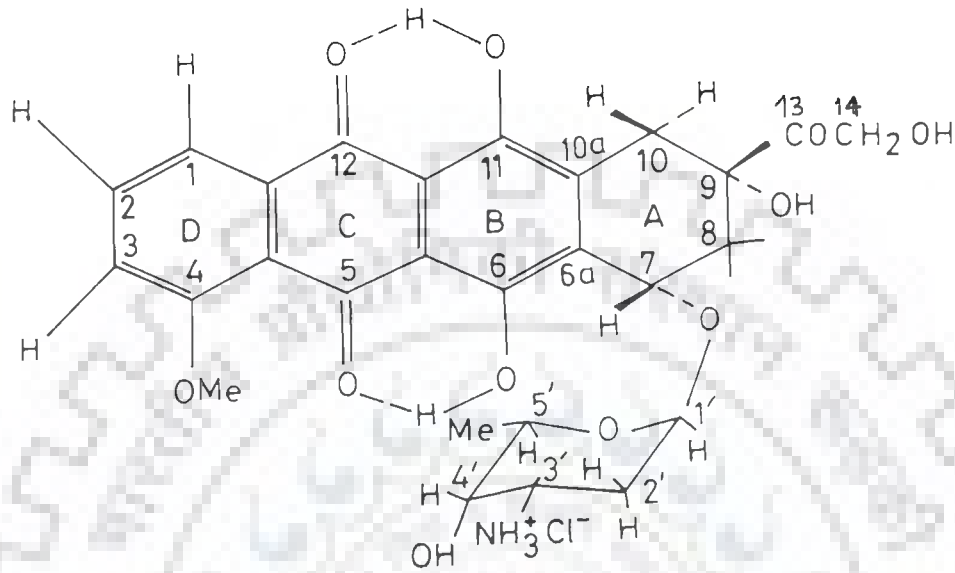

Fig. 1.1 : Structure of adriamycin.

All these analogues have been developed as anticancer drugs in order to reduce their cytotoxicity and enhance their antibiotic activity.

Adriamycin

The anthracycline drugs adriamycin, daunomycin as well as their biosynthetic congeners are all derived from Streptomyces peucetius. Both are established useful agents for the chemotherapeutic treatment of cancer and their primary site of action at tumour cell level is through an interference with deoxyribonucleic acid synthesis and function. Adriamycin is in particular of considerable medicinal value because of its outstanding activity on a number of solid tumours and against acute leukemia. The in vitro growth of a number of normal and neoplastic cell lines is markedly inhibited by adriamycin. This inhibition is characterized by cell damage, particularly to the nucleus. Chromosomal and genetic aberrations of several types are also produced by adriamycin (77).

The biological activities of different anthracyclines have been shown to be dependent on minor modifications in their chemical structure. Efforts to reduce anthracycline toxicity while enhancing the antibiotic nature of adriamycin have resulted in many compounds. One such adriamycin analogue, 4'-epi-adriamycin, has been developed which is better tolerated because of reduced cardiotoxicity. In order to improve the therapeutic effectiveness and to reduce toxicity of adriamycin for cancer

chemotherapy, an in-depth understanding of adriamycin-DNA complex is required.

STRUCTURE OF NUCLEIC ACIDS

Nucleic acids are high molecular weight polymeric compounds. The building blocks of nucleic acids are nucleotide units. Each nucleotide is made up of a purine/pyrimidine base, a sugar and phosphate group.

Purine and pyrimidine bases

Both types of nucleic acids contain the planar purine bases, adenine and guanine and pyrimidine bases, cytosine and thymidine. The latter being replaced by uracil in RNA (Fig. 1.2). The purine and pyrimidine bases can undergo keto-enol tautomerism. Besides these common bases, certain minor bases such as inosine, 7-methyl guanosine, etc. are also found as components of nucleic acids.

Sugar

The sugar component of RNA is ribose while in DNA it is 2-deoxyribose, which in polynucleotides occur in the furanose form (Fig. 1.3(a, b)). This difference has wide ranging effects on chemistry and structure of RNA since the presence of bulky - OH group on the 2nd position of the sugar limits the range of possible secondary structures it can take. The nucleic acid bases are attached to the C1′ position of the sugar moieties. The sugar-base combination is known as nucleoside unit.

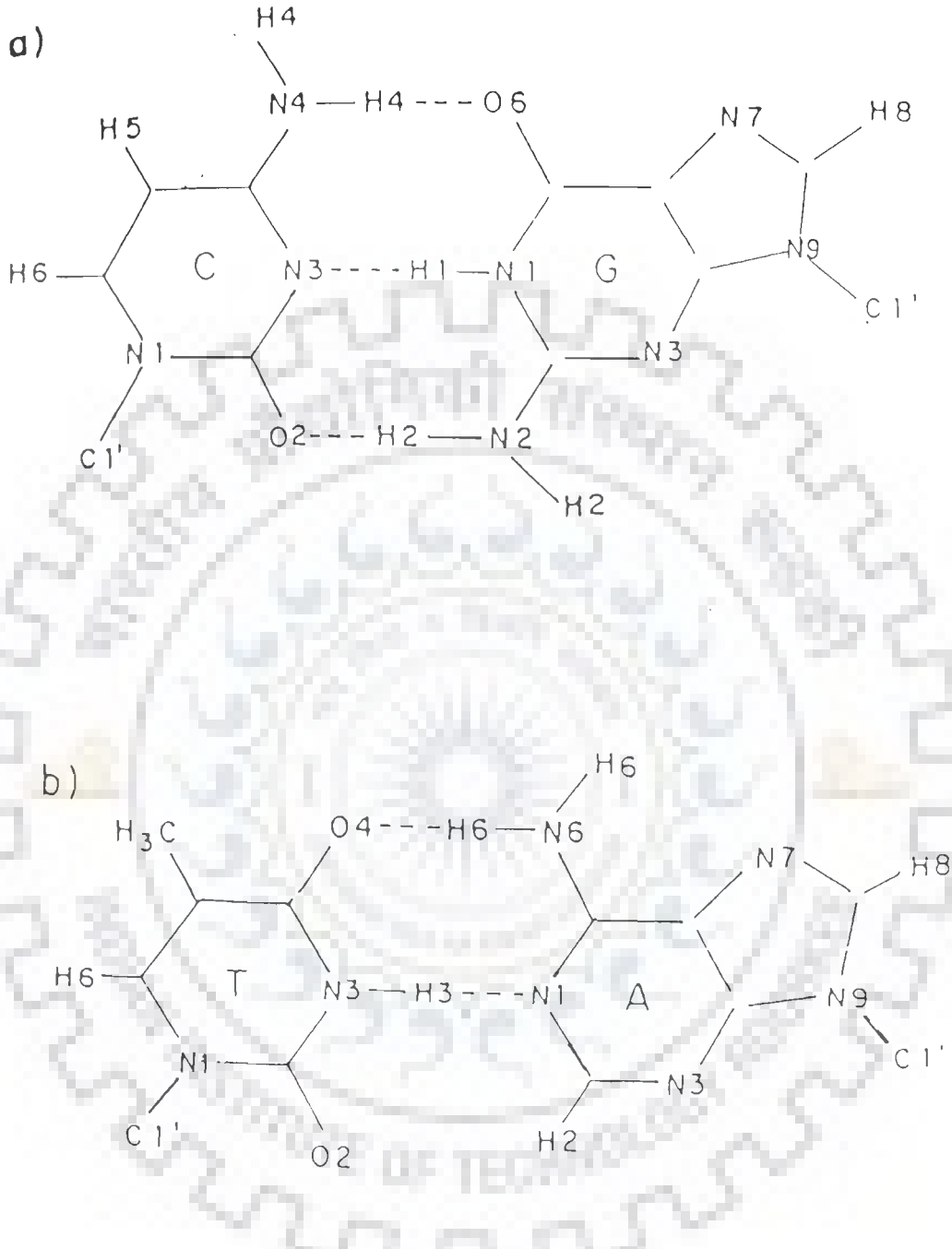

Fig.1.2 : Watson and Crick base pairs showing the hydrogen bonding arrangement in double helical DNA.

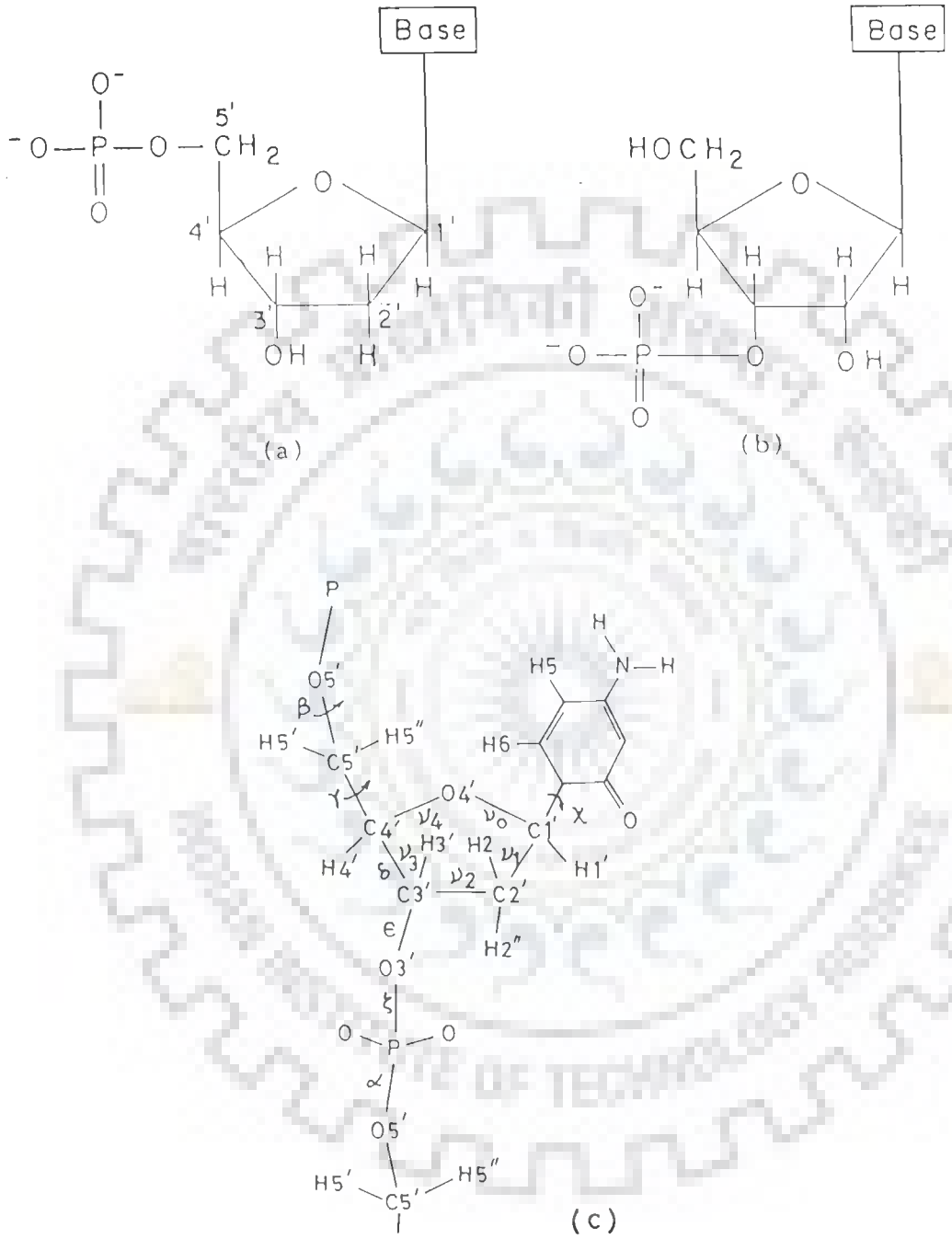

Fig. 1.3 : Five membered furanose ring (a) deoxyribose and (b) ribose found in DNA and RNA, respectively. (c) A nucleotide unit showing the numbering of the atoms in the furanose ring and the backbone torsion angles.

Phosphate group

It is attached to the furanose ring, which bridges successive nucleotide units (Fig. 1.3(c)). Polynucleotide chains are made up of many mononucleotide units, linked by phosphoric acid bridges from the 5′ end of one nucleotide to the 3′ end of the other.

The primary structure of nucleic acids is determined by the sequence of bases along the nucleotide chain and the functions of nucleic acids namely replication, transcription and translation are governed by this sequence. The three-dimensional conformation of nucleic acids is governed by a number of torsion angles shown in Fig. 1.3(c).

There are three sets of torsion angles, which are given as follows :

Glycosidic torsion angle (χ)

The base-sugar linkage is defined by torsion angle, χ, which refers to the orientation of the planar base with respect to the sugar ring. This angle is defined as O4′-C1′-N9-C8 in case of purines and as O4′-C1′-N1-C6 in pyrimidines. The bases can adopt two main orientations relative to the sugar moiety, called anti and syn conformation (Fig. 1.4(a)). In general, the anti conformation in nucleotides have a χ angle of $\simeq 30^{\circ}$, while the corresponding angle for a syn nucleotide is $\simeq 250^{\circ}$, the former being energetically more favourable.

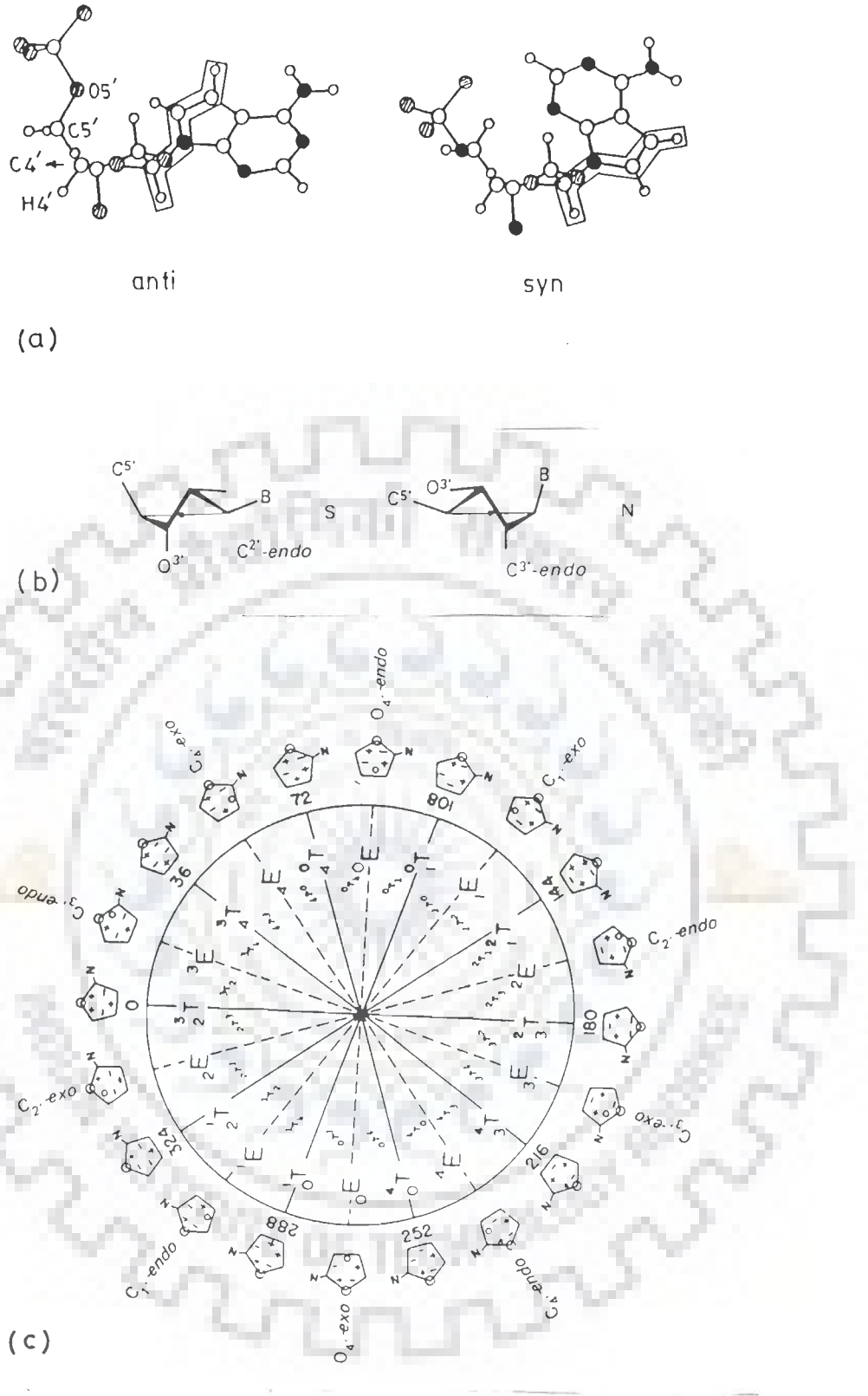

Fig. 1.4 : (a) Anti and syn orientations about the glycosyl bond. (b) Preferred conformations, C2'-endo and C3'-endo of sugar pucker. (c) Pseudorotation cycle of the furanose ring in nucleosides.

Torsion angles within the sugar ring

The sugar ring forms an important part of the backbone unit and side chains. Its conformation is described by five endocyclic torsion angles ν_0, ν_1, ν_2, ν_3 and ν_4 about the bonds O4'-C1', C1'-C2', C2'-C3', C3'-C4' and C4'-O4', respectively. Since sugar has only five atoms and it forms a closed ring structure which introduces constraints, two torsion angles are sufficient to define the three-dimensional geometry of the ring.

The five-membered furanose ring is non-planar. It can be puckered in an envelope (E) form with four atoms lying in a plane and the fifth atom is pointing out by 0.5 A° (Fig. 1.4(b)). Alternatively it is puckered in a twist (T) form with two adjacent atoms displaced on opposite sides of a plane passing through the other three atoms.

The puckering of five-membered furanose ring is described by two pseudorotational parameters P and ν_{max} (1). In nucleotides, the pseudorotational phase angle P is calculated from the endocyclic sugar torsion angles by the equation (Fig. 1.4(c)) :

$$\tan P = \frac{(\nu_4 + \nu_1) - (\nu_3 + \nu_0)}{2.\ \nu_2.\ (\sin 36^{\circ} + \sin 72^{\circ})}$$

The five torsion angles of sugar are related by :

$$\nu_j = \nu_{max}.\mathrm{Cos}\ (P + j\ .\ \phi)$$

where, j = 0 to 4, $\phi = 144^{\circ}$, and maximum torsion angle, ν_{max} is derived by setting j = 0 :

$$\nu_{max} = \nu_0\ /\ \mathrm{Cos}\ P$$

The conformations for P = 0° ± 18 are denoted by N and include the classical C3'- endo and C2'- exo conformations. Those for P = 180° ± 18 are denoted by S and include the C2'-endo and C3'- exo puckers of the ribose ring (38).

Backbone torsion angles

The secondary structure of DNA is determined by backbone torsion angles; α, β, γ, δ, ε, ξ about the bonds P-O5', O5'-C5', C5'-C4', C4'-C3', C3'-O3' and O3'-P, respectively. Under normal physiological conditions of temperature and pH, most double-stranded nucleic acids exist as helices with well defined dihedral angles. Although right-handed B-DNA is presumed to be the predominant conformation in vivo, other stable alternative DNA conformations are also known to exist. These differ in their helical parameters such as pitch, twist, number of bases per turn, sugar pucker, etc. At high temperatures, the secondary structure of DNA gets lost and random coils are obtained.

In naturally occurring nucleic acids, the helix consists of two right-handed strands forming a double helix (Fig. 1.5). The sugar-phosphate backbones run along the outside of the helix in an antiparallel orientation and the bases are paired with each other towards the center of the helix. The DNA double helix is stabilized by base-base hydrogen bonds, stacking interactions and hydrophobic interactions.

In a double helix, the two polynucleotide chains are connected by complementary base pairing. Adenine forms base pair

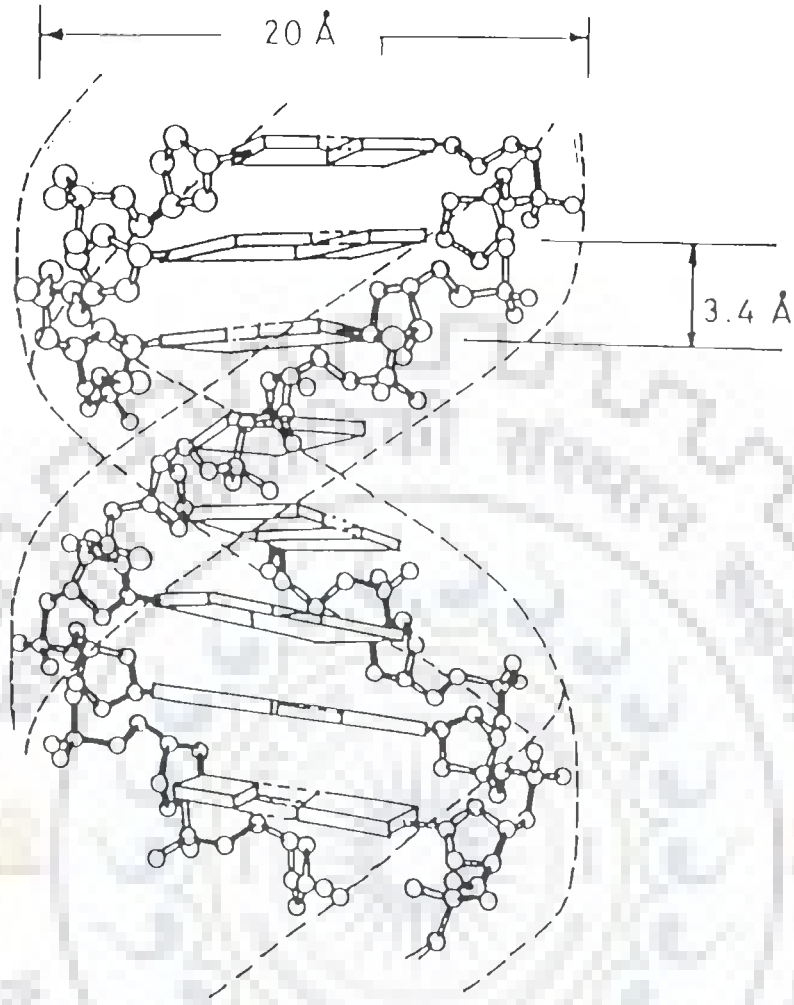

Fig. 1.5 : Schematic representation of the DNA double helix. The sugar-phosphate backbones run at the periphery of the helix in antiparallel orientation. Base pairs are stacked along the centre of the helix.

Table 1.1 Structural characteristics of A, B and Z-type double helices

Family Type	A - Type	B - Type	Z - Type
Bases per turn	11	10	12
Rotation per nucleotide	30° to 32.7°	36° to 45°	-60°
Base per tilt	10° to 20.2°	-5.9° to 16.4°	-7° to 9°
Helix pitch (nm)	3.09 to 3.60	3.38	4.56
Rise per residue	0.20	0.34	0.76/2
Helix diameter (nm)	2.30	1.93	1.81
Helix sense	Right-handed	Right-handed	Left-handed
Glycosidic bond rotation	Anti	Anti	Anti (Cytosine) Syn (Guanosine)
Sugar pucker	C3'-endo	C2'-endo	C3'-endo (Guanosine) C2'-endo (Cytosine)

with thymine and cytosine forms base pair with guanine (Fig. 1.2) by Watson and Crick hydrogen bonding scheme.

In a double helix of DNA, the bases are stacked one over each other and are at a distance of $\simeq$ 3.4 A°. This vertical stacking of base pairs plays an important role in stabilization of DNA helices. Stacking interactions between purines and pyrimidines follow the trend :

Purine-Purine > Pyrimidine-Purine > Pyrimidine-Pyrimidine.

Different forms of DNA can be described in terms of conformation of sugar ring, the base orientation and backbone dihedral angles. DNA can be classified as A, B or Z type of DNA and the main features of these are given in Table 1.1.

ELEMENTS OF DRUG-NUCLEIC ACID INTERACTIONS

Stacking interaction

The increase in viscosity and decrease in sedimentation coefficient of DNA was observed to be associated with stacking interactions of anthracycline antibiotics. These changes in hydrodynamic behaviour are related and could be attributed to lengthening of DNA molecules caused by binding of anthracycline drug. Lerman (58) accounted for these observations by proposing that the planar aromatic drugs like ethidium bromide, proflavine, adriamycin etc. gets intercalated between adjacent base pairs of the double helix. The base pairs remain perpendicular to the helix axis, but they move apart to accommodate the drug molecule which lies in van der Waal's contact with the base pairs above and

below. The drug and DNA stacked complex is stabilized by hydrophobic interactions in aqueous solution. Distortion of the helix occurs because the helix unwinds locally to accommodate the drug molecule. X-ray studies have shown that aglycone chromophore of adriamycin is oriented at right angles to the long dimension of DNA base pairs.

Hydrogen bonding

The phosphate group, sugar and bases in nucleic acids; hydrophilic groups in anthracycline drugs participate in hydrogen bonding. In adriamycin complex with DNA, two hydrogen bonds 9OH...N3 and 9O....N2H between adriamycin and the base G-2 stabilize the conformation of ring A (19,32,71,81,128). The 9OH...N3 hydrogen bond has been found to be necessary for the in vivo antitumour activity of adriamycin (43). There are additional hydrogen bonding interactions linking the C-14 hydroxyl of adriamycin to DNA, which further stabilizes the complex (32).

APPLICATION OF NMR IN STUDYING DRUG-DNA INTERACTIONS

NMR spectroscopy is emerging as a powerful tool in molecular biology and biotechnology. The dynamic and structural information which NMR can provide on the changes in conformation and molecular flexibility, complements X-ray crystallography data and enables mechanistic modes of drug - DNA interactions to be formulated.

The great advantage of NMR technique lies in the truth that molecular structures can be observed under actual biological conditions. Being in solution form, even structural and

biochemical changes in intact cells (in vivo NMR) can be monitored. Characteristic resonance can be obtained from each magnetic nucleus in a biomolecule. The most commonly used resonances in NMR studies are ^{1}H, ^{13}C, ^{31}P and ^{15}N. ^{1}H NMR gives rise to a series of absorption lines in the region 0-10 ppm. A larger spectral dispersion of chemical shifts is observed in ^{13}C NMR. In ^{15}N NMR, chemical shifts are sensitive to primary structure as well as molecular conformation. But it has low sensitivity due to low natural abundance (0.36%) which causes difficulties in its detection hence offers limited applications of ^{15}N NMR. ^{31}P NMR has developed as a powerful probe of the structure and dynamics of DNA due to existence of spin 1/2, 100% natural abundance, moderate relaxation times, wide range of chemical shifts and non-interference from solvent peaks. In ^{31}P NMR, chemical shifts are sensitive to molecular conformation of the phosphate group. Thus it becomes very informative in case of nucleic acid structure elucidation since backbone of DNA and RNA contains phosphorous nuclei.

In the past decade, our understanding of the structural basis of drug-DNA interactions occurring in solution has made great progress; one aspect of it is the use of one and two-dimensional NMR methodologies to investigate these interactions. At the molecular level, the interaction between two kinds of molecules are responsible for specific recognition phenomena. The DNA double helix does not have a monotonous structure, as was once thought, but has sequence specific variations in local

conformation. Different base sequences are also associated with different degrees of molecular flexibility. They too can contribute to the recognition of a given sequence since the binding induces structural distortions in DNA. It is obvious that the three-dimensional (3D) structures of the individual molecules play a crucial role in deciding the nature of the interactions and recognition mechanisms.

The investigation of drug-DNA interactions by NMR spectroscopy requires, as a first step, the separate spectroscopic characterization of the two macromolecules of interest. This characterization starts with assigning NMR resonances to specific nuclei in the molecule. The experiments can then be extended to deduce sugar conformations and to obtain distances between specific nuclei, which can then be used to generate three-dimensional structures of DNA and DNA binding drugs.

LITERATURE REVIEW

ADRIAMYCIN AND ITS COMPLEXES

To this date large number of techniques have been used to understand structure of adriamycin and its mechanism of interaction with nucleic acids. The pioneer studies in this area of drug - nucleic acid interactions are on structurally related anthracycline drug, daunomycin. Several physico-chemical techniques have been used to investigate structure of daunomycin and its interaction with nucleic acids.

Calendi et al. (9) proved that daunomycin binds to both strands of DNA double helix on observing spectroscopic properties of DNA in presence of daunomycin. The existence of a bond between daunomycin and DNA, which stabilizes the association of two strands, is indicated by observed increase in melting point of DNA. The structure and stereochemistry of daunomycin was elucidated by Iwamoto et al. (49) using NMR technique. It was shown that the anomeric proton H1' is equatorially oriented and sugar exists as α-L form, while C7 proton is pseudoequatorially oriented. Ryser (109) showed that the high endocytotic activity characteristic of many tumour cells, allows the transport of the macromolecular drug - DNA complex into the target cell

preferentially. Once inside the tumour cell, the complex would most probably be taken up by the lysosomes, the carrier DNA would then be digested by the enzyme DNase, and the drug would be released. The beneficial effect of using such a complex depends on the fact that the complex is less toxic than the drug alone.

The intercalative binding of drugs, daunomycin, ethidium bromide, nogalamycin etc. has been verified by observing changes in the supercoiling of closed circular DNA, as revealed by changes in the sedimentation coefficient (129). Daunomycin causes a definite decrease in sedimentation coefficient S_{20} of ϕX174 RF, as expected for intercalative binding. The apparent unwinding angle has been calculated for all intercalating drugs by taking the unwinding angle of ethidium $\simeq 12^{\circ}$ as a reference.

The stereochemistry of intercalation of daunomycin in DNA was proposed by Pigram et al. (94) from the X-ray diffraction pattern of a DNA-daunomycin complex. The structural model of intercalated complex had unwinding angle of 12° per drug with amino sugar of daunomycin existing in large groove of DNA and the hydrophobic faces of the base pairs and drug overlapping extensively. The ionised amino group is found to interact strongly with second DNA phosphate away from intercalation site. Zunino et al. (138) carried out spectroscopy , viscometry and thermal denaturation studies to investigate the interaction of daunomycin, adriamycin and its other derivatives with calf thymus DNA. It was observed that binding of daunomycin to DNA involves more than one class of

sites. Adriamycin binds to DNA as strongly as daunomycin itself. The amino sugar residue plays an important role in the stabilization of the complex.

Complexes of calf thymus DNA with daunomycin, nogalamycin and carminomycin were studied by circular dichroism over a range of drug/DNA ratios (25). The existence of intercalative complex is predicted for daunomycin along with presence of free drug and DNA contributions. Comparing the results obtained with that for 9-aminoacridine, which is believed to intercalate in DNA, it was observed that none of these antibiotics appeared to behave exactly as intercalating molecules. This was attributed to difference in chromophoric group present in antibiotics giving rise to transition dipoles in different directions and due to the difference in position of intercalation. The interaction of adriamycin with polydeoxyribonucleotides, double-stranded DNA and double-stranded ribodeoxyribopolynucleotide hybrids were investigated (123) by fluorescence emission and polarization techniques. It was found that alternating deoxyguanylate (dG)-deoxycytidylate (dC) sequence binds to adriamycin in a better way than alternating deoxyadenylate d(A) - deoxythymidylate (dT) sequence. Intercalation of adriamycin in Poly (dG). Poly (dC) resulted in inhibition of DNase II enzyme to an extent two or three times more than that of DNase I.

Gabbay et al. (34) have studied the interaction of salmon sperm DNA with various derivatives of daunorubicin including

adriamycin by circular dichroism, spectral titration and various other techniques. The peptide derivatives substituted at the amino sugar of daunorubicin has lower affinity for DNA whereas adriamycin and daunomycin binds strongly to DNA. The results are consistent with specific hydrogen bonding of amino group of sugar moiety of daunorubicin with DNA as suggested earlier by Pigram et al. (94). In order to ascertain the biochemical specificity of adriamycin Momparler et al. (68) have compared the effect of adriamycin on DNA, RNA and protein synthesis in mammalian cell-free systems and in intact cells. It was found that adriamycin is a more potent inhibitor of DNA dependent DNA polymerase than that of RNA polymerase. In cell-free systems containing t-RNA, polyribosomes, co-factors, adriamycin inhibits protein synthesis significantly. However, in intact cells this antibiotic does not inhibit protein synthesis.

The relation between the stereochemistry of anthracycline antibiotics and their ability to bind to DNA has been investigated by Zunino et al. (139) using homologous series of derivatives of daunomycin. The quenching of fluorescence and high stability of DNA by 4-demethoxy daunomycin shows that 4-methoxy group does not interfere with chromophore / base pair stacking. However inverted configuration at positions 7 and 9 decreases the DNA binding. Using an ethidium bromide fluorescence assay it was demonstrated by Lown et al. (63) that adriamycin and daunorubicin bound to covalently closed circular DNA nick the latter when reduced by sodium borohydride. Both, parent antibiotics adriamycin and

daunomycin as well as their reduced forms, intercalate the DNA and relax it completely as shown by 30% decrease in fluorescence. The interaction of daunomycin with t-RNA was studied using fluorescence quenching and spectral titration studies (115). Fluorescence of daunomycin is quenched and its visible spectrum undergoes hypochromic and slightly bathochromic shift on addition of t-RNA. The curve obtained on spectral titration is biphasic typical of intercalation complexes with nucleic acids. The results obtained provided evidence that interaction of daunomycin with t-RNA is different than with viral double-stranded RNA. In fluorescence quenching and spectral titration studies t-RNA interacts with daunomycin in a similar manner to DNA.

Plumbridge and Brown (95) investigated the nature of binding of ethidium, daunomycin and mepacrine to DNA and Poly (I.C) by spectrophotometric and fluorescence polarization techniques. The results obtained showed that daunomycin, ethidium and mepacrine bind to DNA by intercalation, whereas these drugs do not intercalate into Poly (I.C). In a separate study the crystal structure of daunomycin was reported by Neidle and Taylor (78). The rings B, C and D were found to be planar whereas the cyclohexene ring A was non-planar and in half chair conformation. The methoxy substituent on ring D deviates from the plane with methyl carbon atom, 0.26 A° out of the plane. The C-8, carbon atom of ring A also deviates from the plane of other five atoms by 0.58 A°. An intramolecular hydrogen bond C(7)...O(9) was observed which accounts for stable molecular conformation. Hydrogen

bonding between O(11)...O(12) and O(5)...O(6) were also observed. The structure of daunomycin was found to be similar to that of carminomycin I (91).

The 1D NMR studies of daunomycin-Poly(dA-dT) complex has been studied by Patel and Canuel (86) with varying P_i / drug ratio under high salt conditions. The changes in chemical shift of daunomycin protons on complexation suggested that either ring B and/or C ring of daunomycin overlaps with adjacent nucleic acid base pairs. It has been suggested that electrostatic interactions between amino sugar and backbone phosphates plays an important role in stability of the complex at low salt. The duplex-to-strand transition of daunomycin-dG-dC-dG-dC complex and dG-dC-dG-dC have been monitored by 1D NMR in solution (88). Complexation with daunomycin results in stabilization of dG-dC-dG-dC by 40 $^{\circ}$C. The experimental complexation shifts of ring D protons suggests that ring B and/or C intercalates into tetranucleotide duplex. Courseille et al. (24) studied the complex of daunomycin-butanol by X-ray crystallography. It was found that aromatic part of the molecule was planar, the daunosamine sugar acquires chair form and had protonated amino group, and the cyclohexane ring was in monoplanar or, half-chair form. The hydrogen bond between keto and hydroxyl group of ring B and C were found to have length of 2.53 and 2.47 A$^{\circ}$. The conformation was found to be identical to that obtained for crystals of daunomycin with pyridine and water (78).

The flexibility of daunomycin about the chromophore - sugar linkages, defined by ϕ_1 = C8-C7-O7-C1′ and ϕ_2 = C7-O7-C1′-O5′ have been explored using semi-empirical energy calculations (79). The minimum energy conformation is close to the N-bromoacetyl derivative, which does not have intramolecular O7...O9 hydrogen bond. Hypothetical structural alterations in daunomycin by deleting O9 hydroxyl group and the $COCH_3$ side chain at C9, does not result in shift of global energy minimum. The binding of adriamycin to cellular macromolecules in vivo has been studied by Sinha and Sik (117). Binding of adriamycin to DNA, RNA and proteins decreased rapidly with time as monitored by radioactivity measured in liquid scintillating counter. It was found to decrease rapidly with time. The genetic damage induced by adriamycin may be related to binding of the drug to nucleic acids and proteins in vivo. Quigley et al. (98) investigated the molecular structure of daunomycin-d-$(CGTACG)_2$ complex by X-ray crystallography. Daunomycin was found to intercalate in d(CpG) step of the hexamer. The cyclohexene ring A and amino sugar protruded in minor groove while ring D in the major groove of DNA. The unwinding angle for the two base pairs on either side of intercalator is 0° and the next two base pairs showed unwinding angle of $\simeq 8^\circ$. Changes in sugar pucker, glycosidic bond angle (χ) and backbone conformation of hexamer were observed on intercalation of daunomycin. Strong hydrogen bonds were formed between O9 and ring nitrogen N3 of guanine G2 (2.6 A°) and between O9 and amino group N2 of same guanine (2.9 A°). The positively

charged amino group of daunosamine sugar was not found to interact with phosphates as has been proposed earlier (34,94).

Binding of daunomycin to various dinucleotides was studied by 1D NMR. (82). In pyridine and D_2O solution, the conformation of ring A was found to be such that H-7 proton splits H-8(ax) proton by a larger amount than H-8(eq) proton. The conformation of ring A does not undergo a change on binding while, daunosamine sugar is altered substantially on complexation. Daunomycin formed 1:1 complex with dinucleotides however, it does not bind to all dinucleotide sequences with equal strength. A model has also been proposed for drug/dinucleotide complex on the basis of these results. The conformational analysis of both the neutral (NH_2) and charged (NH_3^+) forms of adriamycin (doxorubicin) has been carried out by metric energy minimization method (75). Three energy minimas were observed for the neutral molecule and the conformer having $\phi_1 = 250^\circ$, $\phi_2 = 260^\circ$ is the most stable one than the other two conformers. This minimum energy conformer was used as respective starting point for energy minimizations of the charged form (NH_3^+) of doxorubicin as well as the neutral and charged form of daunomycin. It was observed that the stable conformation for both doxorubicin and daunomycin was different from their corresponding crystal conformation.

The intercalation of doxorubicin with dinucleotide dimer sequences d-CpG and d-TpC has been modelled using molecular mechanics energy calculations (74). Minor groove intercalation

was preferred. The conformation was characterized by the anthraquinone ring aligned nearly perpendicular to the long axis of the CpG base pairs having alternate C3'-endo 3'-5' C2'- endo sugar ring puckering. The energy preference for minor groove intercalation decreased for the ionized form of doxorubicin. The conformational preference was not found for intercalation with TpC-ApG dimer. Proton nuclear magnetic studies of the self-complementary hexanucleotide $d(pTpA)_3$ and its interaction with daunomycin was investigated by Phillips and Roberts (92). The helix - coil transition of $d(pTpA)_3$ was studied and nucleotide protons were assigned to central, internal and terminal nucleotides. Extensive fraying was observed at 5 °C. The hexanucleotide duplex is stabilized on interaction with daunomycin by 21 °C at a drug/nucleotide ratio of 0.063. Daunomycin was found to be released co-operatively from $d(pTpA)_3$-daunomycin complex on heating. The H1' and aromatic protons of daunomycin shift downfield by ≥ 0.21 and 0.14 ppm, respectively. The chemical shift of $5'CH_3$ proton of daunosamine was found to be independent of temperature. These results suggested that planar aromatic portion of drug (rings B and C) intercalates while ring D protrudes outside the helix and on opposite side of the sugar moiety.

Patel et al. (89) have performed proton and ^{31}P NMR investigations on complexes of daunomycin and its analogue 11-deoxydaunomycin with Poly (dA-dT) respectively in H_2O. The 6-OH and 11-OH protons of ring B, C of daunomycin shift upfield by

≈ 1.6 ppm on complexation which is characteristic of intercalation. One of the ^{31}P signals presumably the one at intercalation site also shifts downfield by ≈ 0.45 ppm on complexation. The 11-H proton of 11-deoxydaunomycin was found to undergo large upfield shift of ≈ 1.42 ppm which suggests that ring B, C intercalate between base pairs while ring D protrudes out. Raman and Resonance Raman spectra of the DNA-adriamycin complex in aqueous solution have been recorded and analysed (64). UV-pre-resonance Raman spectra showed that guanine, cytosine and sugar-phosphate backbone vibrations decreases in intensity on binding. Resonance Raman spectra of adriamycin showed substantial changes in intensity of several bands on binding. The phenolic vibrations of chromophore of adriamycin changed on complexation, which has led them to suggest that phenolic groups are also involved in drug-DNA interactions. Using a theoretical approach Miller and Newlin (67) designed molecules which are capable of intercalation. To design such molecules, intercalating in an optimum manner, characteristic functional groups on a potential intercalant were established for this purpose. The results were used to form three and four fused ring systems that can bind in an optimum manner to form ideal intercalants.

Interactions of anthracycline antibiotics adriamycin, carminomycin and various other analogues with calf thymus (ct) DNA and covalently closed circular PM-2 DNA has been studied using viscometry and fluorimetry techniques (83). The stronger binding affinity of anthracyclines for native ct DNA, as compared to heat

denatured DNA showed that binding depends on the double-strandedness of DNA. An increase in the binding affinity and number of binding sites of adriamycin, carminomycin and marcellomycin with decrease in ionic strength attested the importance of electrostatic forces in these interactions. Viscometric titrations proved that these drugs were able to unwind and rewind CCC PM-2 DNA which is in accord with their intercalative mode of binding. The self association of daunomycin has been characterized by Chaires et al. (13). The increase in apparent extinction coefficient of drug solution on dilution supported dimerization model. However, sedimentation equilibrium experiments proved existence of indefinite association model for daunomycin. It is clear from NMR data that aromatic protons of anthracycline portion of the drug were most affected by aggregation due to stacking of the anthracycline rings. The effect of drug aggregation on the interpretation of drug-DNA binding data has been assessed quantitatively from the indefinite association model.

The binding of daunomycin to calf thymus DNA as a function of ionic strength and temperature has been studied by spectroscopic titration experiments (14). Daunomycin binds tightly to DNA and its binding constant decreases with increasing ionic strength. The results showed that daunomycin prefers G+C base pairs as a binding site and preferentially alters the buoyant density of G+C rich DNAs in CsCl density gradient. It increased the T_m of DNA by $\simeq$ 30 $^{\circ}$C as saturation of all potential sites was approached. The

data from these equilibrium studies were consistent with intercalative binding of daunomycin. Interaction of daunomycin and iremycin, its structural analogue has been investigated by transient electric dichroism and sedimentation analysis of supercoiled closed duplex DNA (33). The apparent increase in length of DNA induced by daunomycin, iremycin and iremycin - Cu(II) complex were 0.31, 0.40 and 0.44 nm/added drug. Intercalation of iremycin between DNA base pairs was supported by unwinding of the supercoiled closed duplex form of pBR322 plasmid DNA. The unwinding angle induced by iremycin was 15.0 ± 1.5°/bound drug whereas that for daunomycin was 15.4 ± 1.5°/bound drug molecule.

Graves and Krugh (39) studied the binding of adriamycin and daunorubicin to calf thymus DNA by phase partition technique and spectrofluorometric titration. Both drugs showed co-operative binding at ionic concentrations comparable to physiological levels (0.1 M NaCl). Adriamycin and daunorubicin bind to poly (dA-dT). poly (dA-dT) and poly (dA-dC). poly (dG-dT) in a highly co-operative manner at low r values. However, adriamycin exhibited higher binding affinity and greater degree of co-operativity than daunorubicin as evidenced by steeper positive slopes in the initial portion of the scatchard plots. Chen et al. (20) reported the effects of adriamycin on B to Z transition of poly (dGm^5dC). poly(dGm^5dC) by using CD and ^{31}P NMR data. Addition of adriamycin to poly (dGm^5dC) in Z-form resulted in its conversion to B-form in presence as well as in absence of $MgCl_2$. This Z $\longrightarrow$

B transition was found to be co-operative. Further, it was observed by CD spectroscopy that high concentration of Mg^{2+} was required to induce B to Z transition in presence of adriamycin. Thus, it was inferred that adriamycin inhibits B to Z transition and binds preferably to B form of DNA.

Equilibrium binding studies have been used to demonstrate that daunomycin inhibits B $\longrightarrow$ Z transition of poly d(G-C) at 4 M NaCl (11). Binding of daunomycin to poly d(G-C) at 4 M NaCl was found to be strongly co-operative and consistent with the role of the drug as an allosteric effector of the B $\longrightarrow$ Z equilibrium. Kinetic experiments showed that the rate and extent of the B $\longrightarrow$ Z transition were inhibited by daunomycin. Under certain conditions, daunomycin caused Z $\longrightarrow$ B transition and the rate of transition depended on molar ratio of daunomycin added. The inhibition of the RNA polymerase - catalyzed synthesis of RNA, by daunomycin was examined by Kriebardis et al. (55). It was observed that daunomycin inhibited the initiation of RNA chains and overall synthesis of RNA at low drug to DNA nucleotide base pair ratios. At low drug concentrations, daunomycin did not interfere with the formation of the enzyme-template complex. However, at high concentration, its formation was curtailed.

The effect of actinomycin D and adriamycin on various polynucleotides, including supercoiled DNA and synthetic polynucleotides have been studied by employing fluorescent probes terbium and lanthanide (116). Lanthanide and terbium have a known

specificity for unpaired guanine residues. Marked displacement of the probe was observed when any deoxyribose containing polynucleotide was pretreated with either drug as shown by decrease in fluorescence intensity. The iron(III) complexes of two anthracyclines adriamycin and daunorubicin have been studied (6). Potentiometric titrations indicated that these complexes are formed by the release of one proton per molecule of anthracycline. CD data substantiated occurrence of two different conformations A and D which could be adopted by both the complexes. These complexes were able to intercalate between DNA base pairs, despite strong coordination to iron(III). They displayed antitumour activity against P 388 leukemia, which were comparable to free drug.

Neumann et al. (80) studied interaction of daunomycin with B and Z helices of a self-complementary DNA fragment d(CGm^{5}CGCG) in solution by proton NMR spectroscopy. It was observed that with increase in daunomycin concentration, proportion of both B and Z free duplexes decreased and only B duplex-daunomycin complex was detected. No signal corresponding to Z duplex-daunomycin complex was observed. It was shown that daunomycin binds exclusively to the B form of d-(CGm^{5}CGCG). Thermodynamics of the daunomycin - DNA (calf thymus) interaction has been studied (12) by spectrophotometric methods over a wide range of temperature and concentration of NaCl. Van't Hoff analysis provided estimates for the enthalpy of the binding reaction for concentration of NaCl range 0.05 - 1.0 M. Binding of daunomycin was found to be

exothermic over this range and the favourable binding free energy was found to arise primarily from the large negative enthalpy.

The interactions of the adriamycin and nogalamycin with calf thymus and sarcoma-180 native chromatin DNA in presence of ethidium bromide and actinomycin D have been studied to elucidate similarities and differences in the nature of binding sites of these drugs (21). Results on absorbance, fluorescence and nuclease sensitivity showed that nogalamycin/adriamycin and ethidium bromide bind to DNA in a non-competitive manner. The total number of binding sites for combination of these drugs was found to be greater than any individual drug, but this increase was not additive due to neighbor exclusion. Adriamycin and nogalamycin was found to have identical specificity for binding sites in DNA and intercalate between purine (3'-5') pyrimidine sequences. Terbium, a sensitive probe was employed to study the effects of adriamycin and daunomycin on a variety of nucleotide substrates (90). The fluorescence of the probe was found to decrease when either of the drug was added to rRNA, linear calf thymus DNA and polyriboguanylic acid. However, daunomycin produced markedly greater effect than adriamycin. Both drugs appeared to have a similar specificity for guanine residues.

Kinetics of interaction of daunomycin with calf thymus DNA has been studied by Chaires et al. (15) by stopped flow and temperature-jump relaxation methods. The minimal mechanism in which the drug binds to DNA in a rapid biomolecular step, followed

by two sequential isomerizations, is consistent with experimental data. The six rate constants derived for this mechanism were used to calculate an overall equilibrium constant which was in agreement with binding constant obtained from independent equilibrium measurements. Chen et al. (18) performed theoretical computations on the energy and the structural factors involved in sequence selective binding of daunomycin to six self-complementary hexanucleotides including d-$(CGTACG)_2$ sequence. The analysis of interaction of individual constituents of daunomycin, namely daunosamine side chain, its two 9-hydroxyl substituents and 9-acetoxy substituent and the chromophore ring revealed that the overall sequence preference found was a result of intricate interplay of intrinsic sequence preferences, in particular, at the level of daunosamine and 9-hydroxyl substituent. The overall preference of daunomycin for intercalation is for d-$(CGATCG)_2$ sequence. It was observed that the selective base pair recognition of daunomycin could not be defined in terms of two base pairs but must be expressed in terms of a triplet of base pairs.

The self association of adriamycin was studied using proton NMR at 400 MHz in D_2O and methanol (66). The ^2H relaxation time measurements have been employed to monitor the extent of self association. The effect of concentration, pH, ionic strength and temperature on chemical shifts of adriamycin have been monitored. The dimerization of adriamycin was characterized by ΔS of $\simeq$ 3 cal deg^{-1} M^{-1} and a ΔH of -3.45 kcal M^{-1}. Analysis of ^2H line widths

of daunomycin, specifically deuterated at 14th position, showed that it forms a dimer in aqueous solution. Islam et al. (48) prepared a series of anthraquinone analogues of doxorubicin (adriamycin) and mitoxantrone and demonstrated their binding to DNA in solution and by computer graphics modelling. All the compounds showed bathochromic and hypochromic shifts on binding to DNA. Computerized model building of these compounds intercalated into d-CpG was carried out and low energy structures were located by systematic energy explorations.

Theoretical computations were performed on the structural and energy factors involved in sequence selective binding of adriamycin to five self-complementary hexanucleotides (19). The model adopted for computation was similar to the one used in a previous study on daunomycin (18). The analysis here revealed overall preference of adriamycin for mixed oligomeric sequence d-$(CGTACG)_2$. The 14-OH of adriamycin participated in additional hydrogen bonding with O1′ oxygen of deoxyribose linked to base on 3′ strand. The selective base pair recognition by adriamycin could be defined only in terms of triplet of base pairs. There was an overall parallelism in the sequence selectivity of adriamycin with that of daunomycin.

The results of circular dichroism first neighbor analysis of the site specificities for the intercalation of adriamycin, steffimycin B, echinomycin and ethidium bromide in DNA were reported by Jones et al. (51). The results indicate that

adriamycin prefers to bind to intercalation sites which possess at least one guanine or cytosine, with GpC being the most preferred site. Steffimycin B binds to sites containing both G and C residues while echinomycin prefers GpC over CpG sequence contrary to the results reported earlier and the binding of ethidium bromide is non-specific. The binding of adriamycin to DNA phosphate was investigated by infra-red spectroscopy and quantum chemical calculations (96). The distinct absorption at 1070 cm^{-1} region corresponding to C14-OH of adriamycin was found to split in presence of DNA. The quantum chemical CNDO/2 calculations performed on those structural fragments of DNA and adriamycin involved in interaction, show diminution of both WIBERG P---O bond index and O----P----O bond angle of phosphate groups on complexation. These results corroborate the speculation about involvement of C14-OH group of adriamycin in binding to DNA phosphate during its interaction.

The inhibition of AMV reverse transcriptase and its associated enzyme activities by daunomycin and adriamycin using synthetic template - primers has been reported by Dhananjaya and Antony (28). Adriamycin and daunomycin inhibits both RNA and DNA-dependent DNA polymerase activities to 70% at 2 μg concentration. Kinetic studies of inhibition of reverse transcriptase suggested competitive type of inhibition. The crystal structure of daunomycin-$d(CGTACG)_2$ complex has been solved by X-ray diffraction analysis (128). The self-complementary DNA was found to have two daunomycin molecules intercalated in the

d-CpG sequences at either end of the helix. The aglycone chromophore of the daunomycin intercalated at the CpG sequence in such a way that ring D of daunomycin protrude on the major groove side and ring A on the minor groove along with its amino sugar. The O9 hydroxyl group of ring A was found to participate in two hydrogen bonds with N3 and N2 of an adjacent guanine base. The amino sugar adopted a chair conformation with all its side chain pointing away from aglycone. The DNA double helix was distorted with an asymmetric rearrangement of the backbone conformation surrounding the intercalator drug. No simple mixed sugar pattern of C3' - endo (3'-5') C2'-endo type was found on either side of intercalators. Only C1 residue has anti glycosyl torsion angle, while the other residues were in high anti range.

The conformation of ring A of daunomycin, adriamycin and its analogues have been studied by 1D proton NMR in different solvents (69). Daunomycin and adriamycin show same long range coupling ($J_{8,10}$ = 2.0 Hz) in both D_2O and $CDCl_3$ solvents and their θ and θ' angles were in range 71-72° and 43-47° respectively. These results correspond to half chair $^{9}H_{8}$ conformation of ring A. The high stability of $^{9}H_{8}$ conformation of ring A was found to be due to two factors : the intramolecular 9(OH)...O(7) hydrogen bond and peri interaction between C-7 substituents and hydroxyl group of ring B. It was observed that strong donor solvents such as DMSO, partially break the hydrogen bond and thus decreases the stability of $^{9}H_{8}$ conformation. As a result, small contribution of skew S_9 was found to occur for daunomycin, adriamycin, N-acetyl daunomycin

and tri-methoxy daunomycinone in DMSO. The conformation of ring A was found to be similar in D_2O and chloroform solvents. In pyridine solvent conformations were intermediate that of $CDCl_3$ and DMSO and the preferred conformations in dioxane were approximately the same as in $CDCl_3$. The conformation of daunosamine moiety is $^{1'}C_{4'}$ (L) for all compounds, at the temperatures and in the solvents examined.

The preferred conformation of the daunosamine sugar with respect to the aglycone moiety has been determined for N-acetyl daunomycin in chloroform (70). Steady-state NOE experiments showed that orientation of the sugar with respect to the aglycone was such that 1'H proton was close to 7H and 6-OH proton and 5'H of daunosamine sugar was close to 8eqH proton of ring A. This rules out anti relationship between 7H and 1'H protons. Interatomic distances were calculated using "two - spin approximation" and were in good agreement with the corresponding X-ray results (24,78). However, the orientation of the sugar with respect to the aglycone moiety are better described by rotational angles ϕ = H(1')-C(1')-O(7)-C(7) and ψ = C(1')-O(7)-C(7) -H(7). The base and sequence specificity of daunomycin-DNA interactions has been studied by Chaires et al. (16). Equilibrium binding studies showed an increase in apparent equilibrium constant, K with increase in overall GC content of DNA. Daunomycin and adriamycin showed same protection pattern when tyr T DNA fragment was digested by DNase I in their presence. The most protected dinucleotide was GpC. Lower concentration of adriamycin was

required to achieve a similar degree of protection as compared to daunomycin, this reflected high affinity of adriamycin for DNA.

The local mobility of the complex between daunomycin and d-$(CGTACG)_2$ has been determined (44) by refinement of the X-ray diffraction data of 1.2 A° resolution (128). An altered mobility of the bases bracketing daunomycin rings was observed. The phosphate linking the intercalated cytosine and guanine residues were least mobile in the complex. The daunomycin intercalated planar ring system also had low mobility than its amino sugar moiety. Xodo et al. (134) studied the interaction of daunomycin with calf thymus DNA and six alternating polydeoxynucleotides using spectrophotometric studies. The intercalation of the drug into DNA was observed to be antico-operative. For each polymer under consideration, a binding stoichiometry of one drug for every two base pairs was found. The binding affinity shown by the drug decreased in the order by Gm^5C > AT > AC - GT > IC > GC > AU. The presence of a guanine residue at the intercalation site was essential in order to have a complete quenching of the intrinsic fluorescence of drug.

^{31}P NMR study of daunorubicin-d-$(CGTACG)_2$ complex in solution has been carried out by Ragg et al. (99). 2D ^{31}P ^{1}H shift correlation method was used for assignment of ^{31}P nuclei in d-$(CGTACG)_2$. On complexation large downfield shift of ^{31}P corresponding to C5pG6 and C1pG2 was observed. It was observed that C5pG6 signal shows remarkable temperature dependence. The

binding constants and the rate of dissociation of the intercalated duplex were also determined. A definitive analysis of the role of flanking sequences on the DNA sequence specificity of adriamycin has been carried out by Trist and Phillips (121) by in vitro transcription assay. Twelve high affinity sites were apparent out of which nine of these involved transcriptional blockage immediately prior to CpA sequences. In almost all cases, this sequence was flanked by T on 5′ end.

The anticancer drug daunomycin has been crystallized with d-$(CGATCG)_2$ and its three-dimensional conformation was studied by Moore et al. (71). The aglycone moiety intercalates between CpG base pairs on either end of the helix with ring D protruding in major groove and daunosamine sugar in the minor groove of duplex. The aglycone is anchored by two direct hydrogen bonds between the drug and the DNA. The O9 of anthracycline forms hydrogen bond with N2 and N3 of the residue G2. In minor groove the amino sugar lies close to the deoxyribose and base edge of residue C11. The N3′ of daunosamine forms direct hydrogen bonds to the minor groove of DNA. The five potential hydrogen bond acceptors are O4′ and O2 of residue C11, O2 of residue T10 and two water molecules. The DNA double helix was distorted with asymmetric rearrangement of backbone conformation surrounding the intercalator drug. All deoxyribose sugars exhibited C1′-exo sugar pattern except the terminal C1 and G6 residues.

Frederick et al. (32) has made two structural comparisons, daunomycin bound to two different DNA sequences d-CGATCG and d-CGTACG and two similar antitumour drugs adriamycin and daunomycin, bound to same DNA sequence, d-CGATCG. In these complexes, the DNA conformation, position of the anthracycline aglycone, intercalation between two G-C base pairs, was conserved. In each complex, it was found that the O9 group of anthracyclines forms direct hydrogen bond to N2 and N3 of G2 residue. Amino sugar was found to be present in the minor groove of all complexes. However, it was observed to form a tighter complex with CGATCG than with CGTACG. In AT complex amino sugar was found to participate in hydrogen bond with O4' and O2 of C11 and with O2 of T10, while TA complex does not have these hydrogen bonding interactions. Additional solvent interactions were observed with adriamycin C14 hydroxyl linking it to DNA. Under the influence of the altered solvation, there was difference in conformation of spermine in daunomycin-d-(CGATCG) and adriamycin-d-(CGATCG) complexes.

Cieplak et al. (22) has performed free energy perturbation studies on B-DNA.daunomycin, B-DNA.9-aminoacridine complexes and B-DNA alone to calculate free energy differences between complexes having different base pair sequences. The results reproduced the trends observed experimentally i.e. preferences of acridine and daunomycin to bind to a specific base sequence in the DNA. It was observed that daunomycin prefers GC as second base pair and TA as

third base pair, which was consistent with studies done earlier (18,128).

DNase I footprinting titration experiments were performed by Chaires et al. (17) to identify preferred daunomycin binding sites within the 160 tyr T DNA fragment. Seven of strongly protected sites were found at the end of the triplet sequences 5' $\frac{A}{T}$ GC and 5' $\frac{A}{T}$ CG. Second class of protected sites, where band area of these sites decreased after a threshold total drug concentration was reached might have been due to binding to a class of sites with weaker affinity or from co-operative binding.

Infra red spectroscopy was used to detect specific DNA interactions with anticancer drugs daunomycin, adriamycin, aclacinomycin A, mitoxantrone and violamycin BI (97). On complexation of DNA with adriamycin, aclacinomycin A, Violamycin H and mitoxantrone a significant decrease in wave number of the band arising from antisymmetric stretching vibration of PO_2^- group of DNA was observed. The drug induced shift was interpreted in terms of formation of a hydrogen bond between PO_2^{-2} moiety of DNA and C14-OH group for adriamycin, C4-OH for both aclacinomycin and violamycin BI and external side chain OH of mitoxantrone, respectively. The three-dimensional structure of another ternary complex, spermine bound to a DNA : anthracycline complex has been studied by Williams et al. (132) by X-ray crystallography. 4'-epiadriamycin has been cocrystallized with the DNA hexamer d-(CGATCG). 4'-epiadriamycin is an structural analogue of

adriamycin and differs from it by inversion of the stereochemistry at the 4'-position. This drug was found to bind at each d-(CpG) step of the hexamer. The 4'-OH group of 4'-epiadriamycin formed direct hydrogen bond to N3 of A(3). This hydrogen bond resulted from inversion of the stereochemistry at 4'-position. It was observed that spermine molecules bind in the major groove of this complex.

The conformational preference of the glycosidic bond of adriamycin in water has been determined by truncated driven nuclear overhauser effect (TOE) difference spectra (23). The cross-relaxation rates between nearby protons has been evaluated by the "two-spin approximation" and the relative interproton distances were deduced. It was observed that saturation of 1'H causes a strong negative effect on 7H, conversely, irradiation at the 7H frequency induced a large negative effect on 1'H. The rotational angles ϕ^1 = C(7)-O(7)-C(1')-H(1') and ϕ^2 = H(7)-C(7)-O(7)-C(1') has also been calculated from the r_{ij} values using CHEM-X programme. The ϕ^1 and ϕ^2 values which were in agreement with experimental interproton distances are 48 ± 5° and -20 ± 5° respectively.

The anticancer drug daunomycin has been cocrystallized with the hexanucleotide sequences d-(TGTACA) and d-(TGATCA) and X-ray studies were carried out (81). In both complexes the aglycone chromophore of daunomycin was found to intercalate between the TpG sites. The amino sugar was found to be present in the minor

groove. The ring A of chromophore was stabilized by hydrogen bonding between hydroxyl oxygen O9 with N2 and N3 of base G2. It was observed that the conformation of ring A and amino sugar was different in both complexes. The amino sugar of d-(TGATCA) duplex interacted directly with the DNA sequence, while in d-(TGTACA) duplex, the interaction is via solvent molecules. Comparison of the four structures with daunomycin bound to the triplet sequences 5'TGT, 5'TGA, 5'CGT and 5'CGA revealed changes in conformation of both DNA hexamer and daunomycin on complexation.

A systematic study of the effect of HCHO on the complexes of daunomycin and DNA oligonucleotides was carried out by HPLC and X-ray diffraction (125). HPLC analysis revealed that adducts were formed between drug and DNA when daunorubicin was mixed with DNA hexamer, d-(CGCGCG) and d-(CGTDCG), in presence of HCHO. X-ray crystal structure of these adducts showed that they contained a methylene bridge between N3' of daunosamine and N2 of guanine or 2-aminoadenine. In the present complexes daunomycin was intercalated between CpG step with ring D protruding in major groove and daunosamine moiety found in the minor groove. HPLC profile of the redissolved crystals exhibited a single peak which was associated with the adduct and this suggested the reaction to be sequence specific.

Rameta et al. (100) determined the binding enthalpies for the complexation of monomeric daunomycin with a series of 10 polymeric DNA duplexes by using stopped flow microcalorimeter. The net

binding enthalpies derived from stopped-flow microcalorimetry was in agreement with binding enthalpy derived from corrected batch calorimetric data. Stopped-flow calorimetric measurements were also performed over a range of different drug-phosphate ratios (r) and it was observed that daunomycin binding enthalpies exhibited small but significant r dependencies. The molecular structure of 4′-epiadriamycin complex with d-(TGATCA) has been determined by X-ray crystallography (56). The overall structure was found to be similar to that observed in the series of hexamer-anthracycline complexes (32,71,81,128). In all these structures it was found that head on insertion of the aglycone chromophore takes place between d-(CpG) or d-(TpG) base pair steps. Ring D was found to protrude out in the major groove and semi-saturated ring A was present in the minor groove side of the helix. The amino sugar was also found to be present in the minor groove. It was observed that the 9-hydroxyl group forms hydrogen bond with N2 and N3 of G(2). The O4′ and N3′ of amino sugar of 4′-epiadriamycin participated in direct hydrogen bonding to three acceptors in minor groove of the duplex : N3 of A(9), O2 of T(4) and O4′ of C(5) respectively. The contact between DNA and sugar moiety of 4′- epiadriamycin was direct with d-(TGATCA) sequence while, water mediated hydrogen bonds were formed in the case of d-(TGTACA) sequence. X-ray diffraction technique has been used to determine the structures of two hexanucleotide-anthracycline complexes d(CGGCCG)/daunomycin and d(TGGCCA)/adriamycin. In both cases the

anthracycline molecule is bound to non-preferred d(YGG) base pair triplet sites (57).

The binding properties of the antitumour drug daunomycin has been reexamined using double helical oligonucleotides 16 base pairs long which contained preferred binding sites for the drug. (108). The strongest core binding site found was CGTACG, but its affinity was only 2-fold higher than that of other core sequences. Association constants ranged from 1.0×10^{8} to 3.0×10^{7} M^{-1}. The binding enthalpy of daunomycin with CGTACG was exothermic while binding to dA_{20}- dT_{20} was endothermic. Appreciable binding to the flanking A tracts was also observed.

Roche et al. (107) further tested the binding affinity of a series of daunomycin analogues to the same group of oligonucleotides containing binding sites specific for daunomycin. The association constants were in the range of 10^{5} - 10^{7} M^{-1}. It was observed that compounds with hydroxyl substituted for the amino group in the sugar ring binds less well to the oligonucleotides, by factors of upto several hundred. Much of binding lost on removal of the charged amino group was restored with compounds containing an iodo substituent on the sugar ring. Binding constants for a given analogue to a set of sequences varied by roughly 5-fold in all cases, but there was no sequence that was consistently preferred from one analogue to another. Quantitative assessment of relationships between water ring size and frequency of its occurrence in the vicinity of nucleic acid

interfaces has been described by Lipscomb et al. (60). Low temperature X-ray crystallographic structures of two anthracyclines, adriamycin and daunomycin bound to d-(CGATCG) and other DNA structures has been used in this study. The results showed that five membered water rings were not preferred over other ring sizes. The thermal mobility of the amino sugar of daunomycin and adriamycin was significantly greater than rest of complex.

Recently, the interaction of daunomycin with dinucleotide d-CpG has been studied in D_2O by 500 MHz NMR spectroscopy (5). The 2D COSY and NOESY spectra of the complex are investigated at 297 K. The base protons of d-CpG, GH8, CH6, CH5 and daunomycin protons, 1H, 2H, 3H and $4OCH_3$ shift upfield by ≃ 0.27 ppm on complex formation. The T_m of d-CpG increases by 10 $^{\circ}$C on complexation which indicates stabilization of d-CpG due to interaction. The sugar conformation is predominantly S-type with χ_S = 0.65 to 0.68 and P_S = 153° and 135° for G and C residues, respectively. The major S conformer is associated with χ in anti conformation centered towards slightly lower angles, χ = -120° for cytosine, and toward high anti conformation, with χ = -90°, for guanine residue. The spin-spin couplings of daunomycin; J(1'H-2'eqH), J(1'H-2'axH), J(4'H-5'CH_3), J(7H-8axH) and J(7H-8eqH) are altered on complexation with d-CpG. Further, the interproton distances : 1'H-2'axH, 7H-8axH, 7H-8eqH, 5'H-8axH and 5'H-8eqH are also altered on complexation significantly. The NOE observed between 1H, 2H protons of daunomycin and CH6 proton

reflects that the planar aromatic ring of daunomycin is close to cytosine base.

RELATED ANTITUMOUR DRUGS

There are many antitumour drugs which are known to interact with DNA molecules to exert their biological activities. Some of them form covalent linkages with DNA, while others form complexes with the DNA double helix using non-covalent interactions. In a broader sense, DNA molecules can be considered as receptors for a variety of antitumour drugs.

High resolution 1D NMR experiments were performed on the complex of proflavine with poly (dA-dT) at P/D = 24 and 8 in high salt solution (87). The T_m of poly (dA-dT) increased on complexation from 72.6 to 78.1 $^{\circ}C$ for P/D = 24 complex and 83.4 $^{\circ}C$ for P/D = 8 complex. Upfield shifts of four proflavine protons were observed in the range of 0.75 to 0.95 ppm on complex formation, which was a direct evidence of intercalation of proflavine between base pairs of poly (dA-dT). Intercalation occurred preferentially at dT-dA sites. The crystal structure of a 3:2 complex of proflavine with the dinucleoside phosphate cytidylyl - 3'-5'- guanosine has been determined (76). The complex has one drug molecule intercalated between Watson-Crick base pairs of the nucleotide duplex. The other two proflavine molecules were bound to the exterior of the miniature double helix. Each amino group of proflavine participated in a hydrogen

bond to a phosphate oxygen on either side of the duplex. All sugars were found to have C(3')-endo sugar puckering.

The theoretical depolarization of the fluorescence emitted by ethidium has been calculated by computer simulation of energy transfer between ethidium bromide molecules bound to DNA. (85). The energy transfer depends on orientation so the angle between two ethidium molecules and thus the local change in winding angle of DNA helix caused by intercalation can be determined. The results showed that the DNA helix was wound by $13^{\circ} \pm 4$, and not unwound, as earlier assumed, after the intercalation of one ethidium bromide molecule. An alternative model for intercalation has been given by Paoletti and Le Pecq (84) which led to winding of DNA helix on intercalation. In this model distortion above and below the intercalation site was assumed, which was not considered earlier in Lerman model (58). When two phosphate - phosphate distances are fully extended, the phosphate backbone stretching permits a positive change of the torsion of helix. The winding angle computed was between 4 to 16°. This model allowed unwinding between -15 to + 16°. It also predicted exclusion of one site per each intercalated molecule.

Saucier et al. (112) measured the relative change of the torsion of the DNA helix caused by intercalation of various drugs by determining the amount of each drug necessary to relax the supercoiled DNA from PM2 bacteriophage. The change of the torsion of the DNA helix observed was variable with the drug intercalated.

If this change of torsion is 12° for ethidium bromide, then this angle was 8-9° for proflavine and quinacrine, 7° for methoxyellipticine and only 4° for daunomycin. X-ray studies have been performed on complex of ethidium bromide + dinucleoside monophosphate 5′- iodouridylyl (3′-5′) adenosine (iodo UpA) (122). The structure contained two iodo UpA molecules hydrogen bonded together by adenine-uracil Watson-Crick base pairing. The phenyl and ethyl substituents of the intercalated ethidium molecule were present in the minor groove of the miniature iodo UpA double helix. The 2:2 stoichiometry of the complex reflected alternate sandwich-like stack formed between ethidium molecule and base pairs. Both iodouridine ribose sugar residues were C3′- endo, while both adenosine ribose sugar residues were C2′- endo.

The structure of a 2:2 complex of 9-aminoacridine and self-complementary dinucleoside monophosphate, 5-iodocytidylyl (3′-5′) guanosine has been studied (111). In the first part of asymmetric unit, the intercalated 9-aminoacridine molecule was found to be oriented such that its amino group pointed towards the narrow groove of the miniature double helix. The stacked 9-aminoacridine was oppositely oriented such that amino group was present in the wide groove of the double helix. The intercalated aminoacridine was pseudo-symmetric with respect to the base pairs.

The structure of intercalated complexes between 9-amino acridine and various nucleic acid in solution has been investigated (104). Induced chemical shifts in the proton NMR

spectrum of 9-aminoacridine as a function of concentration of self-complementary deoxyribosyl dinucleotides d-GpC, d-CpG and d-ApT as well as the hexanucleotide d-ATGCAT has been studied. The pattern of induced chemical shifts in proton resonances of 9-aminoacridine on adding GpC and d-ATGCAT suggested formation of complexes with defined stoichiometry. However, there was no such indication in case of CpG and ApT dinucleotides.

The stereochemistry of binding of actinomycin to d-ATGCAT has been studied by X-ray crystallography (118). The phenoxazone ring system on actinomycin was found to intercalate between the base paired dinucleotide sequence, d-GpC, while the peptide units were present in the minor groove of the DNA helix and interacted with deoxyguanosine residues. A strong hydrogen bond connected the guanine 2-amino group with the carboxyl oxygen of the L-threonine residue. Numerous van der Waal contacts between hydrophobic groups on the actinomycin molecule and the DNA provided additional stabilization to the complex. The two cyclic pentapeptide chains were found to be related by two-fold symmetry.

A detailed study of the three-dimensional structure of actinomycin D in deuterated dimethyl sulfoxide solution by 2D-NMR, distance geometry and restrained molecular dynamics (RMD) calculation were carried out by Chen Yu and Tseng (136). The spin systems of five amino acid residues were identified and resonance assignment of all protons were achieved by homo and heteronuclear 2D NMR experiments. 2D NOE spectra were recorded to deduce the

conformation of actinomycin D. Initial cross-relaxation rates for each proton pair of NOEs were obtained from 2D NOE spectra recorded with four different mixing times, and interproton distances were estimated. The interproton distance constraints were used for distance geometry calculations and subsequently for restrained molecular dynamics calculations. Four best local minima i.e. four structures were selected. The resultant structures satisfied the experimental restraints and were compatible with X-ray crystal structures.

The solution conformation of the complex of actinomycin D and an asymmetric DNA oligomer - d-(TCGCGTTTTCGCGA) has been studied (8). This oligomer forms a hair pin loop. The changes in ^{31}P chemical shifts linking G3-C4 and G11-C12 on complexation confirmed the intercalation of actinomycin. Interproton distances were calculated and these distance constraints were used in molecular dynamics calculations. Two distinct actinomycin D-d(TCGCGTTTTCGCGA) complexes were formed which differ in orientation of intercalation of actinomycin D chromophore. However, these two complexes were not formed in equal concentrations and their conformations were found to be similar.

The binding constants for interaction of the anticancer agents mitoxantrone and ametantrone and several congeners with calf thymus (ct) DNA and the effects of ionic strength changes has been determined spectrophotometrically (62). These agents showed a preference for sequences with GC base pairs. The binding constant

of mitoxantrone with ct DNA in 0.1 M Na^+, pH 7 was approximately 6 x 10^6 M^{-1}.

Earlier studies showed that mitoxantrone binds to a two base pair sequence selectively. In order to further extend the recognition site, mitoxantrone derivatives were designed by theoretical computations, in which the terminal hydroxyl group of each side chain was esterified with oligopeptides (40). Binding affinity of two derivatives, depsi Gly-Lys (D) and depsi Gly-Gly-Orn (L) for the palindromic sequences d-$(CCCGGG)_2$, d-$(GCCGGC)_2$, d-$(GGCGCC)_2$ and d-$(CGCGCG)_2$ were compared. Binding of oligopeptide arms to major groove was shown to be favourable. Two distinct arrangements were investigated in the major groove with the two arms adopting antiparallel directions. A distinct energetical preference was obtained with the depsi Gly-Gly-Orn (L) derivative. The results showed that the two investigated compounds preferably binds to sequences d-$(CCCGGG)_2$ and d$(GCCGGC)_2$ with a tetrameric core CCGG.

X-ray crystallographic study of nogalamycin was carried out to establish its absolute stereochemistry. A model has been proposed for the probable mode of interaction of nogalamycin with DNA (3). The configuration of ring A was found as 7S, 9S, 10R and glucopyranose has α-L configuration. B, C and D rings are planar. Ring A adopts half chair conformation, while the nogalose and glucopyranose has normal chair conformations. The carbomethoxy group at C(10) was axial. The three-dimensional structures of the

complexes between an antitumour drug, nogalamycin and two DNA hexamers, d[CGT(pS)ACG] and d[m^5CGT(pS)A m^5CG], were determined at high resolution by X-ray diffraction analysis (59). Two nogalamycin were found to bind to the DNA double helix in a 2:1 ratio with the aglycone chromophore intercalated between the CpG steps at both ends of the helix. The nogalose and aminoglucose sugars were in the minor and major grooves, respectively, of the distorted B-DNA double helix. Specific hydrogen bonds were found in the complex between drug and guanine bases.

2D NMR spectroscopy has been utilized to study complex formation between nogalamycin and d-CGTACG (106). 2:1 nogalamycin : hexamer symmetrical complex was formed with the aglycone chromophore intercalated between the CpG steps at both the ends of the helix. The nogalose and aminoglucose sugar were found lying in minor and major groove respectively. Specific hydrogen bonds existed in the complex between the drug and guanine - cytosine bases in both grooves of the helix. Three molecular species, free DNA, 1:1 and 2:1 complex were found to be in slow exchange on NMR time scale, when only one drug per DNA duplex was present in solution. At 65 $^{\circ}$C only free single-stranded DNA and the 2:1 complex co-existed, whereas at 35 $^{\circ}$C the equilibrium between free DNA and the 1:1 complex was observed to be relatively fast while that between the 1:1 complex and 2:1 complex was slow.

The structure of nogalamycin.d-(AGCATGCT) complex (2:1, drug : DNA ratio) has been characterized by application of 2D-NMR experiments and molecular dynamics calculations (137). The aglycone chromophore was intercalated at (C-A).(T-G) steps with its long axis perpendicular to the long axis of the flanking C3.G6 and A4.T5 base pairs. The nogalose and bicyclic amino sugar were in chair conformation while aglycone ring A was in half chair conformation. Further, nogalose and bicyclic amino sugar lie in minor and major groove of DNA respectively. Numerous inter-molecular contacts and hydrogen bonds are formed between nogalose and bicyclic amino sugar of nogalamycin and d-(AGCATGCT). On complex formation both sugars move toward each other to maximize intermolecular contacts in both grooves of the duplex. The molecular dynamics calculation were guided by 274 intramolecular nucleic acid distance constraints, 90 intramolecular nogalamycin distance constraints and 104 intermolecular constraints between nogalamycin and the nucleic acid protons in the complex.

The molecular structure of triostin A, a cyclic depsipeptide antibiotic has been solved complexed to a double helical fragment with sequence d-CGTACG (127). The quinoxaline rings of triostin A bisintercalates in the minor groove of DNA surrounding CG base pairs at either end of the hexamer. The alanine residues form hydrogen bond to the guanines. Base stacking in DNA was perturbed, and the major binding interaction involved a large number of van der Waals contacts between the peptides and nucleic acid. The two AT base pairs in the center of the hexamer undergo a remarkable

transformation on complexation. They were not found to be held by Watson and Crick base pairs but instead were held by N-7 and N-6 of adenine i.e. by hoogsteen base pairing. Thus, adenine residue adopted a syn conformation on complexation.

The X-ray crystallography structure of echinomycin, another member of the quinoxaline antibiotic family, with hexamer d-(CGTACG) has been solved and compared with triostin A.d-(CGTACG) complex studied earlier (124). Both structures were similar to each other with differences in some details due to the shorter cross bridge of echinomycin. Both molecules acted as bisintercalators surrounding the d-(CpG) sequence at either end of the double helix. Alanine formed sequence specific hydrogen bonds to guanines in the minor groove. The two central AT base pairs were held together by hoogsteen base pairing with adenine in the syn conformation in both complexes.

The bisintercalation complex between the DNA octamer d-$[(ACGTACGT)]_2$ and cyclic octadepsipeptide antibiotic echinomycin has been studied by one and two-dimensional proton NMR and the results were compared with the crystal structures of related DNA-echinomycin complexes (36). Results indicated that echinomycin binds co-operatively to both of the strong binding sites on the DNA octamer. Quinoxaline rings intercalated on either side of d-CpG and this was confirmed by large upfield shifts observed in imino ^1H spectra and by NOESY cross peaks observed between the quinoxaline and DNA base resonances. NOESY cross peaks between

T(4).A(5) imino proton and A(5)H8 base proton of the complex in D_2O and H_2O confirm that both terminal and interior A.T base pairs adopted hoogsteen conformation at 1 °C. The syn conformation of adenine bases was confirmed by cross peak between terminal and interior A(H8) and their sugar H1′ resonances. The structure observed at 1 °C corresponded to its crystal structure.

The structure of carminomycin I and stereochemistry of ring D substituents has been determined by X-ray crystallography (91). The six chiral centers found were C7(S), C9(S), C1′(R), C3′(S), C4′(S) and C5′(S). The configuration of the daunosamine unit of carminomycin I was same as that for daunomycin. The stereochemistry at C7 was shown to be the desmethyl derivative of daunomycin with identical configuration at all chiral centers.

The crystal structure of a complex containing deoxycytidylyl-(3′-5′)-deoxyguanosine and terpyridine platinum compound (TPH) has been studied (126). The d-CpG was observed as an antiparallel double helix in which the helix unwinds and base pairs unstack for intercalation of TPH. The deoxyguanosine at 3′ end of molecule has a deoxyribose with C2′-endo pucker while, deoxycytidine at 5′ end has C3′-endo pucker. The hydroxy-ethyl side chain attached to the central intercalating TPH molecule effectively prevented the existence of an exact two-fold symmetry. The unwinding angle of DNA was 23° for TPH.

Delepierre et al. (26) has reported on structural elucidation of a bisintercalator, ditercalinium.d-$(CGATCG)_2$ complex by proton and ^{31}P NMR spectroscopy. The strong upfield shifts observed on aromatic protons of drug and bases as well as on the hexanucleotide imino protons, were consistent with bisintercalation of the dimer. The two pyridocarbazole rings were bound in two different sites, a CpG site (I) and a ApT site (III). The intramolecular NOE effects observed in the complex showed that all bases were in anti position relative to the glycosidic bond, implying that the helix retained a right-handed conformation on complexation.

Geierstanger et al. (35) has carried out structural and dynamic characterization of the heterodimeric and homodimeric complexes formed on binding of distamycin (DSt) and 1-methyl-imidazole-2-carboxamide-netropsin (2-ImN) to oligo- nucleotide duplexes d- (GCCTAACAAGG).d- (CCTTGTTAGGC) and d- (CGCAAACTG-GC).d-(GCCAGTTTGCG). 1:1:1 2-ImN.Dst. DNA heterodimeric complex was formed with DSt and 2-ImN bound in the minor groove of d(GCCTAACAAGG).d(CCTTGTTAGGC), by titration experiments. On the basis of 2D NOE spectra it was observed that 2-ImN ligand spans 5′-GTTA-3′ of the TAACA.TGTTA binding site with the imidazole nitrogen specifically recognising the guanine amino group. The DSt ligand was present along the 5′-AACA-3′ sequence and complements, the 2-ImN ligand in formation of the antiparallel side-by-side heterodimeric complex. Homodimeric complexes were obtained by titration of the same site with Dst or 2-ImN alone

(2:1 ligand.DNA) of lower stability. 1:1:1 complex of 2-ImN. Dst. DNA was also formed by titration of 2-ImN and Dst to d(CGCAAA CTGGC). d(GCCAGTTTGCG) sequence. This complex was found to be more stable than previous heterodimeric complex.

The structure of 2:1 antitumour drugs aclacinomycin A and B complexed to d-CGTACG has been studied by 2D NMR using nuclear overhauser effect spectroscopy (135). Aclacinomycin A and B both have an alkavinone aglycone chromophore and a trisaccharide attached at the C^7 of ring A of the alkavinone. SPEDREF refinement procedure revealed that the alkavinone was intercalated between the CpG steps and the trisaccharide was found in the minor groove. The intercalation geometry of aclacinomycin was found to be a hybrid between those of daunorubicin and nogalamycin. Ring D of alkavinone was sandwiched by the C1 and C11 bases. The deoxyfucose ring of the trisaccharide was close to DNA backbone at A4 nucleotide forcing the DNA helix to kink towards the major groove. Multiple molecular species coexisted in the solution of the 1:1 mixture of aclacinomycin and d-(CGTACG) due to slow rate of drug binding to DNA.

SCOPE OF THESIS

It is evident that until year 1980 several physico-chemical techniques absorbance, fluorescence, circular dichroism, etc. were used to study the intercalation, binding specificity and kinetics of daunomycin and adriamycin on interaction with calf-thymus DNA and certain polydeoxyribonucleotide sequences. Certain other

techniques like foot printing titration (17) were also used to determine sequence specificity of daunomycin. The 5'-3' d-CpG sequence is the preferred sequence for daunomycin and can be accounted for in a better way in terms of triplet of base pairs (18,19). However, many research groups have mainly concentrated on anticancer drug daunomycin, and adriamycin, its structural analogue has not been studied in much detail.

Preliminary X-ray, 1D NMR and theoretical computation studies were also performed on daunomycin to deduce its structure. But, the molecular basis of drug interaction, its complete three-dimensional structure, different types of forces involved in binding were not known. Literature showed that there was renewed interest in the field of drug-DNA interaction after 1985. Daunomycin and adriamycin - DNA interaction was studied by theoretical computation (18,19) and X-ray crystallography (32,71,81,98,128) techniques. There was an advancement in instrumentation and X-ray structures were resolved to the tune of 1.2 A° and an attempt was made to study the molecular aspects of drug-DNA interaction in solid state. But, as it is well known that conformation of a biological macromolecule in solution phase depicts the conformation it acquires in, in vivo condition. Further in solution state the conformation of a macromolecule is governed by stacking interactions and hydrogen bonding whereas these forces are not dominant in solid state which results in differences in conformation acquired in both phases. These observed differences suggests that the analysis of

three-dimensional structure of a molecule should be carried out in solution in detail. Two - dimensional NMR techniques can be used to derive information on structure of a biomolecule and study its interaction.

An attempt was made to study the interaction of daunomycin with deoxydinucleotide d-CpG by two-dimensional NMR technique (5). There is not a single study on the structure of adriamycin reported in literature so far. The only corresponding result reported is that of X-ray structure analysis of adriamycin - d-$(CGATCG)_2$ complex (32). In order to understand the molecular basis of interaction of adriamycin with double stranded B-DNA in solution we have chosen deoxyhexanucleotide d-$(CGATCG)_2$ as model system. These studies are carried out using 2D NMR technique.

Such drug-DNA interaction studies by NMR also provide an insight to conformational features of various other biomolecular interactions taking place in vivo like protein/ligand - DNA interaction, recognition of a particular site on DNA etc. Further these anticancer drug have certain side effects and there has been continuous effort to reduce its cardiotoxicity. Such structural studies on interaction of adriamycin aides in drug designing which have different tolerance and toxicity.

MATERIALS AND METHODS

MATERIALS

The deoxyoligonucleotide sequence d-$(CGATCG)_2$ is purchased from DNA Chemical International, U.S.A. Deuterium oxide (D_2O), dimethyl sulphoxide (DMSO) with isotopic purity 99.96% and adriamycin are purchased from Sigma Chemical Co., U.S.A. Sodium 2, 2-dimethyl-2-silapentane-5-sulphonate (DSS), an internal NMR reference is purchased from Merck Sharp and Dohme Canada Ltd., Canada. Nucleotide and drug samples are used without further purification. All other chemicals like Na_2HPO_4 and NaH_2PO_4 etc. used for buffer preparation are from E. Merck, India Ltd.

Further, d-$(CGATCG)_2$ sample is also synthesized for routine 1D NMR experiments. Synthesis is carried out on 10 μmole scale on an Applied Biosystems DNA synthesizer (model 381 A) using cyanoethyl phosphoramidites in Dr. K.B. Roy's laboratory at J.N.U., Delhi. However, all 2D experiments are conducted on the sample purchased from DNA Chemical International, U.S.A.

The starting material is a solid support derivatized with a nucleoside which will become the 3'-hydroxyl end of the oligonucleotide. The 5'-hydroxyl is blocked with a dimethoxytrityl (DMT) group. The steps of the DNA synthesis cycle are as follows :

(i) The treatment of the derivatized solid support with acid removes the DMT group and thus frees the 5'-hydroxyl for the coupling reaction. An activated intermediate is created by simultaneously adding the phosphoramidite nucleoside monomer and tetrazole, a weak acid, to the reaction column. The intermediate is so reactive that addition is complete within 30 seconds.

(ii) The next step, capping, terminates any chains which did not undergo addition. Capping is done with acetic anhydride and 1-methylimidazole. Capping minimizes the length of the impurities and thus facilitates their separation from the final product.

(iii) During the last step, oxidation, the internucleotide linkage is converted from the phosphite to the more stable phosphotriester. Iodine is used as an oxidising agent and water as oxygen donor. This reaction is complete in less than 30 seconds.

After oxidation, the dimethoxytrityl group is removed with trichloroacetic acid, the cycle is repeated until chain elongation is complete. Treatment with concentrated ammonium hydroxide for one hour removes the β-cyanoethyl protecting groups and also cleaves the oligonucleotide from the support. The benzoyl and isobutyryl base protecting groups are removed by heating at room temperature in ammonia for 8 to 15 hours. Purification is carried out using RPLC and ion-exchange chromatography. RPLC is performed

on ABI HPLC instrument with acetonitrile and triethyl ammonium acetate (0.01 M) buffer system (pH-7.0). The buffer system used for ion-exchange chromatogrpahy is 1 M NaCl in 10 mM NaOH and 10 mM NaOH (pH 12.0) Desalting is also carried out after purification using biogel column. The purified d-$(CGATCG)_2$ is annealed by heating it in a water bath up to 70 $^{\circ}C$ and then allowing it to cool until it attains room temperature. Thus a duplex of d-$(CGATCG)_2$ is prepared.

SAMPLE PREPARATION

Solution of adriamycin (11.5 mM) is prepared by dissolving a known quantity of sample in D_2O. It is lyophilised and redissolved in D_2O and the process is repeated twice. The final concentration is checked by absorbance measurements at wavelength (λ) = 480 nm using DU-6 spectrophotometer. The extinction coefficient (ε) value used for adriamycin is $\varepsilon = 9.8 \times 10^3$ $M^{-1}cm^{-1}$. In a separate experiment, 0.4 ml adriamycin solution (11.5 mM) is prepared by the same procedure in DMSO solvent. HDO and DMSO signals are used as an internal NMR reference for recording spectra in these solvents.

Solution of deoxyoligonucleotide, d-$(CGATCG)_2$ (2.98 mM, duplex concentration) is prepared by dissolving a known quantity of sample in deuterated phosphate buffer (16.25 mM) of pH 7.0 having 15 mM Na salt. The sample is lyophilised and redissolved in D_2O and the process is repeated twice. Finally, d-$(CGATCG)_2$ is dissolved in 0.4 ml of D_2O and its concentration is determined by

absorbance measurements at 260 nm. The extinction value (ε) used is 10.2×10^3 M^{-1} cm^{-1}. Ethylene diamine tetra acetic acid (EDTA), 0.1 mM, is added to suppress paramagnetic impurities, which causes line broadening during NMR measurements. HDO signal is used as an internal NMR reference for recording spectra of d-$(CGATCG)_2$. Typically 1 μl of 0.1 M solution of DSS was added to the complex of d-$(CGATCG)_2$ and adriamycin, as an internal reference.

Preparation of Complex

2.98 mM d-$(CGATCG)_2$ and 26.46 mM adriamycin samples are taken as the stock solution for preparation of complex. A complex of d-$(CGATCG)_2$ and adriamycin is prepared by titration. 90 μl of 26.46 mM adriamycin is added in steps of 10 μl to 0.4 ml of 2.98 mM d-$(CGATCG)_2$ sample during titration in order to make 2:1 complex of adriamycin : d-$(CGATCG)_2$. The concentration of d-$(CGATCG)_2$ (N_1) in total volume of 0.41 ml is determined as follows :

$$N_1V_1 = N_2V_2$$

$$N_1 \times 0.41 = 2.98 \times 0.4$$

$$N_1 = 2.91 \text{ mM}$$

The concentration of adriamycin (N_3) in this solution is determined as follows :

$$N_3V_3 = N_4V_4$$

$$N_3 \times 0.41 = 26.46 \times 0.01$$

$$N_3 = 0.65 \text{ mM}$$

Likewise other adriamycin-d-$(CGATCG)_2$ complexes of different drug/nucleotide (D/N) ratio are prepared. The concentration of adriamycin (D), d-$(CGATCG)_2$ (N) and drug/ nucleotide (D/N) ratio are shown in Table 3.1.

NMR METHODS

The phenomenon

NMR is a type of absorption spectroscopy which is dependent on the property of "spin" possessed by the nuclei of certain isotopes - this causes them to behave like small magnets when placed in a static magnetic field. These spins are capable of interacting with a beam of electromagnetic radiations. When the frequency of the beam is same as that of precessing spin, then absorption of energy takes place which causes the nuclei to "flip" from a low energy state to a high energy state by a process termed resonance. These energy levels correspond to the spins aligned along and against the applied field B_0. The spins oriented to oppose B_0 have the higher energy. These spins do not align perfectly along B_0 and this gives rise to a permanent torque. The nucleus also has the property of angular momentum because of its spin and thus as a result the nuclei precess, with frequency of precession given by :

$$\omega_0 = \gamma B_0$$

where, γ is proportionality constant, ω_0 is the resonant or Larmor frequency in radians/second and B_0 is the magnitude of the applied static magnetic field.

Table 3.1 : Various concentration ratios (D/N) for the complex formed between adriamycin and d-$(CGATCG)_2$

Nucleotide Conc. (mM) = N	Drug Conc. (mM) = D	D/N
2.98	0.00	-
2.90	0.65	0.22
2.83	1.26	0.45
2.77	1.85	0.67
2.71	2.41	0.89
2.65	2.94	1.11
2.59	3.45	1.33
2.54	3.94	1.55
2.48	4.41	1.78
2.43	4.86	2.00

On interaction with magnetic field, nuclei with spin I > 1/2 distribute themselves among 2I + 1 energy levels with the separation given by :

$$\Delta E = h \gamma B_0$$

The magnetic quantum number m_I, characteristic of each nuclear energy level, depends on nuclear spin quantum number. Thus, a nucleus of spin I = 1/2 has two allowed energy levels corresponding to the m_I values of + 1/2 and - 1/2, respectively, where m_I is the quantum number characterising Z component of I.

In an NMR sample there are many molecules, each with its spin precessing about B_0 at same frequency and result in a net magnetization of M_z oriented along Z-axis. On application of a rotating radiofrequency field with frequency at or near $\omega_0 = \gamma B_0$, the spins resonate giving rise to net M_{xy} component which is phase coherent.

The following are the spectral parameters in NMR :

Chemical shift

Nuclei are surrounded by electrons, which shield them from the applied magnetic field B_0. The B_0 field induces current in these electron clouds which reduces the effective field experienced at the nucleus because they tend to oppose B_0. The induced fields are directly proportional to B_o. This is represented by the equation :

$$B_{eff} = B_0 (1 - \sigma)$$

where, σ is shielding constant which depends on the nature of electrons around the nuclei. Thus, different nuclei within a sample experience different fields, depending on their immediate chemical environment. Chemical shift expressed in parts per million (ppm) is given as :

$$\delta = 10^6 \times \left[\frac{\delta_{ref} - \delta_{obs}}{\delta_{ref}} \right]$$

where, δ_{ref} is the position observed for a reference compound and δ_{obs} is the position of the signal of interest.

Spin-spin coupling constant

Spin-spin coupling is an important phenomenon occurring between nuclei directly coupled through bonds. The strength of coupling is called spin-spin coupling constant (J) and is expressed in Hertz. This coupling causes splitting of lines. The appearance of a multiplet pattern depends on relative magnitude of δ and J for the coupled nuclei. The most important parameter in deducing three-dimensional conformation of biological macromolecule is vicinal or three bond coupling constant (^3J) between A and D nuclei in A-B-C-D fragment. Vicinal coupling constants (^3J) are related to the dihedral angle θ between planes A-B-C and B-C-D by Karplus relationship (52,53) given as follows :

$$^3J = 8.5\ Cos^2\ \theta - 0.28 \qquad 0^\circ < \theta < 90^\circ$$

$$^3J = 9.5\ Cos^2\ \theta - 0.28 \qquad 90^\circ < \theta < 180^\circ$$

The dihedral angle (θ) can thus be obtained between a pair of coupled protons.

Relaxation time

The spin system returns to its equilibrium state after perturbation by radiofrequency (rf) field. The time taken by the spin system to return to equilibrium after it has been excited is called relaxation time. The spin-lattice relaxation time (T_1) is a measure of the rate of the recovery of Z-component of magnetization, M_z, after perturbation. The rate at which a Boltzman distribution of population is set up among energy levels is $1/T_1$. The term spin-lattice is used because the process involves an exchange of energy between the nuclear spin and their molecular frame work. Spin-lattice relaxation time depends on several factors : dipole-dipole interaction, spin rotation, scalar coupling etc.

The spin-spin relaxation time (T_2) is caused by random local magnetic fields in the sample and is the result of chemical exchange or mutual exchange of energy between spin states of two nuclei in close proximity. Thus, it is the measure of rate of exchange of energy within two spins. The spin-spin relaxation time T_2 is related to the resonance line width in the absorption spectrum by the relation :

$$(\Delta\omega)_{1/2} = \frac{1}{\pi T_2}$$

where $\Delta\omega_{1/2}$ refers to the line width at half height. But, field inhomogeneity affects the observed line width and the transient decay because of the spread of fields produces a spread of frequencies.

Therefore, in practice

$$(\Delta\omega)_{1/2} = \frac{1}{\pi T_2^*}$$

where, T_2^* is effective relaxation time which has contributions from field inhomogeneities and true relaxation time, so that $T_2^* < T_2$.

In experiments involving NMR of biopolymers, it is necessary to use high magnetic fields, a radiofrequency field to stimulate absorption and a detector to record resonance signals. The booming fourier transform NMR field received its primary impetus from Ernst and Anderson (29). In FT-NMR spectrometer, the sample is excited by a short radiofrequency pulse which contains all characteristic frequencies together.

The number of NMR resonances increases greatly, while studying proteins and DNA fragments, due to large number of nuclei present in these molecules. As a result, resonances of individual nuclei overlap and the resolution is limited. This severe problem has been overcome by the advent of 2D NMR, first proposed by Jeener in 1971 (50) and later developed by Aue et al. in 1976 (4).

TWO-DIMENSIONAL (2D) NMR TECHNIQUES

The two-dimensional spectrum has two frequency axis (ω_1, ω_2) and the intensities are represented along the third axis. Thus, each peak in a 2D spectrum occupies volume against an area in the 1D spectrum. The two frequency dimensions, ω_1 and ω_2, of a two-dimensional NMR are obtained after a fourier transformation with respect to a time domain function $S(t_1, t_2)$. The 2D NMR experiment consists, in effect, of a series of one-dimensional experiments in which the time interval t_1 is incremented and free induction decay for each experiment is recorded during the time interval t_2 as in one-dimensional NMR. These two time variables are generated by suitable segmentation of the conventional time axis of the FT-NMR experiment. In all 2D experiments, four different time segments can be distinguished namely preparation period, evolution period (t_1), mixing time (τ_m) and detection period (t_2) (Fig. 3.1).

(i) Preparation period : This consists of a delay time or a sequence of pulses separated by fixed time intervals or saturation sequences. Thermal equilibrium is attained during this period.

(ii) Evolution period (t_1) : The various spins are labelled during this period. Further, one or several radiofrequency pulses may be applied to create coherence. The evolution is not detected directly but

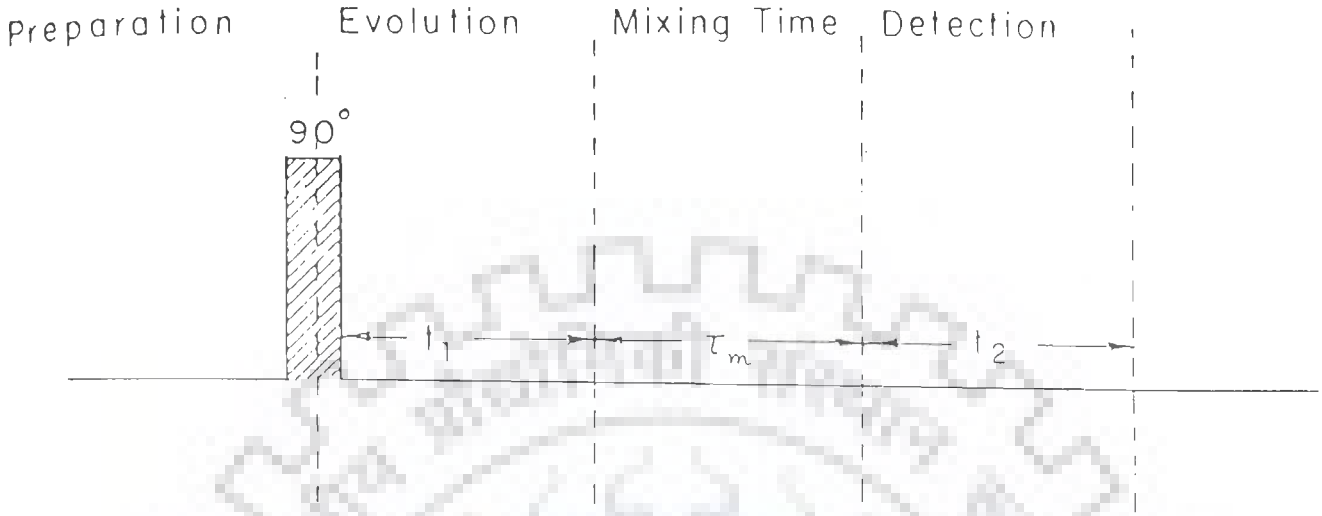

Fig.3.1 : Four different time segments of a 2D NMR experiment namely (i) preparation period (ii) evolution period (t_1) (iii) mixing period (τ_m) and (iv) detection period (t_2).

may be mapped by carrying out many experiments with different evolution times.

(iii) Mixing time (τ_m) : During this period coherence is transferred between spins. The mixing period may include one or several radiofrequency pulses and delay intervals.

(iv) Detection period (t_2) : The amplitudes of signals are detected as a function of evolution time (t_1) during this period.

The kinds of interactions observed in a two-dimensional NMR experiment depend on the exact pulse sequence used (i.e. the number, length and phases of the pulses within and between the three time periods). The purpose of the variety of 2D NMR techniques is to establish a correlation between the behaviour of the spin system during the two periods - t_1 and t_2 which is achieved by mixing period (τ_m).

Correlational spectroscopy (COSY)

The pulse sequence for COSY experiment is the classical Jeener sequence (50) shown in Fig. 3.2. The first 90° pulse creates transverse magnetization after the preparation period. During the evolution period, the various spins are labelled by their characteristic frequencies. The second 90° pulse acts as a mixing pulse and transfers magnetization between J-coupled spins in the system. This establishes a correlation between J-coupled spins and is reflected in the spectrum as an off-diagonal peak.

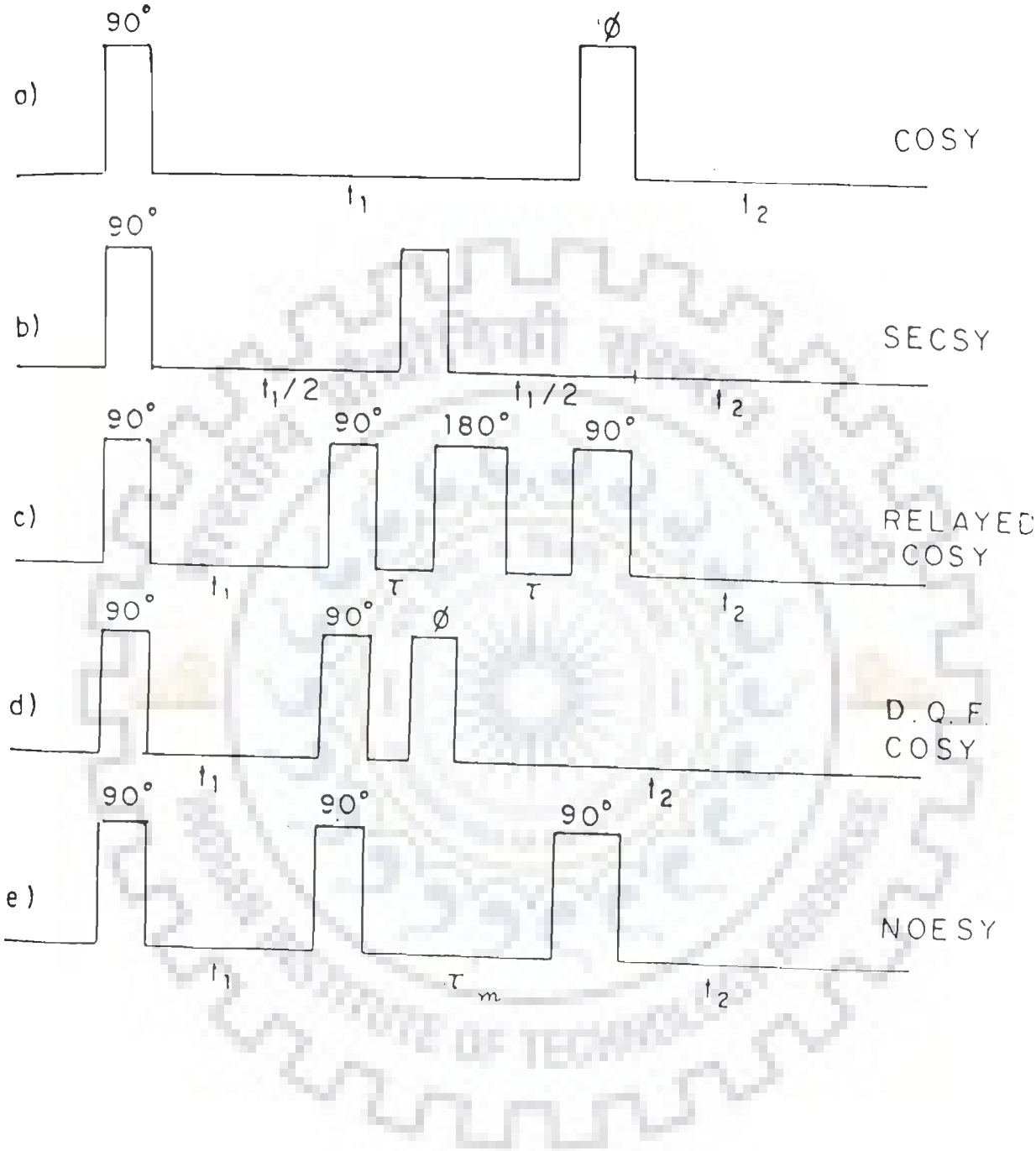

Fig.3.2 : Pulse schemes of various 2D NMR techniques.

Some spins do not exchange magnetization and give rise to peaks along the diagonal in the 2D COSY spectrum. Both diagonal and off-diagonal cross peaks have multiplet structures characteristic of the spins from which they originate.

The COSY spectra is acquired with phase cycling to remove axial peaks and a set of mirror image responses in which the diagonal runs in opposite direction. Special phase cycling and data processing can also be done in a COSY experiment to change 2D line shape into pure 2D absorption mode allowing the use of a phase-sensitive display. There are two different methods in use, the first requires the results of two complete COSY experiments with different phase cycling to be added (119) and the second known as TPPI (Time proportional phase incrementation) method uses a single experiment with phase cycling which changes with t_1 increments (7,54,65,102). The phase-sensitive COSY spectra has cross peaks in antiphase. The active coupling between a pair of protons which gives rise to cross peaks has antiphase multiplet structure. Extra splittings present in multiplet but, which do not give rise to cross peak are called passive couplings and appear inphase. Thus, the advantage of phase-sensitive COSY is that the phase relation between peaks can be used for accurate assignment and calculation of coupling constants.

In a three spin system, e.g. AMX, with J_{AM}, J_{AX} and J_{MX} coupling constants (Fig. 3.3(a)), the AX pattern is split into identical arrays. For example, the cross peak at $\omega_1 = \delta_X$ and $\omega_2 =$

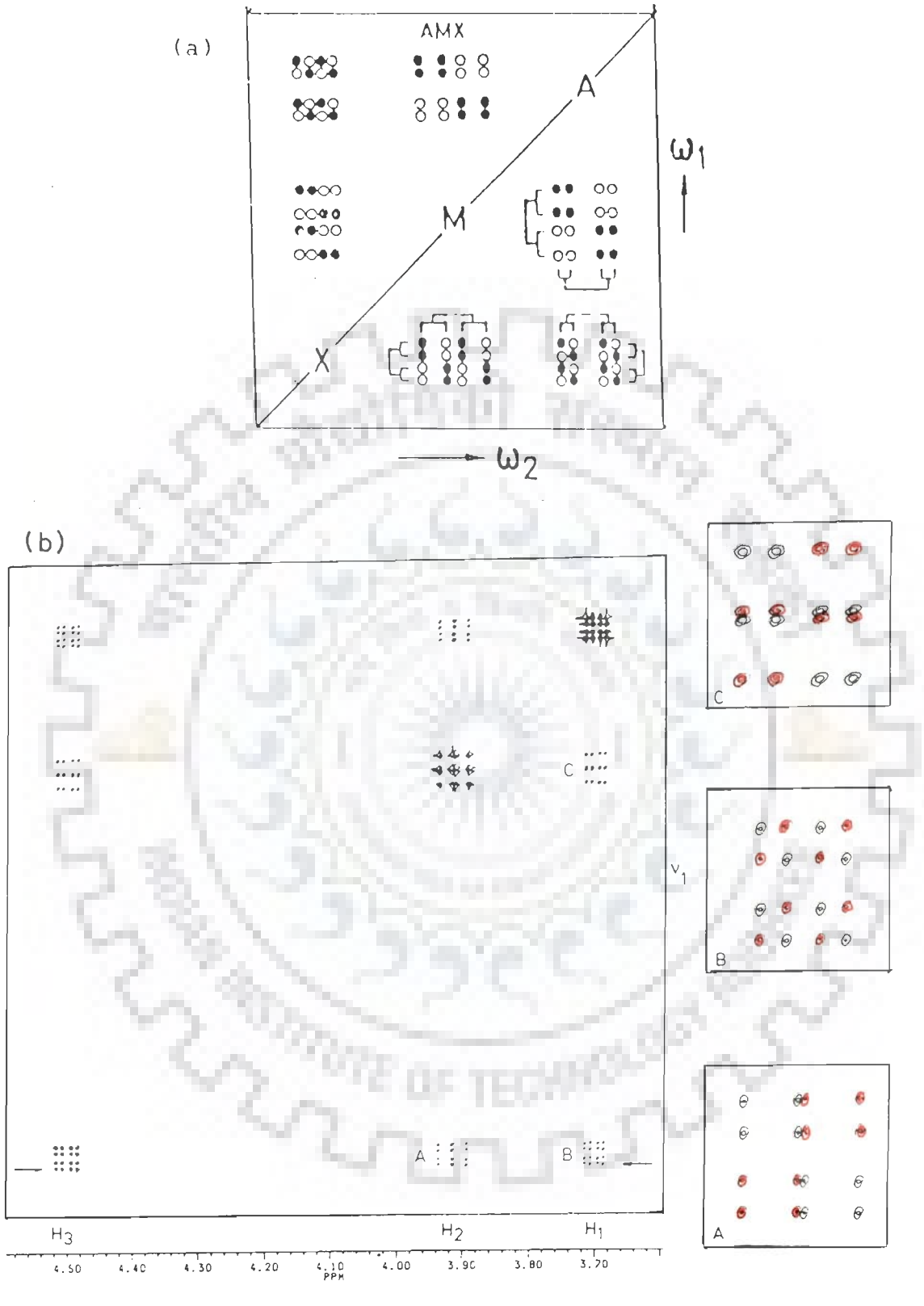

Fig.3.3 : (a) Schematic COSY Spectrum of a three spin system, AMX. Filled circles represent positive signals, open circles represent negative signals. (b) A typical phase-sensitive COSY spectrum for an AMX system. Negative peaks are shaded with red colour.

δ_A, manifests along ω_2 the antiphase (+ -) splitting which gives active coupling J_{AX} and inphase (+ +) splitting J_{AM}. Along ω_1 axis, it manifests antiphase splitting J_{AX} and inphase splitting J_{MX}. A typical phase-sensitive COSY (27) for an AMX system with positive and negative contours in black and red is shown in Fig. 3.3(b). In the cross peak pattern B, the smaller coupling is the active coupling J_{AX} (along both ω_1 and ω_2 axis) and the larger ones along ω_2 and ω_1 axis are passive couplings J_{AM} and J_{MX}, respectively. It is readily apparent from Fig. 3.3(a, b) that the appearance of the cross peaks including the order in which positive and negative components are arranged depends on strength of coupling constants.

Double quantum filtered COSY (DQF-COSY)

This experiment (93) uses the pulse sequence $90_\phi - t_1 - 90_\psi - 90_\xi - t_2$ where ϕ, ψ and ξ are the appropriate phase cycles (Fig. 3.2) and is used for the extraction of information of coupling constants (10,37). In ^{1}H NMR spectra, methyl singlets are often very intense and split due to spin-spin coupling. This creates problems in COSY spectra because multiplet resonances of interest are sometimes buried beneath its noise and spinning side bands from the singlets. INADEQUATE sequence specifically excludes singlets from the spectrum by creating multiple quantum coherence and forcing the phase cycling to follow the latter rather than the single quantum coherence. Combining these two ideas gives a sequence (Fig. 3.2) in which the responses from a COSY experiment

are passed through a double quantum filter, thereby removing methyl and other singlets from the final spectrum. Another advantage of DQF-COSY is that it converts the phase of COSY diagonal signals from dispersive antiphase to absorptive antiphase. Thus, there is less interference of these signals with cross peaks and cross peaks lying close to the diagonal are more clearly discernible than in corresponding COSY spectra. Twice as many as transients are needed in this experiment to achieve the same signal-to-noise as in conventional COSY.

Nuclear overhauser enhancement spectroscopy (NOESY)

The exact three-dimensional conformation of a molecule can be deduced by two-dimensional nuclear overhauser enhancement spectroscopy. It gives us information about cross-relaxation occurring between a pair of protons through dipole-dipole interaction. Thus, it gives us an idea about pairs of protons present in close proximity to each other in space. The pulse sequence used for making correlation through dynamic NOE is shown in Fig. 3.2.

The first 90° pulse produces transverse magnetization which precesses in the X-Y plane during the evolution period. This is followed by mixing time (τ_m) during which transfer of magnetization takes place due to dipolar interactions between pair of protons which are close in space. The transfer of magnetization takes place either directly between spins coupled through bonds or through cross-relaxation in space. The first two pulses label the

magnetization M_z of different spins with their chemical shift frequencies. The exchange of magnetization M_z during the mixing time (τ_m) will lead to signals detected during t_2 which have modulation frequencies different from their precession frequencies during t_1 and hence on fourier transformation, will give rise to cross peaks in the 2D spectrum. The third 90° pulse transforms the resulting Z magnetization into transverse magnetization, which is measured during the detection period.

EXPERIMENTAL PARAMETERS

All proton NMR experiments are carried out at National FT-NMR facility located at TIFR, Bombay and are recorded on 500 MHz high resolution Bruker AM 500 FT-NMR spectrometer equipped with aspect computer. Typical parameters for one-dimensional NMR experiments are : pulse width = 10 μs; number of data points = 8-16 K; spectral width = 4000 Hz; number of scans = 64-128 and digital resolution = 0.25-0.5 Hz/point. Receiver gain was optimised in each instance to obtain the best signal-to-noise ratio. 2D Phase-sensitive DQF-COSY and NOESY experiments on d-$(CGATCG)_2$ and its complex with adriamycin are carried out at 295 K in D_2O. However, 2D experiments on adriamycin are carried out at 297 K. 2D NOESY experiments are recorded with variable mixing times (τ_m) 400, 500, 600 ms for adriamycin; 75, 150, 200, 250 ms for d-$(CGATCG)_2$ and 50, 75, 150, 200, 250 ms for adriamycin-d-$(CGATCG)_2$ complex.

Typical parameters for 2D experiments are : 1024-2048 data points along t_2 dimension; 512 free induction decays in t_1 dimension; pulse width ≃ 9.5 - 12 μs; spectral width ≃ 4000 Hz; number of scans = 64 - 128; digital resolution 2.30-4.60 Hz/point and relaxation delay ≃ 1.0 s.

CONFORMATION OF NUCLEIC ACIDS BY NMR

Assignment of various resonances to specific nuclei in the molecule is the first step in any endeavour (30,31,42, 47,61,73,102,113). Once the assignments have been made, quantitative estimation of various cross peaks in 2D J-correlated and NOE correlated spectra can be used to derive information about sugar geometry, glycosidic angle and backbone structure along the entire sequence of the molecule.

Resonance assignment

Typically in an NMR spectrum, the protons in nucleic acid can be classified into three groups namely the exchangeable NH and non-exchangeable base protons resonating between 7 - 15 ppm; non-exchangeable sugar protons appearing between 2 - 6.5 ppm and finally methyl protons of thymines which resonate between 0.5 - 2 ppm.

The strategy for resonance assignment consists of two steps. In the first stage, the J-correlated spectra are used to identify net work of coupled spins. In the second stage, the spin system so identified are assigned to particular nucleotides along the

sequence of the molecule by making use of the NOESY spectrum as described below.

The sugar protons H1′, H2′, H2", H3′, H4′, H5′ and H5" form a complex J-correlated net work. The various cross peaks observed in a 2D J-correlated spectra between these protons can be used in identification of spin system within individual nucleotide units. The proton - proton coupling constants in the above J-correlated network are sensitive to the type of sugar pucker of deoxyribose ring and lie in the range 0 to 10 Hz. Thus intensity of the various cross peaks in the COSY spectrum varies with sugar pucker.

The H1′ proton shows a cross peak with H2′, H2" sugar protons. The J-coupling corresponding to these cross peaks varies in the range 0.7 to 10.5 Hz and the cross peak may or may not exist depending on the sugar pucker. The H2′ and H2" protons are further coupled to H3′ proton. The cross peaks corresponding to these couplings may or may not be observed as the J value varies in the range 0.7 to 9.7 Hz depending on the sugar pucker.

Similarly, the intensity of cross peak H3′-H4′ and H4′-H5′/H5" protons may vary according to the sugar geometry. We have used phase-sensitive DQF-COSY spectra to estimate spin-spin coupling constants in order to deduce sugar geometry of individual nucleotide along the sequence.

In the second phase, sequential assignment is carried out using NOESY spectrum. Short internucleotide distances between adjacent nucleotide units are used as shown in Fig. 3.4(a) (47).

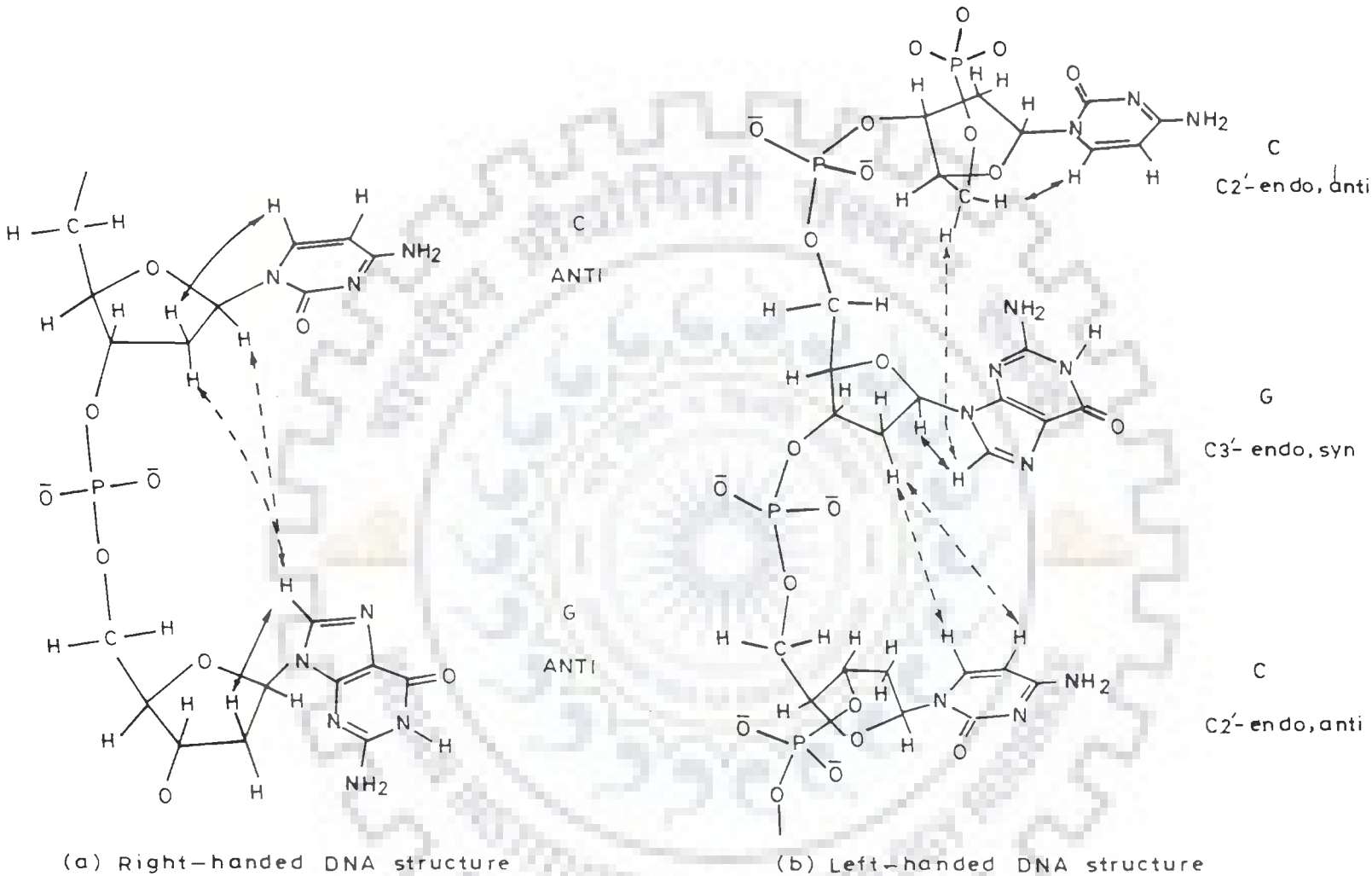

Fig.3.4 : Short interproton distances between adjacent nucleotide units in (a) right-handed DNA (b) left-handed DNA which can be used for sequential assignment.

In right-handed DNA with sugars in C3'-endo/C2'-endo/O1'-endo pucker and glycosidic angle in anti domain, a convenient strategy for sequential assignment is :

$$(H6/H8)_n \longrightarrow (H2', H2")_{n-1}$$

$$(H6/H8)_n \longrightarrow (H1')_{n-1}$$

$$(H6/H8)_n \longrightarrow (H6/H8)_{n-1}$$

where, n stands for nth residue in 5'-3' oligonucleotide sequence.

In case of Z-DNA, where the repeating unit is a dinucleotide, the internucleotide pathway is (101) :

Base(2n-1) .... H5'(2n-1) ..... Base(2n) ..... H1'(2n) .... H2'(2n) and H2"(2n) ..... Base(2n + 1) (Fig. 3.4(b)).

Conformation of deoxyribose sugar

In principle, it should be possible to establish the complete conformation of a deoxyribose ring from the knowledge of all vicinal proton coupling constants (^3J) (38,110). Such a straight forward approach is not feasible for nucleotides for a number of reasons. First, the available evidence overwhelmingly indicates that the furanose ring does not possess a unique rigid structure in solution but is in a dynamic equilibrium between at least two favoured sugar conformations, a type N-conformer and a type S-conformer. If the interconversion rate between conformers is sufficiently rapid then the observed couplings represent weighted average of couplings in individual conformers. A determination of the conformer equilibrium therefore requires knowledge of the

number of allowed conformations and of couplings in specific conformers, which is often not readily available.

Despite the above problems, coupling constants can be related to conformational properties of deoxyribose sugar. The vicinal coupling constants are related to their relevant H-C-C-H dihedral angle (θ). The dihedral angle, θ can be calculated in terms of pseudorotational angle, P. The variation of the vicinal coupling constants in the deoxyribose ring as a function of sugar geometry is shown in Fig. 3.5 (110). A value of 38° has been taken for ν_{max}, the degree of pucker. It is observed that the values of H1'-H2" and H2'-H3' coupling constant vary within a small range of 6 - 10 Hz for different sugar geometries. Thus, these coupling constants are relatively insensitive to the sugar geometry. However, the values of H1'-H2', H2"-H3' and H3'-H4' coupling constants vary considerably and can be used to determine the sugar geometry.

Phase-sensitive COSY/DQF-COSY spectra can be utilised to extract the J-coupling constant information directly from separation between positive (+) and negative (-) components of a cross peak. But, even for a simple AX doublet, both line width and digital resolution significantly affect the actual separation between these components. So, intensity of cross peak depends directly on magnitude of coupling constant. Thus, it is clear that certain cross peaks in the COSY spectrum will be more prominent than others depending on the sugar geometry.

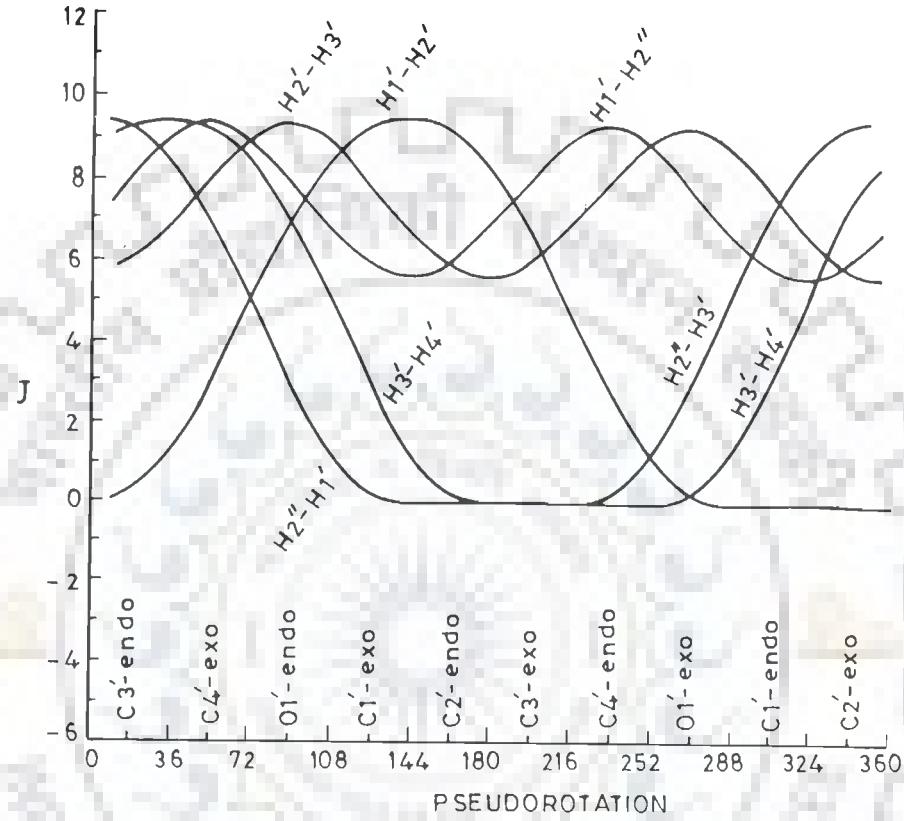

Fig.3.5 : Variation of the vicinal coupling constants in the deoxyribose ring as a function of the ring geometry.

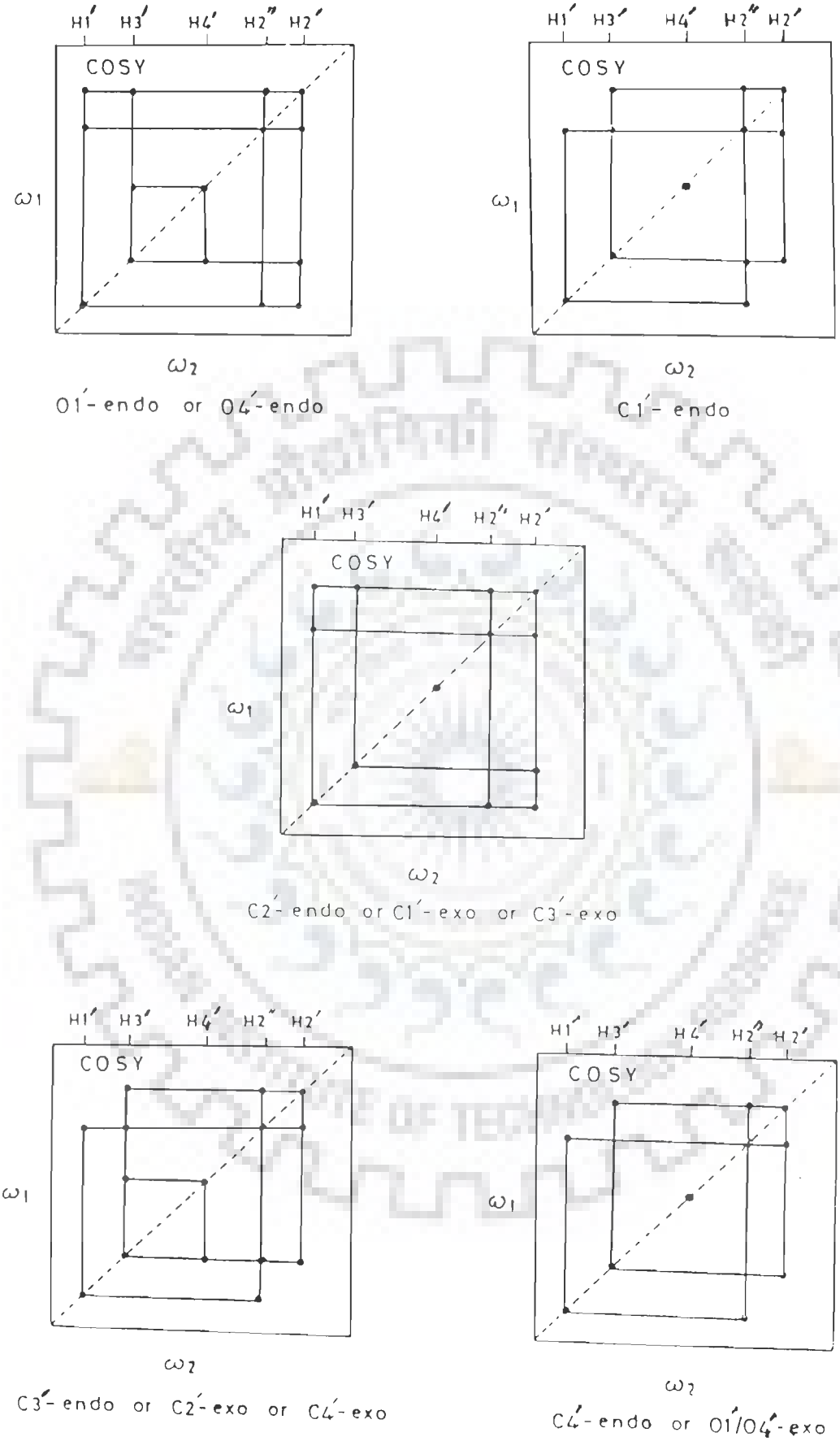

Fig.3.6 : Typical COSY spectra expected for various sugar geometries.

Typical COSY spectra for various sugar conformations are shown in Fig. 3.6 (47). In C2'-endo sugar geometry, H1'-H2' cross peak is more intense (J ≃ 10 Hz) than H1'-H2" (J ≃ 5.5 Hz) and H3'-H4' cross peak would be less intense or absent. While, in C3'-endo sugar geometry H1'-H2" cross peak is more intense (J ≃ 8.0 Hz) than H1'-H2' cross peak (J ≃ 1.4 Hz). The H3'-H4' cross peak is also intense (J ≃ 8.6 Hz). Thus, the information on vicinal coupling constants can lead to important conclusions about the sugar geometry.

The strategy used to determine the sugar conformation is :

(a) Analysis of cross peak patterns of H1'-H2', H1'-H2", H2'-H3', H2"-H3' coupled protons and spin-spin coupling constants measured from DQF-COSY and 1D NMR spectra.

(b) Estimation of intra residue interproton distances from phase-sensitive NOESY spectra as discussed in Chapter V.

In crystal structures of nucleosides and nucleotides, usually a single pure N- or S-type conformer is found but, as discussed earlier, situation is different in aqueous solution where stacking plays a predominant role. Several research groups (10, 105, 114, 130, 131) have developed a strategy to explain the dynamic behaviour of furanose sugar conformations in DNA from analysis of coupling constants. Complete conformational analysis of a given interconverting furanose in the ideal cases involves the determination of P_S, ϕ_S, P_N, ϕ_N and χ_S, where P_S and P_N are pseudorotation angle for S and N-type conformer, ϕ_S and ϕ_N

represent the amplitude of sugar pucker for S and N-type conformer and χ_S is the mole fraction of S-conformer. The mole fraction of S-conformer (χ_S) and N-conformer (χ_N) has been calculated for each residue using this strategy and is discussed in Chapter V.

Conformation about the glycosidic bond

It has been already established that the torsion angle, χ, defining the orientation of a base ring with respect to the deoxyribose ring, can be categorized into two categories designated as syn and anti conformation (120). Information regarding the glycosidic bond rotation (χ) can be obtained from NOESY spectrum (47,101). For this the interproton distances are calculated from intensities of various cross peaks from phase-sensitive NOESY spectra recorded at low mixing time (τ_m) to avoid transfer of magnetization through spin diffusion. The interatomic distances between base (H6/H8) protons and sugar protons (H1', H2', H2") depends on glycosidic bond angle (χ) and the sugar geometry. The sugar geometry can be deduced independently from COSY spectrum, while information on glycosidic torsion angle (χ) is obtained from NOESY spectrum using following strategies :

(i) For a syn conformation, strong NOEs are observed between base (H8/H6) to H1' sugar protons than that with H2'/H2" protons.

(ii) Nucleotide has an anti conformation with respect to the glycosidic bond when base (H8/H6) protons show intense NOEs to the sugar H2′ and H2" protons than that with H1′ proton.

(iii) For high anti conformation, the H2" protons will show intense NOEs to the base protons of the same nucleotide and the following nucleotide on 3′ end.

The (H6/H8)-H1′ distance depends only on χ while, other distances depend on both P and χ. Iso-distance contours have been calculated by Wuthrich (133) in (P, χ) space for H6/H8 - H2′, H2", H3′, H4′ and H5′ distances. In principle P and χ can be estimated using calculated interproton distances and iso-distance contour plots as discussed in detail in Chapter V.

ESTIMATION OF INTERPROTON DISTANCES

The cross peaks in a NOESY spectrum represent dipole-dipole couplings between nuclei which are within a distance of 5 A° from each other. Thus, intensities of these NOE cross peaks provide information about interproton distances. In large molecules satisfying the condition $\omega\tau_c > 1$ (where, τ_c is the effective correlation time and ω is the spectrometer frequency), cross-relaxation is very efficient. When several protons are present in close vicinity to each other then multispin relaxation occurs, leading to spin diffusion and in extreme cases, all NOEs become equal. The extent of diffusion depends on the length of the mixing time (τ_m) used in NOESY experiment. For short τ_m (< 50 ms),

the magnetization transfer is restricted to a single step i.e. direct magnetization transfer is observed between two spins. Under such conditions, the intensity of a cross peak (I_{ij}) is proportional to a single cross-relaxation rate σ_{ij} and is given as:

$$I_{ij} = \sigma_{ij} \tau_m \qquad \ldots(1)$$

where, i and j are the relaxing protons.

The intensity of the cross peak in equation (1) varies linearly with mixing time, therefore, this condition is referred to as "linear regime". Under the conditions of an isotropic tumbling motion of a rigid molecule where all interproton vectors have the same effective correlation time, σ_{ij} is linearly dependent on τ_c (for $\omega \tau_c \geq 1$) and inversely proportional to the sixth power of the interproton distance r_{ij}. The intensity I_{ij} can be written in terms of these parameters as :

$$I_{ij} = \frac{\gamma^4 \hbar^2 \tau_c \tau_m}{10\, r_{ij}^6} \qquad \ldots(2)$$

where, γ is the proton magnetogyric ratio and $\hbar$ is Planck's constant divided by 2π.

It is thus clear that interproton distances can be estimated by measuring the intensities of cross peaks in the linear regime. In order to determine the acceptable value of τ_m, NOE build-up curves are obtained as a function of τ_m for several cross peaks

since spin diffusion can be different for various protons. Estimation of correlation times, τ_c, can be obtained from T_2 and T_1 measurements, according to the following equation :

$$\tau_c = 2\omega^{-1} (3T_2/T_1)^{-1/2} \quad \ldots(3)$$

which holds good for $\omega \tau_c \geq 1$. If protons i, j, k, l have similar τ_c values and if r_{ij} is a known distance, then unknown distance r_{kl} can be calculated by comparing the intensities I_{ij} and I_{kl} in a single spectrum.

$$\frac{I_{ij}}{I_{kl}} = \frac{(r_{kl})^6}{(r_{ij})^6} \quad \ldots(4)$$

The choice of the reference fixed distance is important if the molecule under study exhibits internal motion in addition to the global motion in solution. The r(CH5-CH6) and r(H2'-H2") have different effective correlation times and can be selected depending upon the type of cross peak being compared (41). Thus, the sugar H2'-H2" distance of 1.8 A° can be used as reference distance for all NOEs involving sugar H2', H2" protons and for the rest r(CH5-CH6) of 2.45 A° is used as reference distance (41).

Reid et al. (103) examined H2' - H2" and CH5-CH6 cross-relaxation at 100, 90, 60, 30 and 15 ms in dodecamer DNA duplexes. It was observed that sugars and bases have same correlation times so, all interproton distances in short DNA duplexes, whether sugar -sugar, base-base or sugar-base can be determined using r(CH5-CH6) as reference distance.

ANTHRACYCLINE ANTIBIOTIC : ADRIAMYCIN

The conformation of adriamycin has been investigated by 500 MHz proton NMR spectroscopy. Proton NMR spectra of 11.5 mM adriamycin in D_2O are recorded as a function of temperature over the range 277-355 K. Typical spectra of adriamycin at three different temperatures are shown in Fig. 4.1(a-c). The integral plot of adriamycin at 355 K is also shown here (Fig. 4.1(d)). The changes in chemical shift of the adriamycin protons as a function of temperature are shown in Fig. 4.2(a, b). Two-dimensional phase-sensitive COSY spectra recorded at 297 K and phase-sensitive NOESY spectra at 297 K using τ_m = 500 ms are shown in Fig. 4.3(a, b) and Fig. 4.4(a, b). Expansions of particular regions of the phase-sensitive COSY and NOESY spectra showing specific interproton connectivities are given in Fig. 4.5(a-i) and Fig. 4.6(a, b). 1D and 2D phase-sensitive NOESY spectra recorded in DMSO at 297 K are shown in Fig. 4.7 and Fig. 4.8 (a, b).

Spectral assignments

The non-exchangeable protons of ring D, 1H, 2H and 3H are observed around 7.3-7.6 ppm. The most downfield triplet at 7.61 ppm (Fig. 4.1 (b)) is assigned to the 2H proton. Of the two doublets appearing around 7.45-7.50 ppm at 325 K (Fig. 4.1(b)),

the most downfield doublet is assigned to the aromatic proton 1H (13). The doublet at 7.45 ppm is therefore due to proton 3H. At 297 K, the 1H and 3H proton resonances overlap and appear at 7.34 ppm (Fig. 4.1(a)). The 2H proton gives a cross peak with the 1H and 3H protons in COSY spectra (Fig. 4.3(b)). This confirms the assignment of protons 1H, 2H and 3H. The integral plot of adriamycin (Fig. 4.1(d)) shows that the sharp and intense peak at 3.88 ppm is due to three protons. This resonance gives strong NOE cross peaks with the 2H and 3H protons (Fig. 4.4(b)) and is therefore assigned to the $4OCH_3$ protons of ring D.

In ring A (Fig. 1.1 of chapter I), 8axH and 8eqH; 10axH and 10eqH, are coupled to each other through strong geminal couplings (^2J). The pair of protons appearing as doublets at 2.04 and 2.28 ppm give an intense cross peak in the COSY spectra of Fig. 4.3(a). Similarly, the pair of protons resonating at 2.60 and 2.93 ppm give a cross peak in the COSY spectra of Fig.4.3(a). These are assigned to the pairs 8axH, 8eqH and 10axH, 10eqH, respectively. Due to ring current effects of the aromatic chromophore, protons 8axH and 10axH are shifted upfield with respect to their 8eqH and 10eqH partners, respectively (82).

At 4.8 ppm two sets of resonances are superimposed on each other at 297 K. These resonances shift downfield to varying degrees with temperature and are separated at 355 K. The singlet at 5.05 ppm at 355 K, due to two protons as evident from the integral plot (Fig. 4.1(d)), is assigned to the $9COCH_2$ group. It is noted that this proton is not coupled to any other

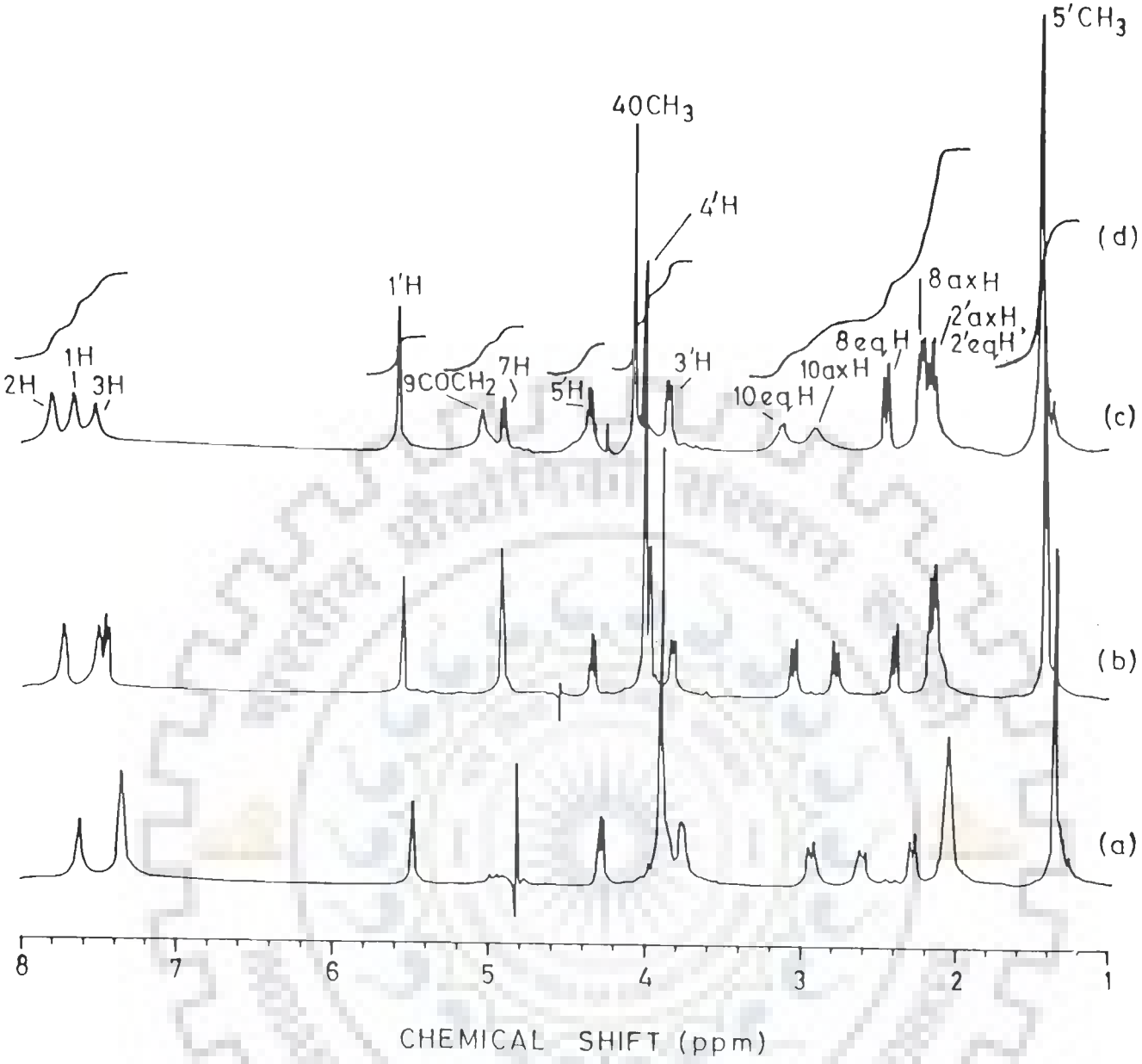

Fig.4.1 : 500 MHz proton 1D NMR spectra of 11.5 mM adriamycin in D_2O at (a) 297 K (b) 325 K (c) 355 K. An integral plot of proton NMR spectra at 355 K is also shown in (d). The HDO signal is used as an internal reference in all spectra.

Table 4.1 : Observed chemical shifts (in ppm) of various protons of adriamycin at 297 K. For comparison, the chemical shift values reported by Mondelli et al.[a] (69) at 298 K.

Proton	Adriamycin	
	Present work	a
2H	7.61	7.66
1H	7.34	7.45
3H	7.34	7.37
1'H	5.48	5.43
7H	4.80	4.82
$9COCH_2$	4.80	4.79
5'H	4.27	4.21
$4OCH_3$	3.88	3.90
4'H	3.88	3.83
3'H	3.76	3.68
10eqH	2.93	2.95
10axH	2.60	2.68
8eqH	2.28	2.28
8axH	2.04	2.06
2'axH	2.04	2.03
2'eqH	2.04	1.98
$5'CH_3$	1.34	1.29
$9COCH_3$	-	-

Table 4.2 : Chemical shift (in ppm) of protons of adriamycin with varying temperature in D_2O.

Temp. (K)	2H	1H	3H	1'H	7H	9$COCH_2$	5'H	5'CH_3
277	7.49	7.23	7.23	5.41	4.76	4.64	4.20	1.26
287	7.56	7.29	7.29	5.45	4.81	4.71	4.24	1.30
297	7.61	7.34	7.34	5.48	4.80	4.80	4.27	1.34
305	7.66	7.39	7.39	5.50	4.87	-	4.30	1.37
315	7.70	7.45	7.42	5.53	4.88	4.90	4.32	1.41
325	7.73	7.50	7.45	5.54	4.88	4.91	4.33	1.42
335	7.73	7.53	7.45	5.52	4.88	4.92	4.31	1.40
345	7.79	7.62	7.51	5.56	4.92	4.99	-	1.44
355	7.83	7.67	7.53	5.58	4.91	5.05	4.36	1.45

Temp. (K)	4OCH_3	4'H	3'H	10eqH	10axH	8eqH	8axH	2'axH	2'eqH
277	3.78	3.78	3.69	2.82	2.46	2.16	1.95	1.95	1.95
287	3.84	3.84	3.73	2.88	2.55	2.23	2.00	2.00	2.00
297	3.88	3.88	3.76	2.93	2.60	2.28	2.04	2.04	2.04
305	3.93	3.93	3.78	2.97	2.66	2.32	2.09	2.07	2.07
315	3.97	3.95	3.81	3.01	2.72	2.37	2.15	2.12	2.12
325	3.99	3.96	3.81	3.04	2.77	2.39	2.16	2.12	2.12
335	3.99	3.94	3.80	3.04	2.78	2.39	2.15	2.10	2.10
345	4.04	3.98	3.84	3.09	2.87	2.43	2.20	2.16	2.16
355	4.06	3.99	3.85	3.13	2.91	2.45	2.21	2.15	2.15

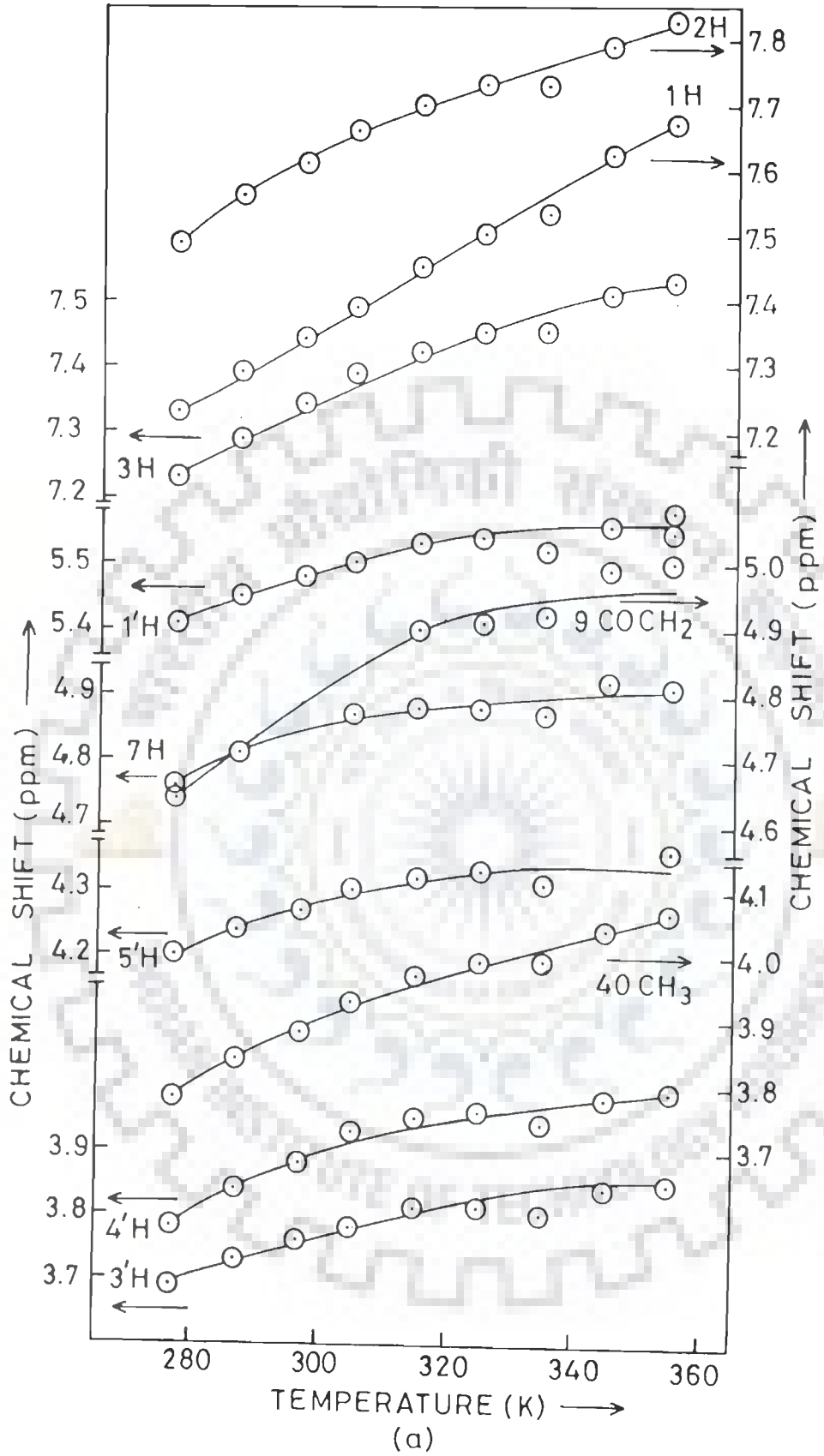

Fig.4.2 : Chemical shifts of adriamycin protons as a function of temperature over the range 277-355 K. (a) Resonances appearing between 3.7-7.8 ppm (b) Resonances appearing between 1.2-3.1 ppm.

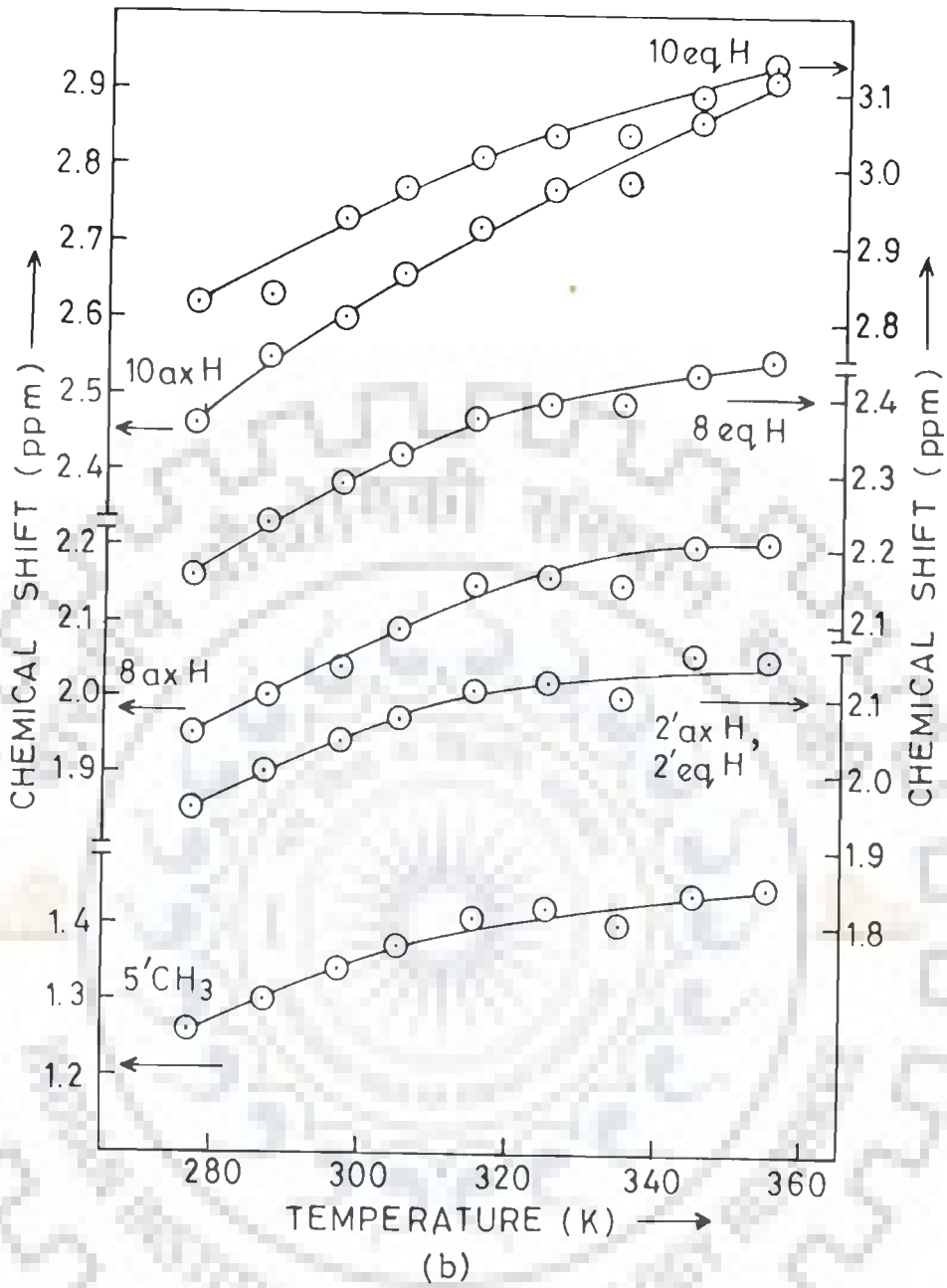
10eq H
10ax H
8 eq H
8ax H
2'ax H,
2'eq H
5'CH3
CHEMICAL SHIFT (ppm)
CHEMICAL SHIFT (ppm)
TEMPERATURE (K)
280
300
320
340
360
2.9
2.8
2.7
2.6
2.5
2.4
2.2
2.1
2.0
1.9
1.4
1.3
1.2
3.1
3.0
2.9
2.8
2.4
2.3
2.2
2.1
2.1
2.0
1.9
1.8
(b)

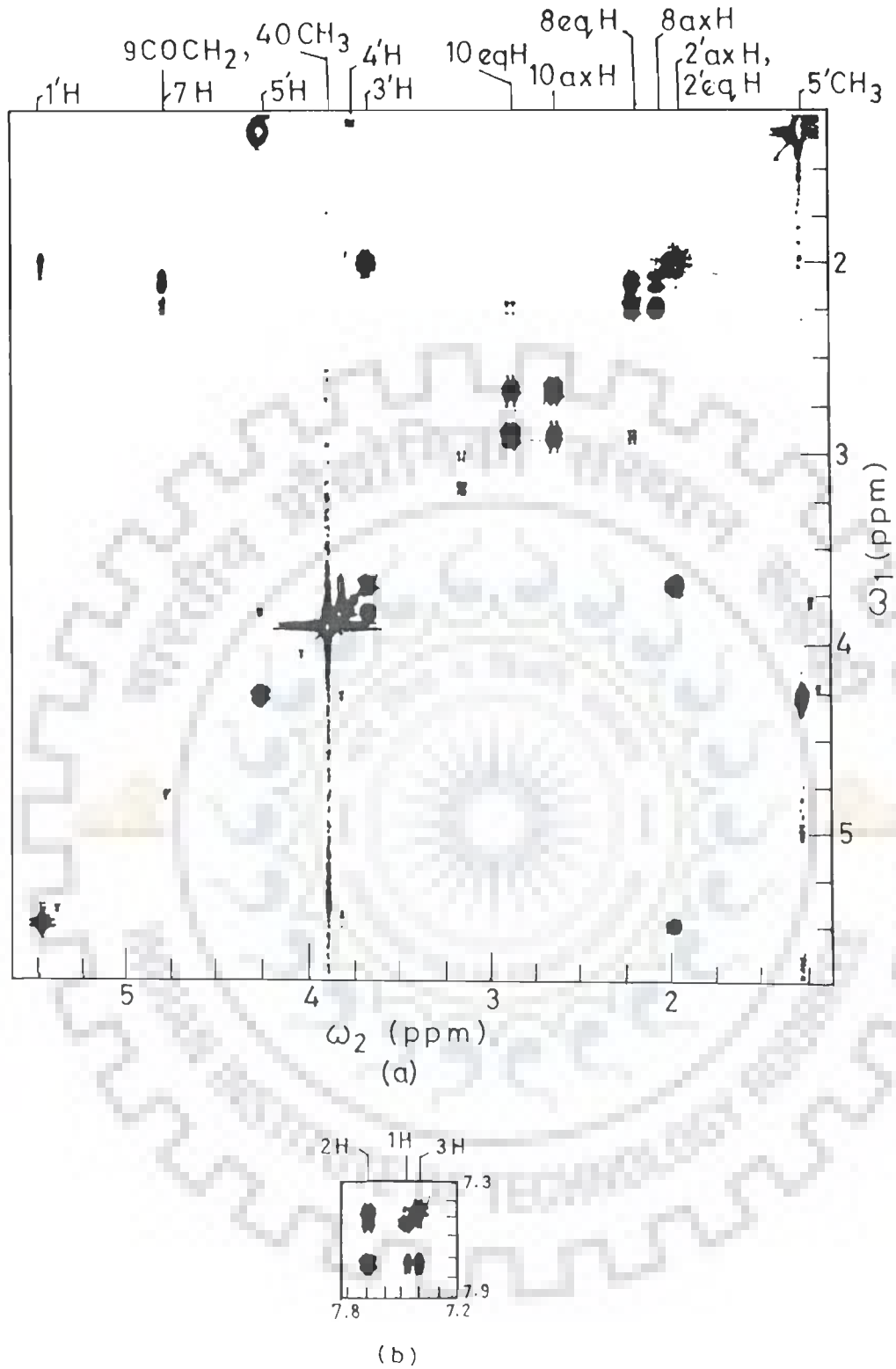

Fig.4.3 : The phase-sensitive COSY spectrum of 11.5 mM adriamycin in D_2O at 297 K showing the observed COSY connectivities between pairs of protons: (a) within the daunosamine sugar moiety and within ring A (b) within ring D.

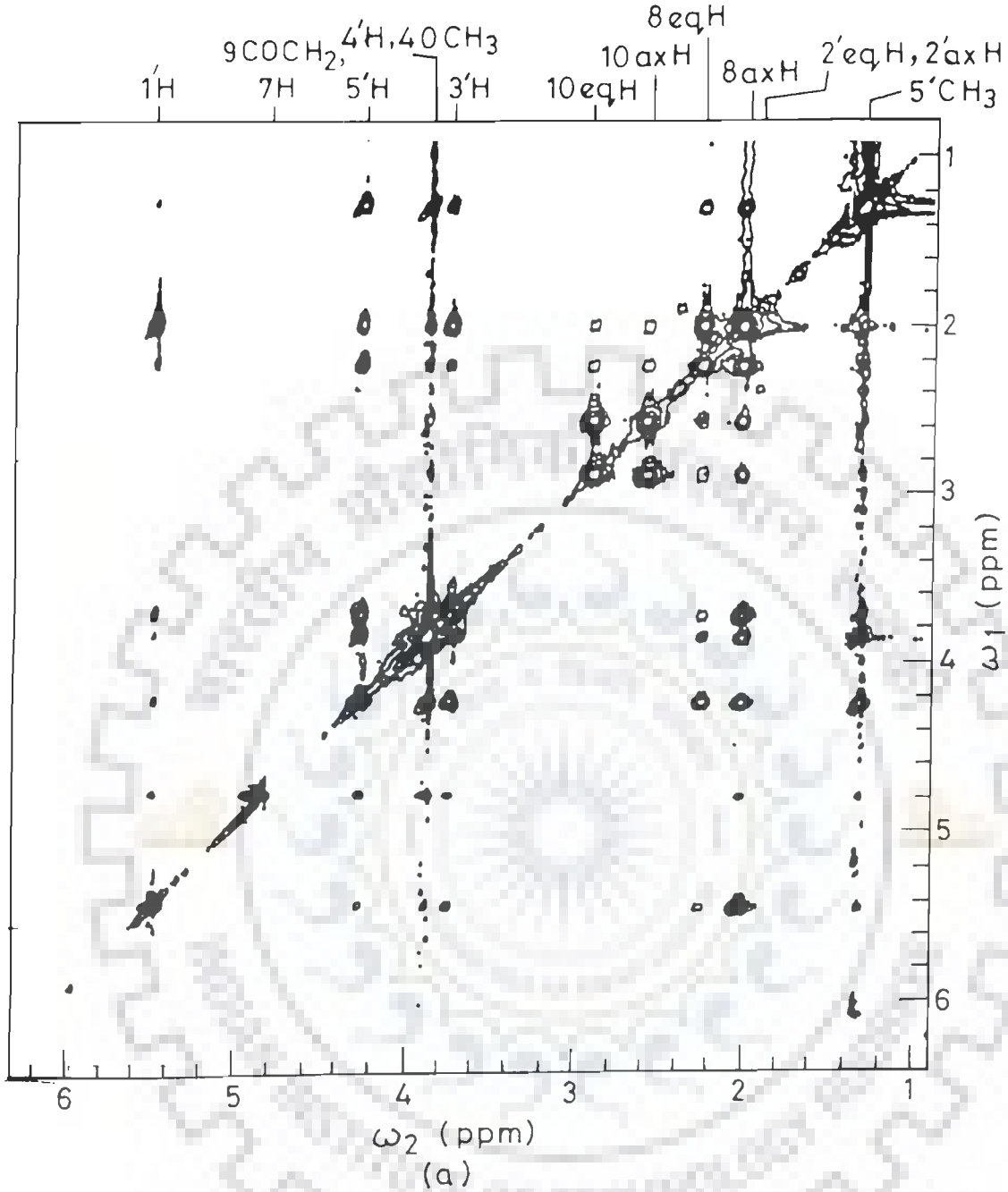

Fig.4.4 : Phase-sensitive NOESY spectrum of 11.5 mM adriamycin in D_2O at 297 K indicating the NOE connectivities for pairs of protons : (a) within ring A and within daunosamine sugar moiety, between ring A and the daunosamine sugar moiety (b) within ring D protons.

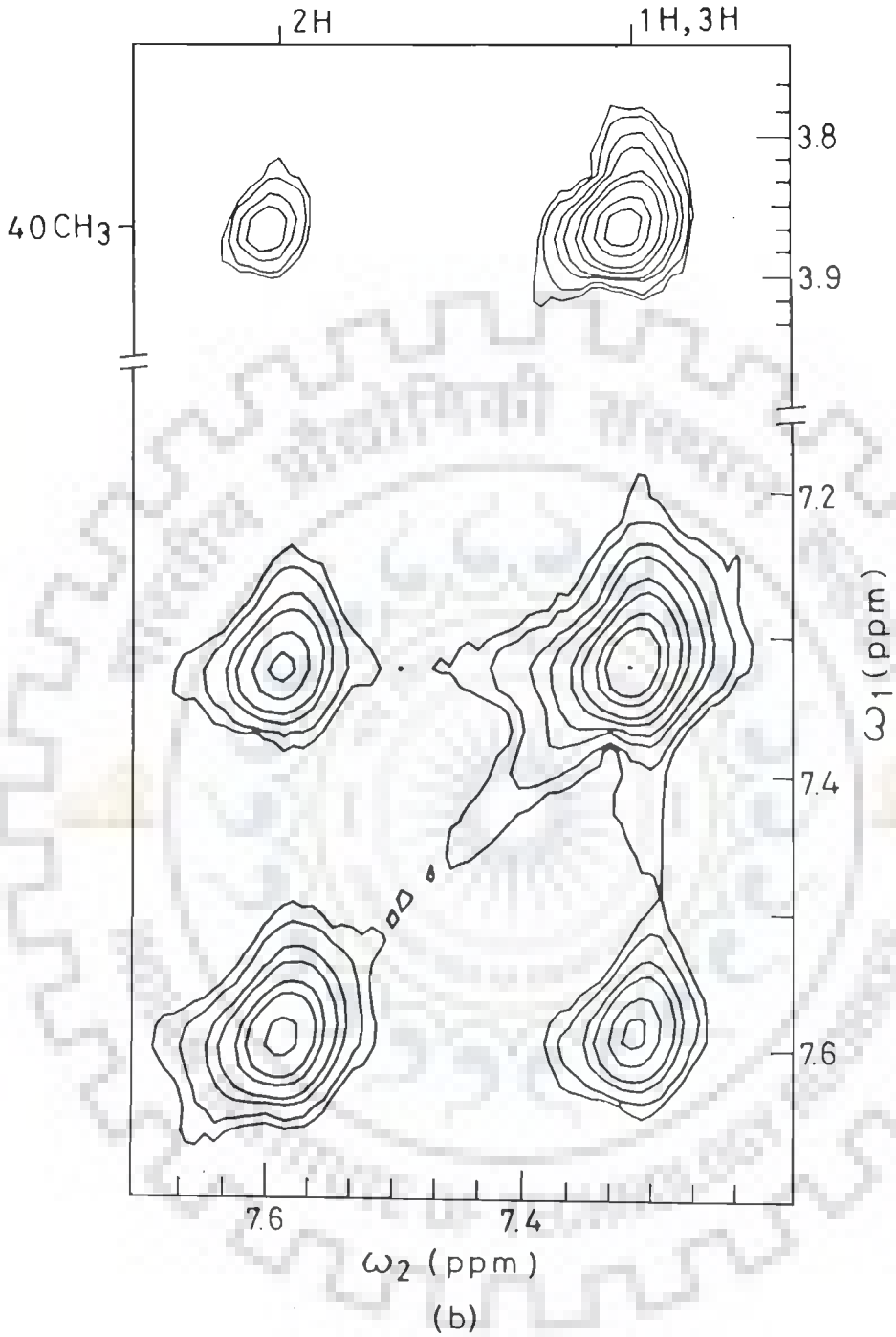

(b)

resonance in COSY spectra, as expected. The other resonance appearing as a doublet at 4.91 ppm at 355 K is coupled to protons 8axH and 8eqH (Fig. 4.3(a)) and is therefore assigned to proton 7H.

The aliphatic $-CH_3$ proton resonances occur in the region 1.2-1.6 ppm. The integral plot shows that the intense peak at 1.34 ppm is due to three protons and is assigned to the 5'CH_3 protons of the daunosamine sugar moiety. This resonance is strongly coupled to another appearing at 4.27 ppm which is assigned to proton 5'H. The 5'H proton is further coupled to the resonance peak at 3.88 ppm, assigned to proton 4'H. In the same way the COSY cross peaks 4'H-3'H; 3'H-2'axH; 3'H-2'eqH; 2'axH-1'H; and 2'eqH-1'H assign the resonances at 3.76, 2.04, 2.04 and 5.48 ppm to 3'H, 2'axH, 2'eqH and 1'H protons, respectively. These spectral assignments are in accord with those reported in the literature (69). The chemical shifts of protons of adriamycin are listed in Table 4.1.

Changes in chemical shift and self association

It has been observed that most of the resonances of adriamycin shift gradually with increase in temperature (Fig. 4.2(a, b)). For almost all protons, this variation in chemical shift is found to cease at ≃ 355 K. The chemical shifts of the various protons with varying temperature in the range 277-355 K are shown in Table 4.2. It is found that the 2H, 1H, 3H and 4OCH_3 protons of adriamycin shift downfield by 0.28-0.44 ppm (Table

4.2). Chaires et al. (13) observed that 2H, 1H, 3H and 4OCH$_3$ protons of daunomycin shift upfield by 0.20, 0.26 , 0.33 and 0.18 ppm, respectively, on increasing the concentration from 10 μm to 7 mM in D_2O solution. This has been attributed to self association of several drug molecules via stacking of their aromatic rings at higher concentrations (13). The self association of adriamycin and daunomycin has also been monitored from the concentration dependence of the ^2H line widths (66). The changes in chemical shift due to stacking interactions have been reported (86,88,92) for drug-nucleic acid complexes also. In our case, the drug is present in a self aggregated form at 277 K. On increasing the temperature, destacking of the rings occurs which is manifested as downfield shift in proton resonances. The drug gradually returns to its monomeric form as the changes in chemical shift cease. Therefore, the chemical shift at high temperature, i.e. 355 K, may be attributed to that of the adriamycin monomer.

Of the ring A protons, the 7H proton shifts downfield by 0.15 ppm with temperature. Although A is a cyclohexane ring, the downfield shift with temperature is apparently due to destacking on dissociation of the self aggregated form suggesting that proton 7H may be present in a pseudoequatorial position with respect to the rings BCD. A relatively large downfield shift of ≃ 0.41 ppm with temperature is observed for the 9COCH$_2$ proton. The 8axH, 8eqH, 10axH and 10eqH protons shift downfield by 0.26-0.46 ppm with temperature which may be attributed to ring current effects from aromatic rings BCD in their proximity. Changes in

chemical shift of various sugar protons due to dissociation of self aggregated adriamycin with temperature are relatively small, being 0.15-0.21 ppm. These protons are not expected to experience the ring current effects of aromatic rings BCD. These protons, however, may have been affected by structural changes accompanying the self association process to accommodate drug molecules stacked on top of each other. Thus it is found that adriamycin exhibits self association in the same way as the drug daunomycin (13).

Spin-spin coupling and torsional angles

Phase-sensitive COSY spectra have been used to delineate scalar coupling interactions through bonds. As discussed earlier in chapter III, the spin system of various pair of protons coupled through bond are identified and the J values are read directly as the separation between the positive and negative contours of the cross peak.

The 8eqH proton is coupled to both 8axH and 10eqH protons. Since, $\Delta\delta$(8eqH-10eqH) > J(8eqH-10eqH), this pair of protons belongs to an AMX spin system. The splitting patterns along ω_2 axis are expected to be as shown in (a) below —

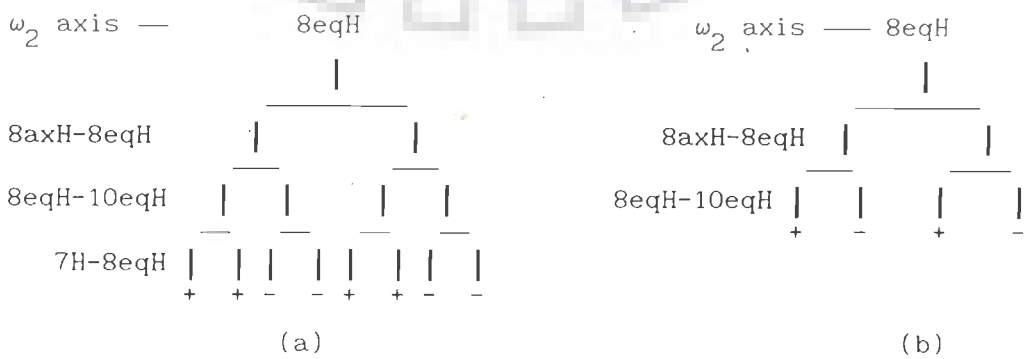

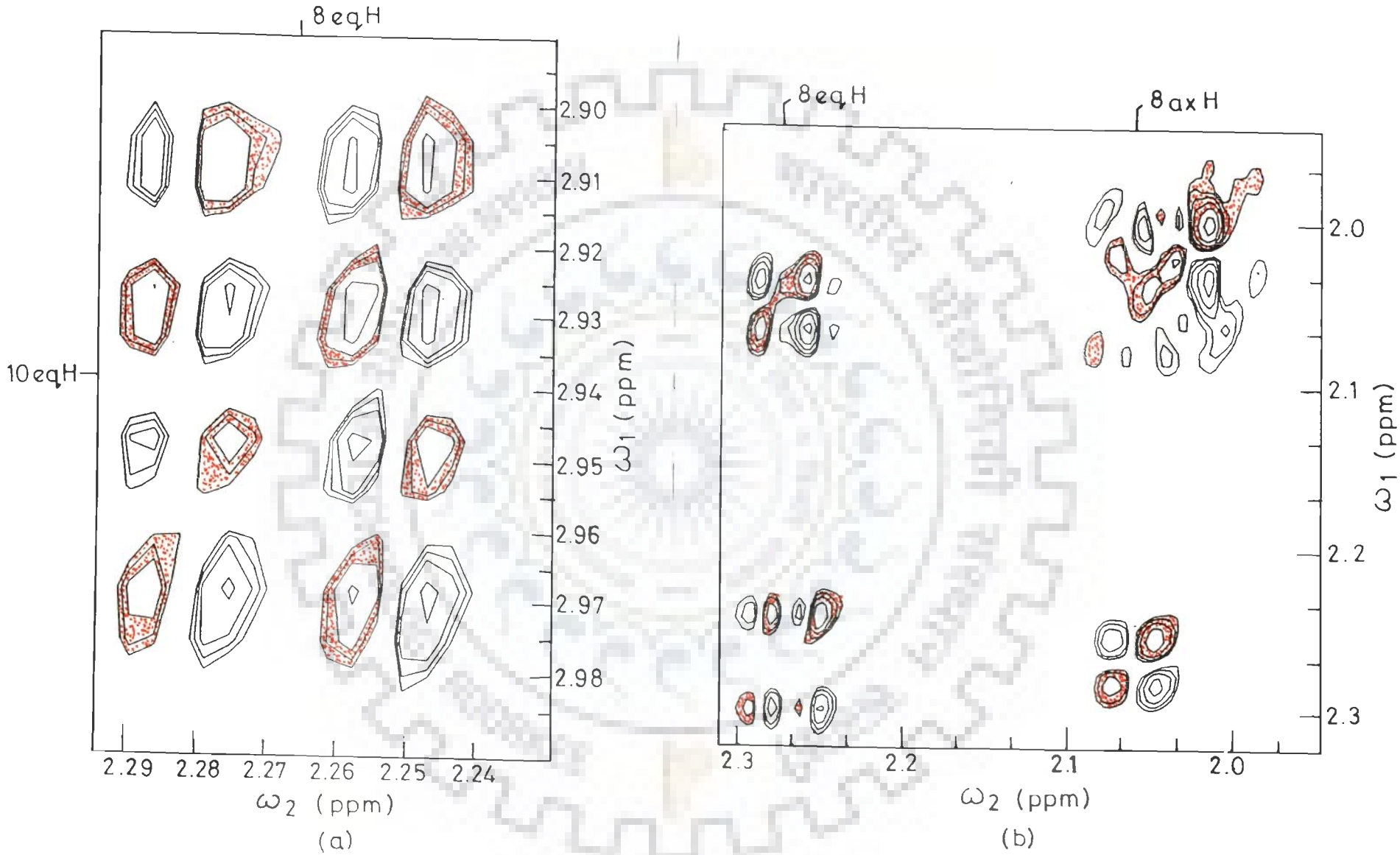

Fig. 4.5 : Portions of the phase-sensitive COSY spectrum (a-i) on an expanded scale showing antiphase components along the ω_1 and ω_2 axis of various cross peaks connecting J-coupled protons.

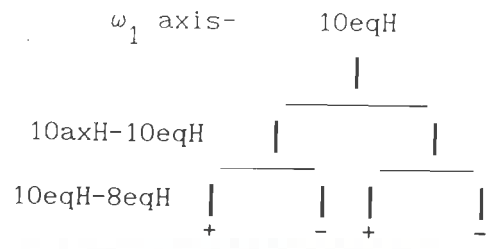

(c)

Since, the 7H-8eqH coupling is small, the splittings along ω_2 axis may effectively be considered as shown in (b). In a similar way the 10eqH proton splits along ω_1 axis and is shown in (c). Fig. 4.5(a) shows the experimentally observed contours of the phase-sensitive COSY spectra showing cross peaks of 8eqH with 10eqH. The negative components are differentiated from the positive ones by its red colour in Figs. 4.5(a-i). The active coupling constant J(8eqH-10eqH) is read off directly as the separation between + and - contours along the ω_2 axis as 5.3 Hz. The larger coupling wherein phase remains constant is due to coupling of 8eqH with 8axH protons and therefore gives a value of J(8axH - 8eqH). Along ω_1 axis the passive coupling constant J(10axH-10eqH) is read off directly. The strong geminal couplings J(8axH-8eqH) and J(10axH-10eqH) are more accurately obtained directly from the AX type spin system along the ω_2 axis (Fig. 4.5(b, c)) as 12.5 Hz and 18.6 Hz, respectively.

Proceeding in a similar way, we find that proton 7H is coupled to both 8ax and 8eq protons, which are coupled to each other by strong geminal coupling. The observed cross peak pattern of 7H with 8axH (Fig. 4.5(d)) gives the active coupling constant J(7H-8axH) read along the ω_2 axis as 7.1 Hz. This

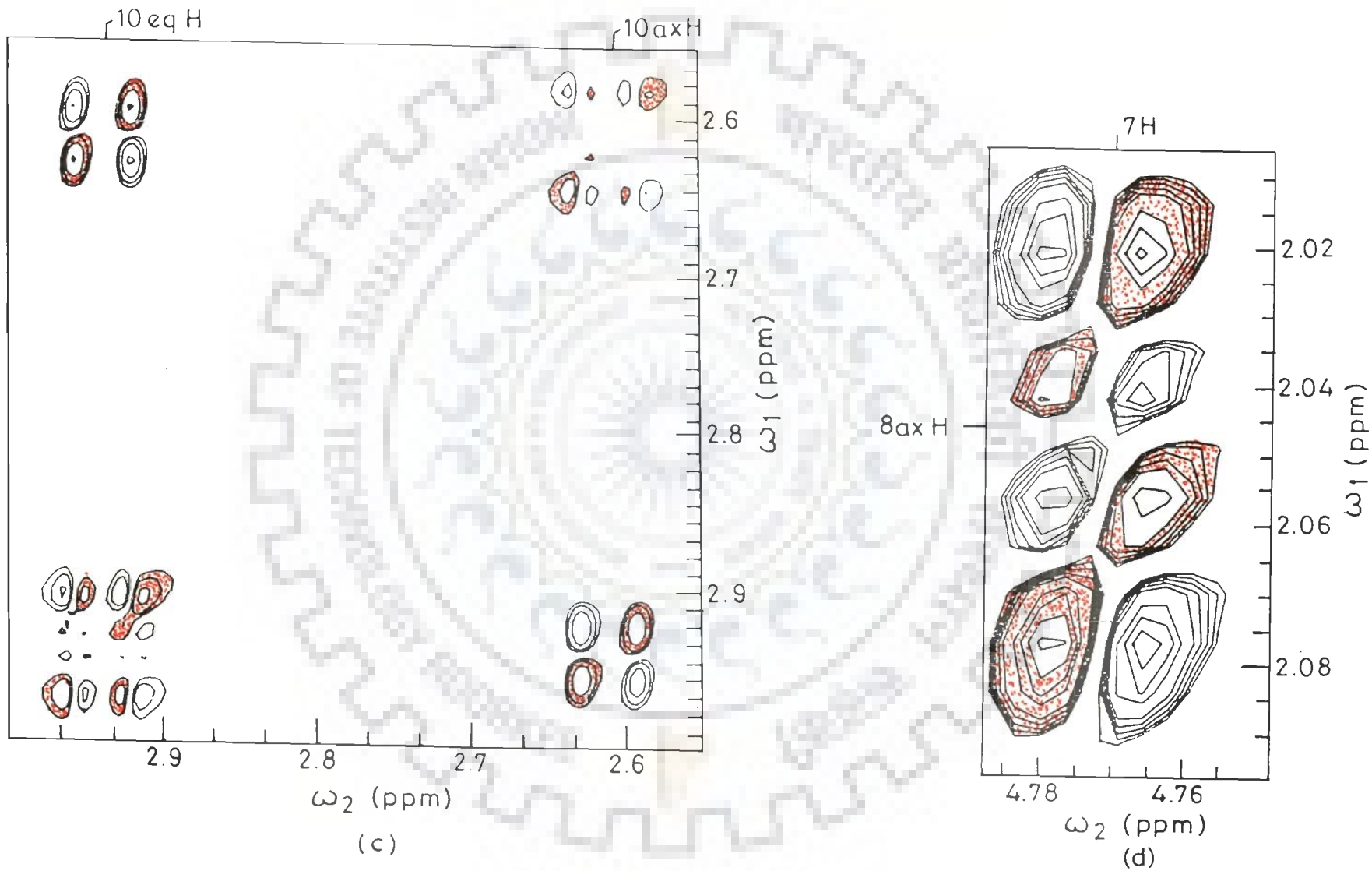
10 eq H
10 ax H
2.6
2.7
2.8
2.9
ω1 (ppm)
2.9
2.8
2.7
2.6
ω2 (ppm)
(c)
7H
8ax H
2.02
2.04
2.06
2.08
ω1 (ppm)
4.78
4.76
ω2 (ppm)
(d)

pattern repeats itself due to passive coupling J(8axH-8eqH) along the ω_1 axis. In contrast, the cross peak of 7H with 8eqH is found to be very weak in intensity. The resolution used by us was not sufficient to resolve the coupling constant J(7H-8eqH) along the ω_2 axis, which is therefore inferred to be < 2.30 Hz. Both 1H and 3H protons of ring D of adriamycin are coupled to 2H proton. The J values are obtained from the active couplings of a typical AX spectra along the ω_2 axis (Fig. 4.5(e)) as J(2H-1H) = 7.7 Hz and J(2H-3H) = 8.5 Hz, respectively.

In the daunosamine sugar moiety of adriamycin, the 5'CH_3 protons are coupled to proton 5'H representing a A_3X spin system. The active coupling of proton 5'H with 5'CH_3 (Fig. 4.5(f)) along the ω_2 axis is 13.3 Hz. Along the ω_2 axis the passive coupling J(4'H-5'H) is 6.6 Hz (Table 4.3). The 5'H proton is further coupled to the 4'H proton. The cross peak 4'H-5'H is shown in Fig. 4.5(g), giving active coupling J(4'H-5'H) along the ω_2 axis as 6.7 Hz. Fig. 4.5(h) shows the cross peak of 3'H with 2'axH and 2'eqH protons. The 2'axH and 2'eqH protons resonate at nearly equal frequencies (Fig. 4.1(a)) and yet are separated in phase-sensitive COSY spectra along the ω_2 axis. The value of J(2'axH-3'H) and J(3'H-2'eqH) are read as active coupling along the ω_2 axis as 13.2 and 7.9 Hz, respectively. The value of J(2'axH-2'eqH) cannot be ascertained accurately as the positive and negative contours of these cross peaks overlap. Fig. 4.5(i) shows the cross peak of 1'H with 2'axH and 2'eqH protons. Along the ω_2 axis, the active coupling J(1'H-2'axH) is 6.1 Hz,

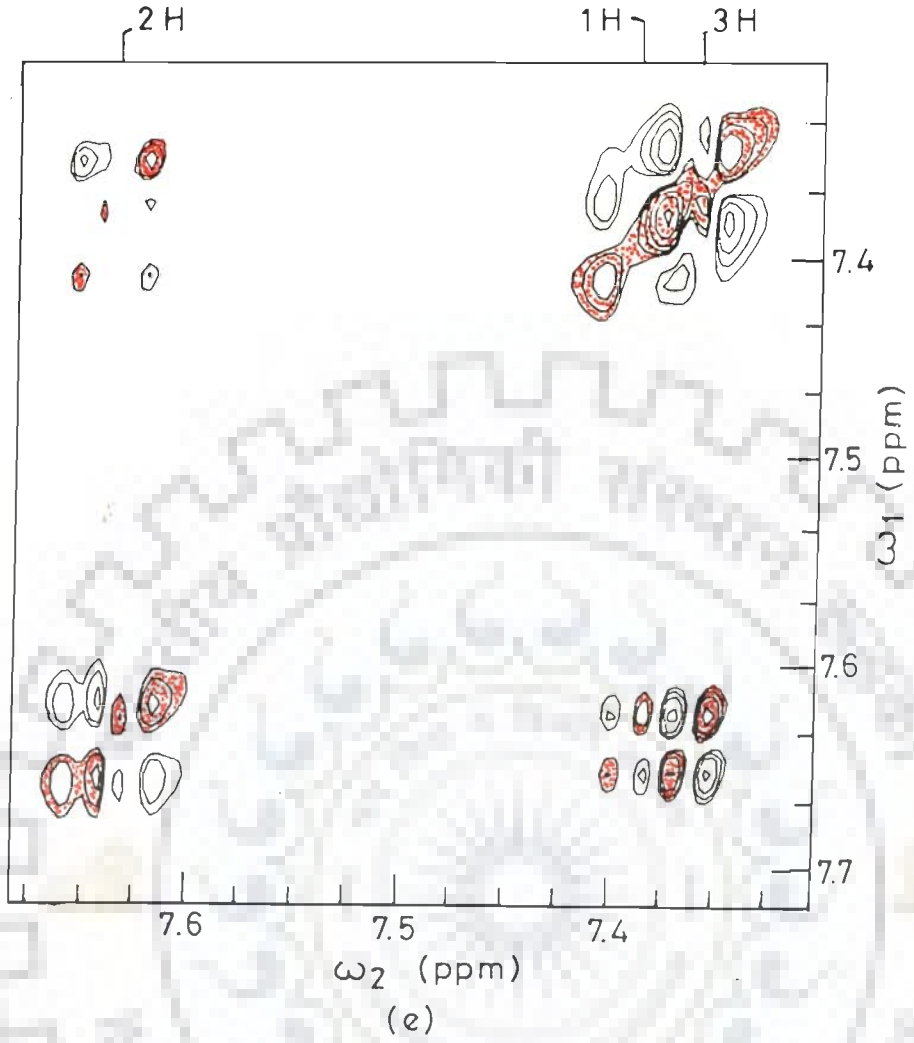

(e)

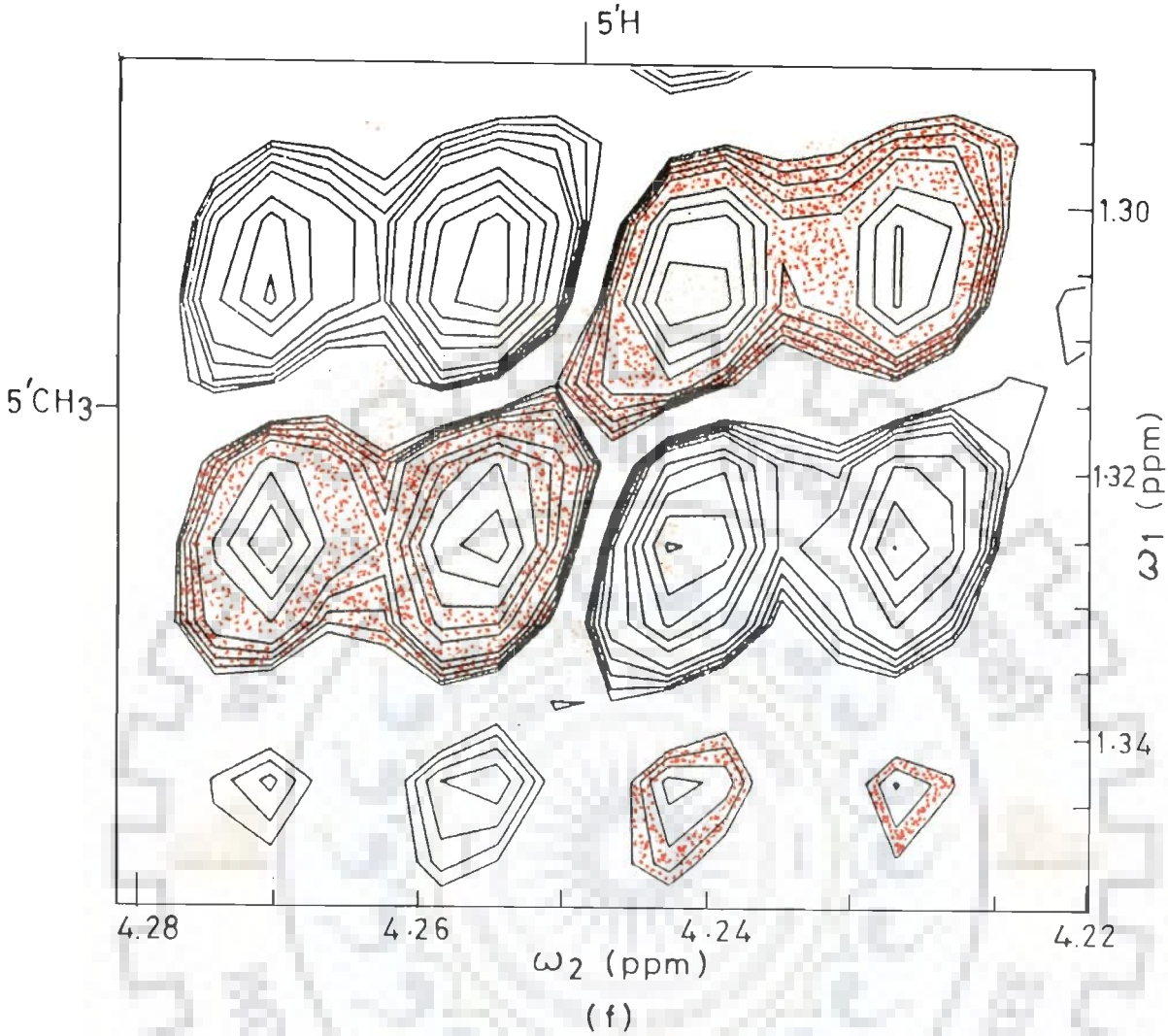

(f)

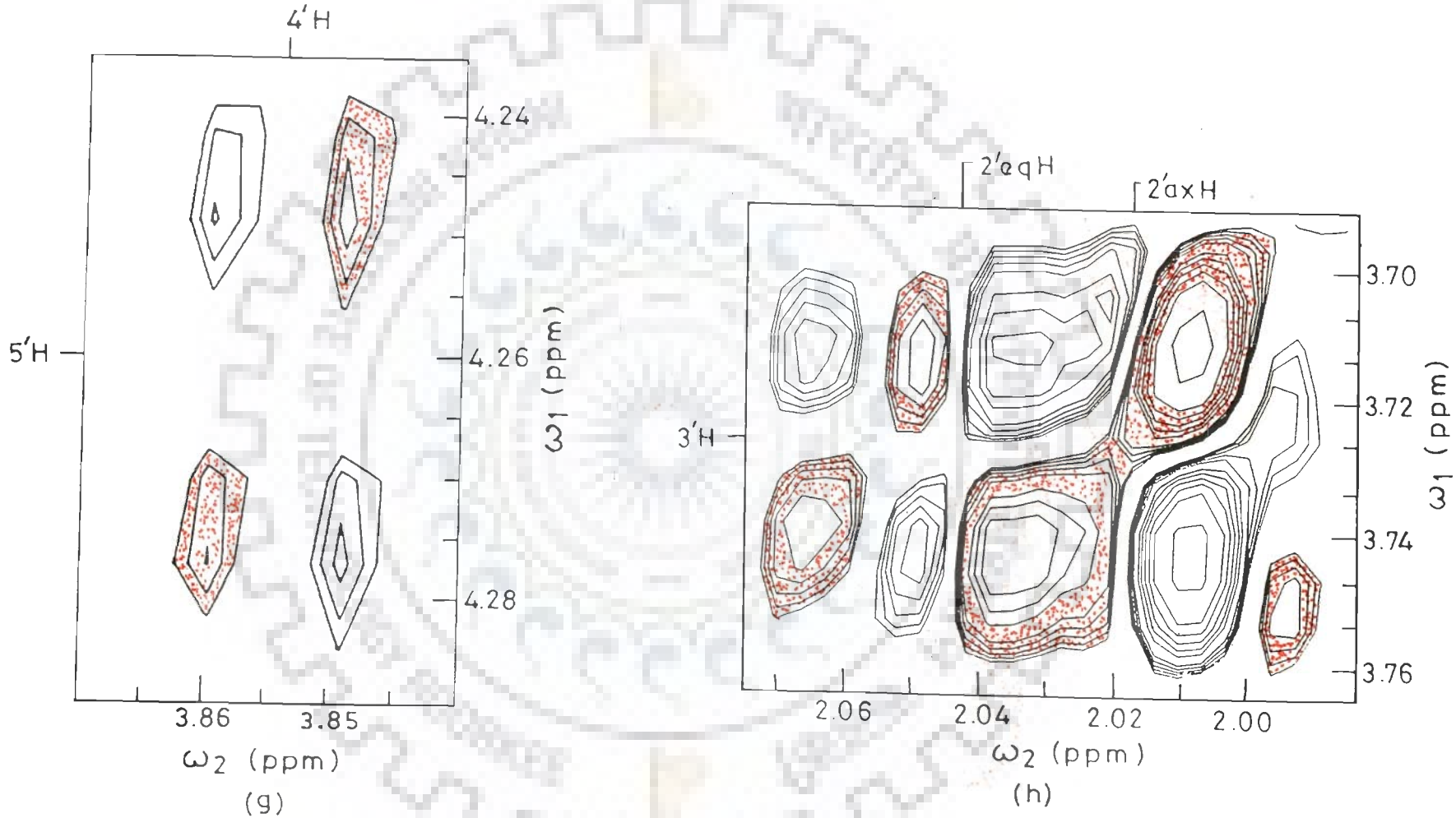
4'H
5'H
4.24
4.26
4.28
3.86
3.85
ω2 (ppm)
ω1 (ppm)
(g)
2'eqH
2'axH
3'H
3.70
3.72
3.74
3.76
2.06
2.04
2.02
2.00
ω2 (ppm)
ω1 (ppm)
(h)

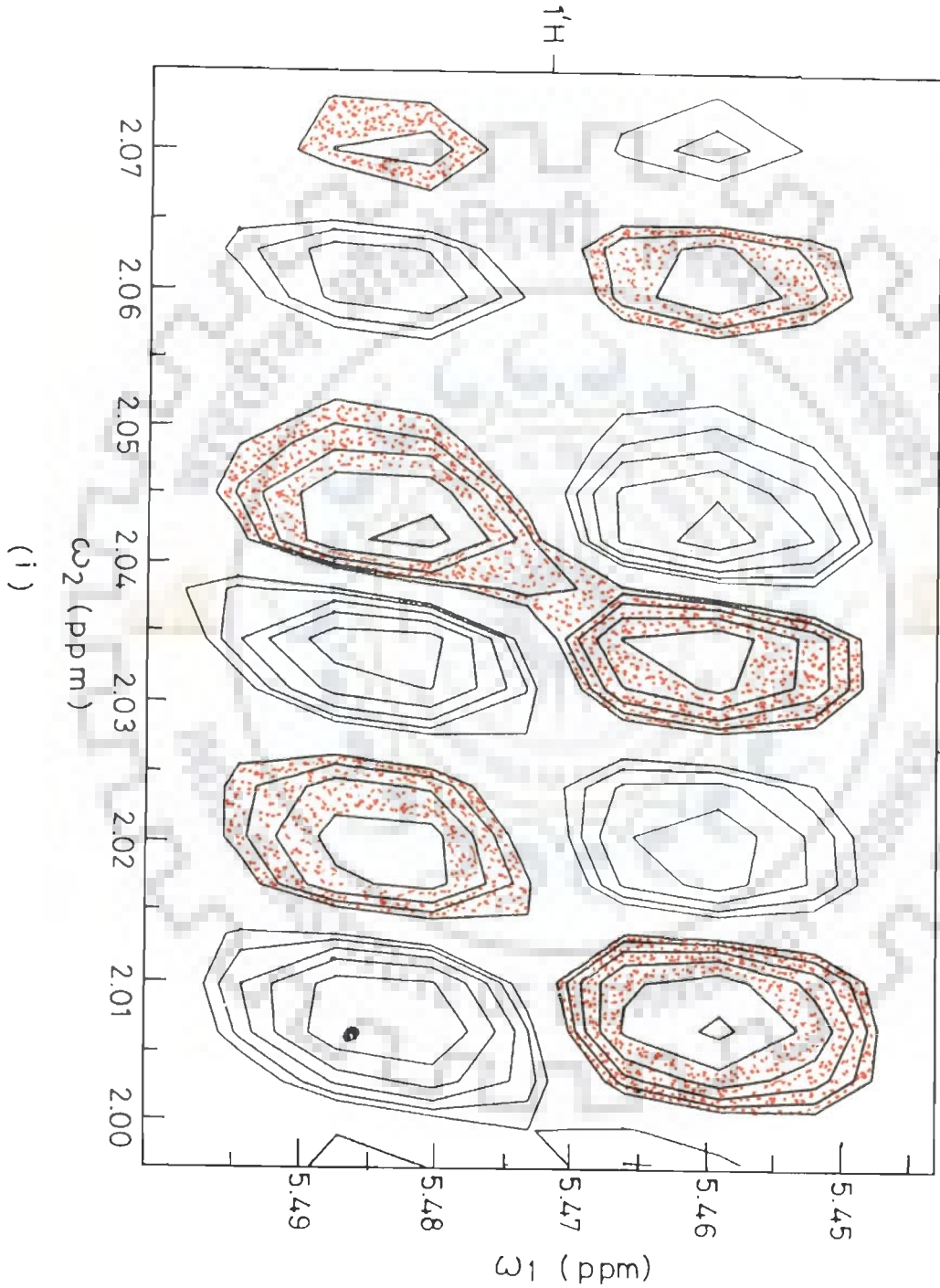
1'H
2'eq H
2'ax H
2.07
2.06
2.05
2.04
2.03
2.02
2.01
2.00
ω2 (ppm)
5.49
5.48
5.47
5.46
5.45
ω1 (ppm)

(i)

Table 4.3 : Observed spin-spin coupling constants, J (Hz), and torsional angles, θ (degree), for vicinal couplings between pairs of protons of adriamycin (for comparison results reported by Mondelli et al. (69) are also given).

Pairs of protons.	Adriamycin		
	Present work		(69)
	J	θ	J
1H-2H	7.7	~ 0	-
2H-3H	8.5	~ 0	-
1'H-2'axH	6.1	29.0	3.8
1'H-2'eqH	5.0	39.1	1.2
3'H-4'H	o	-	2.7
4'H-5'H	6.7	20.0	1.3
3'H-2'axH	13.2	180.0	13.0
3'H-2'eqH	7.9	144.1	4.8
2'axH-2'eqH	14.0	-	13.0
5'H-5'CH_3	13.3	180.0	-
7H-8axH	7.1	135.0	5.1
7H-8eqH	w	60-100	2.5
8axH-8eqH	12.5	-	15.0
10axH-10eqH	18.6	-	18.6
8eqH-10eqH	5.3	-	2.0

o :overlapping.

w : Weak in intensity (see text).

J(1'H-2'eqH) is 5.0 Hz and the passive coupling J(2'axH-2'eqH) is approximately in the range of 12-14 Hz due to overlapping of positive and negative contours. Along the ω_1 axis passive couplings are not expected to be observed for 2'axH and 2'eqH protons as active and passive couplings are similar to one another. Table 4.3 lists the J values obtained from the expansions of phase-sensitive COSY spectra. We have calculated the torsional angles for all vicinal couplings using the standard plot of J versus θ obtained from the Karplus relationship (52,53). The only other available data on spin-spin coupling constants in adriamycin are those reported by Mondelli et al. (69) which are given in Table 4.3 for comparison. It can be seen that the geminal couplings J(2'axH-2'eqH), J(8axH-8eqH) and J(10axH-10eqH) obtained by Mondelli et al. (69) are similar to our results. It should be noted that in a planar aromatic ring, the relative orientation, of the 1H-2H and 2H-3H pairs of protons is nearly cis with torsional angle 0° and hence the J value is expected to be around 8.0 Hz. The observed values of J(1'H-2'axH), J(1'H-2'eqH), J(4'H-5'H) and J(3'H-2'eqH) of daunosamine sugar moiety are different from the corresponding values reported by Mondelli et al. (69). The scalar coupling of 5'CH_3 protons with 5'H proton is relatively large. Of ring A protons, J(7H-8axH) is 7.1 Hz and J(7H-8eqH) < 2.30 Hz. These are different from the corresponding values of 5.1 and 2.5 Hz reported (69) earlier. These differences in spin-spin coupling constants demonstrate that the sugar conformation and the relative orientation of protons 7H,

8axH, 8eqH in our case is different from those reported (69) earlier in solution state.

NOE connectivities and interproton distances

Phase-sensitive NOESY spectra are recorded at different mixing times (τ_m) in the range 400-600 ms. Figs. 4.4(a) and (b) map the protons which are coupled in space through dipolar interactions. Figs. 4.6 (a) and (b) are expansions of 2D phase-sensitive NOESY spectra showing specific NOE connectivities which are listed in Table 4.4. The NOE build-up curves are obtained to determine the acceptable value of τ_m (45) for calculation of interproton distances (data not shown). An increase in intensity of various cross peaks is observed with increase in mixing time. Thus NOESY spectra recorded at lowest mixing time (τ_m = 400 ms) is found to be acceptable for distance measurements. The intensities of these NOE cross peaks are used to obtain the distance between protons. The X-ray structure analysis of various closely related drugs, carminomycin I (91), n-bromoacetyl daunomycin (2) and daunomycin (24), have shown that the distance between 1H and 2H protons of ring D vary over the narrow range 2.30-2.36 A°. In the absence of any crystal structure data for adriamycin, the distance r(1H-2H) = 2.36 A° of daunomycin (24) has been used as an internal standard. The volume integral of all other NOE cross peaks is then used to obtain interproton distances. The values thus calculated are shown in Table 4.4.

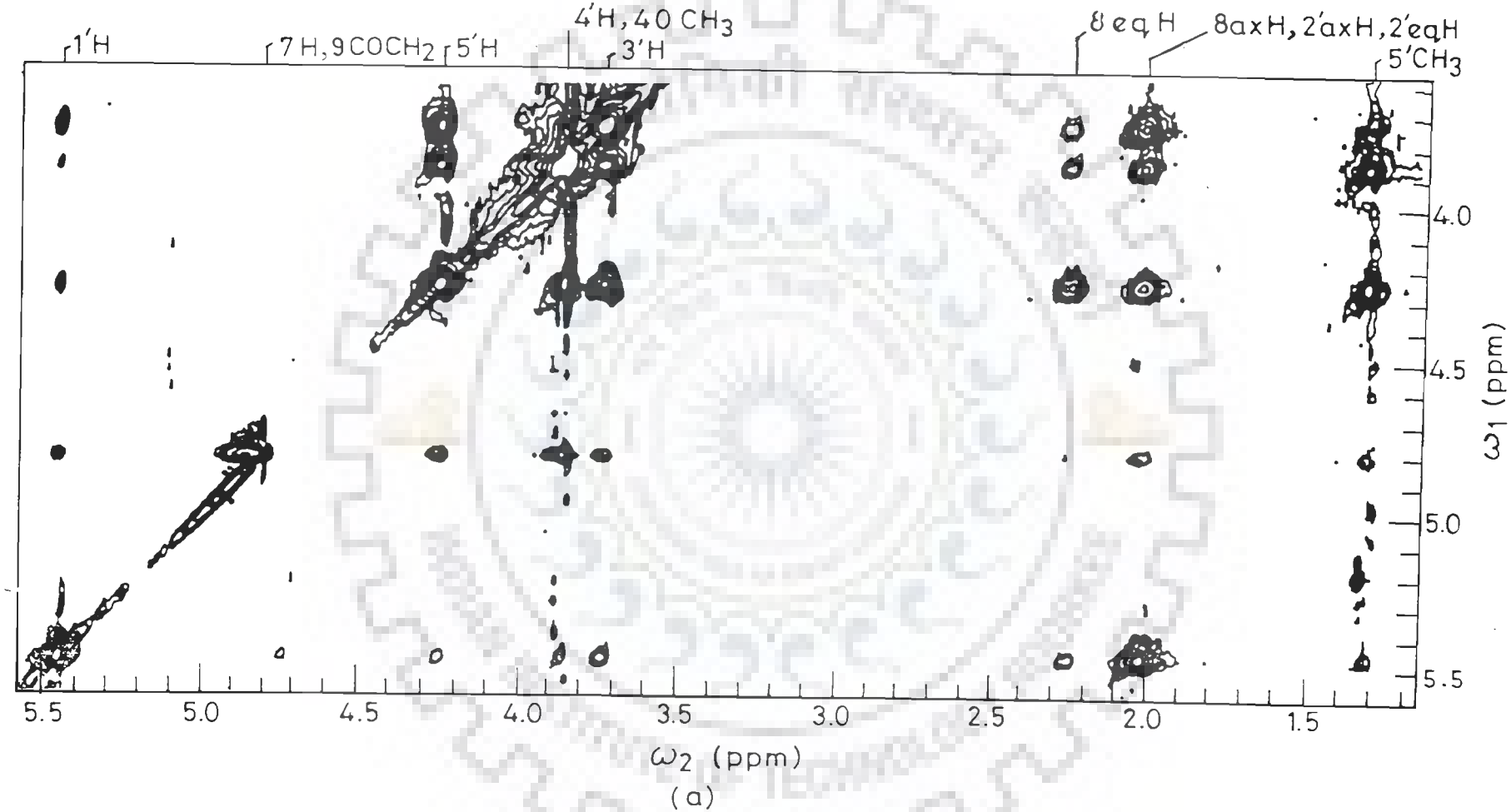

Fig.4.6 : Portions of the phase-sensitive NOESY spectrum (a,b) on an expanded scale showing specific NOE connectivities.

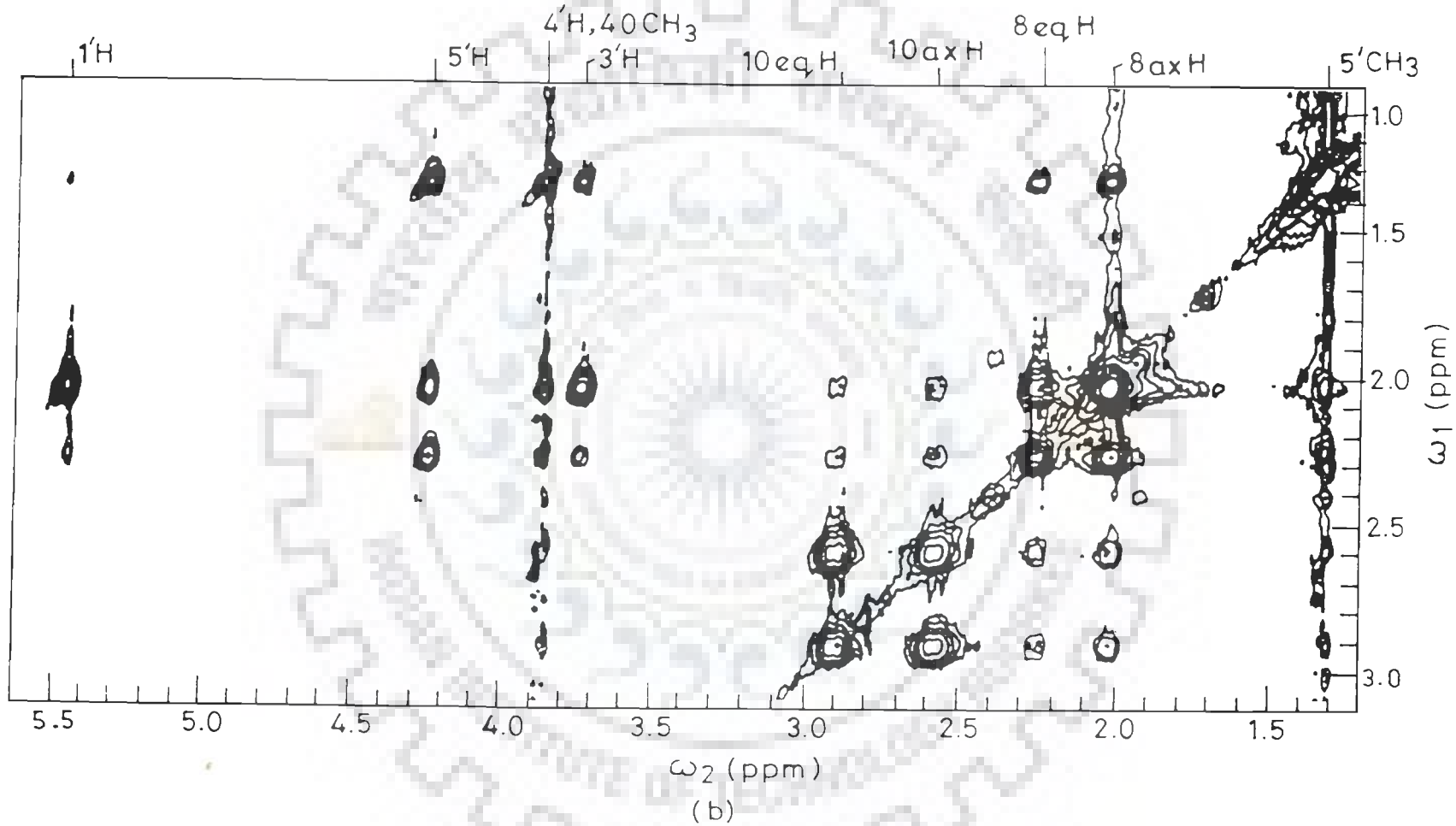
1'H
5'H
4'H,4OCH3
3'H
10eqH
10axH
8eqH
8axH
5'CH3
1.0
1.5
2.0
2.5
3.0
ω1 (ppm)
5.5
5.0
4.5
4.0
3.5
3.0
2.5
2.0
1.5
ω2 (ppm)

(b)

Under the resolution used all pairs of protons at a distance of < 5.0 A° are expected to exhibit NOE cross peaks. It is observed that the pairs of protons correlated by spin-spin coupling give rise to NOE cross peaks and have interproton distances < 3.3 A°. The r(2'axH-2'eqH) could not be ascertained due to overlap of resonances in this region. Although the pair of protons 7H-8eqH shows NOE connectivity, its distance could not be obtained due to the weak intensity of the signal. Since the resonance positions of protons 2'ax, 2'eq and 8ax are very close to each other, each of the exact distances 1'H-2'axH, 1'H-2'eqH, 1'H-8axH cannot be ascertained accurately. X-ray crystal structure analysis (78) has shown that the distances 1'H-2'axH, 1'H-2'eqH and 1'H-8axH are 2.56, 2.53 and 4.47 A°, respectively. Assuming these distances are in the same ratio as the distances determined from X-ray structural analysis, it is found that the observed intensity of NOE cross peaks 1'H-2'axH, 1'H-2'eqH and 1'H-8axH corresponds to a distance of 2.31, 2.28 and 4.03 A° respectively (given in Table 4.4). Proceeding in the same way, the interproton distances between 3'H-2'axH, 3'H-2'eqH and 3'H-8axH are found to be 3.89, 2.95 and 5.70 A°, respectively, from X-ray crystal structure analysis (78). These distances are estimated as 3.07, 2.33 and 4.50 A° respectively, (Table 4.4) from the intensity of NOE cross peaks 3'H-2'axH, 3'H-2'eqH and 3'H-8axH. Similarly, the distances 4'H-2'axH, 4'H-2'eqH and 4'H-8axH are 5.11, 3.72 and 6.70 A°, respectively, determined by X-ray crystallography (78) and are estimated as 3.69, 2.68 and

Table 4.4 : Interproton distances[a] calculated from observed NOE connectivities between pairs of protons coupled by dipolar interaction.

Connectivities	Adriamycin	Daunomycin[c]	
		NMR	X-ray
Spin-spin coupled protons			
2H-1H	2.36	-	-
2H-3H	2.12	-	-
1'H-2'axH	2.31[o]	2.21	2.56
1'H-2'eqH	2.28[o]	2.35	2.53
3'H-4'H	1.92	-	2.55
4'H-5'H	2.16/ 2.37[b]	2.35	2.45
3'H-2'axH	3.07[o]	-	3.89
3'H-2'eqH	2.33[o]	-	2.95
2'axH-2'eqH	o	-	1.76
5'H-5'CH_3	2.60, 2.59, 3.24	-	2.41, 2.40, 3.00
7H-8axH	3.30	2.30	2.36
7H-8eqH	w	2.45	2.40
8axH-8eqH	1.95	-	1.81
10axH-10eqH	1.92	-	1.77
8eqH-10eqH	2.96	-	4.25

Within Sugar -			
1′H-3′H	3.30	-	3.76
1′H-4′H	3.22	-	4.90
1′H-5′H	3.69	-	3.66
1′H-5′CH_3	5.68, 4.90, 4.75	-	5.36, 4.63, 4.49
3′H-5′H	2.28	-	2.40
3′H-5′CH_3	4.61, 5.55, 5.62	-	4.24, 4.61, 4.67
4′H-2′axH	3.69[o]	-	5.11
4′H-2′eqH	2.68[o]	-	3.72
4′H-5′CH_3	2.25, 2.79, 3.41	-	2.43, 3.01, 3.68
Within ring D -			
2H-4OCH_3	2.96	-	-
3H-4OCH_3	2.05	-	-
Within ring A -			
10axH-8axH	2.82	-	2.64
10axH-8eqH	2.78	-	3.86
10eqH-8axH	3.01	-	3.71
Ring A with sugar protons -			
7H-1′H	3.24/ 2.16[b]	2.19	2.22
7H-3′H	3.30	-	4.67
7H-4′H	2.70	-	5.78
7H-5′H	3.02	-	3.65
7H-5′CH_3	5.18, 4.81,	-	5.41, 5.03,

	3.90		4.08
8axH-1'H	4.03[o]	-	4.47
8axH-3'H	4.50[o]	-	5.70
8axH-4'H	4.84[o]	-	6.70
8axH-5'H	2.50	-	4.35
8axH-5'CH_3	3.32,3.42, 2.60	-	6.05,4.75, 6.24
8eqH-1'H	3.16	-	3.94
8eqH-3'H	3.13	-	4.30
8eqH-4'H	3.29	-	5.07
8eqH-5'H	2.40/ 2.49[b]	2.40	2.61
8eqH-5'CH_3	3.75,2.84, 4.10		4.33,4.74, 3.28

o : denotes overlapping peaks, since 2'axH, 2'eqH, 8axH peaks are very close to each other (see text) and are being used as guideline only.

w : denotes cross-peak weak in intensity.

[a]The distance between protons 1H and 2H is used as an internal reference.

[b,c]For comparison, interproton distances for adriamycin in D_2O (23), in n-acetyl daunomycin obtained by NMR (70), and by X-ray are also given (78).

4.84 A°, respectively, from the intensity of cross peaks 4'H-2'axH, 4'H-2'eqH and 4'H-8axH (Table 4.4). Owing to the unavoidable inaccuracy, the estimated interproton distances 1'H-2'axH, 1'H-2'eqH, 1'H-8axH, 3'H-2'axH, 3'H-2'eqH, 3'H-8axH, 4'H-2'axH, 4'H-2'eqH and 4'H-8axH having overlapping 2'axH, 2'eqH and 8axH peaks are used in further analysis as a guideline only. Apart from the spin-spin coupled protons, other NOE contacts between protons within the daunosamine sugar unit, within ring A and between ring A and daunosamine sugar protons are observed. The distances corresponding to these contacts are given in Table 4.4. Within ring D, we find that $4OCH_3$ is close to 3H and 2H protons, the distances being 2.05 and 2.96 A°, respectively. This fact has been used previously for spectral assignment. Within ring A, the 8ax and 8eq protons are oriented with respect to protons 10ax and 10eq in such a way that their relative distances are fixed within 2.7-3.0 A°. Within the daunosamine sugar unit, proton 1'H is close to 3'H, 4'H, 5'H and $5'CH_3$ protons. Further, the 3'H proton is spatially close to protons 5'H and $5'CH_3$. All other NOE contacts are between protons of ring A and the daunosamine sugar protons. These NOEs help to determine the relative position of ring A and the sugar atoms. It is observed that proton 7H is close to protons 1'H, 3'H, 4'H, 5'H and $5'CH_3$, the distances being in the range 2.70-3.90 A°. Further, 8ax and 8eq protons are close to 1'H, 3'H, 4'H, 5'H and $5'CH_3$ with distances varying in the range 2.40-3.80 A°. Since, 2'ax and 2'eq protons resonate at positions that are very close to the

corresponding position for 8axH, the connectivity of the 1'H, 3'H, 4'H protons with 8axH may well be due to their connectivity with the 2'ax or 2'eq proton. In addition, 5'H and 5'CH_3 are expected to be at a distance > 4.0 A° from 2'axH and 2'eqH. However, the distances between 5'H - 8axH, 8eqH are 2.50 and 2.40 A°, respectively. Therefore these correspond to connectivities with 8axH and 8eqH protons rather than with 2'ax, 2'eq protons. This is in accord with the dreiding stereo model discussed later.

It is observed that the interproton distances estimated from NOE cross peaks agree with coupling constants obtained from COSY spectra. The value of J(2H-3H), 8.5 Hz, gives a torsional angle of 0° or 150°. In a planar ring, it is well known that the relative orientation of an ortho proton is the cis configuration and thus, the torsional angle is about 0°. A torsional angle of 0° corresponds to a distance of 2.2 A°. We have estimated the distance to be 2.12 A° from NOESY spectra which is in accord with J-values. The J(4'H-5'H) value of 6.7 Hz gives a torsional angle of 20° or 135°. Since the 4'H-5'H distance is observed as 2.16 A°, the torsional angle θ is confirmed as 20°. Similarly the 7H-8axH distance of 3.3 A° is in accord with J(7H-8axH)= 7.1 Hz giving θ as 135°.

Exchangeable protons and their connectivities

To observe exchangeable protons, the spectrum of adriamycin is investigated in DMSO solvent. Fig. 4.7 and Fig. 4.8(a, b) show the 1D and 2D NOESY spectra of adriamycin recorded in DMSO. The 6OH and 11OH protons of ring B resonate in the region 13-14

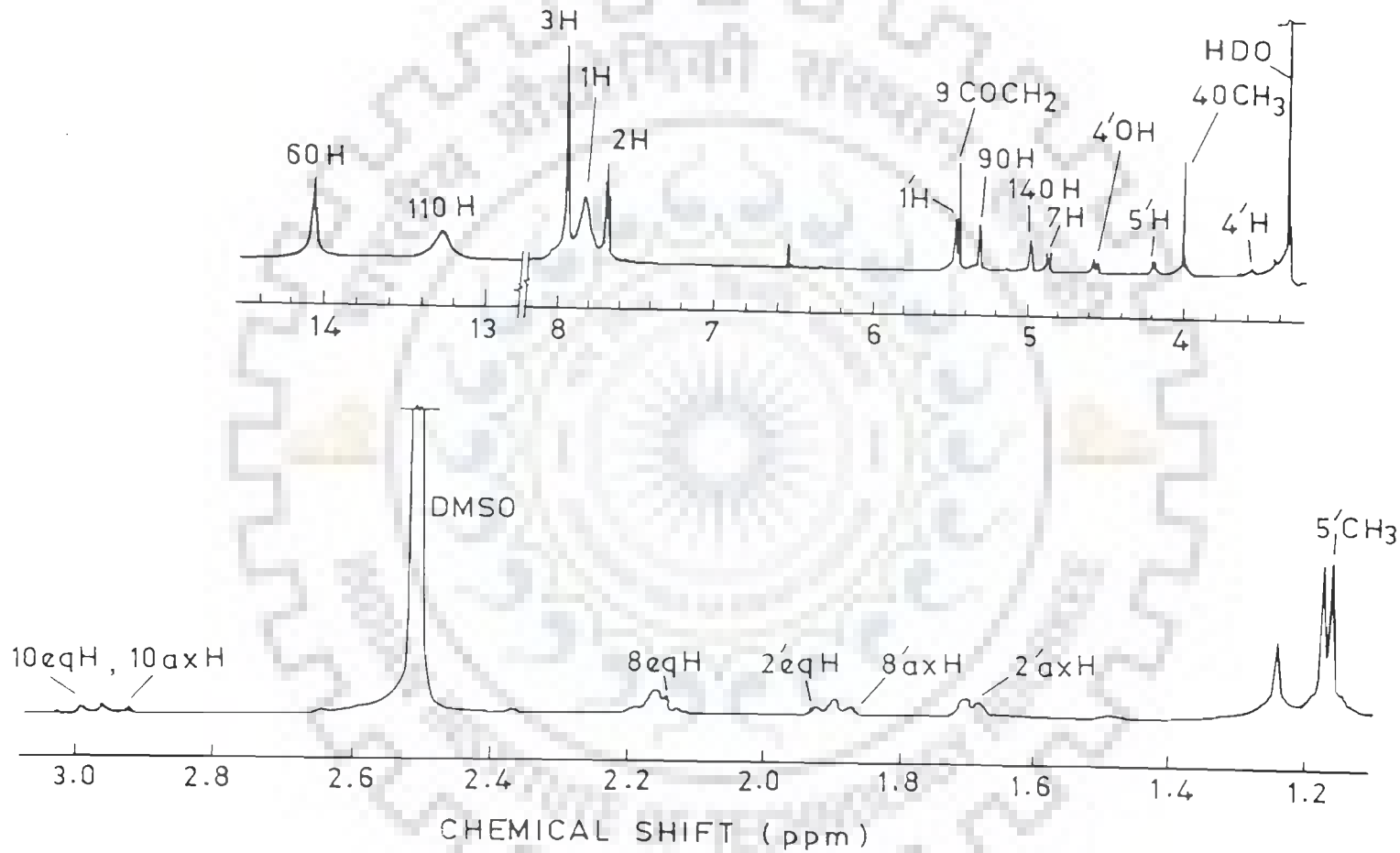

Fig.4.7 : 1D proton NMR spectra of 11.5 mM adriamycin in DMSO at 297 K. DMSO signal is used as an internal reference in all spectra.

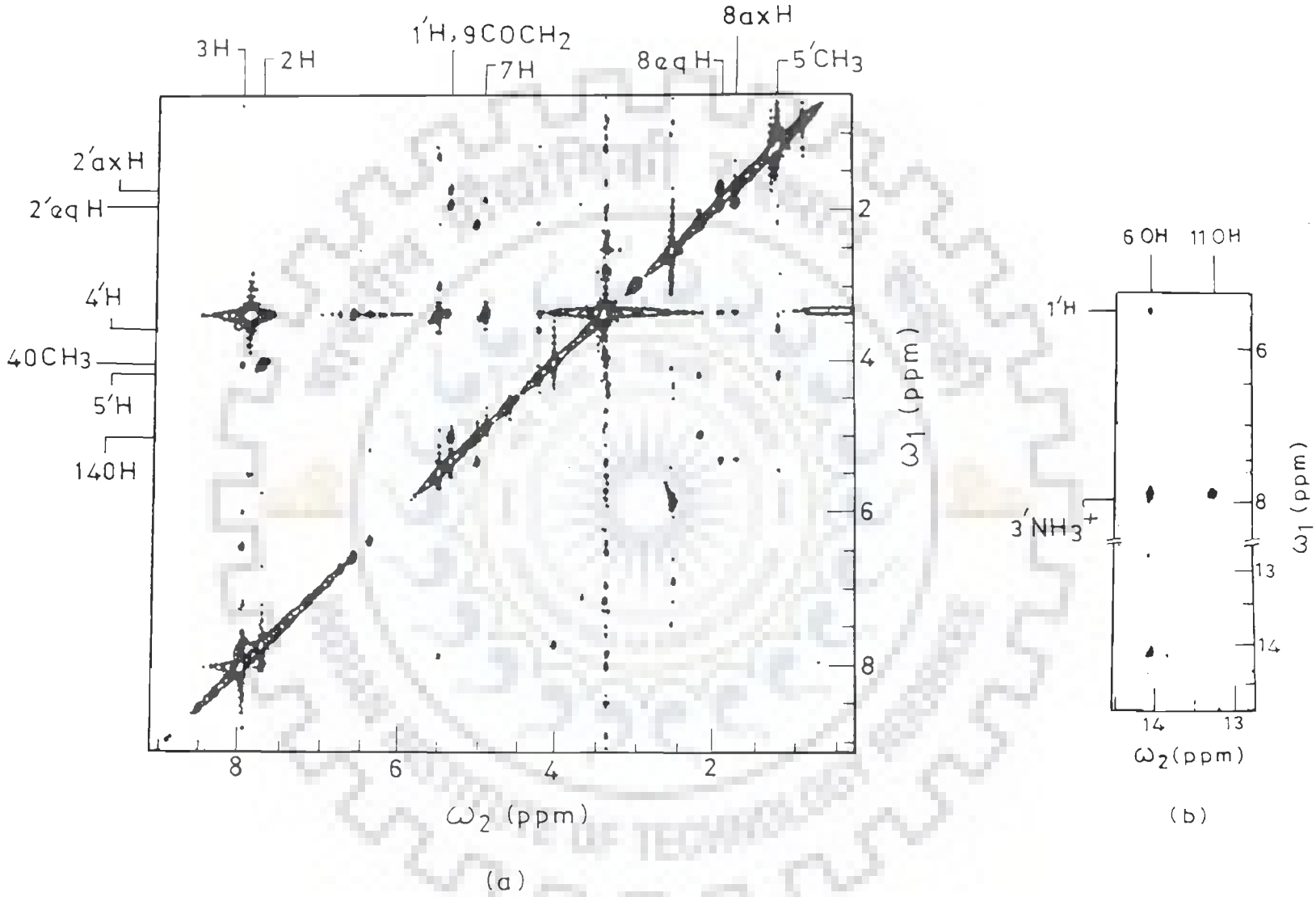

Fig.4.8 : Phase-sensitive NOESY spectrum of 11.5 mM adriamycin in DMSO at 297 K indicating observed NOESY connectivities for pairs of protons : (a) within ring A and ring D and withir daunosamine sugar (b) ring B with daunosamine sugar.

ppm (69). Of these two protons, the resonance at 14.05 ppm gives rise to a NOE cross peak with proton 1'H of the daunosamine sugar unit and is therefore assigned to proton 6OH (69) while the other resonance at 13.03 ppm is assigned to proton 11OH. Further, the 6OH proton gives rise to an NOE cross peak with the $3'NH_3^+$ proton of the daunosamine sugar moiety. The resonance at 4.98 ppm gives an NOE cross peak with the proton resonating at 5.40 ppm which is assigned to the 14OH and $9COCH_2$ protons, respectively. The 4'OH proton and 9OH protons resonate at 4.6 and 5.31 ppm, respectively. The non-exchangeable protons of adriamycin are also observed in spectra recorded in DMSO but they are shifted downfield with respect to their chemical shift positions in D_2O. The chemical shifts of exchangeable and non-exchangeable protons of adriamycin in DMSO solvent are listed in Table 4.5. It is observed that most of the protons resonate at positions close to those reported in the literature (69). Several NOE between pairs of protons observed in D_2O (Fig. 4.4(a, b)) are also seen here (Fig. 4.8(a, b)). Apart from these we observe the additional NOE contacts 6OH-$3'NH_3^+$, 6OH-1'H and 14OH-$9COCH_2$. The NOE cross peaks of 14OH-$9COCH_2$ and 6OH-$3'NH_3^+$ are relatively strong and their distances are estimated as $\simeq$ 2.6 A°. The 6OH-1'H NOE is comparatively weak and corresponds to a distance $\simeq$ 3.0 A°.

CONFORMATION OF ADRIAMYCIN

The present investigation is the first attempt to obtain all the interproton distances. The other investigations in the literature of adriamycin (23,69) gives chemical shift, J values

Table 4.5 : Chemical shift (in ppm) of protons of adriamycin in DMSO at 297 K.

Protons	Chemical shifts	Protons	Chemical shifts
6OH	14.05	4'OH	4.58
11OH	13.03	5'H	4.19
3H	7.94	$4OCH_3$	4.00
1H	7.82	4'H	3.60
2H	7.68	10eqH	2.96
1'H	5.46	10axH	2.96
$9COCH_2$	5.44	8eqH	2.15
9OH	5.31	8axH	1.91
14OH	4.98	2'eqH	1.91
7H	4.97	2'axH	1.70
$5'CH_3$	1.16		

and few interproton distances. We have therefore compared the distances obtained here with those reported for a similar drug, daunomycin, by X-ray crystal structure analysis (78). Several distances obtained by NMR spectroscopy (23,70) for adriamycin in D_2O and n-acetyl daunomycin in $CDCl_3$ solution are also given in Table 4.4.

We find that the distances 1'H-2'axH, 1'H-2'eqH, 4'H-5'H, 5'H-8eqH are nearly the same as those obtained for adriamycin and n-acetyl daunomycin (23,70). However, the distances 7H-8axH and 1'H-7H observed as 3.3 and 3.24 A° are significantly different from the corresponding distances reported in literature (23,70). Further, on irradiating proton 8eqH a very weak NOE signal was observed for proton 5'H suggesting an interproton distance of greater than 4.0 A° (70) whereas we observe the 5'H-8eqH distance to be 2.40 A°. Cirilli et al. (23) observed the 5'H-8eqH distance to be 2.49 A°, which is consistent with our results. This suggests that the positions of hydrogen atoms in adriamycin in the present investigation are not identical to those of n-acetyl daunomycin observed by Mondelli et al. (70).

Comparing our distances with those obtained by X- ray crystal structure analysis (78), we find that most of the interproton distances are similar (within ± 0.5 A°). There are major differences in the distances between the 7H proton and protons 1'H, 3'H, 4'H, 5'H, 8axH; and in the distances 5'H-8axH; 1'H-8eqH; 3'H-8eqH; 4'H-8eqH; 1'H-4'H. It may be noted that three of

these distances i.e. 7H-8axH; 5'H-8axH and 1'H-7H are also found to differ from those reported in literature (23,70). In order to understand how these differences in interproton distances are reflected in the conformation of adriamycin, we have constructed a model of adriamycin by using dreiding stereo model. The rings B, C and D are planar. The carbon and oxygen atoms in ring A and the daunosamine sugar moiety are positioned in such a way that the torsional angles within ring A and the amino sugar are the same as those obtained by Neidle and Taylor (78) from crystal structure analysis. The protons attached to these atoms are then oriented so as to satisfy the observed spin-spin couplings and hence the torsional angles. Finally subtle changes to the positions of various atoms are made so that all interproton distances observed from NOESY spectra are consistent with the model. The torsional angle between 7H-8axH and 7H-8eqH are fixed as 135° and 60-100° with 8axH perpendicular and 8eqH parallel to ring A. Then proton 1'H is placed relative to 7H so that it is at a distance of 3.24 A°. Assuming this position of 1'H, we have fixed the position of 2'axH and 2'eqH using J values of 6.1 and 5.0 Hz and hence torsional angles of 29° and 39°, respectively, and NOEs of 2.31 and 2.28 A°, respectively. Subsequently we have placed 3'H atom relative to 2'axH and 2'eqH; 4'H relative to 3'H; and so on. The glycosidic linkages are readjusted so that the distances of the 7H, 8axH and 8eqH atoms from daunosamine sugar protons agree with the observed distances from NOESY spectra. It is found that it is

possible to arrive at a single specific geometry for the drug molecule. The various torsional angles in the final conformation of the drug thus obtained differ from Neidle's X-ray crystal structure by ± 15° (78). This is in accord with the observation that in the X-ray structure determined for similar drugs such as carminomycin I (91), n-bromoacetyl daunomycin (2) and daunomycin (24), the torsional angles within ring A and the daunosamine sugar moiety differ by 0° and 17°. It has also been found that on complexation of daunomycin with d-CGATCG (71), d-CGTACG (128), d-TGTACA and d-TGATCA (81) the torsional angles within ring A and the daunosamine sugar moiety change by ± 15° and glycosidic linkage differ by ± 25°. Thus it may be presumed that the positions of all carbon and oxygen atoms in adriamycin and related drugs do not differ very much. Further, all these structures correspond to a minimum energy conformation. The position of hydrogen atoms are however quite different in the solution structure and are best known directly from NOESY spectra as shown in the present investigations. It may be noted that the torsional angles , ϕ, ψ defined as H1'-C1'-O7-C7 and C1'-O7-C7-H7 in n-acetyl daunomycin in $CDCl_3$ were found to be 40° and 0° (70) as compared to the corresponding crystal structure value of 41° and 18° (2) suggesting that position of hydrogen atoms is different in these two structures. This observation corroborates our results. Thus we arrive at a solution conformation specified by the spin-spin couplings and interproton distances derived from NOE contacts while the positions of C, N, O and other

atoms is dictated by bond angle and bond distance constraints as in X-ray structure analysis. The present study has direct implications on the binding action of the drug and hence its anticancer action.

CONFORMATION OF DEOXYHEXANUCLEOTIDE d-$(CGATCG)_2$

SEQUENTIAL ASSIGNMENT

The conformation of deoxyhexanucleotide d-$(CGATCG)_2$ is investigated in D_2O by proton NMR at 500 MHz. 1D proton NMR spectra of 2.98 mM (duplex concentration) d-$(CGATCG)_2$ are recorded at varying temperatures in the range of 277-325 K. Fig. 5.1(a-d) and Fig. 5.2(a-d) show expansions of specific regions of one-dimensional NMR spectrum at 295 and 325 K, respectively. The stack plot of one-dimensional spectrum of d-$(CGATCG)_2$ at different temperatures, in the range 277-325 K is shown in Fig. 5.3(b).

The bases in hexanucleotide, d-$(CGATCG)_2$ are numbered from 5′-3′ end as follows :

```
          1 2 3 4 5 6
    5′  d-C G A T C G   3′
    3′    G C T A G C   5′
```

Fig. 5.1(a) shows resonances of non-exchangeable ring protons H2, H8 and H6 of bases appearing in the region of aromatic protons in the range 7.2 - 8.5 ppm. The triplets of all six deoxyribose sugar H1′ protons along with a pair of CH5 protons resonate in the range of 5.6 - 6.3 ppm (Fig. 5.1(b)). However, the triplets of all

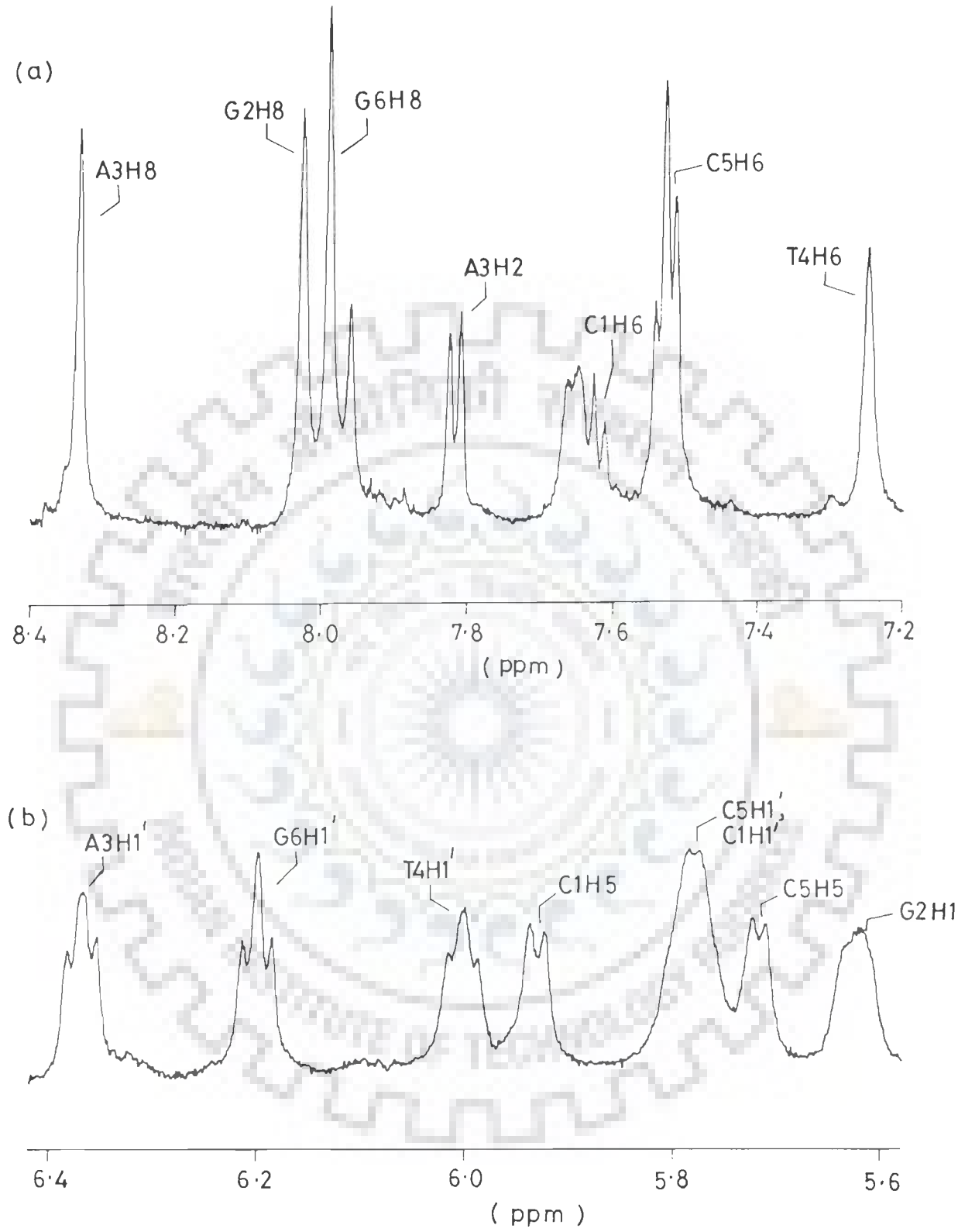

Fig. 5.1(a,b) : 1D proton NMR spectra of d-$(CGATCG)_2$ in D_2O at 295 K. (a) Base protons of all residues. (b) H1′ of all residues along with C1H5 and C5H5.

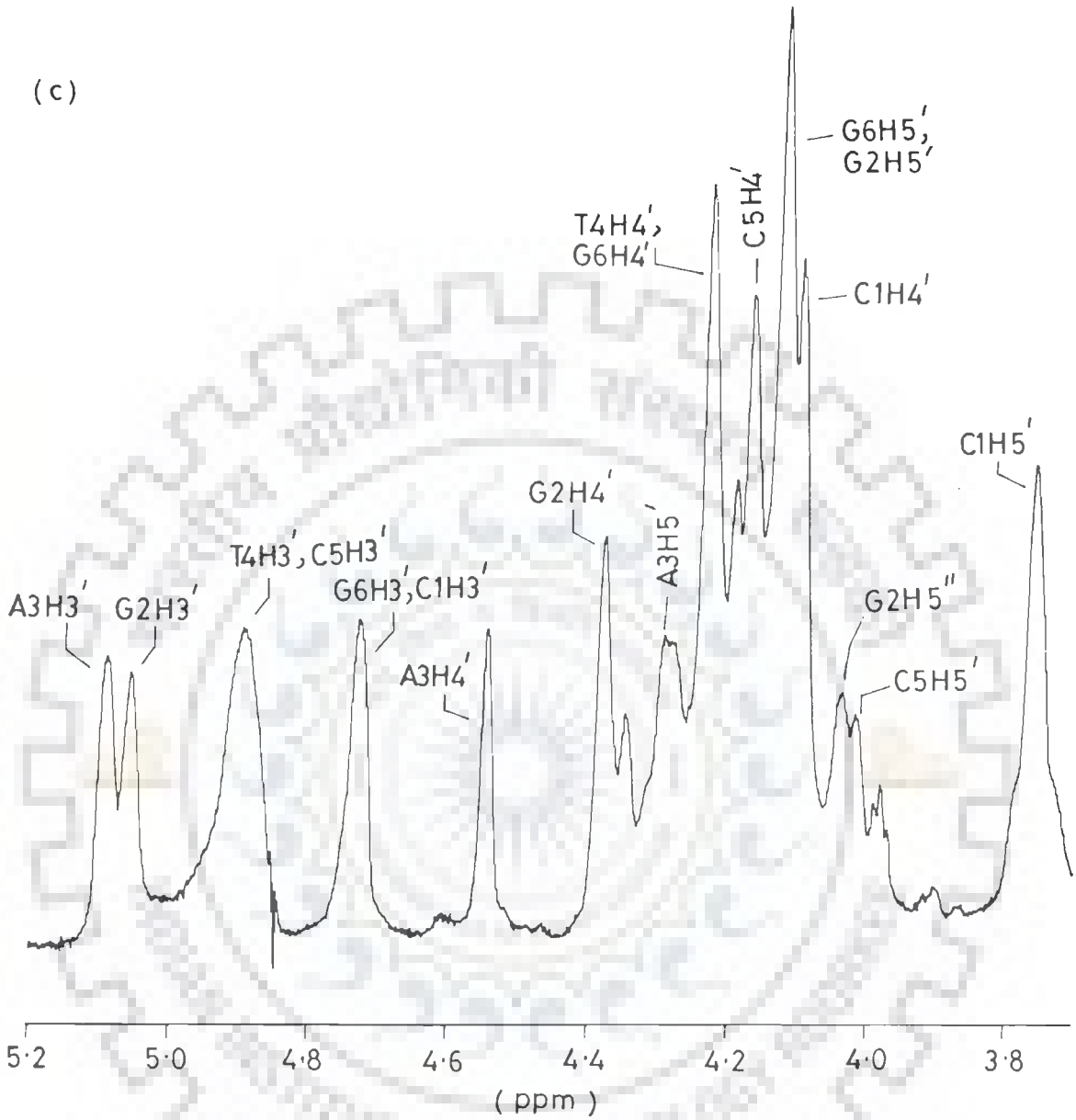

Fig. 5.1(c) : Expanded portion of 1D proton NMR spectra showing H3′, H4′, H5′ and H5" resonances of d-$(CGATCG)_2$ at 295 K in D_2O.

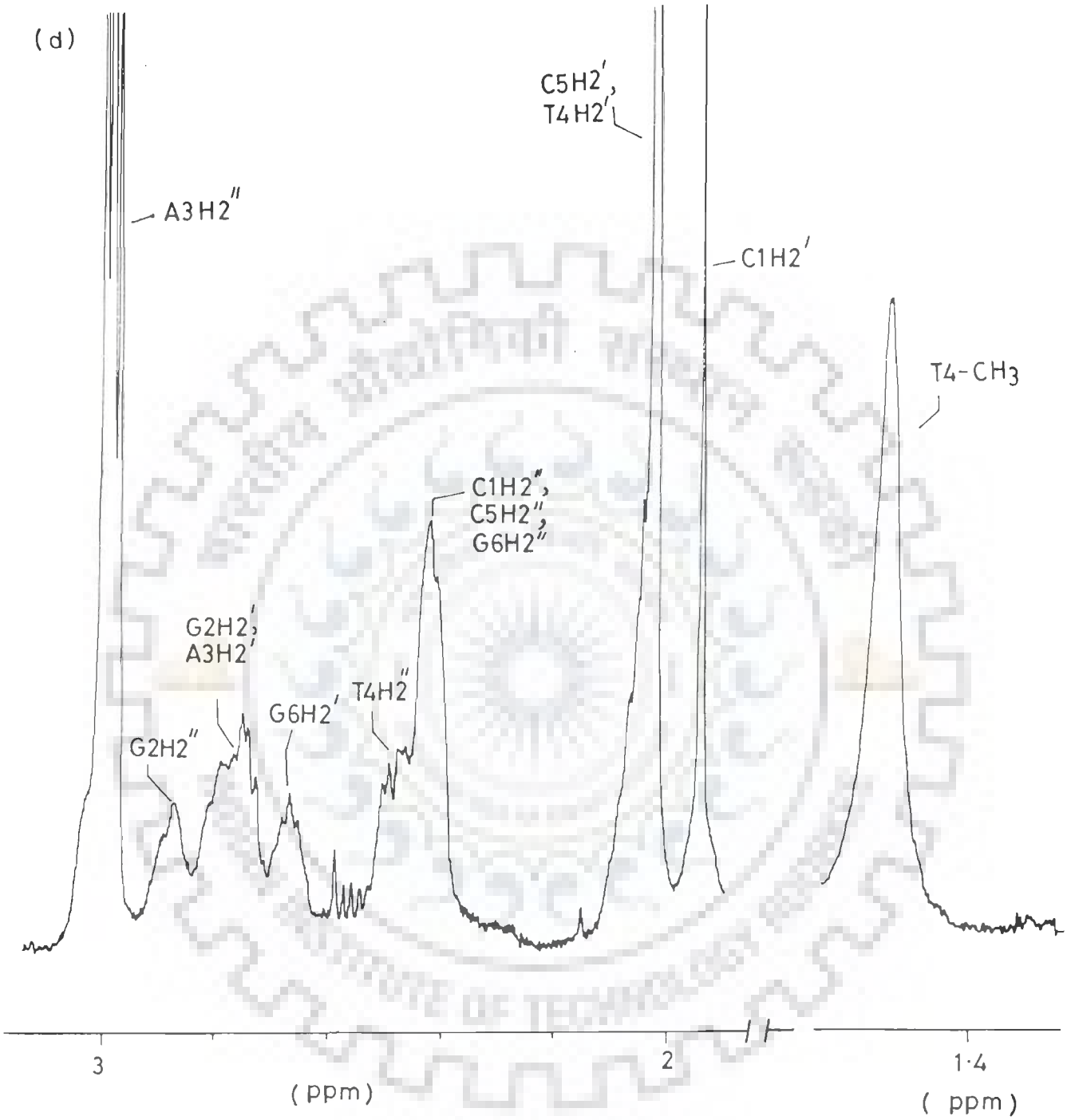

Fig. 5.1(d) : Expanded portion of 1D proton NMR spectra showing H2', H2" and CH_3 protons of d-$(CGATCG)_2$ at 295 K in D_2O.

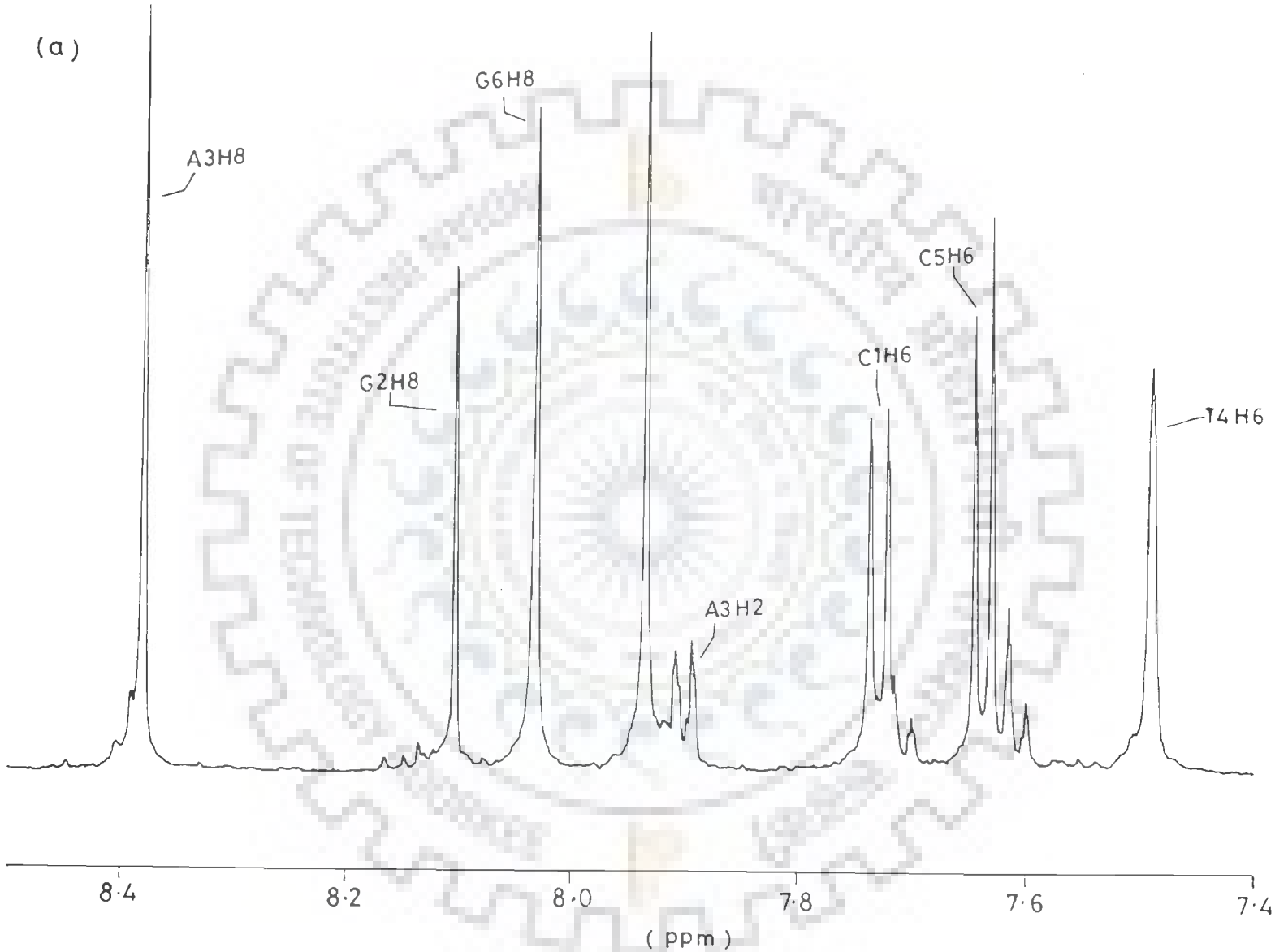

Fig. 5.2(a) : Expanded portion of 1D proton NMR spectra of d-$(CGATCG)_2$ in D_2O at 325 K showing base protons of all residues.

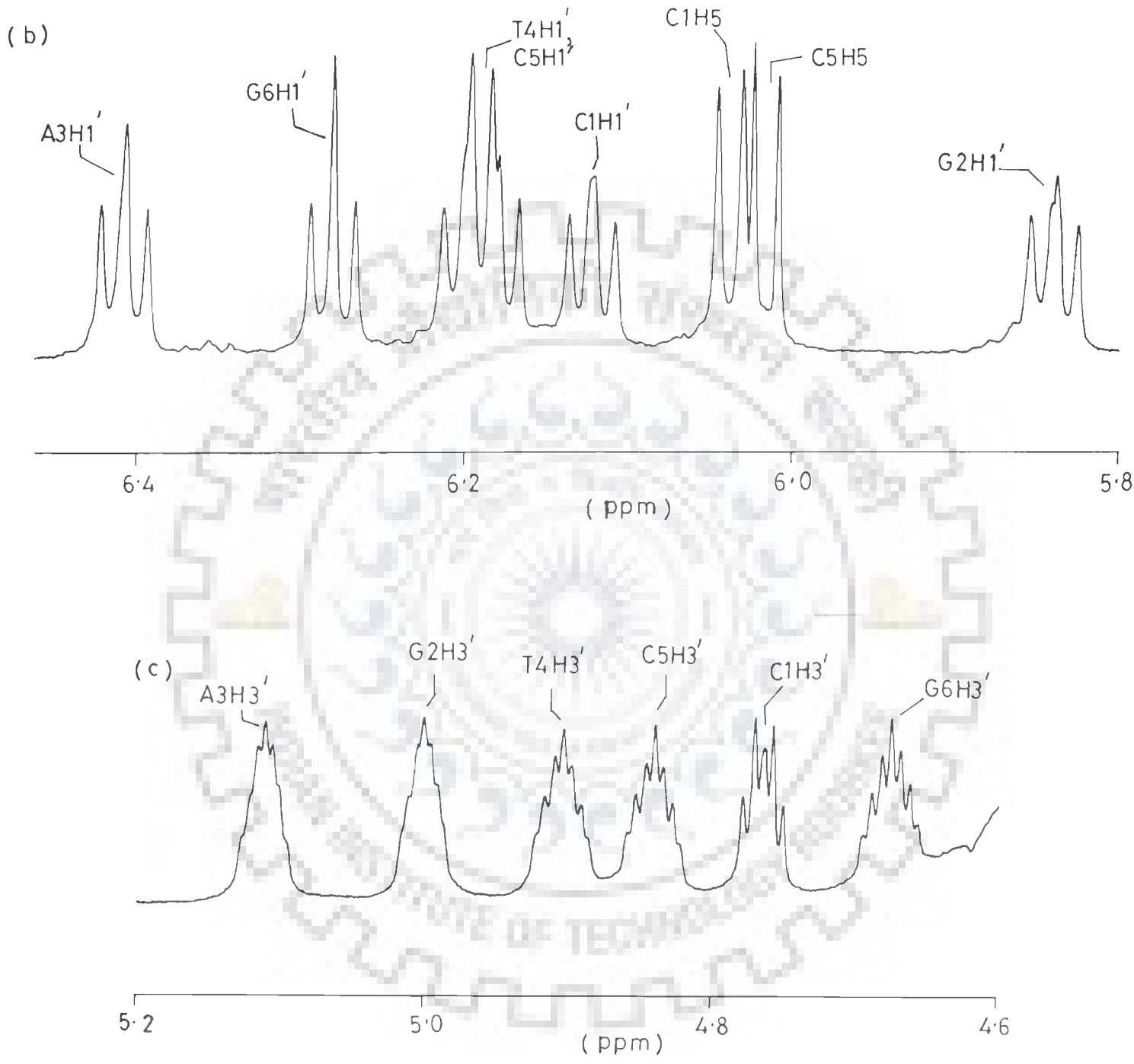

Fig. 5.2(b,c) : Proton NMR spectra of d-$(CGATCG)_2$ at 325 K showing H1', H3' resonances of all residues along with C1H5 and C5H5.

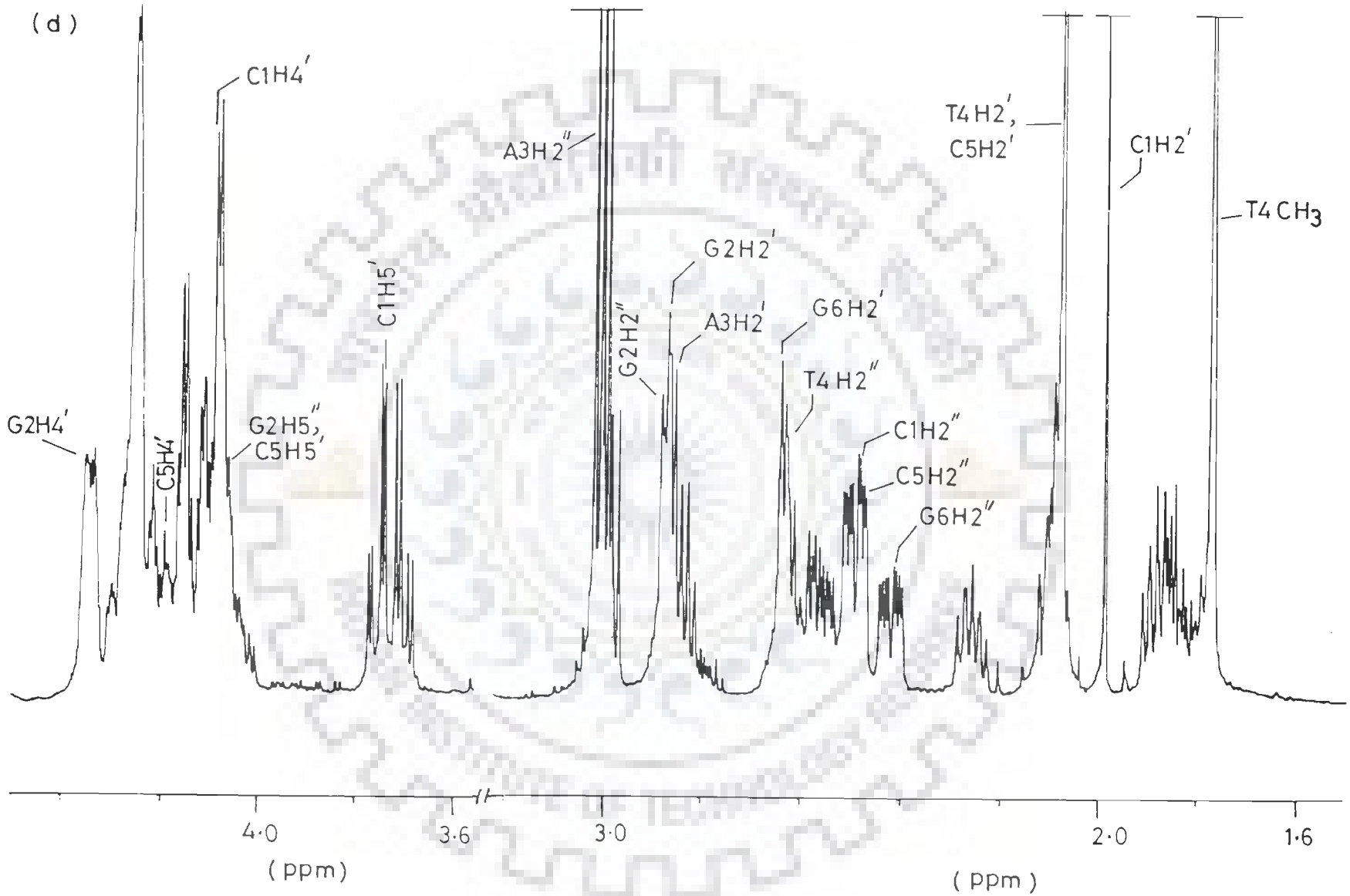

Fig. 5.2(d) : Expanded portion of proton NMR spectra of d-$(CGATCG)_2$ at 325 K showing H4′, H5′, H5", H2′, H2" and CH_3 protons.

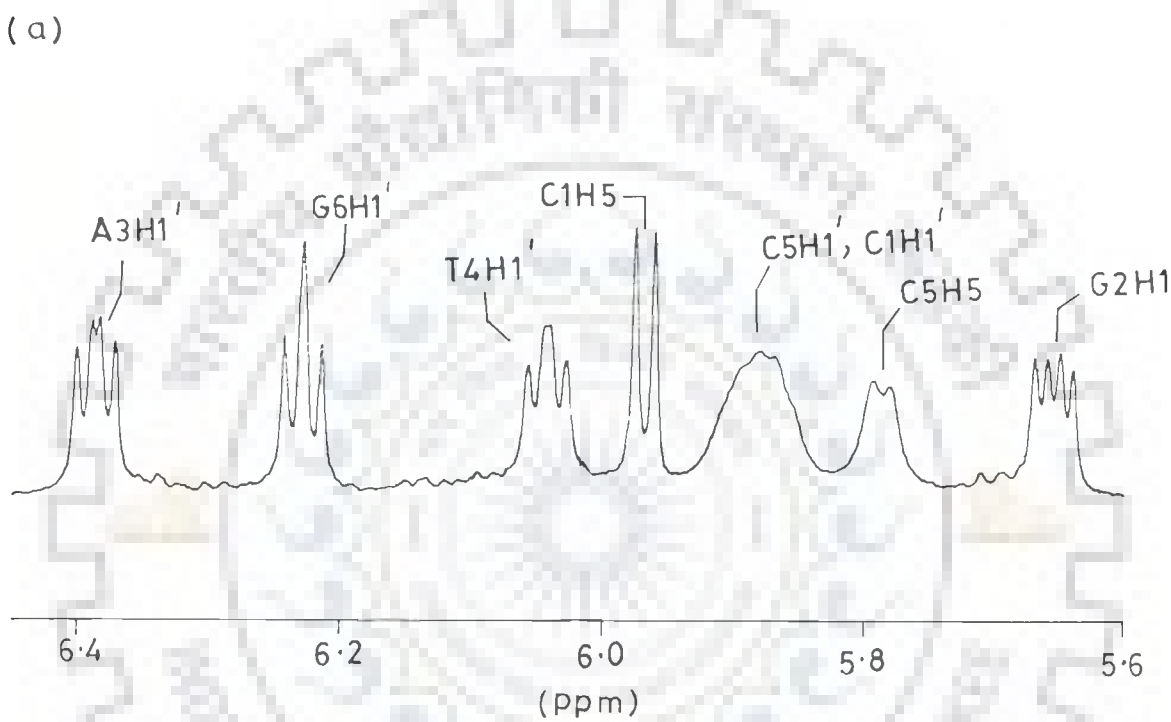

Fig. 5.3(a) : Expanded portion of proton NMR spectra of d-$(CGATCG)_2$ at 305 K showing H1' and CH5 protons of all residues.

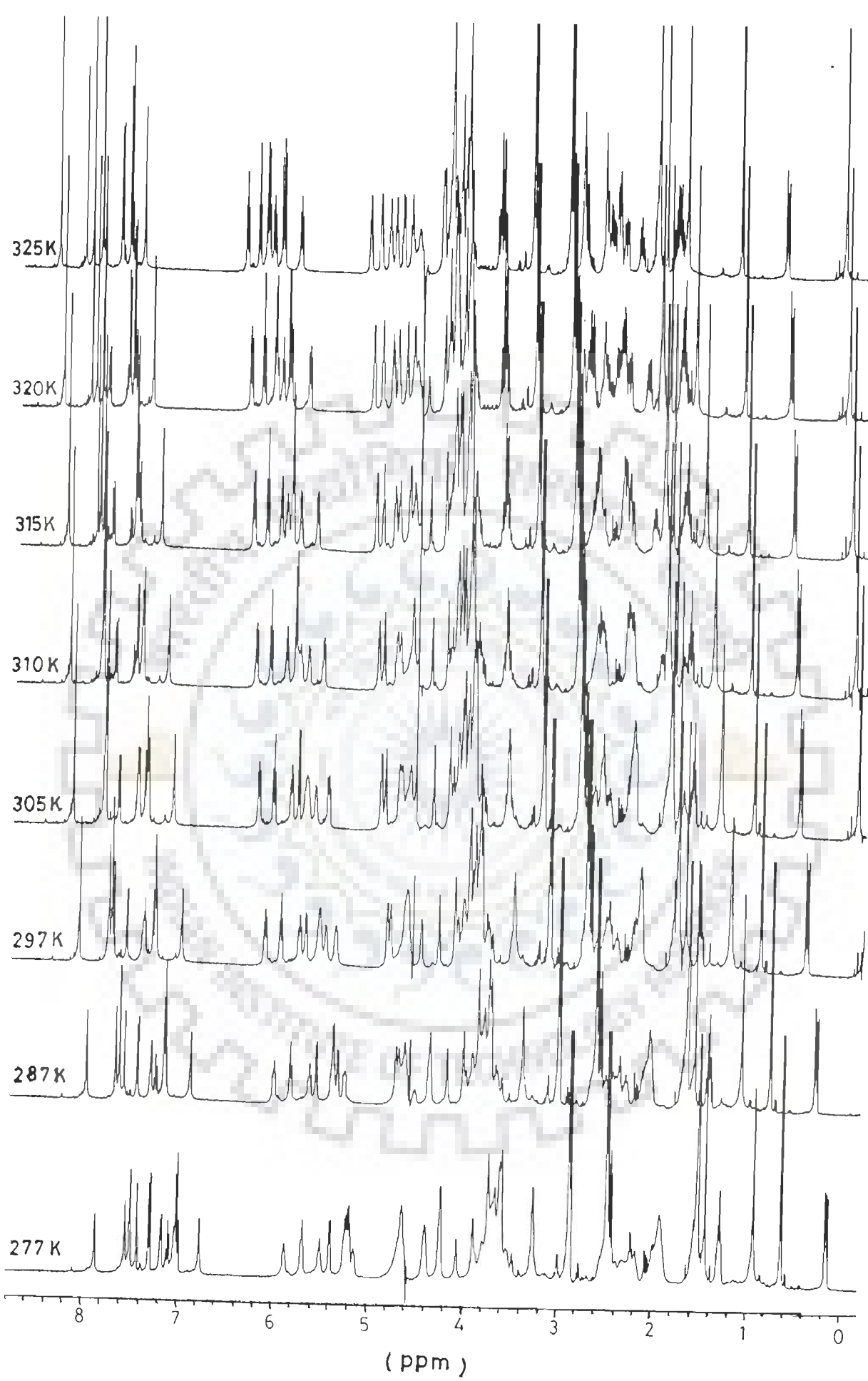

Fig. 5.3(b) : Stack plot of 1D proton NMR spectra of d-$(CGATCG)_2$ recorded with varying temperatures in the range 277-325 K.

sugar H1′ are not resolved at room temperature. At 325 and 305 K triplets of all six H1′ (Fig. 5.2(b) and 5.3(a)) are clearly seen. These give valuable information about J(H1′-H2′), J(H1′-H2") and ΣH1′, used later for deducing the conformation of sugar. The sugar H3′, H4′, H5′/H5" protons resonate in the region 3.4 - 5.2 ppm (Fig. 5.1(c)), while H2′, H2" protons resonate between 1.9 - 3.1 ppm. The aliphatic CH_3 proton resonance occur in the region 1.2 - 1.6 ppm (Fig. 5.1 (d)). It is evident from Fig. 5.2 (a-d) that all sugar and base protons are more resolved at 325 K. It is observed that most of the resonances of d-$(CGATCG)_2$ shift gradually with increase in temperature (Fig. 5.3(b)). This is due to duplex to strand transition of d-$(CGATCG)_2$ affected by an increase in temperature, which is manifested as downfield shift of proton resonances. On increasing the temperature, sharpening of all nucleotide resonances are observed. The chemical shifts of various nucleotide protons over the entire temperature range are listed in Table 5.1. Fig. 5.4 shows the plot of chemical shift of some of the nucleotide protons as a function of temperature. Large changes in chemical shifts, $\Delta\delta$, due to increase in temperature are observed for T4H6, C5H5, C1H5 and C5H6 protons, being $\simeq$ 0.30, 0.41, 0.22 and 0.22 ppm, respectively (Table 5.1). These changes are quite pronounced for C1H1′, C5H1′, T4H1′ and G2H1′ protons as well, since being close to the aromatic ring they experience ring current effects to a large extent. Mid point transition, T_m value, calculated from curves of GH8, AH8, CH5 and CH6 protons is in the range 306 to 311 K. Thus, it may be assumed that a major

Table 5.1 : Chemical shifts (in ppm) of protons of d-$(CGATCG)_2$ with varying temperature in D_2O.

Temp. (K)	C1H6	C1H5	G2H8	A3H8	A3H2	T4H6	$T4CH_3$	C5H6
277	7.59	5.82	7.97	8.29	7.70	7.19	1.36	7.42
287	7.64	5.90	8.01	8.32	7.77	7.23	1.42	7.49
295	7.64	5.93	8.03	8.33	7.81	7.25	1.46	7.52
297	7.62	5.93	8.01	8.32	7.81	7.24	1.46	7.52
305	7.66	5.97	8.02	8.34	7.85	7.28	1.52	7.56
310	7.65	5.98	8.02	8.35	7.86	7.32	1.57	7.58
315	7.64	5.99	8.05	8.36	7.88	7.37	1.63	7.62
320	7.68	6.00	8.08	8.37	7.89	7.43	1.71	7.64
325	7.73	6.04	8.10	8.38	7.89	7.49	1.79	7.64

Temp. (K)	C5H5	G6H8	C1H1'	G2H1'	A3H1'	T4H1'	C5H1'	G6H1'
277	5.61	7.93	5.65	5.56	6.29	5.92	5.65	6.11
287	5.68	7.97	5.72	5.60	6.34	5.97	5.72	6.17
295	5.72	7.99	5.79	5.62	6.37	6.00	5.79	6.20
297	5.72	7.98	5.79	5.62	6.36	6.00	5.79	6.20
305	5.79	8.00	5.88	5.65	6.39	6.04	5.88	6.23
310	5.84	8.01	5.93	5.68	6.39	6.07	5.93	6.24
315	5.90	8.01	6.03	5.72	6.39	6.10	6.03	6.25
320	5.98	8.02	6.07	5.78	6.40	6.14	6.12	6.27
325	6.02	8.03	6.12	5.84	6.41	6.19	6.19	6.28

Temp. (K)	C1H2′	G2H2′	A3H2′	T4H2′	C5H2′	G6H2′	C1H2"	G2H2"
277	1.87	2.64	2.64	1.95	1.95	2.60	2.36	2.74
287	1.91	2.78	2.71	2.02	2.02	2.65	2.40	2.85
295	1.94	2.75	2.75	2.05	2.05	2.67	2.43	2.87
297	1.94	2.77	2.77	2.05	2.05	2.66	2.42	2.86
305	1.96	2.77	2.77	2.07	2.07	2.70	2.44	2.85
310	1.97	2.78	2.76	2.08	2.08	2.75	2.47	2.81
315	1.98	2.76	2.75	2.09	2.09	2.74	2.48	2.80
320	1.98	2.83	2.80	2.09	2.09	2.69	2.49	2.90
325	1.99	2.87	2.82	2.09	2.09	2.63	2.49	2.88

Temp. (K)	A3H2"	T4H2"	C5H2"	G6H2"	C1H3′	G2H3′	A3H3′	T4H3′
277	2.92	2.40	2.36	2.36	4.49	4.82	4.82	4.66
287	2.94	2.45	2.40	2.40	4.71	5.04	5.07	4.97
295	2.98	2.50	2.43	2.43	4.73	5.06	5.09	4.90
297	2.98	2.49	2.42	2.42	4.72	5.05	5.08	4.88
305	3.00	2.50	2.44	2.44	4.79	5.06	5.11	4.90
310	3.00	2.50	2.45	2.44	4.76	5.05	5.11	4.91
315	3.00	2.49	2.44	2.41	4.76	5.03	5.11	4.90
320	3.01	2.53	2.45	2.40	4.76	5.02	5.11	4.91
325	3.01	2.60	2.48	2.41	4.77	5.00	5.11	4.90

Temp (K)	C5H3′	G6H3′	C1H4′	G2H4′	A3H4′	T4H4′	C5H4′	G6H4′
277	4.66	4.49	4.02	4.29	4.32	4.16	4.09	4.16
287	4.97	4.71	4.07	4.36	4.53	4.21	4.14	4.21
295	4.90	4.73	4.10	4.38	4.55	4.23	4.17	4.23
297	4.88	4.72	4.11	4.37	4.54	4.22	4.16	4.22
305	4.88	4.79	4.12	4.39	4.55	4.24	4.21	4.24
310	4.89	4.75	4.12	4.39	4.55	4.25	4.21	4.25
315	4.86	4.72	4.12	4.37	4.54	4.24	4.22	4.24
320	4.85	4.69	4.11	4.36	4.53	4.26	4.22	4.26
325	4.84	4.68	4.09	4.34	0	0	4.20	0

Temp. (K)	C1H5′	G2H5′	A3H5′	G6H5′	C1H5"	G2H5"
277	3.69	4.04	4.22	4.04	3.41	3.97
287	3.74	4.10	4.27	4.10	3.47	4.02
295	3.76	4.12	4.29	4.12	3.50	4.04
297	3.75	4.12	4.28	4.12	3.48	4.03
305	3.77	4.15	4.28	4.15	3.50	4.06
310	3.77	4.15	4.28	4.15	3.50	4.06
315	3.76	4.15	4.28	4.15	3.50	4.05
320	3.75	4.15	4.32	4.15	3.49	4.06
325	3.71	4.12	0	4.12	3.50	4.09

0 : Overlap.

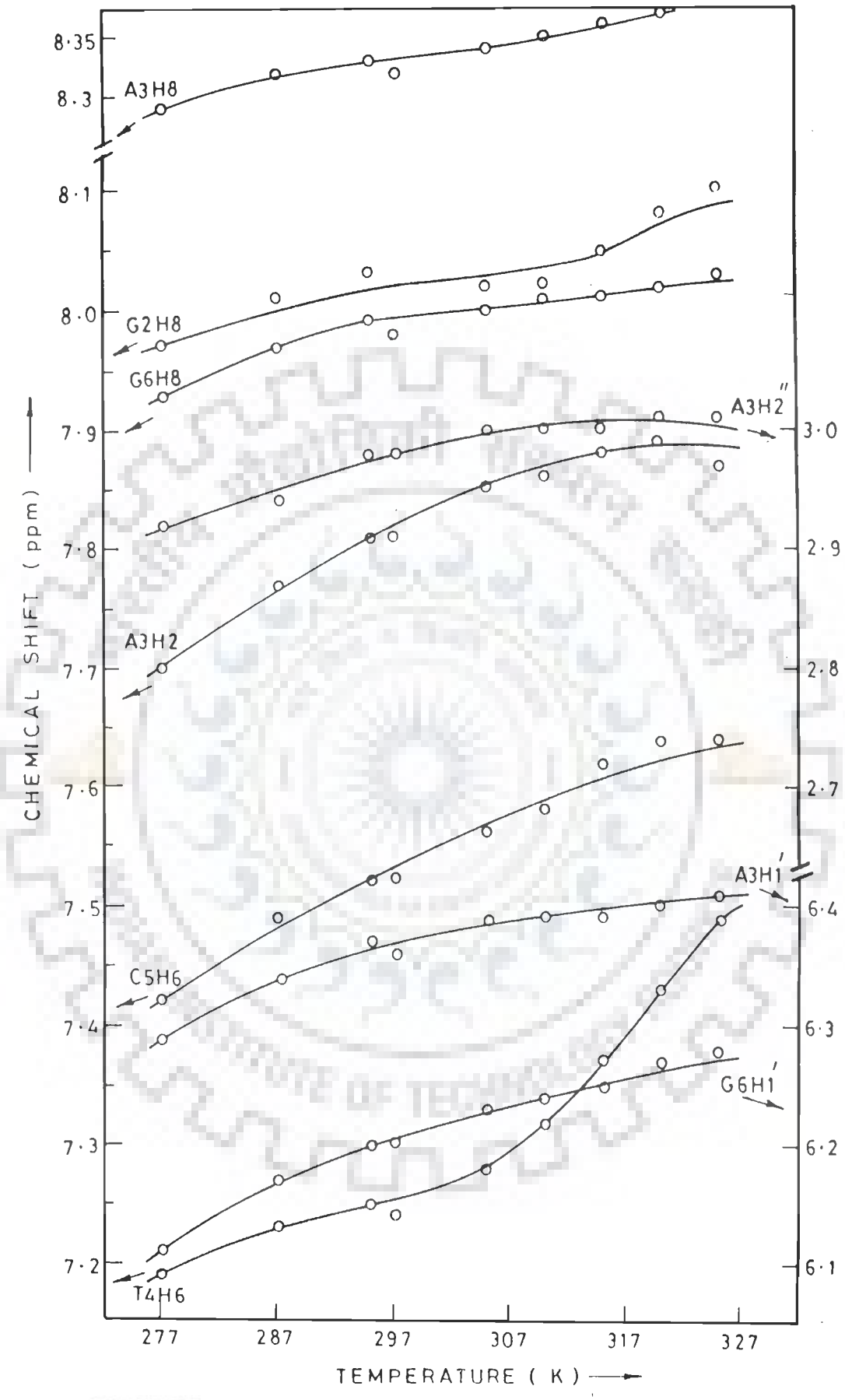

Fig. 5.4 : Chemical shift of various protons of d-$(CGATCG)_2$ as a function of temperature in the range 277-325 K.

fraction of d-$(CGATCG)_2$ is in double-helical state at room temperature.

The sequence specific assignment of various protons to a specific residue is achieved with the help of two-dimensional NMR experiments. The 2D phase-sensitive double-quantum filtered COSY (DQF - COSY) and NOESY spectra recorded at τ_m 75, 150, 200 and 250 ms are shown in Fig. 5.5(a-i) and 5.6(a-j), respectively along with expansions of certain regions to highlight specific connectivities. The chemical shifts, δ (in ppm), of various protons of d-$(CGATCG)_2$ at 295 K are presented in Table 5.2.

All the six sets of deoxyribose sugar protons are assigned using DQF-COSY spectra. The H2′ and H2" protons show strong geminal coupling (^2J) with each other. Fig. 5.5(b,c) shows six pairs of H2′ - H2" sugar protons. The H2′, H2" protons are coupled to their corresponding H1′ and H3′ protons. Fig. 5.5(d-f) shows six sets of H1′ - H2′, H2" and H3′ - H2′, H2" cross peaks. These H3′ protons are coupled to their corresponding H4′ protons. The H4′ protons are coupled to H5′ protons which are further coupled to H5" protons (Fig. 5.5(g)). The CH5 and CH6 protons of cytosine are coupled through three bonds (^3J), giving a cross peak in COSY spectra. A pair of CH5-CH6 cross peak is evident in Fig. 5.5(h). The thymine base proton T4H6 is also coupled to $T4CH_3$ proton and is shown in Fig. 5.5(i). The sets of sugar protons identified in DQF-COSY spectra are assigned to specific residues of d-$(CGATCG)_2$

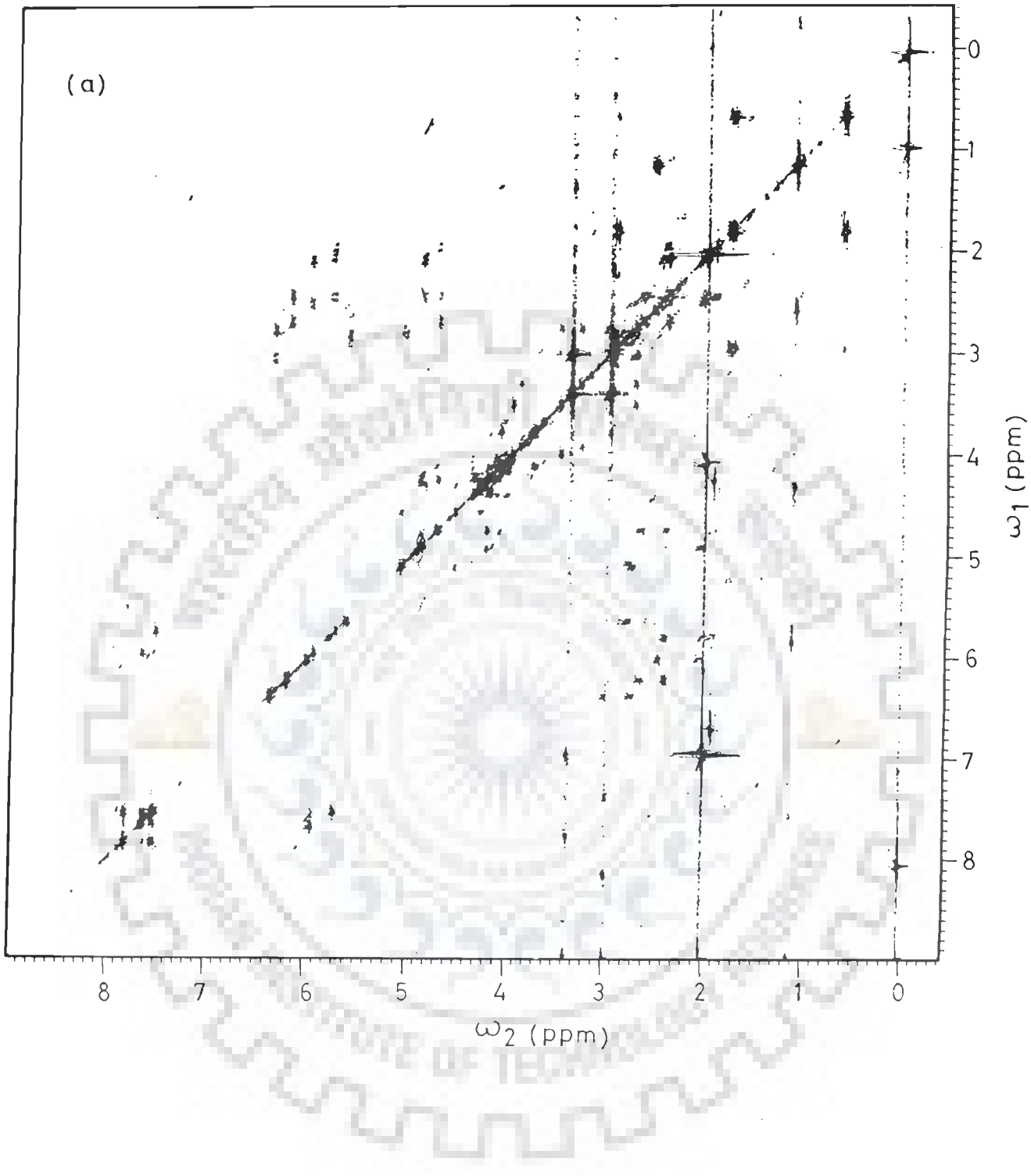

Fig. 5.5(a) : Phase-sensitive double quantum filter COSY spectrum of d-$(CGATCG)_2$ at 295 K in D_2O.

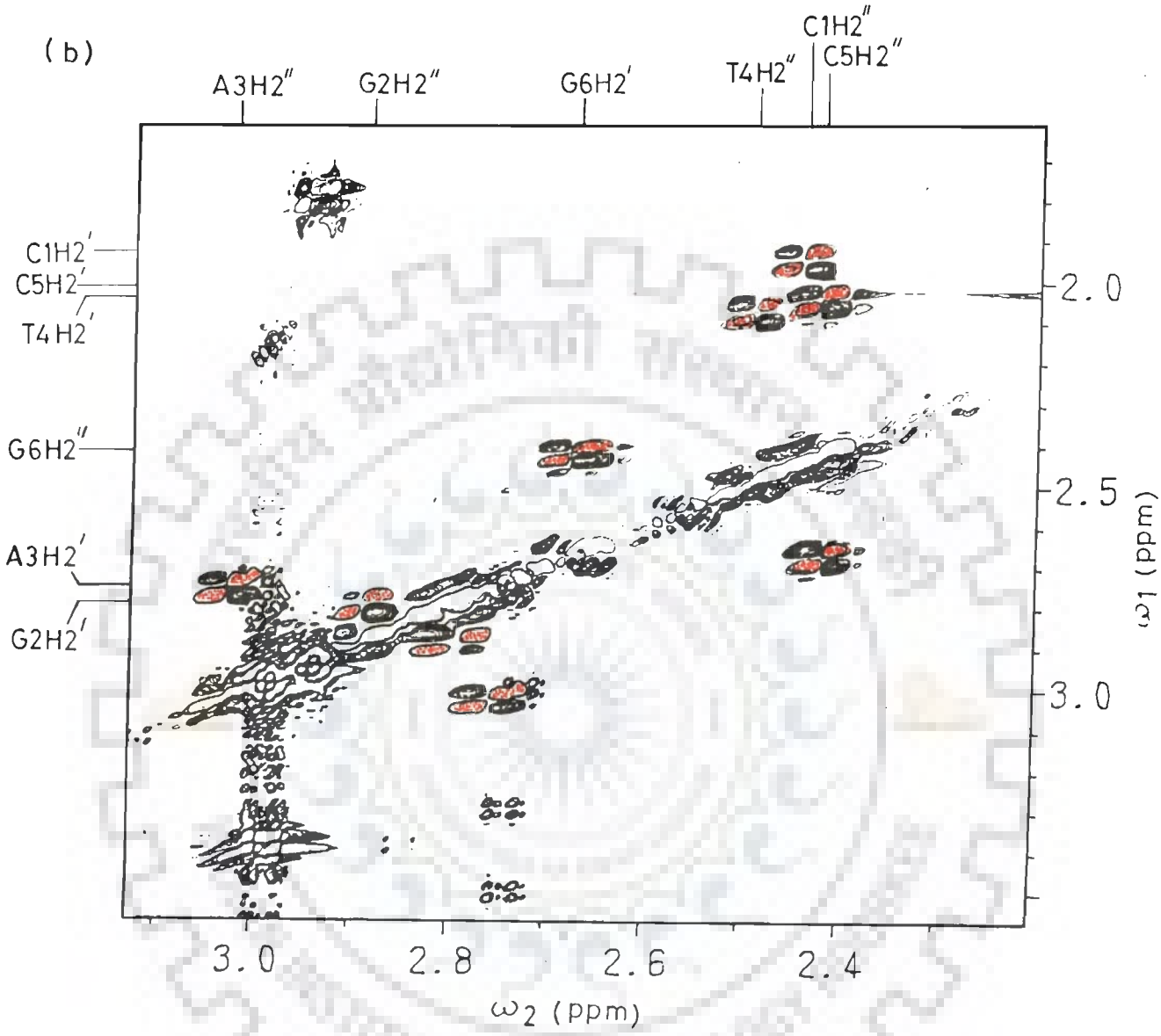

Fig. 5.5(b) : Expanded portion of phase-sensitive double quantum filter COSY spectrum of d-$(CGATCG)_2$ showing H2′-H2" connectivities.

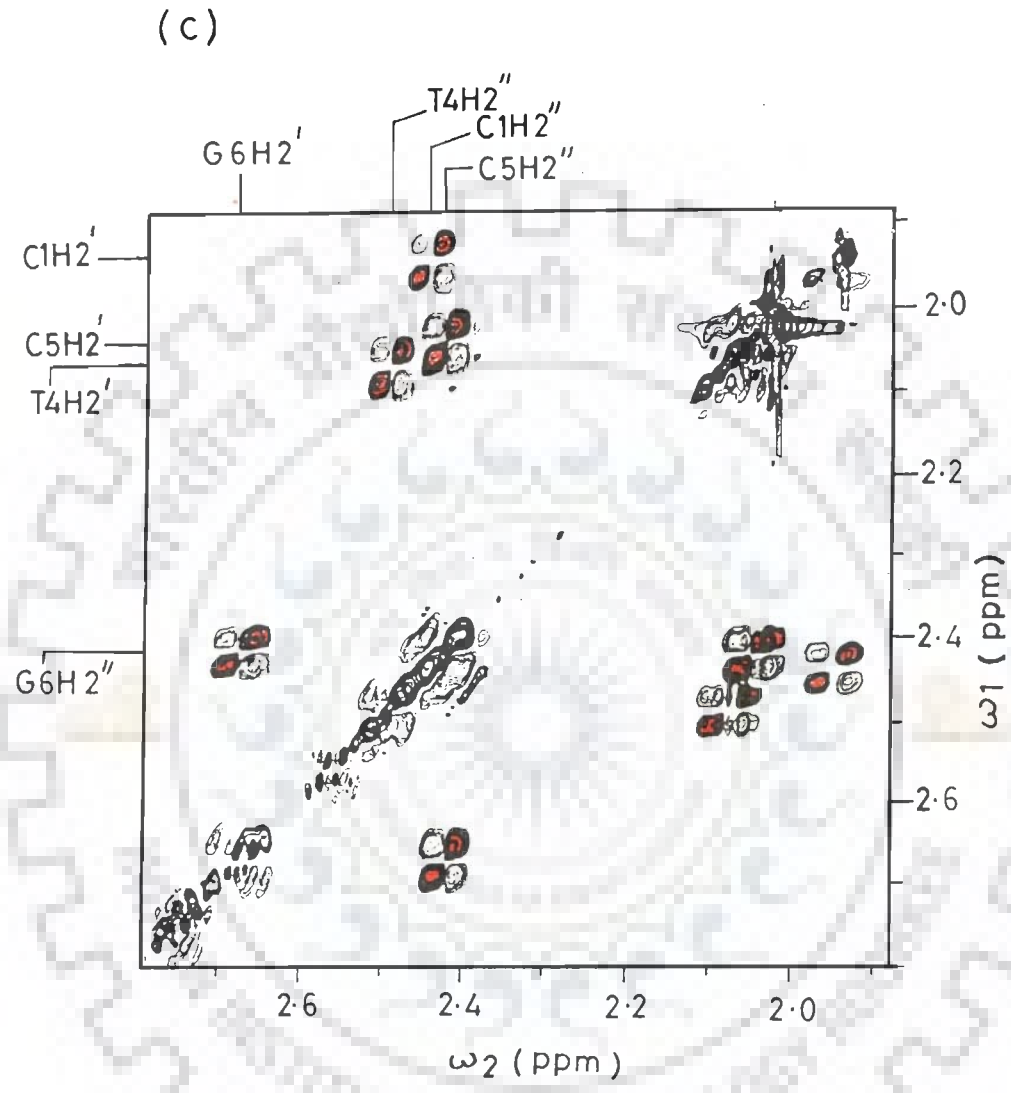

Fig. 5.5(c) : Expanded portion of phase-sensitive double quantum filter COSY spectrum of d-$(CGATCG)_2$ highlighting specific H2'-H2" connectivities.

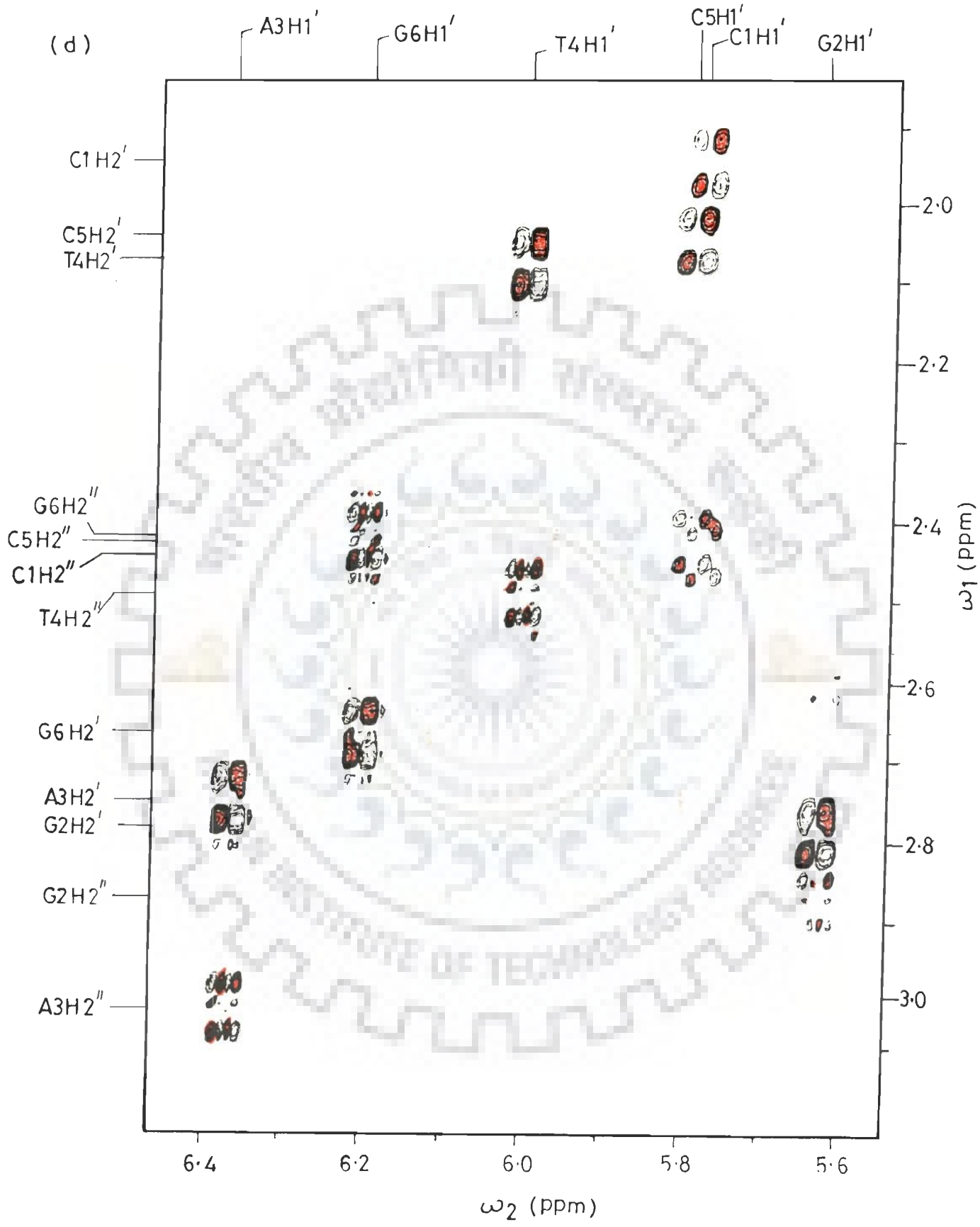

Fig. 5.5(d) : Portion of phase-sensitive double quantum filter COSY spectrum of d-$(CGATCG)_2$ showing H1′-H2′, H2" connectivities.

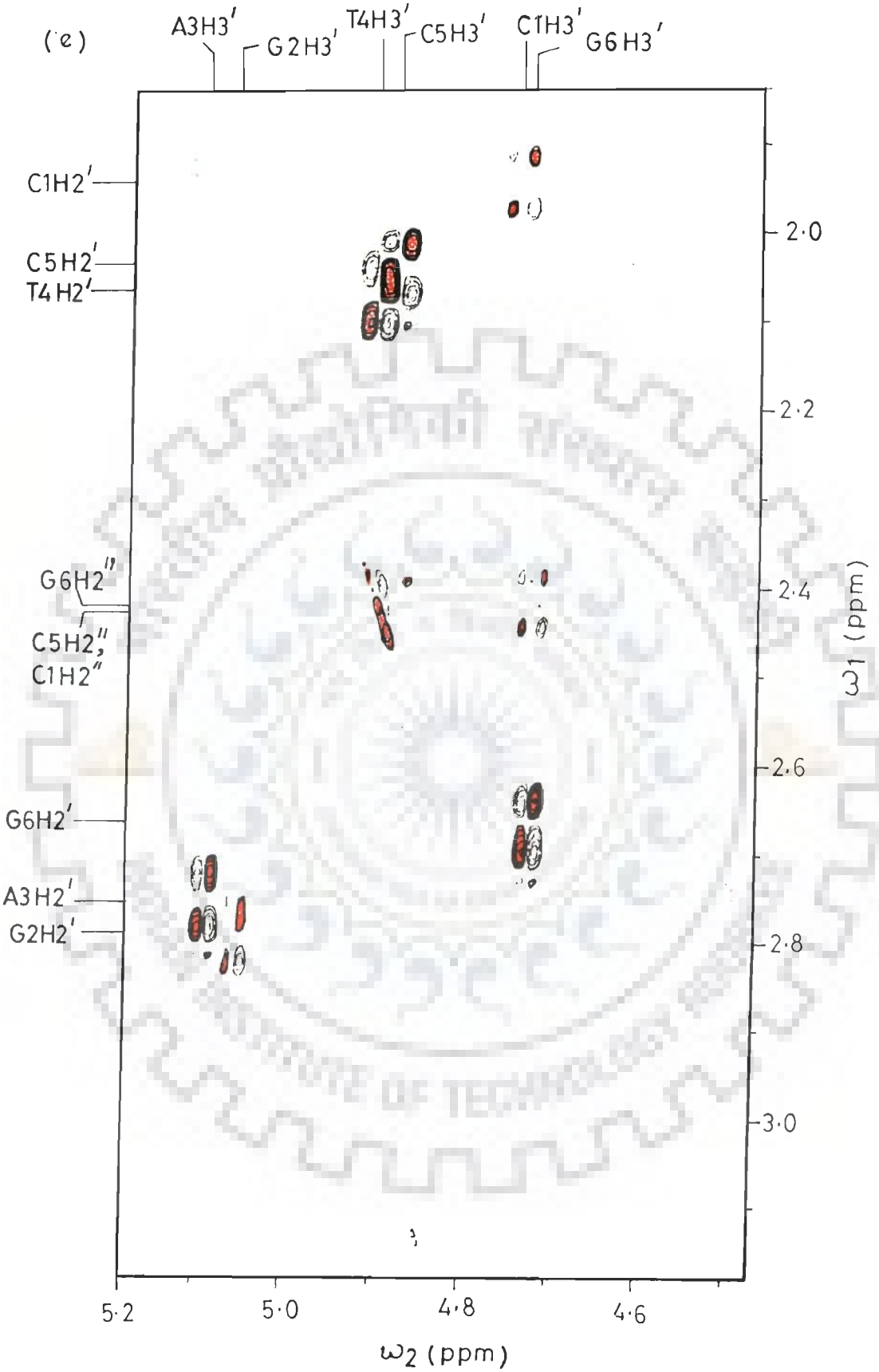

Fig. 5.5(e) : Expanded region of phase-sensitive double quantum filter COSY spectrum of d-$(CGATCG)_2$ showing H3′-H2′, H2" connectivities.

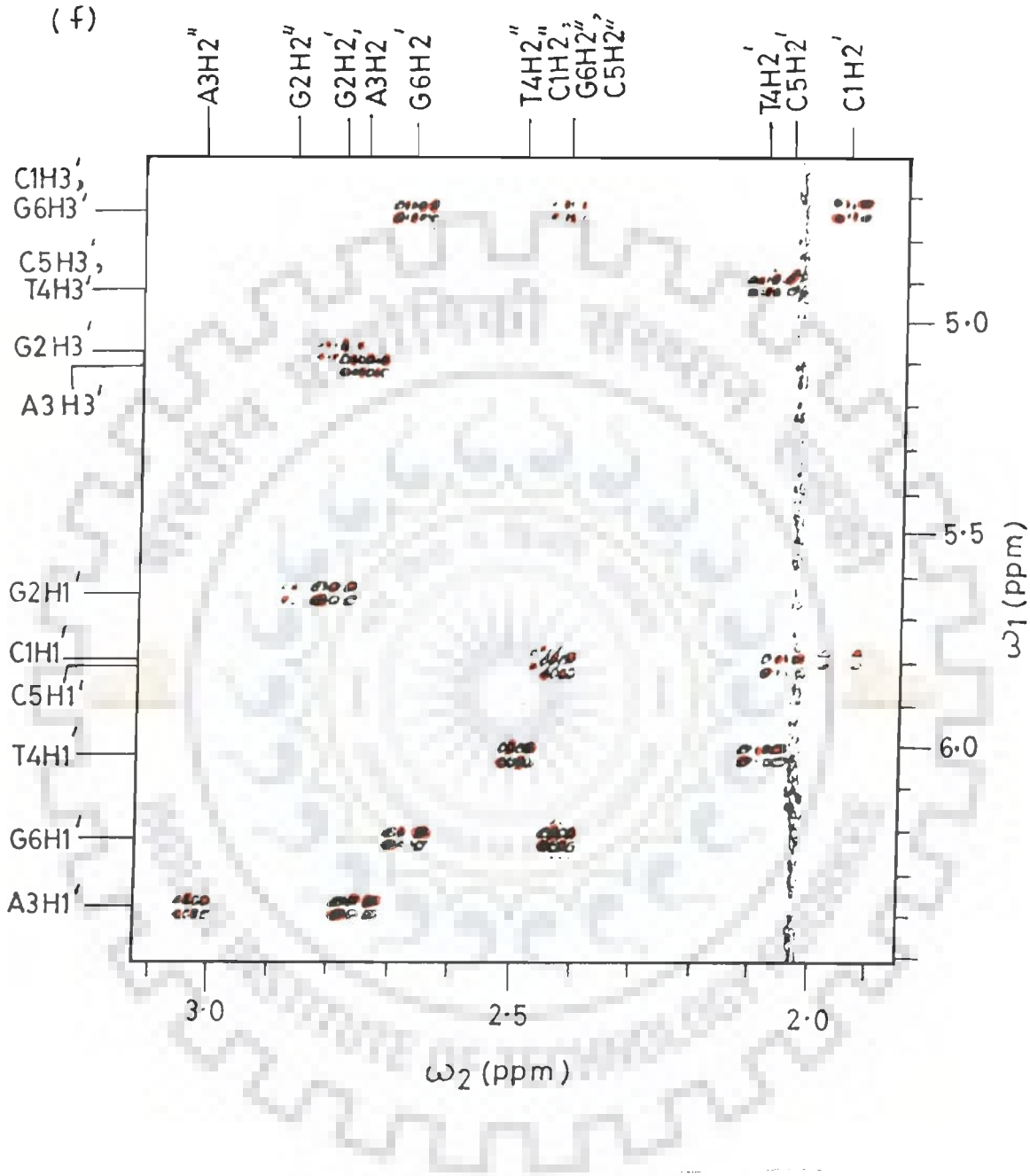

Fig. 5.5(f) : Expanded portion of phase-sensitive double quantum filter COSY spectrum of d-$(CGATCG)_2$ showing cross peak patterns of H1'-H2', H2" and H3'-H2', H2" connectivities.

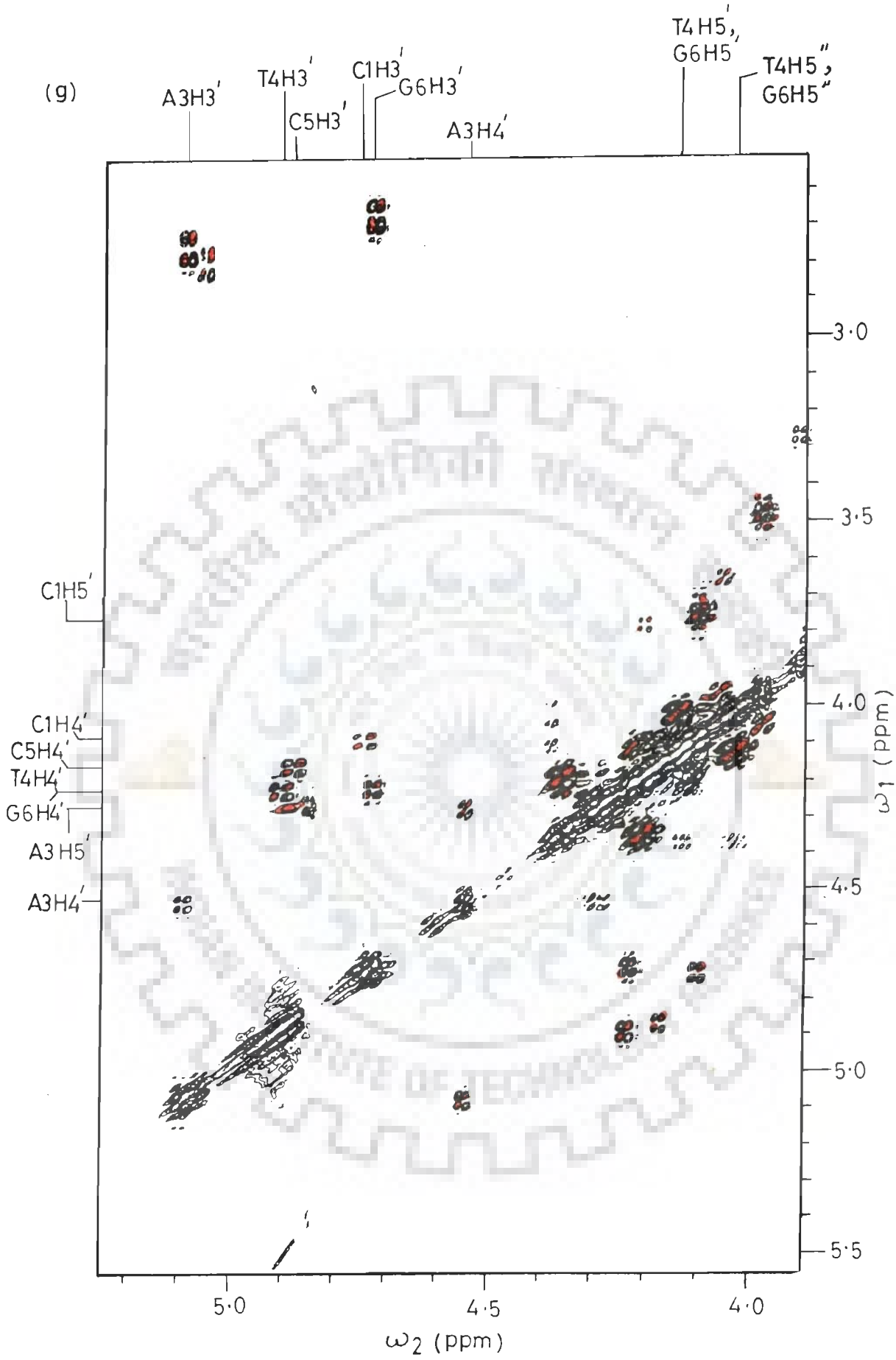

Fig. 5.5(g) : Portion of phase-sensitive double quantum filter COSY spectrum of d-$(CGATCG)_2$ showing H3'-H4', H4'-H5', H5'-H5" connectivities.

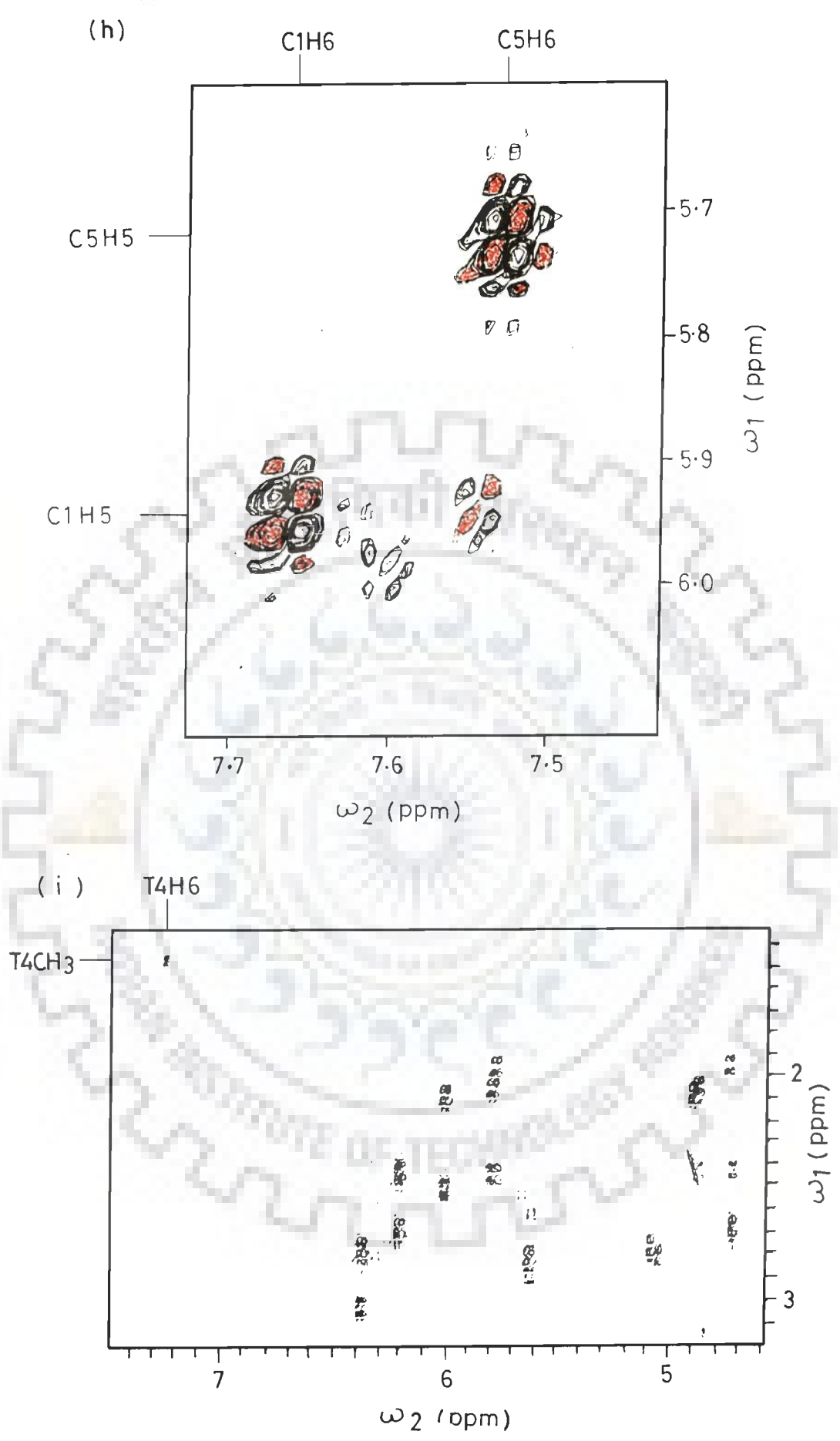

Fig. 5.5(h, i) : Expanded region of phase-sensitive double quantum filter COSY spectrum of d-$(CGATCG)_2$ showing base-base proton cross peaks.

Table 5.2 : Chemical shift positions (in ppm) of d-$(CGATCG)_2$ at 295 K in D_2O.

Proton	C1	G2	A3	T4	C5	G6
H8/H6	7.66	8.02	8.35	7.23	7.52	7.97
H1′	5.78	5.62	6.37	6.01	5.81	6.21
H2′	1.94	2.79	2.75	2.08	2.04	2.67
H2"	2.44	2.89	3.01	2.49	2.43	2.42
H3′	4.74	5.05	5.08	4.91	4.88	4.73
H4′	4.11	4.38	4.54	4.22	4.18	4.22
H5′	3.75	4.13	4.29	4.13	O	4.13
H5"	3.45	4.03	O	4.03	O	4.03
H5/H2/CH_3	5.93	-	7.81	1.44	5.71	-

O : Overlap.

Table 5.3 : Presence (marked as +) and absence (marked as -) of intra-residue cross peak patterns as observed in phase-sensitive double quantum filter COSY spectra of d-$(CGATCG)_2$ at 295 K in D_2O.

Connectivities	C1	G2	A3	T4	C5	G6
H2'-H2"	+	+	+	+	+	+
H1'-H2'	+	+	+	+	+	+
H1'-H2"	+	+	+	+	+	+
H2'-H3'	+	+	+	+	+	+
H2"-H3'	+	-	-	-	+	+
H3'-H4'	+	-	+	+	+	+
H4'-H5'	+	-	+	+	+	+
H5'-H5"	O	-	+	+	+	+
B-B	+	-	-	+	+	-

B : Base proton.

O : Overlap.

by following standard strategies available in literature (30,41, 45-47,113) for sequential assignment in right-handed B-DNA.

The distances of base H8/H6/H5 protons from H1′, H2′ and H2" (133) sugar protons are less than 4.0 A° so that the following internucleotide connectivities are expected :

$$(H8/H6)_n \quad \text{------} \quad (H1')_{n-1}$$

$$(H8/H6)_n \quad \text{------} \quad (H2')_{n-1}$$

$$(H8/H6)_n \quad \text{------} \quad (H2")_{n-1}$$

The intra residual NOEs between H2′ - H2", H1′-H2′, H1′-H2", H2′-H3′, H2"-H3′, H3′-H4′, H4′-H5′ and H5′-H5" protons are shown in Fig. 5.6(b-g). The internucleotide NOE connectivities, used for sequential assignment are seen in NOESY spectra (Fig. 5.6(c-f)). Each base proton (H8/H6) is thus expected to give two intranucleotide cross peaks with its corresponding H2′, H2" protons and two internucleotide cross peaks with H2′, H2" of preceeding nucleotide. One of the CH6 residue gives only two intraresidual NOE cross peaks and is thus assigned as the terminal one at 5′ end (Fig. 5.6(c-f)). Table 5.3 and 5.4(a,b) lists various intraresidue and inter residue connectivities observed in d-$(CGATCG)_2$. Two NOE cross peaks are observed between base protons A3H8 and T4CH_3; C5H5 and T4H6 (Fig. 5.6(c-f), 5.6(j)), showing their proximity and which are expected to be at a distance $\simeq$ 3.8-3.9 A° (Table 5.4(b)). Further all base protons except G2H8 give NOE cross peak with H1′ of the base preceeding to it (Fig. 5.6(j), Table 5.4(b)).

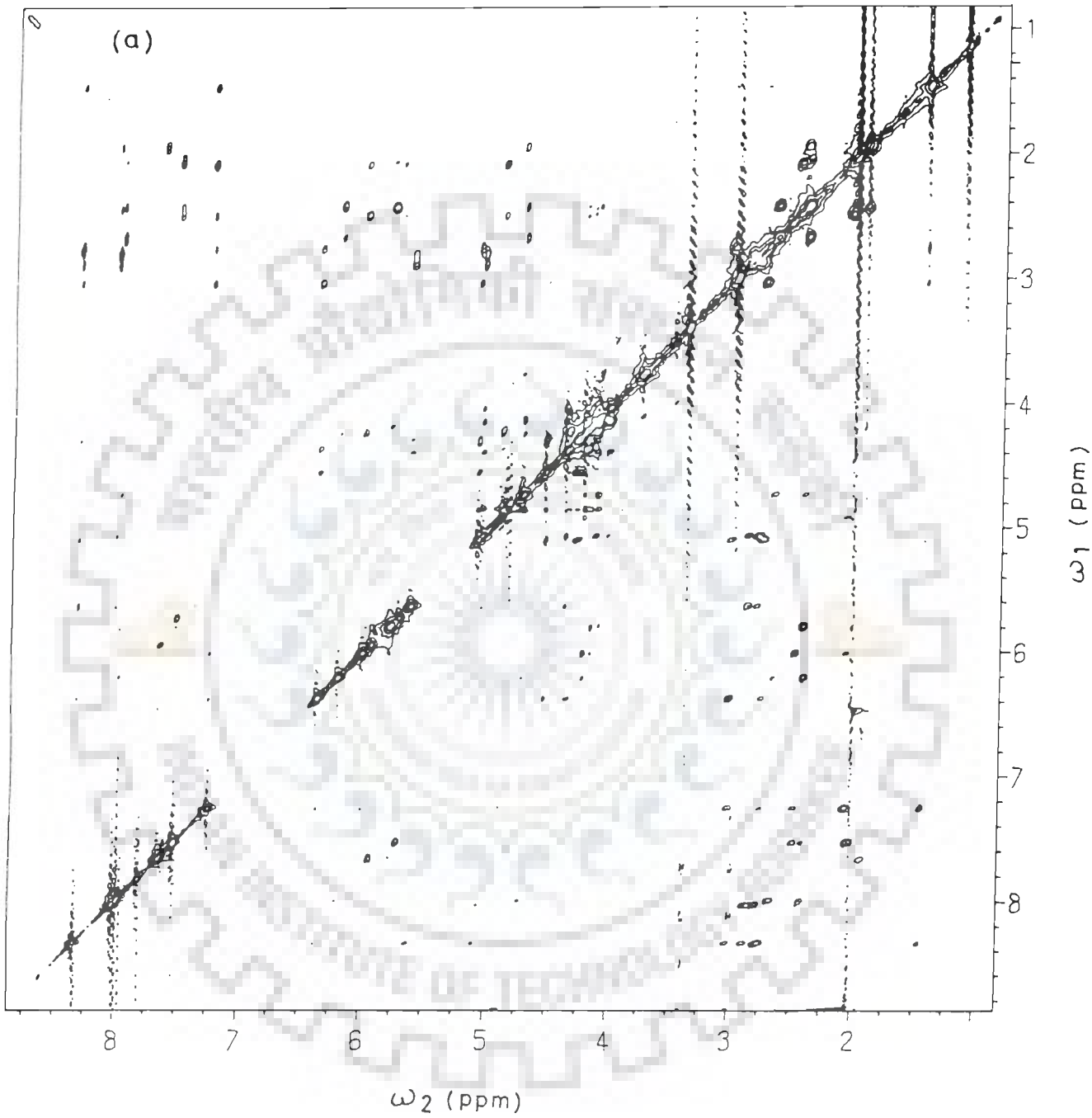

Fig. 5.6(a) : Phase-sensitive NOESY spectrum (at τ_m 200 ms) of d-$(CGATCG)_2$ at 295 K in D_2O.

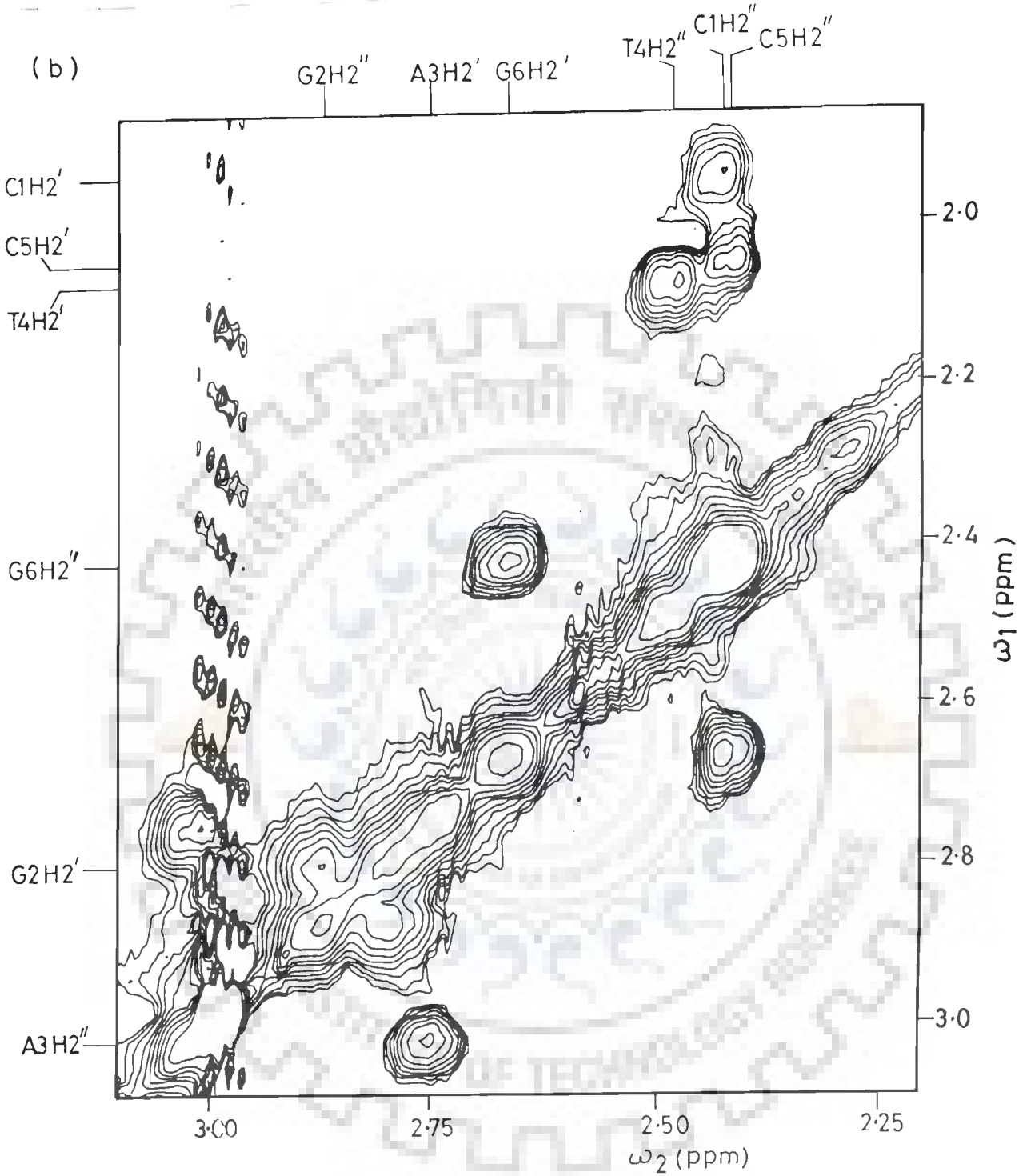

Fig. 5.6(b) : Expanded portion of phase-sensitive NOESY spectrum (at τ_m 200 ms) of d-$(CGATCG)_2$ showing H2'-H2" connectivities.

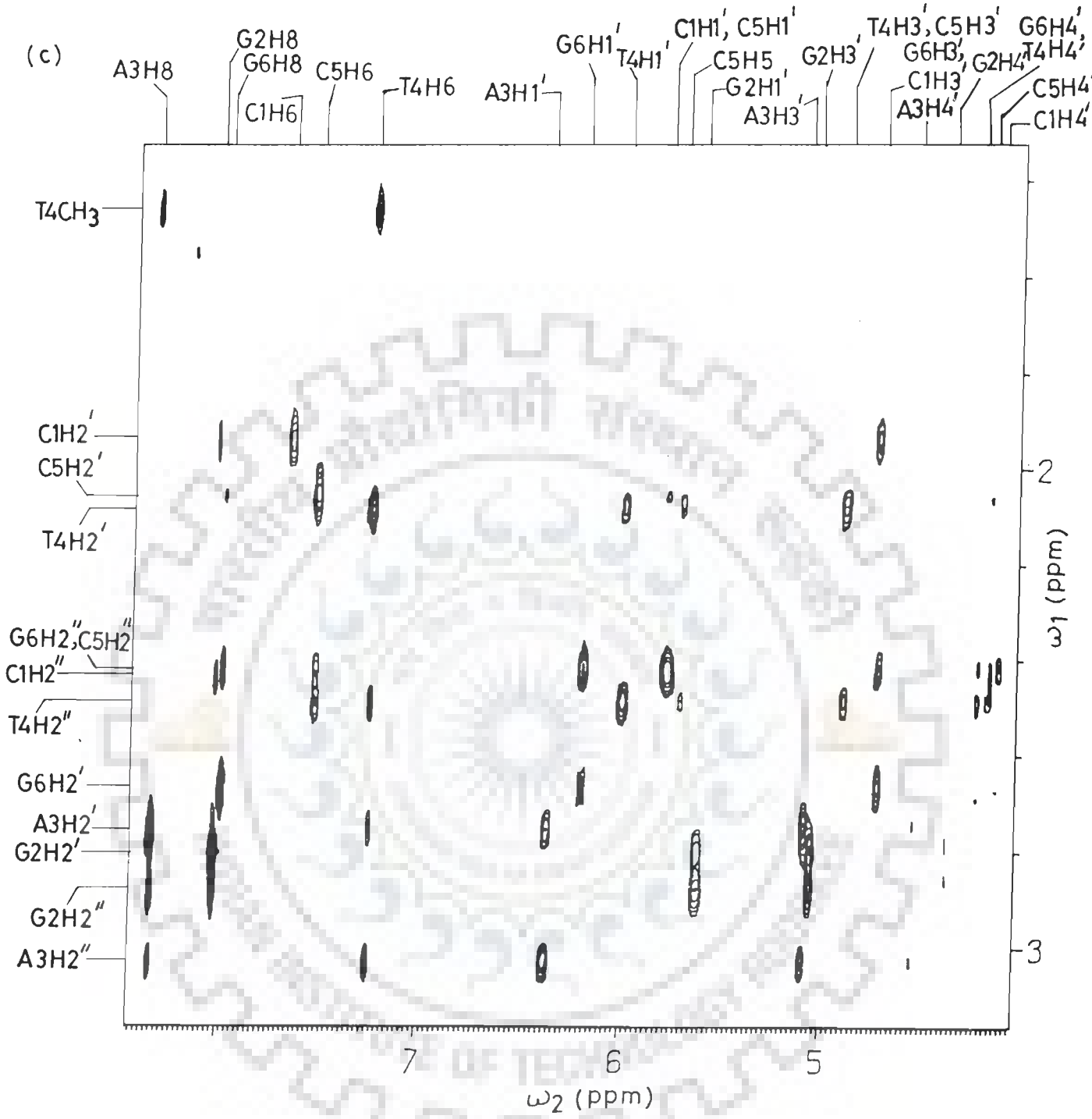

Fig. 5.6(c) : Expanded portion of phase-sensitive NOESY spectrum (at τ_m 200 ms) of d-$(CGATCG)_2$ showing H1'-H2', H2"; H3'-H2', H2"; H2'-H4', H2"-H4', intra and inter-residue connectivities.

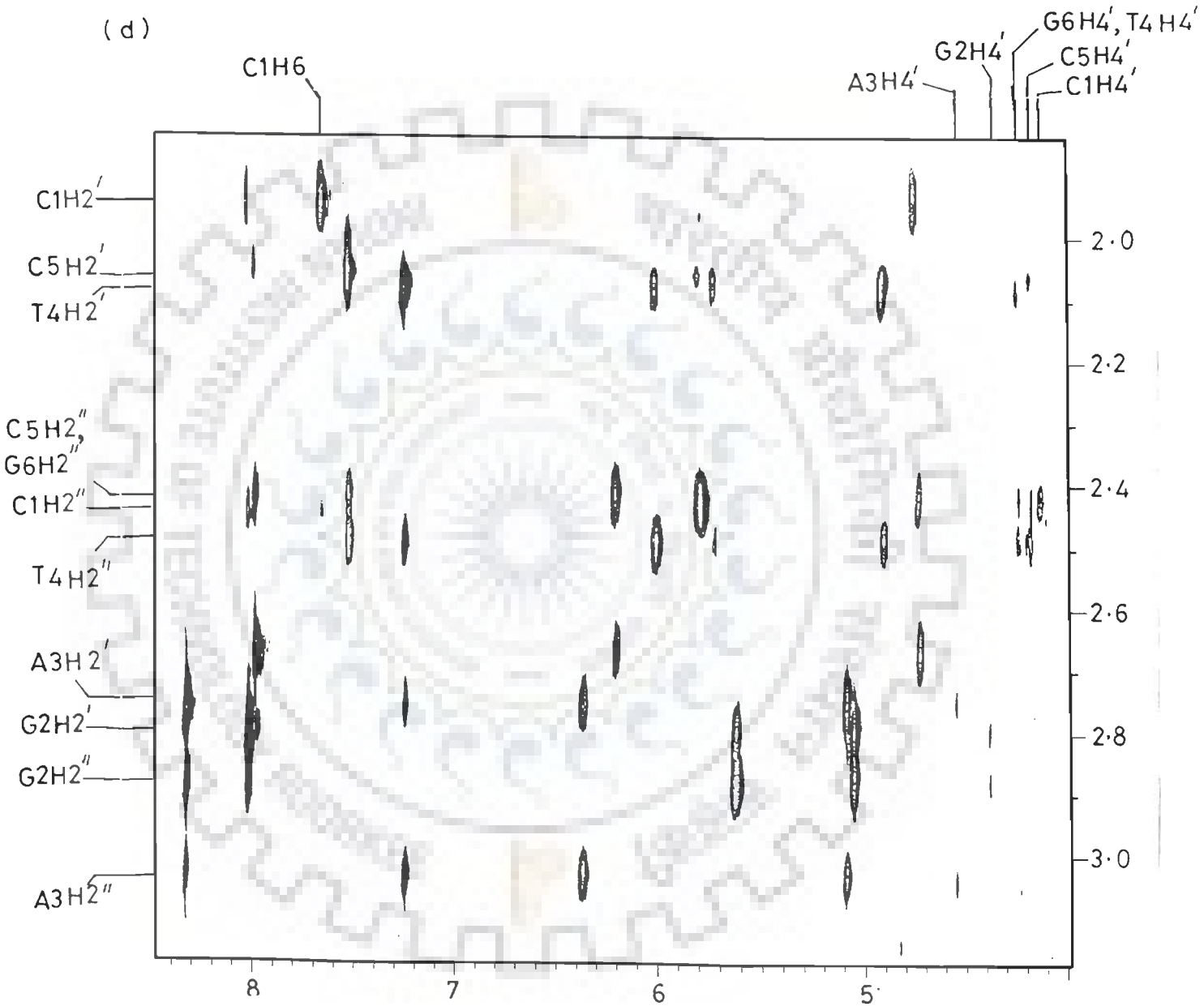

Fig. 5.6(d) : Expanded portion of phase-sensitive NOESY spectrum (at τ_m 250 ms) of d-$(CGATCG)_2$ showing H1′-H2′, H2"; H3′-H2′, H2"; H2′-H4′, H2"-H4′, intra and inter-residue connectivities.

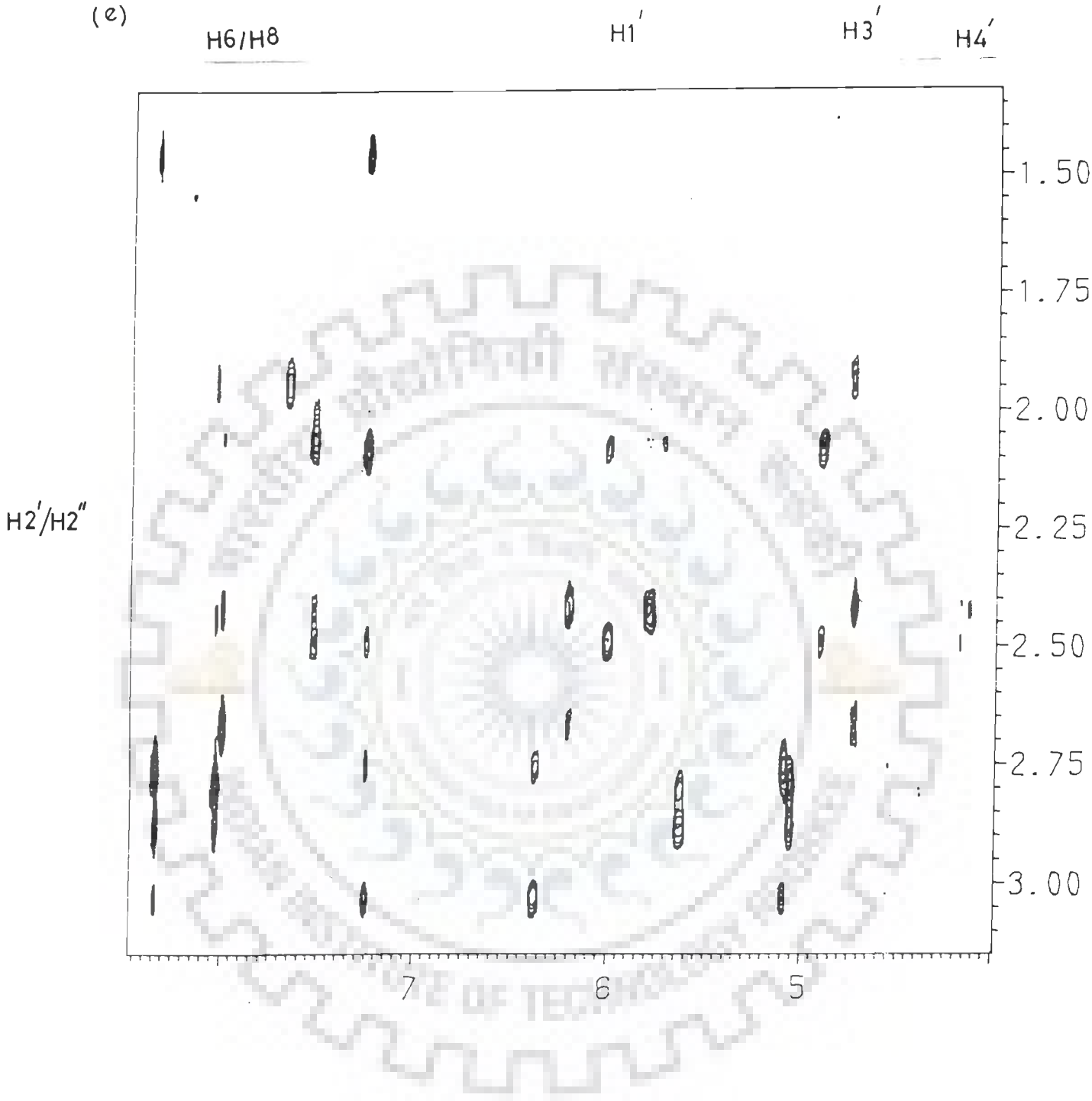

Fig. 5.6(e) : Expanded portion of phase-sensitive NOESY spectrum (at τ_m 150 ms) of d-$(CGATCG)_2$ showing H1′-H2′, H2"; H3′-H2′, H2"; H2′-H4′, H2"-H4′, intra and inter-residue connectivities.

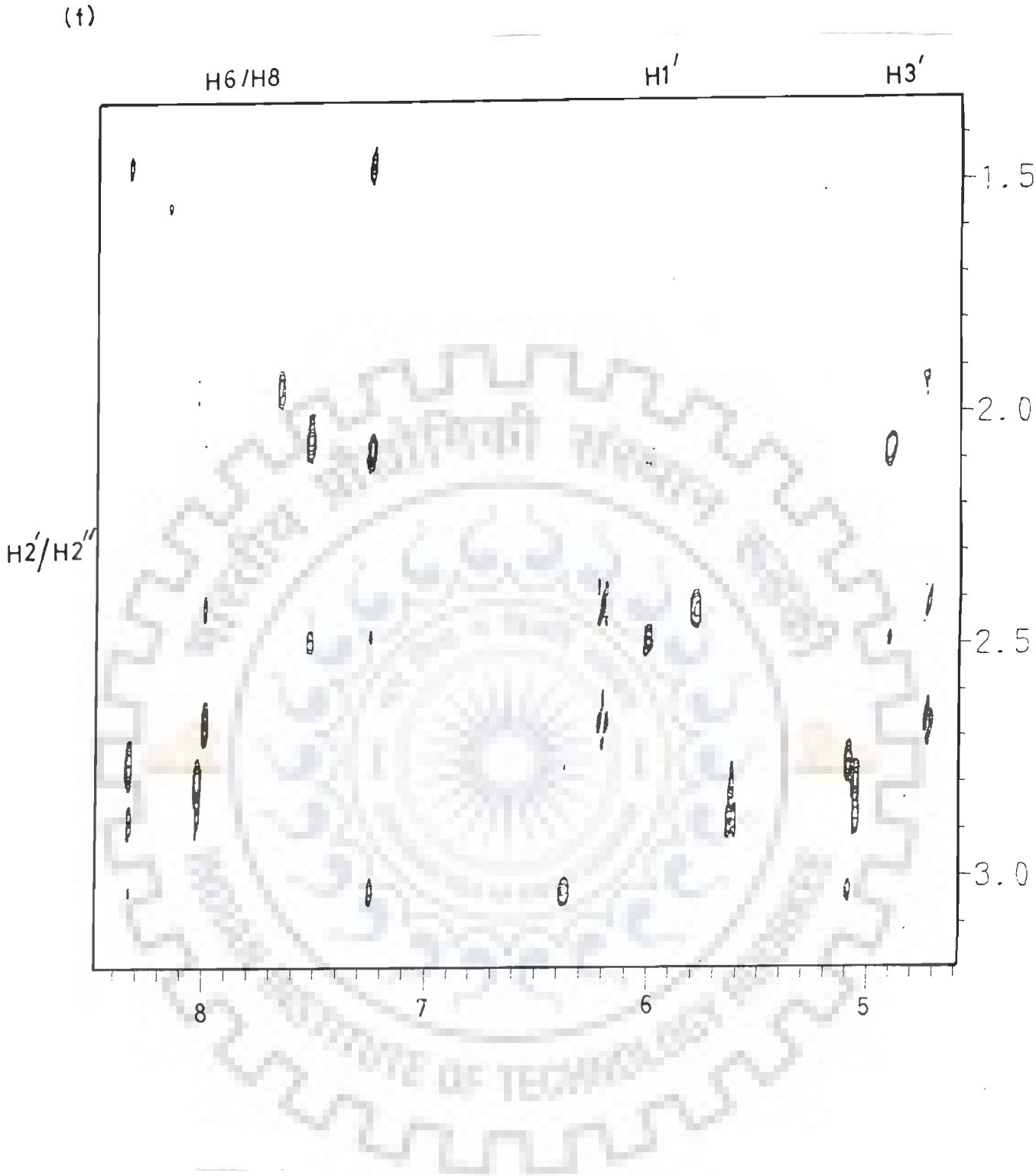

Fig. 5.6(f) : Expanded portion of phase-sensitive NOESY spectrum (at τ_m 75 ms) of d-$(CGATCG)_2$ showing H1′-H2′, H2"; H3′-H2′, H2"; intra and inter-residue connectivities.

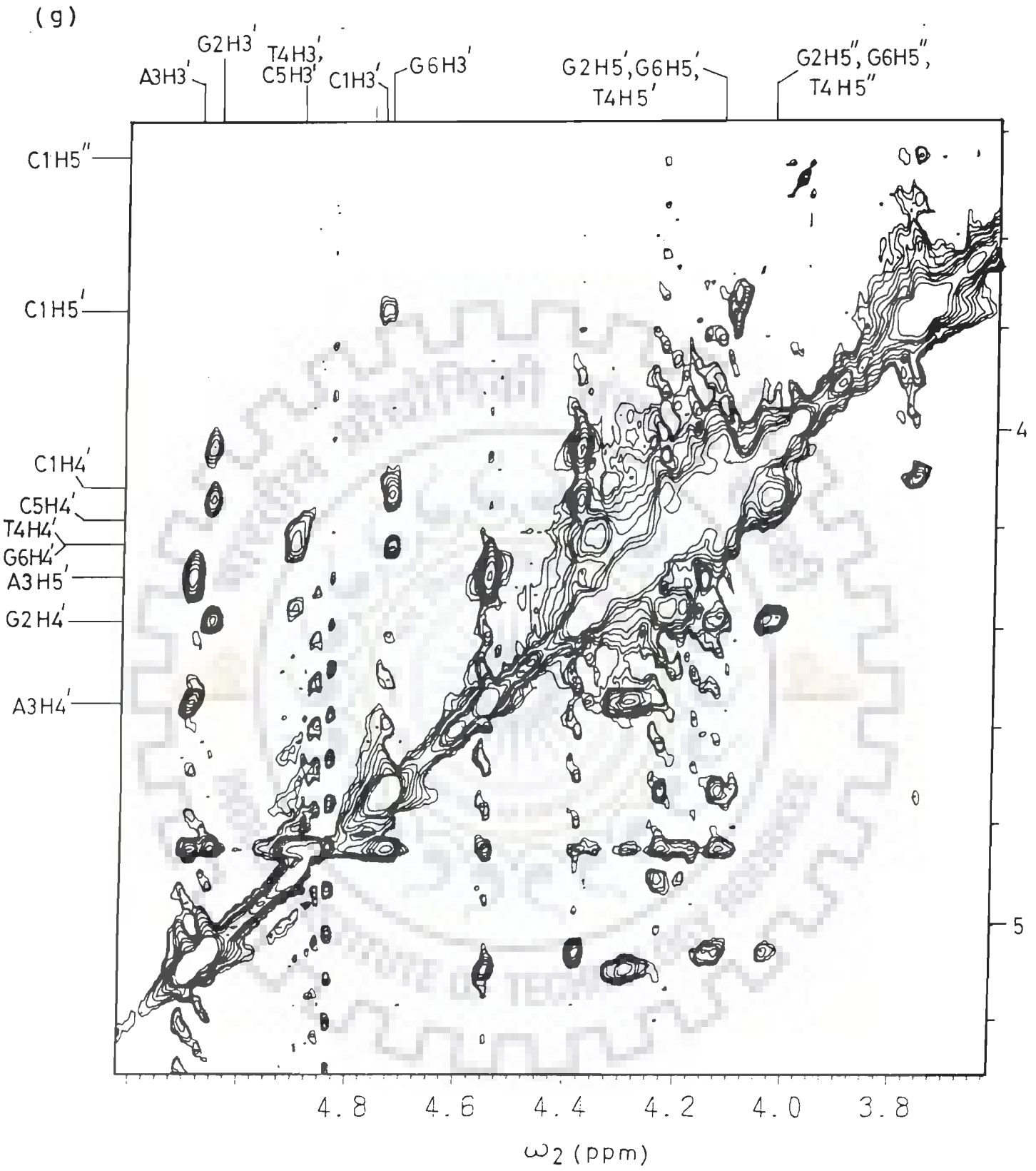

Fig. 5.6(g) : Expanded portion of phase-sensitive NOESY spectrum (at τ_m 200 ms) of d-$(CGATCG)_2$ showing H3'-H4', H4'-H5', H5'-H5" connectivities.

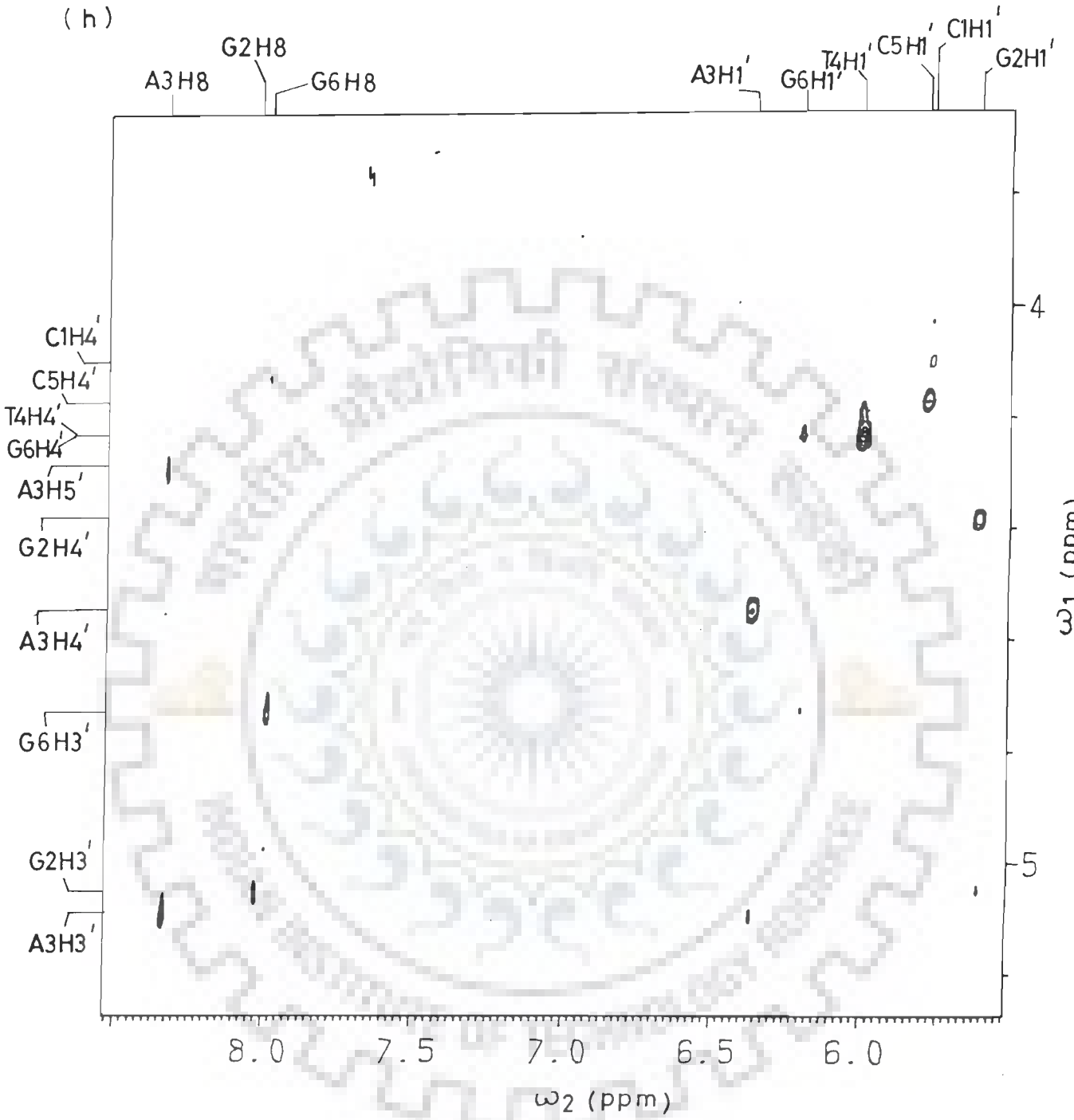

Fig. 5.6(h) : Expanded portion of phase-sensitive NOESY spectrum (at τ_m 200 ms) of d-$(CGATCG)_2$ showing H1'-H3', H1'-H4', base-H3', base-H5' connectivities.

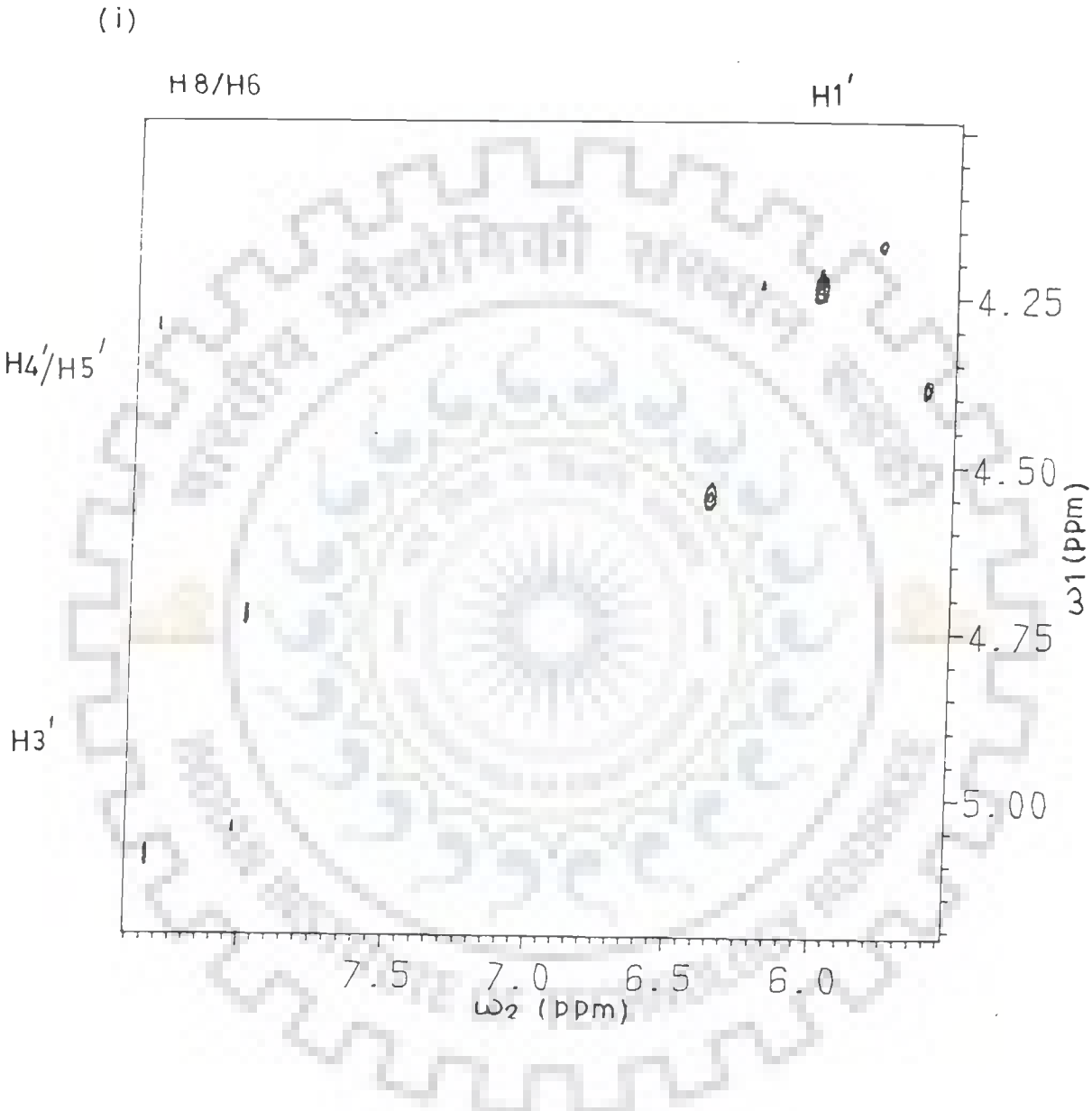

Fig. 5.6(i) : Expanded portion of phase-sensitive NOESY spectrum (at τ_m 150 ms) of d-$(CGATCG)_2$ showing H1'-H4', base-H5', base-H3' connectivities.

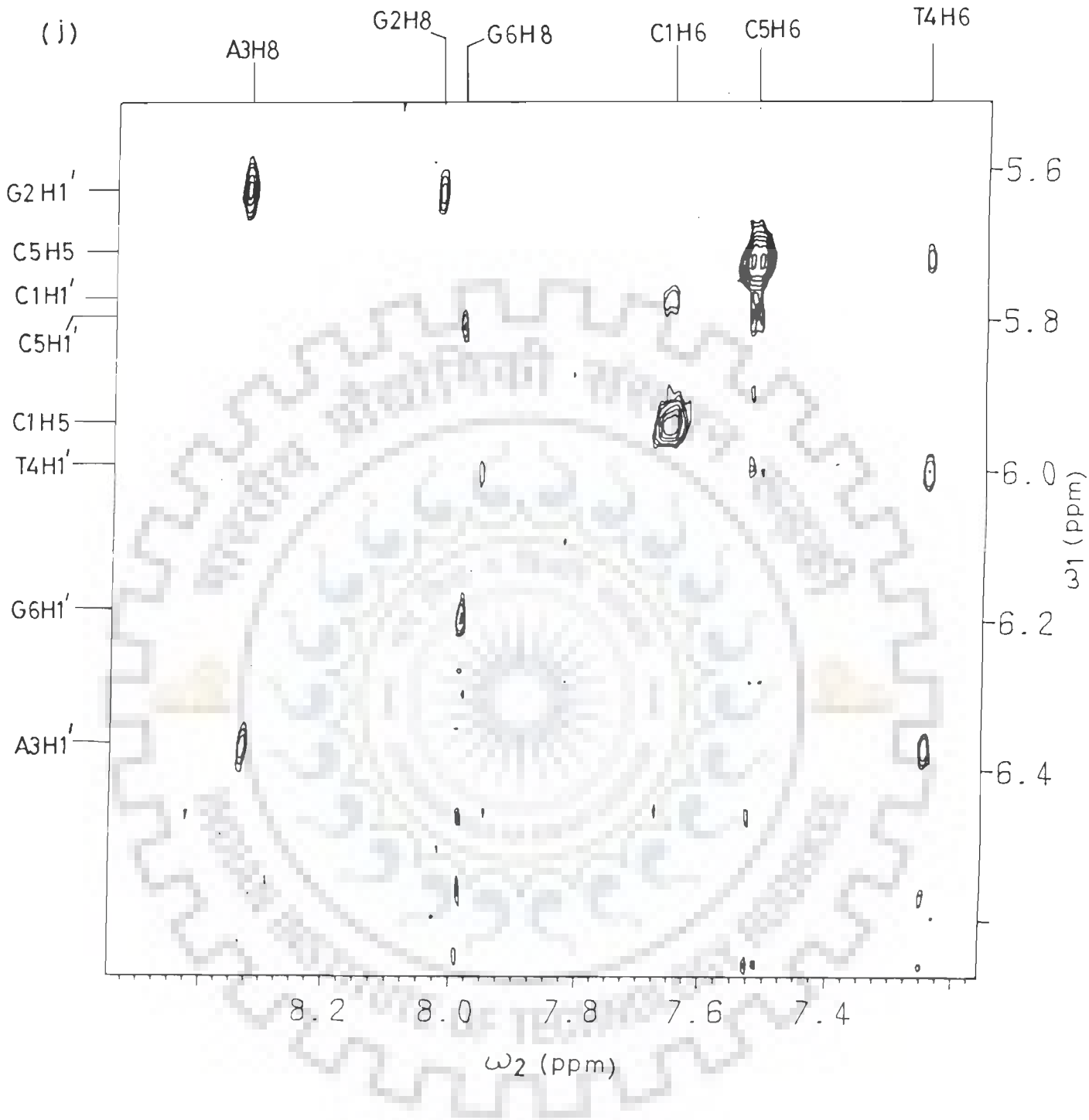

Fig. 5.6(j) : Expanded portion of phase-sensitive NOESY spectrum (at τ_m 200 ms) of d-$(CGATCG)_2$ showing intra and inter-residue base-H1', base-base connectivities.

Table 5.4(a) : Presence (marked as +) and absence (marked as -) of intra-residue cross peaks as observed in phase-sensitive NOESY spectra (at τ_m 75, 150, 200 and 250 ms) of d -(CGATCG) at 295 K in D_2O.

Connectivities	C1	G2	A3	T4	C5	G6
H2'-H2"	+	+	+	+	+	+
H1'-H2'	+	+	+	+	+	+
H1'-H2"	+	+	+	+	+	+
H2'-H3'	+	+	+	+	+	+
H2"-H3'	+	+	+	+	-	+
H3'-H4'	+	+	+	+	+	+
H4'-H5'	+	+	+	+	+	+
H3'-H5'	+	+	+	-	-	+
H3'-H5"	-	+	-	-	-	-
H5'-H5"	+	+	O	O	O	O
H4'-H5"	-	+	-	-	-	-
H1'-H4'	+	+	+	+	+	+
H1'-H3'	-	+	+	-	-	+
H2'-H4'	-	+	+	+	+	+
H2"-H4'	+	+	+	+	+	+
B-H1'	+	+	+	+	+	+
B-H2'	+	+	+	+	+	+
B-H2"	+	+	+	+	+	+
B-H3'	-	+	+	-	-	+
B-H5'	-	-	+	-	-	-
B-B	+	-	-	+	+	-

B : Base proton, O : Overlap.

Table 5.4(b): Inter-residue NOE connectivities as observed in phase-sensitive NOESY spectra (at τ_m 75, 150, 200 and 250 ms) of d-$(CGATCG)_2$ at 295 K in D_2O.

G6H8 - C5H2′
G6H8 - C5H2"
C5H6 - T4H2′
C5H6 - T4H2"
C5H5 - T4H2′
C5H5 - T4H2"
T4H6 - A3H2′
T4H6 - A3H2"
$T4CH_3$ - A3H8
A3H8 - G2H2′
A3H8 - G2H2"
G2H8 - C1H2′
G2H8 - C1H2"
A3H8 - G2H1′
G6H8 - C5H1′
C5H6 - T4H1′
T4H6 - A3H1′
C5H5 - T4H6

Thus each set of sugar resonances gets assigned to its respective base in the sequence d-$(CGATCG)_2$ and unambiguous spectral assignment is thus made. Several additional NOE connectivities are observed in Fig. 5.6(c-j), Table 5.4(a). These include intrasugar NOE cross peaks H3'-H5'/H5", H1'-H3', H2'-H4', H2"-H4', base-H1'/H2'/H2"/H3'/H4'/H5' protons which are used for conformational analysis and are discussed later.

SUGAR GEOMETRY OF d-$(CGATCG)_2$

There are two ways of determining sugar geometries as from the NMR parameters : (a) from the knowledge of three bond $^1H - ^1H$ coupling constants determined from correlation spectroscopy and splitting patterns in 1D NMR spectra and (b) from the knowledge of interproton distances in the sugar ring determined from NOESY spectra. Both the methods can be used in a complimentary fashion. It is recognized (10, 114, 131) that the very nature of pseudorotation phenomena in combination with conformational heterogeneity, virtually precludes an unambiguous and precise determination of sugar geometry from interproton distances. The dependence of distance constraints on glycosyl torsional angle (χ), the pseudorotation (P), pucker amplitude (ϕ_m) and mole fraction of S-conformer in case of a dynamic S to N interconversion show that the NOE data needs to be supplemented by other experimental factors before a reliable picture of the behaviour of an individual deoxyribose ring in a DNA duplex can be obtained. As discussed earlier in chapter III, spin diffusion is

different for various pairs of protons and it increases with mixing time (τ_m) of the NOESY experiment. It is evident from Fig. 5.7 that spin diffusion is least for τ_m 75 and 150 ms for d-$(CGATCG)_2$ therefore interproton distances have been calculated at τ_m 75 ms and are used in further analysis.

We have followed the strategy of determining the sugar geometry from analysis of J values and then supplementing it with distance data to arrive at a specific conclusion.

Determination of deoxyribose pucker in d-$(CGATCG)_2$ by coupling constant analysis

The proton-proton coupling constants of interest in oligonucleotides are J(H1'-H2'), J(H1'-H2"), J(H2'-H3'), J(H2"-H3'), J(H3'-H4') and J(H2'-H2"). Among these five, three bond coupling constants define the sugar geometry. Of these, the J(H2'-H3') and J(H1'-H2") vary in a narrow range and are insensitive to sugar geometry. The other three coupling constants vary significantly between 0-10 Hz depending on sugar geometry (45,105,131), and thus their estimation from experimental spectra provides an effective tool for fixing the sugar geometries in oligonucleotides.

The coupling constants can be determined by analysing the patterns of cross peak components in COSY spectra. However since the patterns depend on the magnitudes of J, which in turn depend on sugar geometry, it is necessary to have a dictionary of expected patterns for various sugar geometries. The

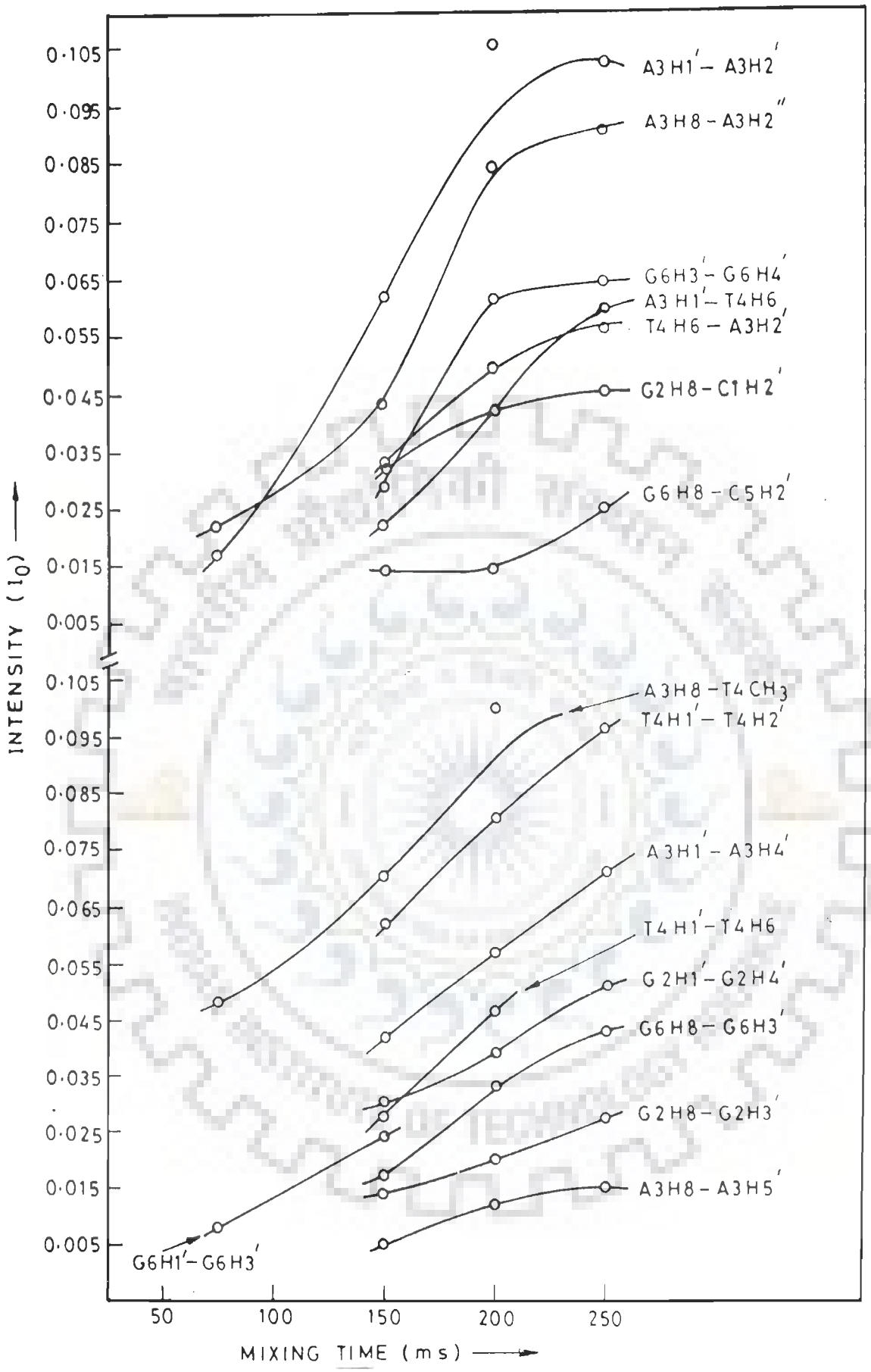

Fig. 5.7 : NOE build-up curves for various pairs of protons of d-$(CGATCG)_2$ as a function of mixing time (τ_m) in the range of 75-250 ms.

experimentally observed patterns are then matched with calculated patterns to derive the coupling constant information. The procedure used by us is described below.

The five coupling constants J(H1'-H2'), J(H1'-H2"), J(H2'-H3'), J(H2"-H3') and J(H3'-H4') are calculated as a function of the sugar geometry using the Karplus type relationship (52,53). For the flip angle ϕ of the read pulse (Fig. 3.2) as $\pi/2$, the multiplet structure is simply calculated by combining the + and - along the ω_1 axis with those along the ω_2 axis. This is illustrated in Fig. 5.8(a-c) for four cross peaks H1'-H2', H1'-H2", H2'-H3', H2"-H3', for three standard sugar geometries, that is, C2'-endo, O1'-endo and C3'-endo. For example, it may be noted that in case of H1'-H2" that is, H2" along ω_1 axis and H1' along ω_2 axis cross peak of C2'-endo sugar pucker, the fine structure along the ω_1 axis arises from the H1'-H2", H2"-H3' and H2'-H2" coupling constants while that along the ω_2 axis arises from the H1'-H2' and H1'-H2" coupling constants. Only the active coupling H1'-H2" leads to antiphase components along both the axis. Similarly, for the H1'-H2' cross peaks, only the H1'-H2' coupling leads to antiphase components. This feature helps in identifying the coupling constants as indicated in Fig. 5.8 (a-c).

Fig. 5.9 shows several patterns generated for H1'-H2" and H1'-H2' cross peaks for flip angle of read pulse, ϕ, as $\pi/2$ for three different sugar geometries. For C3'-endo geometry, the H1'-H2" cross peak looks more elongated along the ω_1 axis and is

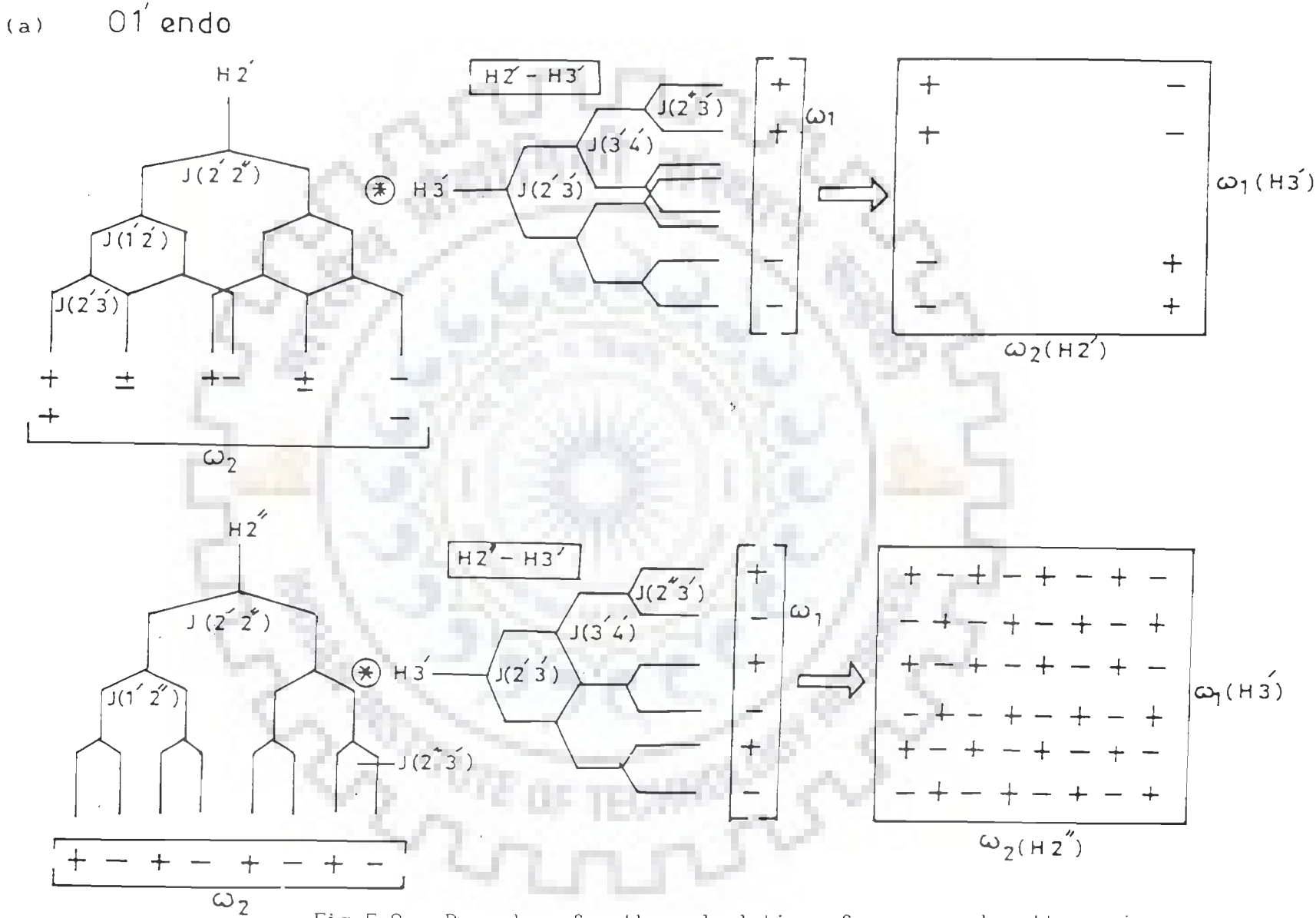

Fig 5.8 : Procedure for the calculation of cross peak patterns in COSY spectra, illustrated for (a) O1′-endo (b) C2′-endo and (c) C3′-endo for (i) H1′-H2′ (ii) H1′-H2" (iii) H2′-H3′ and (iv) H2"-H3′.

(a) 01´ endo

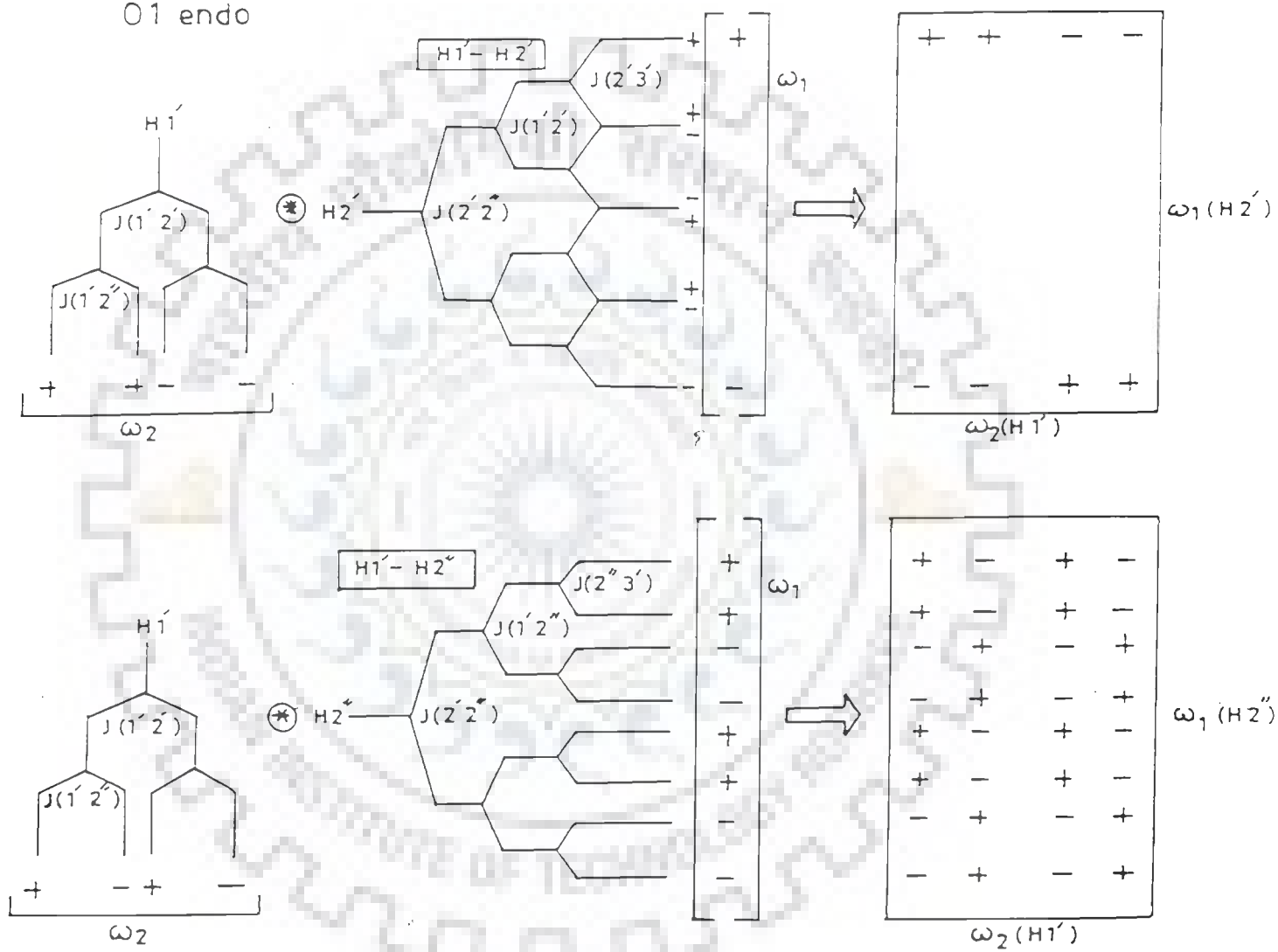
H1´
J(1´2´)
J(1´2´´)
ω2
H1´- H2´
J(2´3´)
J(1´2´)
H2´
J(2´2´)
ω1
ω1(H2´)
ω2(H1´)
H1´
J(1´2´)
J(1´2´´)
ω2
H1´- H2´´
J(2´´3´)
J(1´2´´)
H2´´
J(2´2´´)
ω1
ω1(H2´´)
ω2(H1´)

(b) C 2′ endo

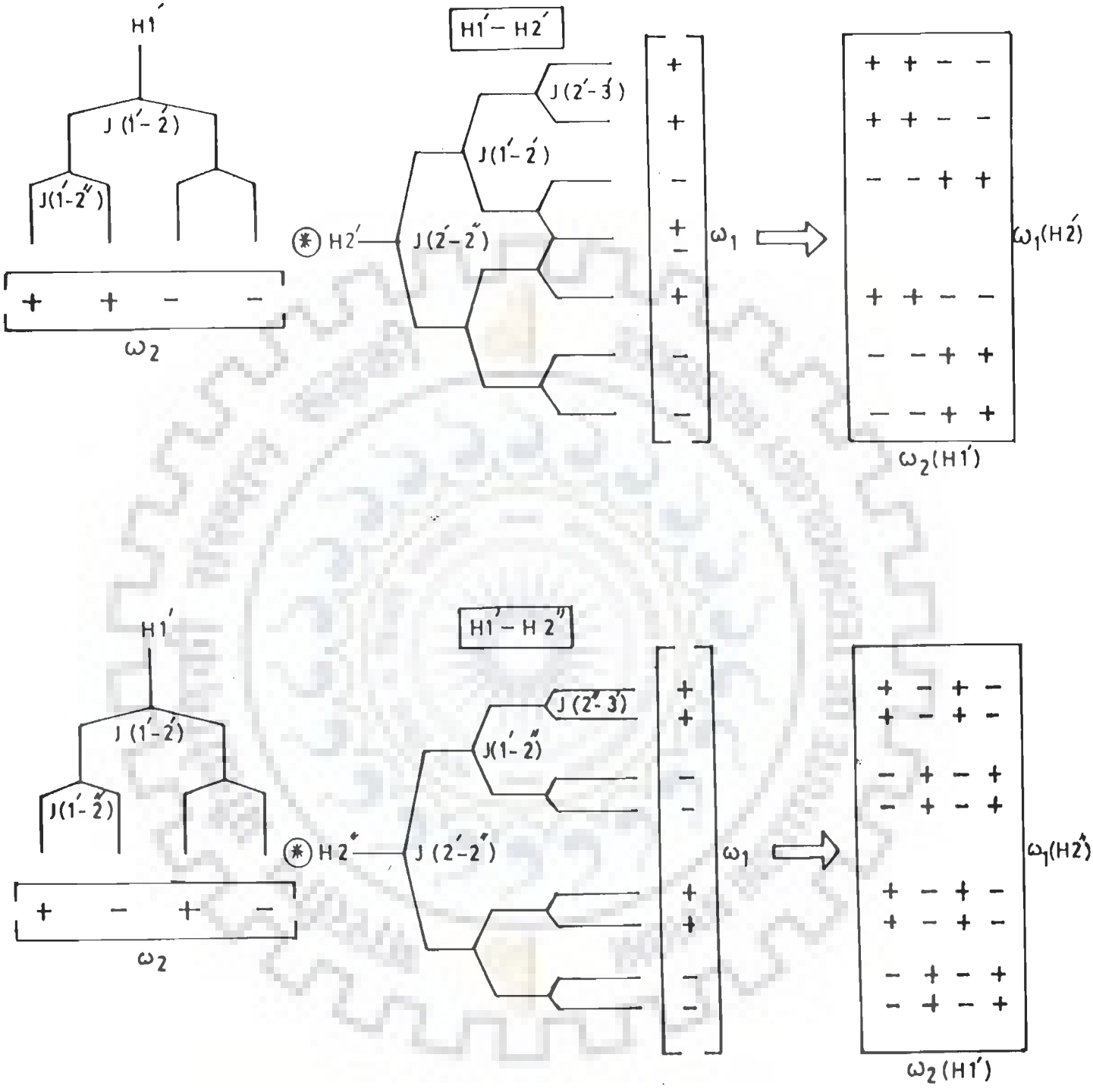
H1′
J (1′- 2′)
J(1′- 2″)
+ + - -
ω2
H1′ – H2′
J (2′- 3′)
J(1′- 2′)
⊛ H2′
J (2′- 2″)
+ + - + - + - -
ω1
+ + - -
+ + - -
- - + +
+ + - -
- - + +
- - + +
ω1(H2′)
ω2(H1′)
H1′
J (1′- 2′)
J(1′- 2″)
+ - + -
ω2
H1′ – H 2″
J (2″- 3′)
J(1′- 2″)
⊛ H2″
J (2′- 2″)
+ + - - + + - -
ω1
+ - + -
+ - + -
- + - +
- + - +
+ - + -
+ - + -
- + - +
- + - +
ω1(H2″)
ω2(H1′)

(b) C2′endo

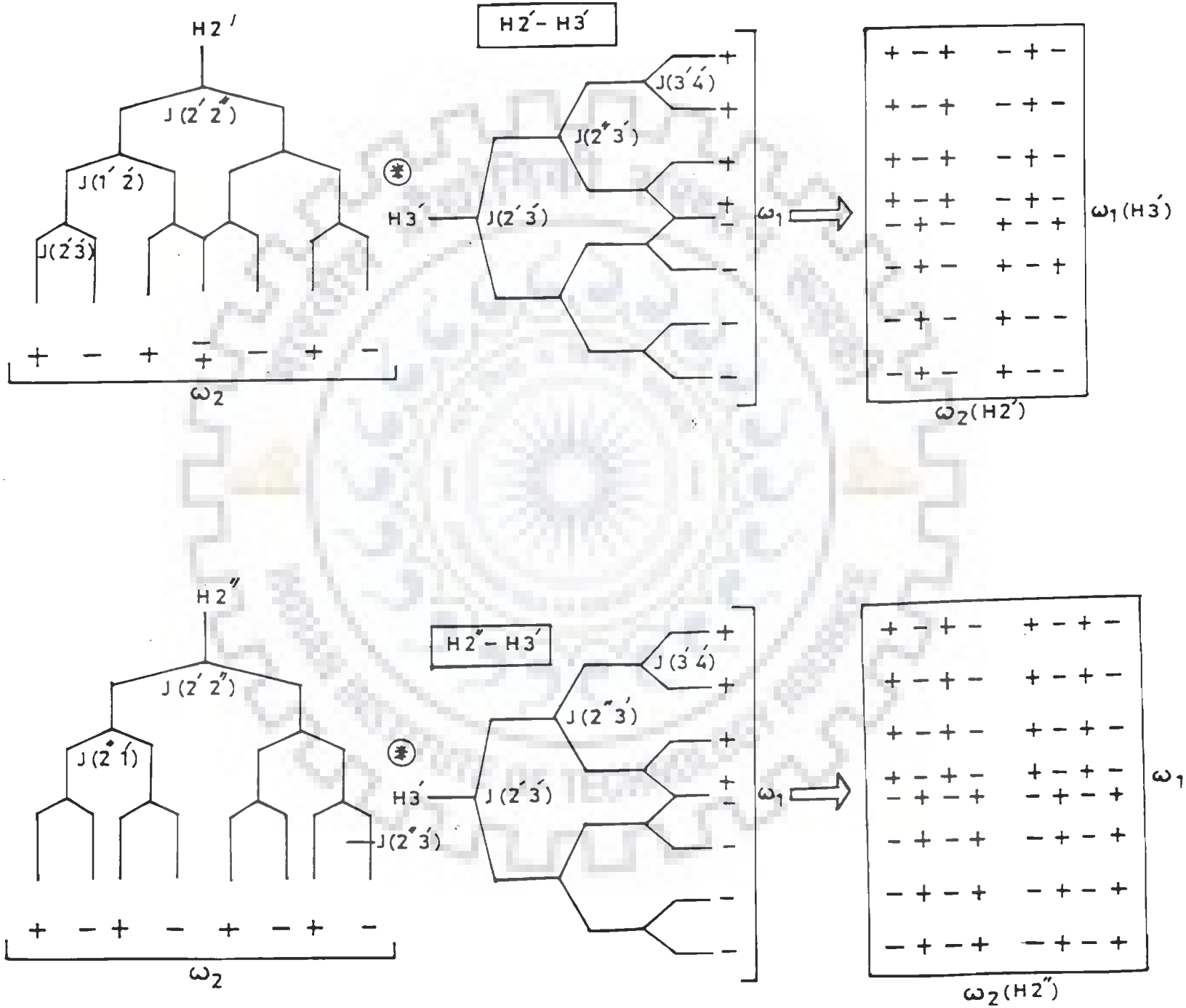
H2′
J(2′2″)
J(1′2′)
J(2′3′)
+ − + − − + −
ω2
H2′- H3′
J(3′4′)
J(2″3′)
H3′
J(2′3′)
ω1
+ − + − + −
ω1(H3′)
ω2(H2′)
H2″
J(2′2″)
J(2″1′)
J(2″3′)
H2″- H3′
J(3′4′)
J(2″3′)
H3′
J(2′3′)
ω1
ω1(H3′)
ω2(H2″)

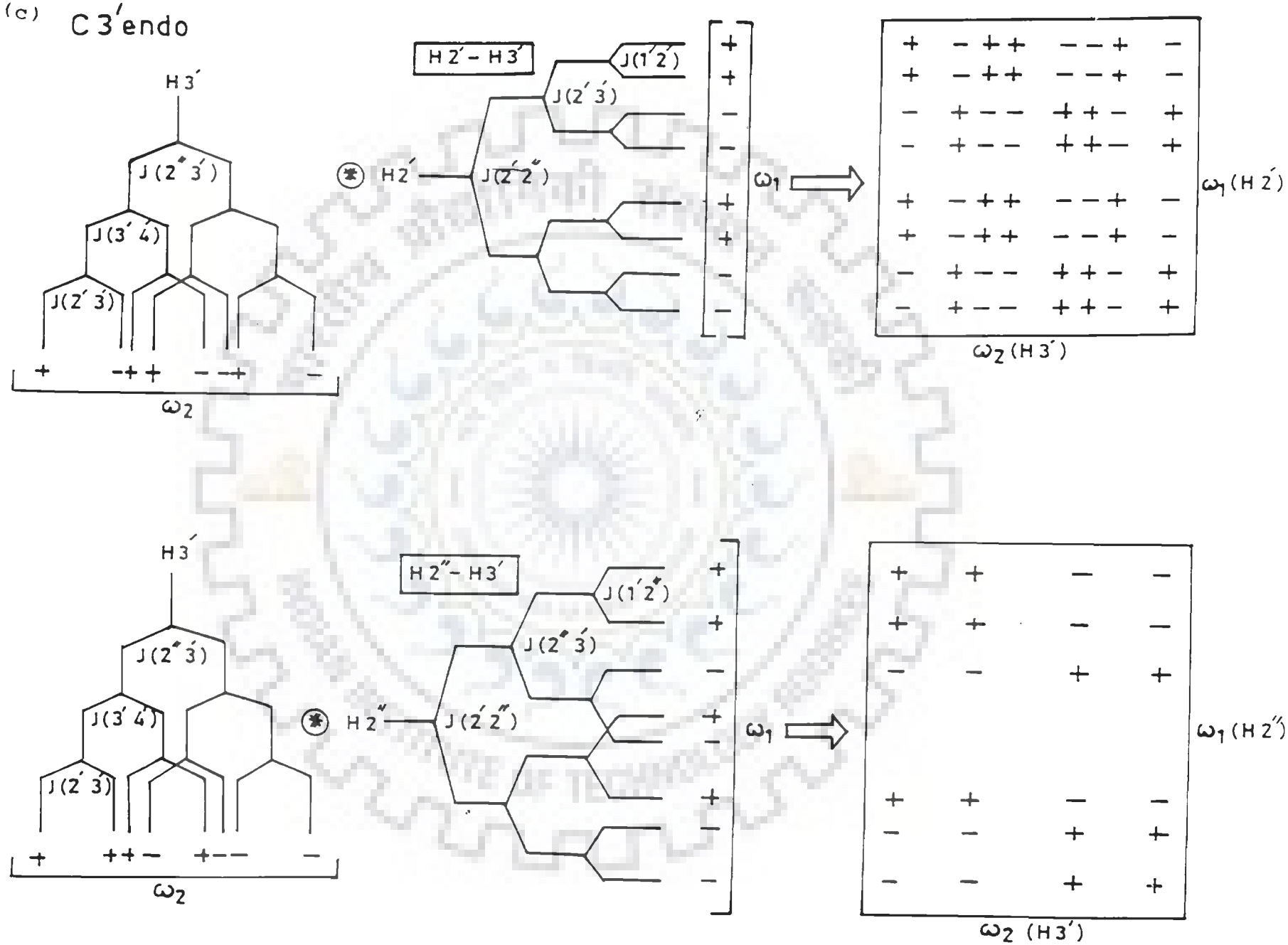
(c) C3′endo
H3′
J(2″3′)
J(3′4′)
J(2′3′)
+ -+ + - -+ -
ω2
H2′-H3′
J(1′2′)
J(2′3′)
H2′
J(2′2″)
ω1
+ - + + - - + -
+ - + + - - + -
- + - - + + - +
- + - - + + - +
+ - + + - - + -
+ - + + - - + -
- + - - + + - +
- + - - + + - +
ω1(H2′)
ω2(H3′)
H3′
J(2″3′)
J(3′4′)
J(2′3′)
+ ++ - +-- -
ω2
H2″-H3′
J(1′2″)
J(2″3′)
H2″
J(2′2‴)
ω1
+ + - -
+ + - -
- - + +
+ + - -
- - + +
- - + +
ω1(H2″)
ω2(H3′)

(c) C3´endo

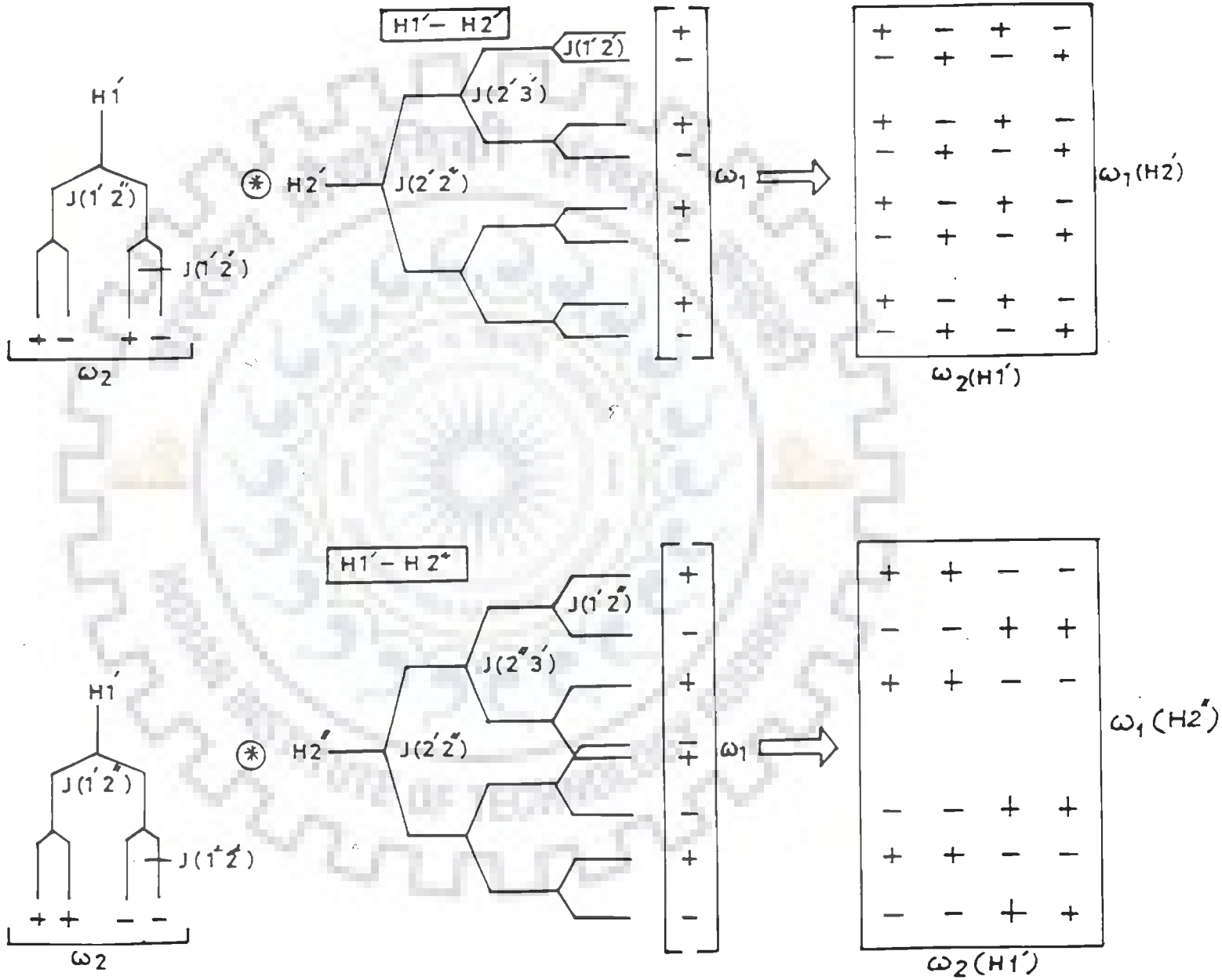
H1´
J(1´2´´)
J(1´2´)
+ − + −
ω2
H1´− H2´
J(1´2´)
J(2´3´)
H2´
J(2´2´´)
ω1
ω1(H2´)
ω2(H1´)
H1´− H2´´
J(1´2´´)
J(2´´3´)
H2´´
J(2´2´´)
ω1(H2´´)
ω2(H1´)

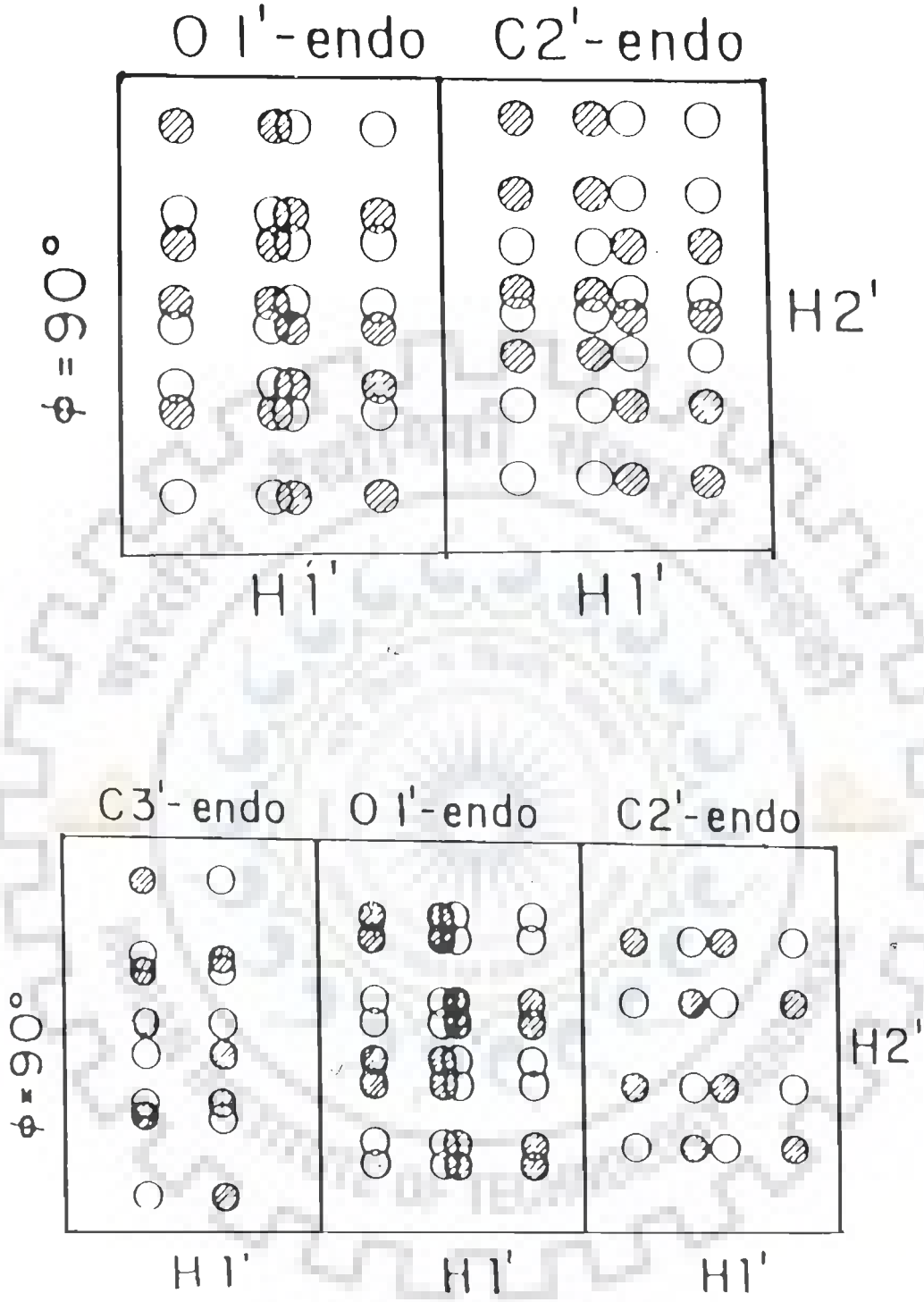

Fig. 5.9 : Calculated H1′-H2′ and H1′-H2" cross peak patterns for flip angle $\phi = \pi/2$ for C2′-endo, O1′-endo and C3′-endo sugar geometries (45).

compressed along the ω_2 axis. For C2'-endo pucker, the H1'-H2" ω_1 cross peak pattern gives rise to four components along each ω_2 as well as ω_1 axis and hence a total of sixteen components. The H1'-H2" ω_1 cross peak pattern, on the other hand, gives rise to four major components due to overlap of inphase components and cancellation of antiphase components in the middle of the pattern. The peak separations (indicated in Fig. 5.9) are directly read from the scale along ω_2 axis. The active coupling is always the separation between the antiphase components, irrespective of sugar geometry. The success in the estimation of coupling constants is crucially connected with the resolution of the multiplet components. If the required resolution is not achieved then the separation can be simulated by taking into consideration line widths and the line shapes along both the frequency axis. A low resolution COSY technique assesses the cross peak intensities to evaluate the relative size of the coupling constants (10(a,b),45), assuming that active coupling is the prevailing factor determining intensities. The success of this method is highly dependent on the actual line widths of the pertinent peaks. We have not carried out spectral simulation as the relevant programs were not available. Instead we have tried to match the observed patterns with those available in literature (10,72,72(a),114,114(a),130, 130(a)) particularly the DQF - cross peaks simulated by Schmitz et al. (114) using SPHINX and LINSHA programs (130,130(a)) which are reproduced here in Fig. 5.10. The extraction of coupling constant value is complicated due to peak overlap and increase in line

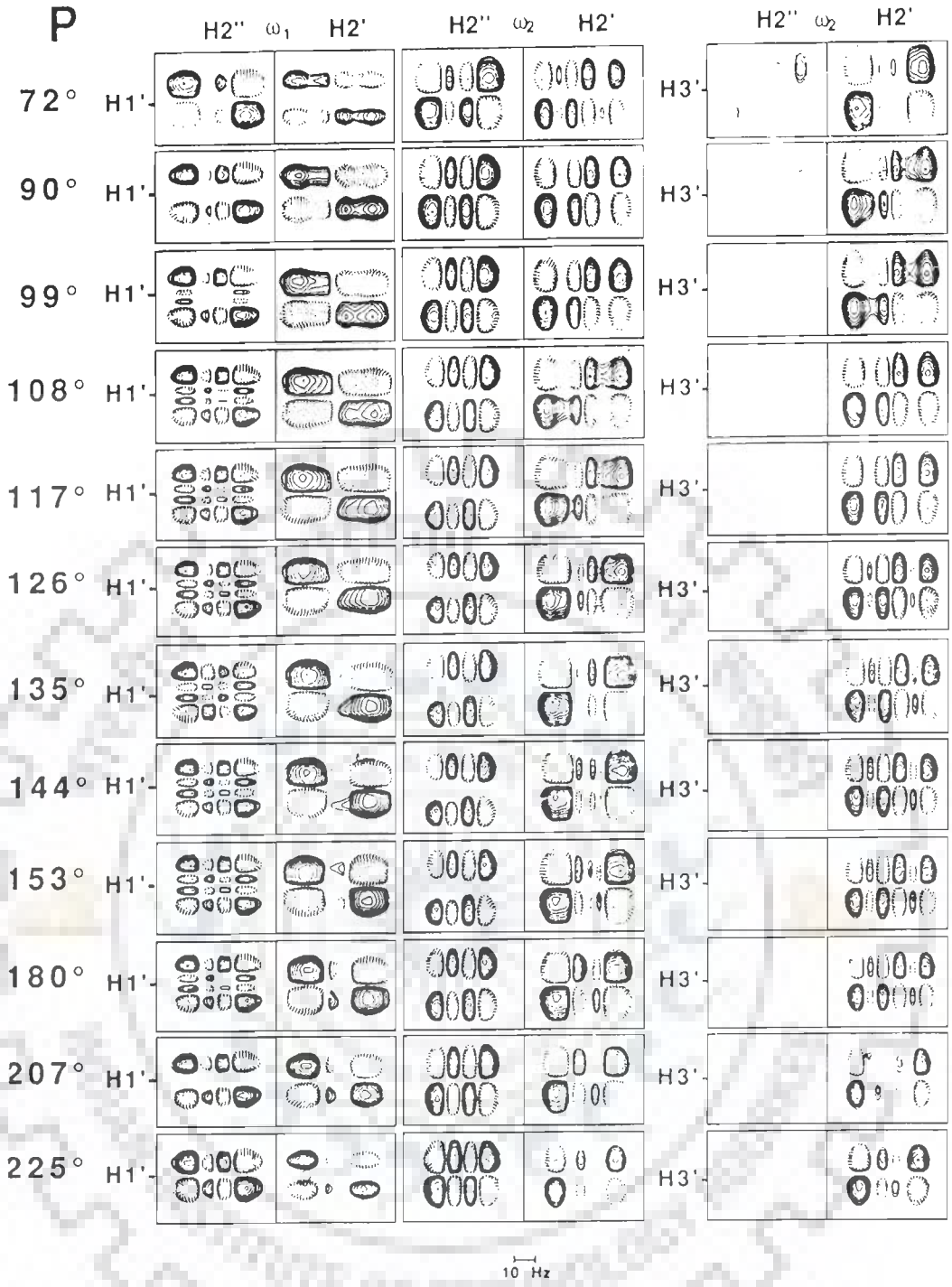

Fig. 5.10 : Simulated DQF-COSY cross peaks for different rigid deoxyribose conformations, described by a pseudorotation phase angle, P an amplitude $\phi_m = 35^\circ$: H1' H2"-ω_1, H1' H2'-ω_1, H1' H2"-ω_2, H1' H2'-ω_2, H3' H2"-ω_2 and H3' H2'-ω_2 from left to right. Negative peaks are indicated by dashed lines. An empty box indicates that the corresponding cross peak is of negligible intensity (114).

widths. The limitation of 2D NMR technique the digital resolution of about 2.3 Hz/point (in our case) in the better resolved dimension ω_2 axis allows an estimate of the range of J(H1'-H2'), J(H1'-H2") etc. values assuming that the line width does not vary even within the residue (114).

Initially we have tried to match the observed patterns with those obtained (Fig. 5.10) for different rigid sugar puckers, defined by pseudorotation phase angle P and the pucker amplitude $\phi_m = 35^\circ$ (1(a)). Values of J(H2'-H2") = 14 Hz and J(H3'-^{31}P) = 5.8 Hz and a line width of 9 Hz has been employed here. We find that there are lot of difficulties in interpreting the data. Table 5.3 gives the presence/absence of intra residue cross peak patterns as observed in DQF COSY spectra of d-$(CGATCG)_2$ at 295 K in D_2O. For three of the residues viz G2, A3 and T4 (that is all except C1, C5 and G6 residue) we did not observe the H2"-H3' cross peak indicating that active coupling constant involved is < 2.3 Hz and the pseudorotation phase angle lies in the range 90° to 225° (Fig. 5.10). The H3'-H4' cross peak pattern is however observed for all residues except G2 residue indicating that P lies in the range 9°-108° or ≃ 324° (72(a)). Therefore the non occurrence of H2"-H3' and occurrence of H3'-H4' cross peak would restrict the P value to a range of 90° - 108° i.e. close to O1' endo sugar pucker for most of the residues. However the observed H1'-H2", H1'-H2' and H2'-H3' cross peak patterns (Fig. 5.5 (d-f)) do not qualitatively agree with the corresponding simulated patterns for P_S = 90° to 108° (Fig. 5.10).

We then looked into possibility of existence of rapid interconversion on the NMR time scale between two sugar conformations observed in several studies on deoxyoligonucleotide (5,10,45,72,72(a),105,114,114(a),131) instead of rigid structure with P angle restricted to a small domain. A dynamic two state model commonly employed (105,131) with DNA uses one conformer from the S region and one from the N region of the pseudorotation cycle. In this model, the two conformation states are defined : (a) a minor conformer (N) with pseudorotation phase angle, P_N, and pucker amplitude, ϕ_N, essentially same as those of C3'-endo geometry i.e. $P_N = 18^\circ$, $\phi_m = 36^\circ$ (131) or that observed for A-DNA structures i.e. $P_N = 9^\circ$, $\phi_m = 36^\circ$ (110,114) and (b) a dominant S conformer with a pucker amplitude range $\phi_S = 28^\circ - 44^\circ$ and a pseudorotation phase angle P_S corresponding to approximately the C2'-endo range of puckers but subject to some variation (131) in the range 108° to 162°. The resulting observed coupling constant J between two protons is calculated as :

$$J = \chi_S J_S + \chi_N J_N$$

where χ_S and χ_N are the fractional populations of S and N conformers ($\chi_S + \chi_N = 1$), respectively and J_N and J_S are the ^1H-^1H vicinal coupling constants for N and S conformers respectively. The sums of coupling constants usually measured to a fairly good accuracy than the individual couplings are defined as follows :

$$\Sigma H1' = J(H1'-H2') + J(H1'-H2")$$

$$\Sigma H2' = J(H1'-H2') + J(H2'-H3') + J(H2'-H2")$$

$$\Sigma H2" = J(H1'-H2") + J(H2"-H3') + J(H2'-H2")$$

$$\Sigma H3' = J(H2'-H3') + J(H2"-H3') + J(H3'-H4') + J(H3'-^{31}P)$$

These summations include the absolute value of the geminal coupling J(H2'-H2"), which is not related to the deoxyribose conformation. It is expected to be close to ~ 14.0 Hz (25(a)) and this value has been used in analysis wherever required. The sums correspond to the distance in Hertz measured between the outer peaks of the H1', H2', H2" and H3' resonance patterns. For ΣH2' and ΣH2" the above statement is only strictly true when first order conditions apply (105,131). In the present case, the Δδ (H2'-H2") = δ(H2') - δ(H2") exceeds 40 Hz in all cases so that the nearest lines of the H2' and H2" resonance multiplets are separated from each other by at least 15 Hz and hence ΣH2' and ΣH2" can be trusted. The sums ΣH1' and ΣH3' are independent of Δδ (H2'-H2") although deceptively simple pattern are seen, when Δδ (H2'-H2") < 4 Hz a triplet for the H1' resonance and a quartet for H2'/H2" (105,131). The summation ΣH3' includes J (H3'-^{31}P) which affects the H3'-H2', H3'-H2" and H3'-H4' cross peak patterns. It does not directly pertain to the deoxyribose conformation and a fixed value of 5.8 Hz has been used (114) wherever required. For our analysis we have used spin-spin coupling values given by Van Wijk et al. (131) which are reproduced here in Table 5.5 (a-c) and Fig. 5.11. Structures with the motions of the sugar ring

Table 5.5(a)

CALCULATED COUPLING CONSTANTS FOR RANGE OF SUGAR GEOMETRIES OF DEOXYRIBOSE RING IN NUCLEOSIDES AND NUCLEOTIDES, ENCOUNTERED ALONG PSEUDOROTATION ITINERARY

	$J_{1'2'}$ for Φ_m			$J_{1'2''}$ for Φ_m			$J_{2'3'}$ for Φ_m			$J_{2''3'}$ for Φ_m			$J_{3'4'}$ for Φ_m		
p(°)	28°	36°	44°	28°	36°	44°	28°	36°	44°	28°	36°	44°	28°	36°	44°
0	1.3	0.8	0.7	7.9	7.5	6.8	7.5	6.6	5.5	8.6	10.0	11.0	7.0	8.0	8.7
9	1.5	1.1	0.8	8.1	7.7	7.3	7.5	6.6	5.6	8.5	9.9	10.9	7.4	8.3	9.0
18	1.9	1.4	1.0	8.2	8.0	7.7	7.6	6.8	5.8	8.3	9.7	10.8	7.6	8.6	9.2
27	2.4	1.9	1.5	8.3	8.2	8.1	7.7	7.1	6.2	8.0	9.3	10.4	7.8	8.7	9.3
36	3.0	2.6	2.2	8.4	8.3	8.3	7.9	7.4	6.6	7.5	8.8	9.9	7.8	8.8	9.3
45	3.7	3.4	3.2	8.3	8.3	8.3	8.1	7.7	7.2	6.9	8.1	9.2	7.8	8.7	9.3
54	4.4	4.4	4.4	8.2	8.2	8.2	8.3	8.0	7.7	6.2	7.2	8.2	7.6	8.6	9.2
63	5.3	5.5	5.7	8.0	8.0	7.9	8.4	8.3	8.1	5.4	6.2	7.0	7.4	8.3	9.0
72	6.1	6.6	7.1	7.8	7.6	7.4	8.5	8.5	8.4	4.6	5.1	5.6	7.0	8.0	8.7
81	6.9	7.6	8.3	7.5	7.2	6.8	8.5	8.5	8.5	3.8	4.0	4.2	6.5	7.4	8.2
90	7.6	8.5	9.3	7.2	6.7	6.2	8.4	8.4	8.4	3.0	3.0	3.0	6.0	6.8	7.5
99	8.2	9.2	10.1	6.9	6.3	5.6	8.2	8.2	8.1	2.3	2.1	1.9	5.3	6.0	6.6
108	8.7	9.8	10.6	6.6	5.8	5.0	8.0	7.8	7.6	1.7	1.4	1.2	4.6	5.0	5.5
117	9.1	10.2	11.0	6.3	5.5	4.6	7.7	7.4	7.0	1.3	1.0	0.8	3.9	4.1	4.3
126	9.4	10.5	11.2	6.1	5.2	4.2	7.4	6.9	6.4	1.0	0.7	0.6	3.2	3.2	3.2
135	9.6	10.6	11.3	6.0	5.1	4.0	7.0	6.4	5.7	0.8	0.6	0.7	2.5	2.3	2.2
144	9.6	10.7	11.3	6.0	5.0	4.0	6.7	6.0	5.1	0.7	0.6	0.9	1.9	1.6	1.4
153	9.6	10.6	11.3	6.0	5.1	4.0	6.5	5.6	4.6	0.6	0.7	1.1	1.5	1.1	0.9
162	9.4	10.5	11.2	6.1	5.2	4.2	6.3	5.3	4.3	0.6	0.8	1.4	1.1	0.8	0.6
171	9.1	10.2	11.0	6.3	5.5	4.6	6.1	5.1	4.1	0.6	0.9	1.5	0.9	0.6	0.5
180	8.7	9.8	10.6	6.6	5.8	5.0	6.1	5.1	4.0	0.6	0.9	1.6	0.7	0.5	0.6
189	8.2	9.2	10.1	6.9	6.3	5.6	6.1	5.1	4.1	0.6	0.9	1.5	0.6	0.5	0.7
198	7.6	8.5	9.3	7.2	6.7	6.2	6.3	5.3	4.3	0.6	0.8	1.4	0.6	0.5	0.8
207	6.9	7.6	8.3	7.5	7.2	6.8	6.5	5.6	4.6	0.6	0.7	1.1	0.6	0.6	0.9
216	6.1	6.6	7.1	7.8	7.6	7.4	6.7	6.0	5.1	0.7	0.6	0.9	0.5	0.6	0.9
225	5.3	5.5	5.7	8.0	8.0	7.9	7.0	6.4	5.7	0.8	0.6	0.7	0.6	0.6	0.9
234	4.4	4.4	4.4	8.2	8.2	8.2	7.4	6.9	6.4	1.0	0.7	0.6	0.6	0.5	0.8
243	3.7	3.4	3.2	8.3	8.3	8.3	7.7	7.4	7.0	1.3	1.0	0.8	0.6	0.5	0.7
252	3.0	2.6	2.2	8.4	8.3	8.3	8.0	7.8	7.6	1.7	1.4	1.2	0.7	0.5	0.6
261	2.4	1.9	1.5	8.3	8.2	8.1	8.2	8.2	8.1	2.3	2.1	1.9	0.8	0.6	0.5
270	1.9	1.4	1.0	8.2	8.0	7.7	8.4	8.4	8.4	3.0	3.0	3.0	1.0	0.8	0.6
279	1.5	1.1	0.8	8.1	7.7	7.3	8.5	8.5	8.5	3.8	4.0	4.2	1.5	1.1	0.9
288	1.3	0.8	0.7	7.9	7.5	6.8	8.5	8.5	8.4	4.6	5.1	5.6	1.9	1.6	1.4
297	1.1	0.7	0.7	7.8	7.2	6.4	8.4	8.3	8.1	5.4	6.2	7.0	2.5	2.3	2.2
306	1.0	0.7	0.7	7.6	7.0	6.1	8.3	8.0	7.7	6.2	7.2	8.2	3.2	3.2	3.2
315	0.9	0.7	0.8	7.6	6.8	5.9	8.1	7.7	7.2	6.9	8.1	9.2	3.9	4.1	4.3
324	0.9	0.7	0.8	7.5	6.8	5.8	7.9	7.4	6.6	7.5	8.8	9.9	4.6	5.0	5.5
333	0.9	0.7	0.8	7.6	6.8	5.9	7.7	7.1	6.2	8.0	9.3	10.4	5.3	6.0	6.6
342	1.0	0.7	0.7	7.6	7.0	6.1	7.6	6.8	5.8	8.3	9.7	10.8	6.0	6.8	7.5
351	1.1	0.7	0.7	7.8	7.2	6.4	7.5	6.6	5.6	8.5	9.9	10.9	6.5	7.4	8.2

(Reproduced from ref.(131)).

Table 5.5(b)

CALCULATED SUMS OF COUPLING CONSTANTS FOR RANGE OF SUGAR GEOMETRIES OF DEOXYRIBOSE RING IN NUCLEOSIDES AND NUCLEOTIDES, ENCOUNTERED ALONG PSEUDOROTATION ITINERARY

	Σ 1′ for Φ_m			Σ 2′ for Φ_m			Σ 2″ for Φ_m			Σ 3′ for Φ_m		
P(°)	28°	36°	44°	28°	36°	44°	28°	36°	44°	28°	36°	44°
0	9.2	8.3	7.5	22.7	21.4	20.2	30.5	31.4	31.8	23.1	24.5	25.3
9	9.6	8.8	8.0	23.0	21.7	20.4	30.6	31.6	32.2	23.4	24.9	25.6
18	10.1	9.4	8.7	23.5	22.2	20.9	30.5	31.7	32.5	23.5	25.1	25.8
27	10.7	10.1	9.6	24.1	23.0	21.7	30.3	31.5	32.5	23.5	25.1	25.9
36	11.3	10.9	10.5	24.9	24.0	22.9	29.9	31.1	32.2	23.3	24.9	25.9
45	12.0	11.8	11.6	25.8	25.1	24.4	29.2	30.4	31.5	22.8	24.5	25.6
54	12.7	12.7	12.7	26.7	26.5	26.1	28.4	29.4	30.4	22.1	23.8	25.1
63	13.3	13.5	13.6	27.7	27.8	27.8	27.5	28.2	28.9	21.2	22.8	24.1
72	13.9	14.2	14.5	28.6	29.0	29.5	26.4	26.7	27.0	20.1	21.5	22.7
81	14.4	14.8	15.1	29.4	30.1	30.8	25.3	25.2	25.1	18.8	19.9	21.0
90	14.8	15.2	15.5	30.0	30.9	31.7	24.2	23.7	23.2	17.4	18.1	18.9
99	15.1	15.5	15.7	30.5	31.4	32.2	23.1	22.4	21.5	15.8	16.2	16.6
108	15.3	15.6	15.7	30.7	31.6	32.2	22.3	21.3	20.2	14.3	14.3	14.3
117	15.5	15.7	15.6	30.8	31.6	32.0	21.6	20.5	19.3	12.8	12.4	12.1
126	15.5	15.7	15.4	30.8	31.4	31.5	21.1	19.9	18.9	11.5	10.8	10.1
135	15.6	15.7	15.3	30.6	31.0	31.0	20.8	19.7	18.7	10.3	9.4	8.6
144	15.6	15.7	15.3	30.4	30.6	30.4	20.6	19.6	18.9	9.3	8.3	7.4
153	15.6	15.7	15.3	30.0	30.2	29.9	20.6	19.8	19.2	8.6	7.4	6.7
162	15.5	15.7	15.4	29.7	29.8	29.5	20.8	20.0	19.6	8.0	6.9	6.2
171	15.5	15.7	15.6	29.3	29.3	29.0	20.9	20.4	20.1	7.6	6.6	6.1
180	15.3	15.6	15.7	28.8	28.9	28.6	21.2	20.8	20.6	7.5	6.5	6.1
189	15.1	15.5	15.7	28.4	28.3	28.1	21.5	21.2	21.1	7.4	6.5	6.3
198	14.8	15.2	15.5	27.9	27.8	27.6	21.8	21.5	21.6	7.5	6.7	6.4
207	14.4	14.8	15.1	27.4	27.2	26.9	22.1	21.9	22.0	7.6	6.9	6.7
216	13.9	14.2	14.5	26.8	26.5	26.2	22.5	22.3	22.3	7.9	7.2	6.9
225	13.3	13.5	13.6	26.3	25.9	25.5	22.8	22.6	22.6	8.4	7.6	7.3
234	12.7	12.7	12.7	25.8	25.3	24.8	23.2	22.9	22.8	8.9	8.1	7.8
243	12.0	11.8	11.6	25.3	24.8	24.3	23.6	23.3	23.1	9.6	8.9	8.4
252	11.3	10.9	10.5	24.9	24.4	23.9	24.1	23.8	23.5	10.4	9.8	9.4
261	10.7	10.1	9.6	24.6	24.1	23.6	24.6	24.3	24.0	11.4	10.9	10.5
270	10.1	9.4	8.7	24.3	23.8	23.4	25.2	25.0	24.7	12.5	12.2	12.0
279	9.6	8.8	8.0	24.0	23.6	23.3	25.8	25.7	25.5	13.7	13.6	13.6
288	9.2	8.3	7.5	23.8	23.3	23.1	26.5	26.5	26.4	15.0	15.2	15.4
297	8.9	7.9	7.1	23.5	23.0	22.8	27.2	27.4	27.4	16.4	16.8	17.2
306	8.6	7.7	6.8	23.3	22.7	22.4	27.9	28.2	28.3	17.7	18.4	19.0
315	8.5	7.5	6.7	23.0	22.4	21.9	28.5	28.9	29.1	18.9	19.9	20.6
324	8.4	7.4	6.6	22.8	22.0	21.4	29.1	29.6	29.8	20.0	21.2	22.0
333	8.5	7.5	6.7	22.7	21.7	20.9	29.6	30.2	30.3	21.0	22.3	23.2
342	8.6	7.7	6.8	22.6	21.5	20.5	30.0	30.7	30.9	21.9	23.3	24.1
351	8.9	7.9	7.1	22.6	21.4	20.3	30.3	31.1	31.4	22.6	24.0	24.8

Table 5.5(c)

CALCULATED SUMS OF COUPLINGS FOR VARIOUS CONFORMATIONAL EQUILIBRIUM COMPOSITIONS AND S-TYPE GEOMETRIES

	P_s 108°				P_s 153°				P_s 180°			
X_s	Σ 1′	Σ 2′	Σ 2″	Σ 3′	Σ 1′	Σ 2′	Σ 2″	Σ 3′	Σ 1′	Σ 2′	Σ 2″	Σ 3′
0	9.4	22.2	31.7	25.1	9.4	22.2	31.7	25.1	9.4	22.2	31.7	25.1
5	9.7	22.7	31.2	24.6	9.7	22.6	31.1	24.2	9.7	22.5	31.1	24.2
10	10.0	23.1	30.7	24.0	10.0	23.0	30.5	23.3	10.0	22.9	30.6	23.2
15	10.3	23.6	30.1	23.5	10.3	23.4	29.9	22.4	10.3	23.2	30.1	22.3
20	10.6	24.1	29.6	22.9	10.7	23.8	29.3	21.6	10.6	23.5	29.5	21.4
25	11.0	24.6	29.1	22.4	11.0	24.2	28.7	20.7	11.0	23.9	29.0	20.4
30	11.3	25.0	28.6	21.8	11.3	24.6	28.1	19.8	11.3	24.2	28.4	19.5
35	11.6	25.5	28.0	21.3	11.6	25.0	27.5	18.9	11.6	24.5	27.9	18.6
40	11.9	26.0	27.5	20.8	11.9	25.4	26.9	18.0	11.9	24.9	27.3	17.7
45	12.2	26.4	27.0	20.2	12.2	25.8	26.3	17.2	12.2	25.2	26.8	16.7
50	12.5	26.9	26.5	19.7	12.5	26.2	25.7	16.3	12.5	25.5	26.2	15.8
55	12.8	27.4	26.0	19.1	12.9	26.6	25.1	15.4	12.8	25.9	25.7	14.9
60	13.1	27.8	25.4	18.6	13.2	27.0	24.5	14.5	13.1	26.2	25.1	13.9
65	13.5	28.3	24.9	18.1	13.5	27.4	23.9	13.6	13.5	26.5	24.6	13.0
70	13.8	28.8	24.4	17.5	13.8	27.8	23.4	12.7	13.8	26.9	24.0	12.1
75	14.1	29.3	23.9	17.0	14.1	28.2	22.8	11.9	14.1	27.2	23.5	11.2
80	14.4	29.7	23.4	16.4	14.4	28.6	22.2	11.0	14.4	27.5	22.9	10.2
85	14.7	30.2	22.8	15.9	14.7	29.0	21.6	10.1	14.7	27.9	22.4	9.3
90	15.0	30.7	22.3	15.4	15.0	29.4	21.0	9.2	15.0	28.2	21.9	8.4
95	15.3	31.1	21.8	14.8	15.4	29.8	20.4	8.3	15.3	28.5	21.3	7.4
100	15.6	31.6	21.3	14.3	15.7	30.2	19.8	7.4	15.6	28.9	20.8	6.5

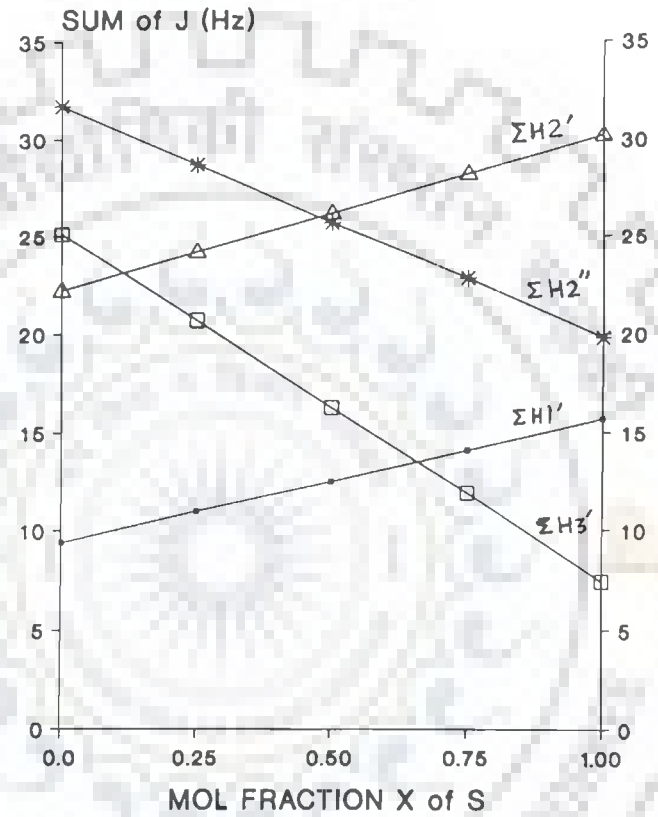

Fig. 5.11 : Predicted sums of coupling constants plotted versus mole fraction of S-type conformer for deoxyribofuranose rings in nucleosides and nucleotides that occur in a fast conformational equilibrium between an N-type conformer (P_N 18°, ϕ_N 36°) and an S-type conformer (P_S 153°, ϕ_S 36°) (131).

restricted to a small region of the P angle, the following observations about J values are made from the data of Table 5.5 (a) (131), when P value is gradually changed from 162° to 9° :

(a) J(H1'-H2') decreases significantly by ~ 9 Hz from a value of 10.5 Hz to 1.1 Hz.

(b) J(H1'-H2") increases to a lesser extent by ~ 2.5 Hz from a value of 5.2 Hz to 7.7 Hz.

(c) J(H2'-H3') first increases from 5.3 Hz to 8.5 Hz then decreases to 6.6 Hz so that the net change is rather small ~ 1.3 Hz.

(d) J(H2"-H3') first increases slowly then rapidly to a significant extent from 0.8 Hz to 9.9 Hz.

(e) J(H3'-H4') increases at a uniform rate but significantly from 0.8 Hz to 8.3 Hz.

Hence the change in sugar conformation gets reflected in J(H1'-H2'), J(H2"-H3') and J(H3'-H4').

From Table 5.5(b) (131), it is seen that when P value is gradually changed from 162° to 9°, the :

(f) ΣH1' decreases from 15.7 Hz to 8.8 Hz.

(g) ΣH2' increases from 29.8 to 31.6 Hz and then decreases ultimately to 21.7 Hz.

(h) ΣH2" increases from 20.0 Hz to 31.6 Hz.

(i) ΣH3′ increases most dramatically from 6.9 Hz to 24.9 Hz and hence is very sensitive to the pseudorotation angle.

These observations are very useful in ascertaining the presence of C3′-endo ⇌ C2′-endo equilibrium in solutions. Starting from the pure S conformer with P = 162°, as the fraction population of N conformer is increased from 0 to 1, the following will result (45) :

(j) J(H1′-H2′) decreases significantly from 10.5 to 1.1 Hz.

(k) J(H1′-H2") increases to a lesser extent from 5.2 to 7.7 Hz.

(l) J(H2′-H3′) does not show any variation and hence is independent of the proportion of S and N conformer (due to (g) stated above). Its value is ~ 6 Hz (45).

(m) J(H2"-H3′) increases significantly from 0.8 Hz to 9.9 Hz.

(n) J(H3′-H4′) increases significantly from 0.8 to 8.3 Hz in a manner similar to J(H2"-H3′).

The last observation, that is, (n) is particularly crucial since this allows the identification of the presence of a C3′-endo ⇌ C2′-endo (N ⇌ S) equilibrium even without actually measuring the magnitudes of the coupling constants and by simply monitoring the relative intensities of the cross peaks in a low resolution COSY spectrum (45). In a low resolution COSY spectrum, the intensity

of a cross peak is largely determined by the magnitude of the active coupling constant. Thus the intensities of the H2"-H3′ and H3′-H4′ cross peaks are largely determined by the respective coupling constants, the multiplicities in both these cross peaks are similar. Thus in a given COSY spectrum, if these two types of cross peaks have dissimilar intensities, it would imply that the sugar geometry is different to C3′-endo [J(H2"-H3′) ≃ J(H3′-H4′) ~ 9 Hz] or C2′-endo [J(H2"-H3′) = J(H3′-H4′) = 0.8 Hz] or there is no C3′-endo ⇌ C2′-endo equilibrium. [J(H2"-H3′) = J(H3′-H4′) ≃ 0.9 Hz for χ_S= 0.90; J(H2"-H3′) = J(H3′-H4′) ≃ 1.8 Hz for χ_S = 0.80; and so on]. In the present investigations, which are not exactly a low resolution COSY experiment, the cross peak pattern of H2"-H3′ as well as H3′ - H4′ are observed for G6, C1 and C5 residue (Fig. 5.5 (e-g)). A quick approximate inference may be drawn that these are likely to be in a dynamic C3′-endo ⇌ C2′-endo conformers equilibrium (Table 5.3). Further for G2 residue, both the cross peak patterns, i.e. H2"-H3′ and H3′-H4′ are not observed (Fig. 5.5 (e-g)) which may also be either a pure C2′-endo conformer or a dynamic C3′-endo ⇌ C2′-endo conformers with relatively very low fractional population of C3′-endo conformer. For A3 and T4 residues, the H2"-H3′ cross peak patterns are not seen (may be very weak) but relatively intense H3′-H4′ cross peak patterns are found to exist. It is possible that these have a dynamic N ⇌ S conformer equilibrium with P_S value quite different from that of C2′-endo i.e. 162° or else a single conformer other than that for P_S = 162° or else a more complex deoxyribose

conformation. However a more systematic analysis is carried out by following strategies discussed below.

Van Wijk et al. (131) have shown the importance of sums of couplings and have predicted those for different mole fractions of S-conformer for sugars existing in a fast conformational equilibrium between an N type conformer ($P_N = 18^\circ$, $\phi_m = 36^\circ$) and an S-type conformer ($P_S = 153^\circ$, $\phi_m = 36^\circ$) which are reproduced in Table 5.5(c) and Fig. 5.11. The following observations useful in ascertaining the presence of N $\rightleftharpoons$ S equilibrium are made for an increase in mole fraction of N conformer from 0 to 1 :

(o) ΣH1′ decreases from 15.7 Hz to 8.8 Hz.

(p) ΣH2′ decreases from 30 Hz to 22 Hz.

(q) ΣH2" increases from 20 Hz to 31.6 Hz.

(r) ΣH3′ increases dramatically from 6.9 to 24.9 Hz.

For most oligonucleotides, χ_S is found to lie in the range 0.65 to 1.0 (5,72,114,114(a),131). Fig. 5.11 shows that the difference between ΣH2′ and ΣH2" is least for $\chi_S = 0.50$; it being ~ 0.5 Hz. The difference increases to 2.5, 6.4 and 10.4 Hz for χ_S = 0.6, 0.8 and 1.0, respectively. It is notable since inspite of poor resolution in 2D DQF-COSY spectra, the ΣH2′ and ΣH2" values along the better resolved ω_2 axis can still be differentiated. A smaller difference in ΣH2′ and ΣH2" will correspond to a greater fraction of N conformer to be present in solution. This observation is however to be used more cautiously since it has

been observed (114) that the line width for H2′ proton are generally 2-3 Hz larger than that for H2" protons due to different environment and molecular motions. Further the smallest line width are found for terminal residues (6-9 Hz) while the non terminal ones exhibit larger variations (7-12 Hz).

In order to analyse the deoxyribose sugar conformation we have first attempted to match the cross peak patterns obtained in DQF COSY spectra with Fig. 5.10. As a second step, we followed the strategy of Van Wijk et al. (131) in which the first marker used is ΣH1′. It was possible to measure these from the peak print outs of the 1D NMR spectra to an accuracy of 0.5 Hz (resolution in 1D NMR spectra) particularly at 305, 310, 315, 320 and 325 K. In few cases, ΣH1′ was obtained at 295 and 297 K also. The observed values are found in the range 13.5-15.0 Hz. It has been shown (131) that a value in excess of 13.2 Hz indicates a predominance of the S-type conformer ($\chi_S \geq 65 \pm 5\%$). If that is the case a relatively safe conclusion follows: of the two H2′/H2" multiplets the one with the largest separation between the outer lines (typically 26-32 Hz) can be identified with H2′; the signal with the smaller separation (typically 19-25 Hz) is then assigned to H2". In the majority of cases an S/N conformer ratio no less than 65/35 also implies that the larger of the two couplings present in the H1′ multiplet belongs to J(H1′-H2′). The value of ΣH1′ is not very sensitive (Table 5.5 (c) and Fig. 5.11) to variations in P_S and ϕ_S and is used to determine the approximate

fraction for S-type conformer ($\chi_S \pm 0.05$) whenever the S form predominates :

$$\chi_S = (\Sigma H1' - 9.4) / (15.7 - 9.4) \qquad ...(5.1)$$

We have also looked into the fine splitting of H1′ resonance which allows a good insight into the population ratio of the sugar ring χ_S / χ_N (105). It has been shown that the H1′ resonance appears as a quartet (Fig. 5.12) and the distance between the outer peaks exceeds 14.5 Hz; the larger the distance between the inner two peaks of the quartet the higher the conformational purity. In contrast, the observation of a H1′ resonance of a given residue which occurs as a triplet and for which the corresponding H2′ and H2" resonances are not (near) isochronous, indicates that the sugar ring of this residue displays a relatively high conformational flexibility, $0.40 \leq \chi_S \leq 0.70$. We observed a quartet with maximum separation between inner two peaks for G2 residue (Fig. 5.3 (a)) at 305-325 K. The G6 residue on the other hand is a triplet (Fig. 5.1 (b) and 5.2 (b)) while all other residues show a pattern in between the two extremes.

Once χ_S is known to a first approximation the next step (third step) is to use the simulated DQF-COSY cross peaks for different mixtures using a dynamic two state model for deoxyribose with $P_S = 162^\circ$ and $P_N = 9^\circ$ for the interconverting conformers available in literature (10,72,72(a),114,114(a),130,130(a)). We have used those obtained by Schmitz et al. (114) more frequently which are reproduced here as Fig. 5.13. We made an attempt to

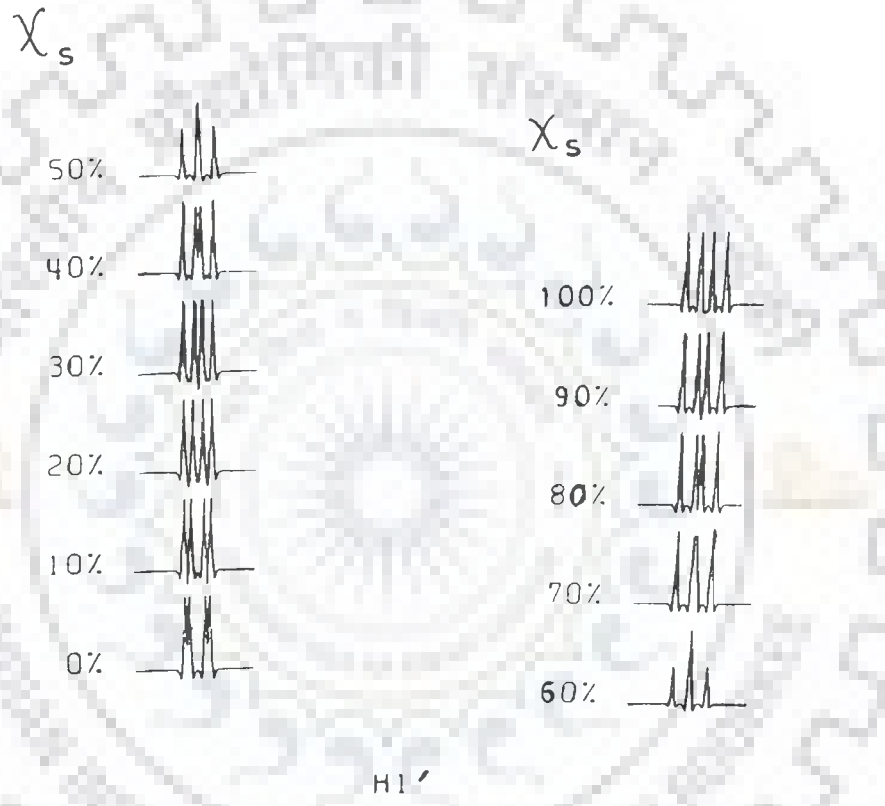

Fig. 5.12 : Predicted splitting patterns of the H1′ resonance for different values of the fraction S-type conformer (105).

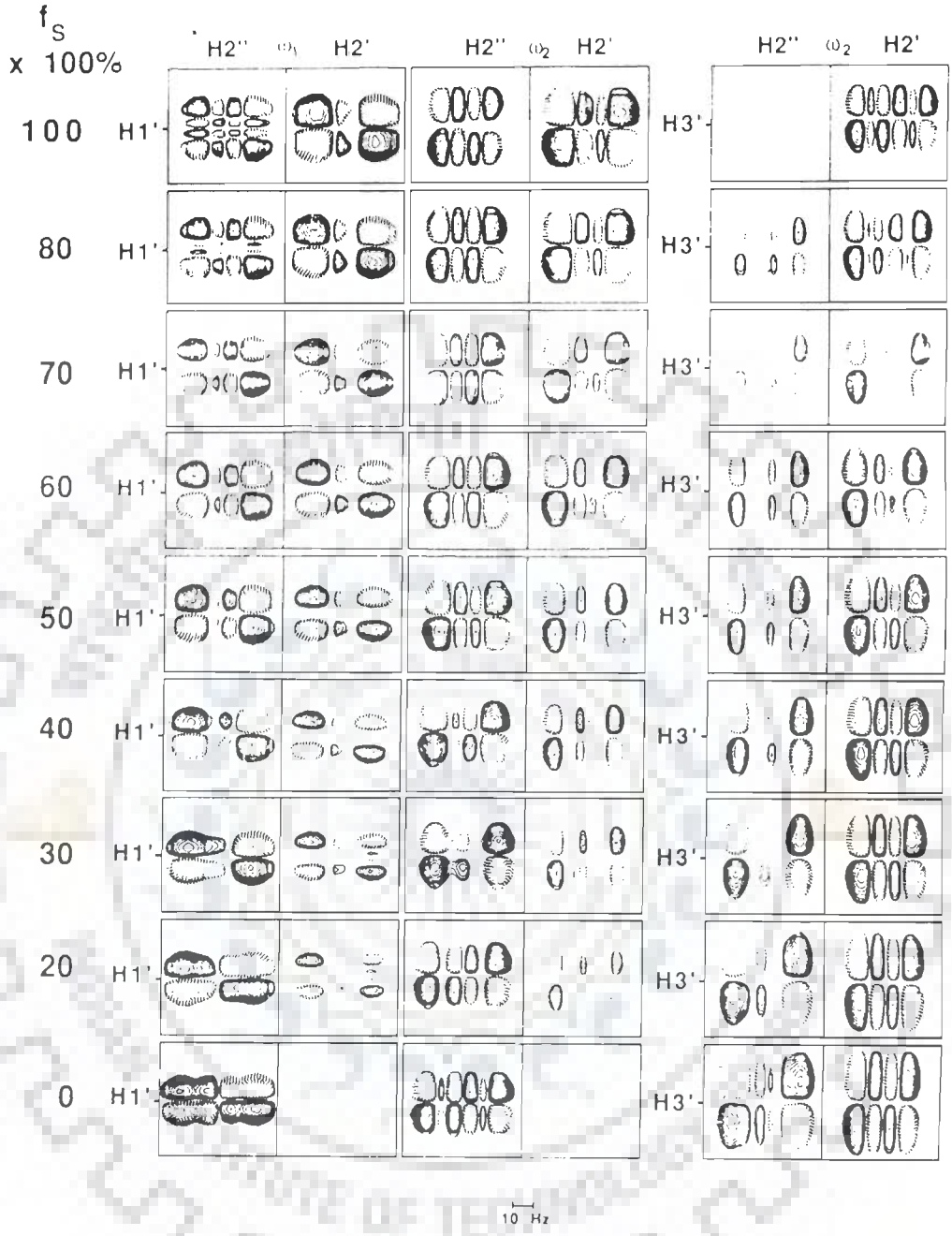

Fig. 5.13 : Simulated DQF-COSY cross peaks for different mixtures using a dynamic two-state model for deoxyribose, with $P_S = 162^\circ$ and $P_N = 9^\circ$ for the interconverting conformers ($\phi_m = 35^\circ$) : H1' H2"-ω_1, H1' H2'-ω_1, H1' H2"-ω_2, H1' H2'-ω_2, H3' H2"-ω_2 and H3' H2'-ω_2 from left to right (114). Vicinal coupling constants for the conformers are taken from Rinkel and Altona (105).

match the observed patterns with Fig. 5.13 and arrived at a value of χ_S. In most cases, the value obtained matched with that obtained from ΣH1′ using 1D NMR spectra and equation (5.1) within ± 10%. In a particular case, where in the observed cross peak pattern did not match with Fig. 5.13, an alternate, such as presence of three conformations in equilibrium was looked into.

The fourth step is to use the sum of couplings for $P_N = 18^\circ$, $\phi_N = 36^\circ$ or $P_N = 9^\circ$, $\phi_N = 36^\circ$ (Table 5.5 (a,b)) and the same for unknown S-type form at hand for $P_S = 108^\circ$, 153° and 180°, $\phi_S = 36^\circ$ (Table 5.5(c) and Fig. 5.11). The corresponding observed values from 1D NMR (to an accuracy of ± 0.5 Hz) are fitted in three sets of predicted lines at χ_S = ± 0.05 simultaneously (Table 5.5(c)). With some experience we are able to narrow the possible P_S range of solutions. As a final step, we calculated J values and sums of couplings by adjusting P_S untill all the observed results are in agreement with the calculated values.

The analysis of deoxyribose sugar of each residue following this procedure is illustrated below :

G2

The observed values of couplings, sums of couplings, separation between inner two peaks of H1′ quartet from 1D NMR spectra at different temperatures are given in Table 5.6(a,b). The average value of ΣH1′ at 305 K = 15.0 Hz is used to evaluate χ_S as follows :

$$\chi_S = \frac{15.0 - 9.4}{15.7 - 9.4} = 0.89$$

Since ΣH1′ is accurate to a value of ± 0.50 Hz, the χ_S value may essentially lie in the range 0.83 to 0.95 within the experimental errors. The H1′ peak is found to be quartet from 305-325 K (Fig. 5.2(b), 5.3(a)). Further, of all the residues, G2 residue has maximum value of ΣH1′ and maximum separation between the inner two peaks of quartet (105) and therefore has the least mixing with N conformer. Since south/north conformer ratio (105) is rather high, it also implies (131) that the larger of the two couplings is J(H1′-H2′) in the H1′ quartet (Fig. 5.3(a)). Due to overlapping ΣH2′ is not available from 1D NMR spectra but ΣH2" is ≃ 21 Hz at 297 K. The rough estimate from DQF COSY (Fig. 5.5(b)) of ΣH2′ and ΣH2" with distance equal to about one line width added to them are about 39 and 30 Hz (± 2.3 Hz), respectively (Table 5.7) while the ΣH3′ value at 325 K is ≃ 15.1 Hz (± 0.5 Hz) (Fig. 5.2(c)). The cross peaks of both H2" - H3′ as well as H3′ - H4′ are not observed (Table 5.3) in DQF COSY spectra (Fig. 5.5(e-g)) so that the active couplings involved are low and < 2.3 Hz, that is, below the digital resolution of 2.3 Hz/point used along ω_2 axis. It is only G2 residue which does not show H3′ - H4′ cross peak (Table 5.3) which is in confirmity with the fact that it has the maximum content of S conformer (highest χ_S value observed). The observed patterns of H1′ -H2′, H1′ - H2" and H2′ - H3′ cross peaks obtained in DQF COSY spectra (Fig. 5.5(d-f)) are matched with the simulated patterns shown in Fig. 5.10 (114) for a rigid

sugar conformer. For patterns above the diagonal (Fig. 5.5(d,e)) we get the following :

(a) H1′ - H2′ pattern indicates (Fig. 5.10) P = 135°- 180°.

(b) H1′ - H2" pattern indicates (Fig. 5.10) P = 108°- 180°.

(c) H2′ - H3′ pattern indicates (72(a)) P = 144°- 162°.

(d) Absence of H2" - H3′ pattern indicates (72(a),114) P = 99°- 252°.

(e) Absence of H3′ - H4′ pattern indicates (72(a)) P = 144°- 288°.

For patterns below the diagonal (Fig. 5.5 (f)), we have :

(f) H1′ - H2′ pattern indicates (Fig. 5.10) P = 153°- 207°.

(g) H1′ - H2" pattern indicates (Fig. 5.10) P = 108° - 225°.

(h) H2′ - H3′ pattern (a six peak pattern) indicates (Fig. 5.10) P = 153° - 180°.

(i) Absence of H2" - H3′ pattern indicates (Fig. 5.10) P = 99°- 225°.

Combining (a-i), it is found that P_S = 153° - 180° fits into all the observed DQF patterns satisfactorily. We also attempted to compare the observed patterns with those for a dynamic two

state model (114), and it is found (Fig. 5.13) that the observed patterns match with that expected between those for 100% S and 80% S conformer and are rather more close to that for 100% S conformer with $P_S = 162^\circ$. Finally, we calculated the various couplings and sums of couplings by considering $P_N = 9^\circ$, 18° and $P_S = 144^\circ$, 153°, 162°, 180° for $\chi_S = 0.87 - 0.95$ and attempted to match particularly the observed values of J(H1′ - H2′), J(H1′ - H2") and ΣH1′ as 10.0, 5.0 and 15.0 Hz (Table 5.6(b)). Table 5.6 (a) shows that the values of J(H1′ - H2′), J(H1′ - H2"), ΣH1′ increase (8.9 to 10.0), decrease (5.9-5.0) and increase (14.8 to 15.0) with decrease in temperature from 320 to 297 K systematically and hence exhibits increase in proportion of S conformer (Table 5.5 (a-c)). The ΣH3′ observed at 325 K as 15.1 Hz is therefore expected to be lower at 297 K (Table 5.5 (a-c)). We also applied the constraint that J(H2" - H3′), J(H3′ - H4′), ΣH2′, ΣH2" and ΣH3′ be < 2.3, < 2.3, 19-23, 26-32 and ≃ 9 Hz (that observed at 325 K - J(H3′-P) coupling i.e. 15.1 - 5.8 = 9.3), respectively. Table 5.7 shows the results of such calculations and it is easily seen that P_S = $153^\circ/162^\circ$, $\chi_S = 0.94$ with $P_N = 9^\circ/18^\circ$, $\chi_N = 0.06$ fits into all the observed results (Table 5.7, 5.8).

A3

Considering A3 residue in d-$(CGATCG)_2$ since ΣH1′ = 14.6 Hz, the S conformer is the predominant one, the $\chi_S = 0.83$ with the exact value possibly in the range $\chi_S = 0.77$ to 0.89 by taking the error in the ΣH1′ to be ± 0.5 Hz. The H1′ peak is seen as a

Table 5.6(a) : The observed values of coupling constants (in Hertz) and sum of couplings (in Hertz) from 1D NMR spectra of d-$(CGATCG)_2$ at different temperatures.

Temp. (K)	C1	G2	A3	T4	C5	G6
J(H1′ -H2′)						
325	7.3	8.1	7.6	0	0	6.8
320	7.2	8.9	8.5	8.1	0	6.9
315	7.4	9.4	8.7	8.5	0	7.0
310	0	10.0	8.8	8.5	0	7.0
305	0	10.0	8.8	8.3	0	7.1
297	0	-	8.4	8.1	0	7.2
295	0	-	7.8	8.1	0	7.4
J(H1′ -H2")						
325	6.5	6.6	6.6	0	0	6.8
320	6.6	5.9	5.9	6.4	0	6.8
315	0	5.4	5.8	6.1	0	6.9
310	0	5.1	5.8	6.2	0	7.0
305	0	5.0	5.9	6.2	0	7.0
297	0	-	6.1	6.7	0	7.0
295	0	-	6.8	6.7	0	7.0
ΣH1′						
325	13.9	14.7	14.3	0	0	13.5
320	13.9	14.8	14.4	14.5	0	13.7
315	0	14.9	14.5	14.6	0	13.8
310	0	14.9	14.6	14.7	0	14.0

305	0	15.0	14.6	14.5	0	14.1
297	0	-	14.6	14.7	0	14.2
295	0	-	14.6	14.5	0	14.4
Separation						
325	0.8	1.6	1.0	0	0	0.0
320	0.6	3.0	2.6	1.7	0	0.1
315	0	4.0	2.9	2.4	0	0.1
310	0	4.7	3.0	2.3	0	0.0
305	0	5.1	2.9	2.1	0	0.1
297	0	-	2.3	1.4	0	0.2
295	0	-	1.0	1.4	0	0.4

Separation = J(H1'-H2')-J(H1'-H2")

All values are within accuracy of ± 0.5 Hz

O : Overlapping of peaks.

Table 5.6 (b) : Observed average values of J(in Hertz) and sum of couplings (in Hertz) from 1D NMR spectra (Fig. 5.1 (b) and 5.2 (b,c) to an accuracy of ± 0.5 Hz. The average value at 305 K extrapolated and used for analysis is shown below.

	C1	G2	A3	T4	C5	G6
J(H1'-H2')	7.3	10.0	8.8	8.3	0	7.1
J(H1'-H2")	6.6	5.0	5.9	6.2	0	7.0
ΣH1'	13.9	15.0	14.6	14.5	0	14.1
ΣH3'	14.1	15.1	15.8	18.3	18.4	18.9
ΣH3'-J(H3'-P)	8.3	9.3	10.0	12.5	12.6	13.1

ΣH3' is measured at 325 K and it includes J(H3'-P) coupling of 5.8 Hz.

Table 5.7 : Calculated value of J (in Hertz) and sum of couplings (in Hertz) for a mixture of deoxyribose sugar at various P_S and P_N values and those observed experimentally for all residues.

	Coupling constants					Sum of couplings			
	1'-2'	1'-2"	2'-3'	2"-3'	3'-4'	ΣH1'	ΣH2'	ΣH2"	ΣH3'
G2									
P_S=162°, χ_S = 0.94, P_N = 18°, χ_N = 0.06									
	10.0	5.4	5.4	1.3	1.3	15.3	29.3	20.7	8.0
P_S = 162°, χ_S = 0.94, P_N = 9°, χ_N = 0.06									
	9.9	5.1	5.4	1.4	1.2	15.0	29.3	20.7	8.0
P_S = 153°, χ_S = 0.94, P_N = 18°, χ_N = 0.06									
	10.0	5.3	5.6	1.2	1.6	15.3	29.7	20.5	8.5
P_S = 153°, χ_S = 0.94, P_N = 9°, χ_N = 0.06									
	10.0	5.3	5.7	1.3	1.5	15.3	29.6	20.5	8.5
Observed									
	10.0	5.0	>2.3	<2.3	<2.3	15.0	~29.0	~21.0	~9.0
A3									
P_S = 162°, χ_S = 0.82, P_N = 18°, χ_N = 0.18									
	8.9	5.7	5.6	2.4	2.1	14.6	28.4	22.1	10.0
P_S = 162°, χ_S = 0.82, P_N = 9°, χ_N = 0.18									
	8.8	5.6	5.5	2.4	2.0	14.5	28.3	22.1	10.1
P_S = 153°, χ_S = 0.82, P_N = 18°, χ_N = 0.18									
	8.9	5.6	5.8	2.3	2.5	14.6	28.4	22.1	10.1
P_S = 144°, χ_S = 0.82, P_N = 18°, χ_N = 0.18									
	9.0	5.5	6.1	2.2	2.9	14.6	29.1	21.8	11.3

	Coupling constants					Sum of couplings			
	1′-2′	1′-2"	2′-3′	2"-3′	3′-4′	ΣH1′	ΣH2′	ΣH2"	ΣH3′
$P_S = 153^\circ$, $\chi_S = 0.81$, $P_N = 18^\circ$, $\chi_N = 0.19$									
	8.8	5.7	5.8	2.4	2.7	14.5	28.7	22.1	10.8
$P_S = 153^\circ$, $\chi_S = 0.80$, $P_N = 18^\circ$, $\chi_N = 0.20$									
	8.7	5.6	5.8	2.5	2.6	14.4	28.6	22.2	10.8
$P_S = 144^\circ$, $\chi_S = 0.80$, $P_N = 18^\circ$, $\chi_N = 0.20$									
	8.8	5.6	6.2	2.4	3.0	14.4	28.9	22.0	11.7
Observed									
	8.8	5.9	>2.3	<2.3	>2.3	14.6	-	-	~10
G6									
$P_S = 99^\circ$, $\chi_S = 0.75$, $P_N = 18^\circ$, $\chi_N = 0.25$									
	7.2	7.2	7.9	4.0	6.7	14.4	29.1	24.7	18.4
$P_S = 117^\circ$, $\chi_S = 0.75$, $P_N = 18^\circ$, $\chi_N = 0.25$									
	8.0	6.0	7.3	3.2	5.2	14.1	29.3	23.3	15.6
$P_S = 135^\circ$, $\chi_S = 0.75$, $P_N = 9^\circ$, $\chi_N = 0.25$									
	8.2	5.7	6.4	2.9	3.8	14.0	28.7	22.7	13.3
$P_S = 135^\circ$, $\chi_S = 0.75$, $P_N = 18^\circ$, $\chi_N = 0.25$									
	8.3	5.8	6.5	2.9	3.9	14.1	28.8	22.7	13.3
$P_S = 153^\circ$, $\chi_S = 0.75$, $P_N = 18^\circ$, $\chi_N = 0.25$									
	8.3	5.8	5.2	3.0	3.0	14.1	27.9	22.8	11.8
$P_S = 189^\circ$, $\chi_S = 0.75$, $P_N = 18^\circ$, $\chi_N = 0.25$									
	7.3	6.7	5.5	3.1	2.5	14.0	26.8	23.8	11.1
$P_S = 189^\circ$, $\chi_S = 0.75$, $P_N = 9^\circ$, $\chi_N = 0.25$									
	7.1	6.6	5.5	3.2	2.4	13.8	26.7	23.8	11.0

	Coupling constants					Sum of couplings			
	1′-2′	1′-2"	2′-3′	2"-3′	3′-4′	ΣH1′	ΣH2′	ΣH2"	ΣH3′
$P_S = 198^\circ$, $\chi_S = 0.75$, $P_N = 18^\circ$, $\chi_N = 0.25$									
	6.7	7.0	5.7	2.6	2.5	13.7	26.4	24.0	11.3
$P_S = 207^\circ$, $\chi_S = 0.75$, $P_N = 18^\circ$, $\chi_N = 0.25$									
	6.1	7.4	5.9	2.9	2.6	13.5	26.0	24.4	11.3
Observed									
	7.1	7.0	>2.3	>2.3	>2.3	14.1	-	-	~11.6
T4									
$P_S = 135^\circ$, $\chi_S = 0.80$, $P_N = 18^\circ$, $\chi_N = 0.20$									
	8.7	5.6	6.4	2.4	3.5	14.3	29.1	22.1	12.5
$P_S = 144^\circ$, $\chi_S = 0.80$, $P_N = 18^\circ$, $\chi_N = 0.20$									
	8.8	5.6	6.2	2.4	3.0	14.4	28.9	22.0	11.7
$P_S = 153^\circ$, $\chi_S = 0.80$, $P_N = 18^\circ$, $\chi_N = 0.20$									
	8.7	5.6	5.8	2.5	2.6	14.4	28.6	22.2	10.8
$P_S = 126^\circ$, $\chi_S = 0.77$, $P_N = 18^\circ$, $\chi_N = 0.23$									
	8.3	5.8	6.9	2.7	4.4	14.2	29.3	22.6	14.1
$P_S = 135^\circ$, $\chi_S = 0.77$, $P_N = 18^\circ$, $\chi_N = 0.23$									
	8.4	5.8	6.5	2.7	3.7	14.2	29.0	22.5	13.0
$P_S = 144^\circ$, $\chi_S = 0.77$, $P_N = 18^\circ$, $\chi_N = 0.23$									
	8.5	5.7	6.2	2.8	3.2	14.2	28.7	22.4	12.2
$P_S = 135^\circ$, $\chi_S = 0.77$, $P_N = 9^\circ$, $\chi_N = 0.23$									
	8.4	5.7	6.5	2.7	3.5	14.1	28.9	22.4	13.0

	Coupling constants					Sum of couplings			
	1′-2′	1′-2"	2′-3′	2"-3′	3′-4′	ΣH1′	ΣH2′	ΣH2"	ΣH3′
$P_S = 144^\circ$, $\chi_S = 0.77$, $P_N = 9^\circ$, $\chi_N = 0.23$									
	8.5	5.6	6.1	2.7	2.9	14.1	28.6	22.4	12.1
Observed									
	8.3	6.2	>2.3	<2.3	>2.3	14.5	-	-	12.5

ΣH3′ are calculated at 325 K and does not include J(H3′-P) coupling, however for G6 residue ΣH3′ is showed at 297 K.

All observed values are within accuracy of ± 0.5 Hz.

χ_S and χ_N is the mole fraction of S and N conformer.

Table 5.8 : Average P_S, P_N (in degrees), χ_S, χ_N values for mixture of deoxyribose sugar for all residues which fits best to the observed J (in Hertz) and sum of couplings (in Hertz).

	C1	G2	A3	T4	C5	G6
P_N	18	9/18	18	9/18	18	18
P_S	225	162	153	135/144	225	189/198
P_S	117/126	-	-	-	117/126	-
χ_S	0.70	0.94	0.82	0.77	0.60	0.75
χ_S	0.27	-	-	-	0.37	-
χ_N	0.03	0.06	0.18	0.23	0.03	0.25

χ_S and χ_N is the mole fraction of S and N conformer.

χ_S may vary ± 0.05 and P_S may vary ± 9°.

quartet in the temperature range 305 - 320 K with the separation between inner two peaks to be 2.3 - 3.0 Hz at different temperatures in the range 297-320 K. From Table 5.6(b), it is also clear that A3 has higher population of S conformer than all residues except G2 (which has maximum χ_S). The cross peak for H2" - H3' connectivity is not observed while that for H3' - H4' connectivity is seen (Fig. 5.5(e-g)). The observed DQF COSY cross peak patterns of H1' - H2', H1' - H2", H2' - H3' and H3' - H4' are matched with Fig. 5.10 i.e. for a rigid sugar conformer. The comparison shows that for peaks above the diagonal (Fig. 5.5 (d,e,g)) :

(a) H1' - H2' pattern indicates (Fig. 5.10) P = 126° - 144°.

(b) H1' - H2" pattern indicates (Fig. 5.10) P = 108° - 180°.

(c) H2' - H3' pattern indicates (72(a)) P = 144° - 162°.

(d) Absence of H2" - H3' cross peak indicates (72(a),114) P = 90° - 225°.

(e) H3' - H4' pattern indicates (72(a)) P = 9° to 90°.

For patterns below the diagonal (Fig. 5.5(f,g)) we find :

(f) H1' - H2' pattern indicates (Fig. 5.10) P = 117° - 180°.

(g) H1' - H2" pattern indicates (Fig. 5.10) P = 108° - 207°(wide range).

(h) H2′ - H3′ pattern indicates (Fig. 5.10) P = 135°, 144°, 153°.

(i) Absence of H2" - H3′ cross peak indicates (Fig. 5.10) P = 90° - 225°.

(j) H3′ - H4′ pattern indicates (72(a)) P = 9° to 90°.

Combining (a-f) we find that the observed patterns do not fit into existence of a single rigid sugar conformer. A value of P_S = 144° fits in best to (a) to (d) and (f) to (i), i.e. all except (e) and (j), because for this P_S value, H3′ - H4′ cross peak is not expected as the corresponding J value is rather low, < 1.6 (131). The results of (e) and (j) are in contradiction to those in (a) to (d) and (f) to (i), clearly the existence of a single rigid sugar conformer does not explain the observed DQF cross peak patterns. Since ΣH1′ is considerably less than 15.7 Hz within the experimental errors and $\chi_S \simeq 0.83$ we looked into the possibility of two state model. We compare the observed patterns with those simulated for two interconverting conformers P_N = 9° and P_S = 162° (Fig. 5.13) we find that for above diagonal (Fig. 5.5 (d, e) :

(k) H1′ - H2′ pattern indicates (114) χ_S = 0.8 - 1.0.

(l) H1′ - H2" pattern indicates (114) χ_S = 0.8 - 1.0 (more close to 1.0).

(m) H2′ - H3′ pattern indicates (72(a) deduced from COSY 45 pattern) χ_S = 0.9 -1.0.

(n) Absence of H2" - H3′ cross peak indicates (72(a)) χ_S = 1.0, > 0.8.

For patterns below the diagonal (Fig. 5.5 (f)) comparison with Fig. 5.13 gives the following:

(o) H1′ - H2′ pattern indicates χ_S = 0.8 - 1.0.

(p) H1′ - H2" pattern indicates χ_S = 0.7 - 1.0 (wide range possible).

(q) H2′ - H3′ pattern indicates χ_S = 1.0 (a typical six peak pattern) or > 0.8.

(r) Absence of H2" - H3′ pattern indicates χ_S = 1.0, > 0.8.

From (k-r) it is found that χ_S = 1.0 generally satisfies all the observed results but the deviation in H1′ - H2′ pattern below the diagonal (Fig. 5.5(f)) is notable. Also J(H1′ - H2′), J(H1′ - H2") and ΣH1′ values (Table 5.6 (a,b)) clearly show that χ_S is not equal to 1.0. It may therefore be inferred that P_S value is not close to 162° and therefore the observed DQF cross peak patterns do not match satisfactorily. The observed average value of J(H1′ - H2′), J(H1′ - H2") and ΣH1′ at 305 K (Table 5.6 (a,b)) as 8.8, 5.9 and 14.6 Hz restricts the value of χ_S as 0.80 - 0.82. As a next step we calculated the J values for P_N = 9/18°, ϕ_N = 36° and P_S = 144°, 153°, 162°, ϕ_S= 36° using Tables 5.5 (a-c) (131). Some of these values along with the observed value are shown in Table 5.7. It is clear that the observed results fits satisfactorily with P_S = 153°, $\chi_S \simeq$ 0.81-0.82 and P_N = 18°, χ_N =

0.18 - 0.19. The expected value of J(H2" - H3′) = 2.3 - 2.4 Hz is not likely to give a cross peak in the present case as this value is close to the resolution in 2D spectra.

G6

Considering G6 residue it is observed that this is the only residue which gives H1′ as sharp triplet at all temperatures. It also has the least value of ΣH1′ as 14.1 Hz, J(H1′ - H2′) ≃ J(H1′ - H2") ≃ 7.0 Hz as well as maximum observed value of ΣH3′ as 18.9 Hz (including 5.8 Hz as the J(H3′-P) coupling at 325 K) (Table 5.6(b)). It is the only residue which gives a clear good cross peak pattern in DQF COSY spectra for H2" - H3′ coupling above (Fig. 5.5(e)) and below (Fig. 5.5(f)) the diagonal (the other residue C5 gives very weak corresponding patterns). Since ΣH1′ = 14.1 Hz, the average χ_S value is 0.75 and lies in the range 0.68 to 0.82 within the experimental errors (± 0.5 Hz). This shows that G6 residue has maximum population of N conformer and is certainly not close to the standard B-DNA geometry. Comparing the observed DQF cross peak patterns with those simulated for the rigid conformer (114) we find for the peaks above the diagonal (Fig. 5.5 (d,e,g)) :

(a) H1′ - H2′ pattern indicates (Fig. 5.10) P = 135°, 144°.

(b) H1′ - H2" pattern indicates (Fig. 5.10) P = 108°, 180°.

(c) H2′ - H3′ pattern indicates (72(a)) P = 144°, 162°.

(d) H2" - H3′ pattern indicates (72(a)) P = 36°, 288°.

(e) H3′ - H4′ pattern indicates (72(a),114) P = 72°, 90°.

For peaks below the diagonal (Fig. 5.5 (f,g)) :

(f) H1′ - H2′ pattern indicates (Fig. 5.10) P = 153°- 207°.

(g) H1′ - H2" pattern indicates (Fig. 5.10) P = 90°- 225° (wide range).

(h) H2′ - H3′ pattern indicates (characteristic six peak patterns) (Fig. 5.10) P = 135°- 180°.

(i) H2"-H3′ pattern indicates (Fig. 5.10) (72(a)) P = 36°, 72°, 288°.

(j) H3′ - H4′ pattern indicates (72(a)) P = 72°, 90°.

Certainly (a-j) shows that a rigid conformer cannot explain the observed results which is in confirmity with low χ_S value. Comparing the observed patterns above the diagonal (Fig. 5.5 (d,e,g)) with those for two interconverting conformers (Fig. 5.13) we find :

(k) H1′ - H2′ pattern indicates (Fig. 5.13) $\chi_S \simeq 1.0$ (certainly > 0.8).

(l) H1′ - H2" pattern indicates (Fig. 5.13) $\chi_S = 0.8 - 1.0$.

(m) H2′ - H3′ pattern indicates (72(a)) $\chi_S = 0.9 - 1.0$.

(n) H2" - H3′ pattern indicates (72(a)) $\chi_S = 0.6 - 0.7$.

For peaks below the diagonal (Fig. 5.5(f)), comparison with Fig.5.13 gives the following :

(o) H1′ - H2′ pattern indicates χ_S = 0.6 - 0.8.

(p) H1′ - H2" pattern indicates (Fig. 5.13) χ_S = 0.7 - 1.0.

(q) H2′ - H3′ pattern indicates (characteristic six peak pattern) $\chi_S \simeq 1.0$.

(r) H2" - H3′ pattern indicates χ_S = 0.5 - 0.8.

The single χ_S value does not explain all the observed results, in particular the results of observed patterns (k), (q), (r) cannot be reconciled with each other. Therefore a variation in P_S value is required to get a good fit. The next step is to calculate the J and summation values by varying both χ_S and P_S. The χ_S value is restricted to the range 0.68 - 0.75 in order to have J(H1′ - H2′) ≃ J(H1′ - H2"). Some of the calculated values are shown in Table 5.7. Selecting $P_N = 9^\circ$ or 18° does not make a significant difference and confining the sugar conformation close to a P_S value of 135° - 162° will make J(H1′ - H2′) and J(H1′ - H2") different by about 2.5 Hz. Since the resolution in 1D NMR spectra is ± 0.5 Hz and the observed difference between J(H1′ - H2′) and J(H1′ - H2") is ≃ 0 and at the most ± 0.5 Hz at all temperatures. Therefore P_S value is to be selected significantly lower or higher than $P_S = 135^\circ$ to 162°, selecting low P_S such as 99° fits into these two results but gives very high value of ΣH3′ = 18.4 Hz. We observe ΣH3′ and ΣH1′ at 325 K as 13.1 and 13.5 Hz (Table 5.6(a,b)) respectively. ΣH3′ could not be measured at 297

K due to broadening of resonance lines. It may however be deduced that ΣH3′ at 297 K will be ~ 11.0 - 12.0 Hz by using Table 5.5(c). Therefore a higher value of P_S is now explored. It is noted from the table of calculated values $P_S = 189^\circ - 198^\circ$ will yield J(H1′ - H2′) = J(H1′ - H2") ≃ 7.0 Hz and ΣH3′ ≃ 11.2 Hz i.e. close to the observed values. Hence G6 residue is a mixture of $P_N = 18^\circ$, χ_N = 0.25 and $P_S = 189^\circ - 198^\circ$, χ_S = 0.75. It may be noted that we have not deviated any where in our analysis so far from $\phi_m = 36^\circ$ for the major S conformer since we did not consider our resolution to be so high so as to get into fine details such as variation in amplitude of pucker as suggested by Wijk et al. (131). If ϕ_m is lowered from 36° to 28° we find, the pair of couplings J(H1′ - H2′), J(H1′ - H2") for $P_S = 171^\circ$ and 180° are 9.1, 6.3 and 8.7, 6.6 Hz, respectively. The corresponding values for $P_S = 189^\circ$ and 198° for $\phi_m = 36^\circ$ are 9.2, 6.3 and 8.5, 6.7 Hz respectively. (Table 5.6(a)). Therefore, $P_S = 171/180^\circ$, $\phi_m = 28^\circ$ fits as well into experimental data as $P_S = 189^\circ / 198^\circ$, $\phi_m = 36^\circ$ by considering χ_S = 0.75 in all cases.

T4

Considering T4 residue, the observed average value of J(H1′ - H2′), J(H1′ - H2"), ΣH1′ at 305 K are 8.3, 6.2, 14.5 Hz, respectively (Table 5.6(a,b). Assuming the corresponding values at 295 K to be close to that at 305 K, the ΣH1′ = 14.5 Hz yields χ_S as 0.81 (± 0.5).

The ΣH3′ value at 325 K is 18.3 Hz including J(H3′-P) coupling of 5.8 Hz (Table 5.6(b)). Since the J values at 320 K and 305 K are not very different from each other, it may be assumed that ΣH3′ at 295 K ≃ 18.3 - 5.8 = 12.5 Hz. The H1′ resonance of T4 residue is observed as a quartet from 310 - 320 K with the separation between inner two peaks as 1.7 - 2.4 Hz. Comparing the observed values of J(H1′ - H2′) , J(H1′ - H2"), ΣH1′ for A3 and T4 residues (Table 5.6 (a)), we find that for both residues ΣH1′ ≃ 14.5 Hz giving χ_S = 0.81 but the difference of couplings J (H1′ - H2′) and J(H1′ - H2") is 2.9 Hz and 2.1 Hz at 305 K for A3 and T4 residues, respectively. Obviously the P_S values of the major conformer are different in two cases which also yield different values of ΣH3′, i.e. ≃ 10.0 and 12.5 Hz for A3 and T4 residues respectively (Table 5.6 (b)). A quick look at Table 5.5 (b,c) shows that P_S for T4 should be lower than that for A3 residue i.e. $P_S = 153^\circ$ or be > $P_S = 225^\circ$. Comparing the observed cross peak patterns in DQF COSY spectra with those simulated for a rigid conformer (114), we find for peaks above the diagonal (Fig. 5.5 (d,e,g)), that :

(a) H1′ - H2′ pattern indicates (Fig. 5.10) P = 153°-180°.

(b) H1′ - H2" pattern indicates (Fig. 5.10) P = 108°-150°.

(c) H2′ - H3′ pattern indicates (72(a)) P = 144°-216°.

(d) Absence of H2" - H3′ cross peak indicates (72(a),114) P = 90°-252°.

(e) H3′ - H4′ pattern indicates (72(a)) P = 72°- 108°, 324°.

For peaks below the diagonal (Fig. 5.5(f,g)) we find that :

(f) H1′-H2′ pattern indicates (Fig.5.10) P = 153°- 207°.

(g) H1′-H2" pattern indicates (Fig. 5.10) P = 108°- 225°.

(h) H2′-H3′ pattern (characteristic six peak pattern) indicates (Fig. 5.10) P = 144°, 153°, 180°.

(i) Absence of H2"-H3′ indicates (Fig. 5.10) P = 90°- 252°.

(j) H3′-H4′ pattern indicates (72(a)) P = 72°- 108°, 324°.

The P_S value in the range 144°- 180° may explain all the observed patterns but the existence of H3′ - H4′ cross peak indicates that a rigid sugar conformer does not exist. We therefore compare the observed patterns with those simulated for two interconverting N and S conformers (114). For peaks above the diagonal (Fig. 5.5 (d,e,g)) we find :

(k) H1′ - H2′ pattern indicates (Fig. 5.13) $\chi_S \simeq 0.8 - 1.0$.

(l) H1′ - H2" pattern indicates (Fig. 5.13) $\chi_S = 1.0$.

(m) H2′ - H3′ pattern indicates (72(a)) $\chi_S = 0.8 - 1.0$.

(n) Absence of H2" - H3′ cross peak indicates (72(a),114) $\chi_S = 0.8 - 1.0$.

For peaks below the diagonal (Fig. 5.5 (f)) comparison with Fig. 5.13 gives the following :

(o) H1′ - H2′ pattern indicates χ_S = 0.8 - 1.0.

(p) H1′ - H2" pattern indicates χ_S = 0.7 - 1.0.

(q) H2′ - H3′ pattern indicates $\chi_S \simeq 1.0$.

(r) Absence of H2" - H3′ pattern indicates χ_S = 0.8 - 1.0.

Although the above observed results fit into χ_S = 0.81 obtained from 1D NMR results, some of the patterns like H1′ - H2" (l) fit better with χ_S = 1.0. In the simulated pattern $P_S = 162^\circ$ and therefore a variation in χ_S value is to be explored. We have calculated the various J and summation values for different values of P_S by taking χ_S = 0.77, 0.80 and $P_N = 9^\circ/18^\circ$. The calculated values (Table 5.7) are compared with the observed average value of J(H1′ - H2′), J(H1′ - H2"), ΣH1′, ΣH3′ as 8.3, 6.2, 14.5 and 12.5 Hz respectively. It is found that $P_N = 9^\circ/18^\circ$, χ_N = 0.23 and $P_S = 135/144^\circ$, χ_S = 0.77 fits into observed results satisfactorily. Further decrease in ϕ_m from 36° to 28° provides a fit with χ_S = 0.82 and $P_S = 153^\circ/162^\circ$.

C1

Considering C1 residue, the average J (H1′ - H2′), J(H1′ - H2") and ΣH1′ value at 325 K / 320 K are found to be 7.3, 6.6 and 13.9 Hz, respectively (Table 5.6(a,b)). At lower temperatures it is not possible to determine these values from 1D NMR spectra due to severe overlap with C5H1′. It is also found that it has a H3′ multiplet (Fig. 5.2 (c)) at 325 K which is quite different from that observed for all other residues. The observed ΣH3′ value is

minimum (Fig. 5.2 (c)), being 14.1 Hz (including H3'-P coupling) or 8.3 Hz assuming the H3'-P coupling to be ~ 5.8 Hz. The H1' - H2" cross peak pattern in DQF COSY spectra is also observed (as also for C5 residue) to be different and the characteristic 16 peak (4 peak along ω_2 axis) pattern is not seen. The observed pattern has 4 peaks in all with 2 each along ω_2 axis and ω_1 axis (Fig. 5.5 (d,f)). We compared the J(H1' - H2'), J(H1' - H2") and ΣH1' values obtained for C1 residue with the corresponding ones for G6 residue (Table 5.6 (a,b)). We find that ΣH1' are similar but the difference between J(H1' - H2') and J(H1' - H2") is larger (~ 0.6 - 0.8 Hz) than that for G6 residue and the ΣH3' is significantly lower (by ~ 5 Hz) in C1 residue than that for G6 residue. Therefore although χ_S for these two residues may be close to each other, the P_S values for the major S conformer are certainly quite different in C1 and G6 residue. The H1' - H2' and H1' - H2" cross peak patterns in DQF COSY spectra (Fig. 5.5 (d)) of C1 and C5 residue are quite similar but the ΣH3' values are different by ~ 4 Hz (Table 5.6(b)).

We compare the observed cross peak pattern with those for a rigid sugar conformer (114). We find that for peaks above the diagonal (Fig. 5.5 (d,e,g)) we have :

(a) H1' - H2' pattern indicates (Fig. 5.10) P = 153°-225°.

(b) H1' - H2" pattern indicates (Fig. 5.10) P = 90°, 99°.

(c) H2' - H3' pattern indicates (72(a)) P = 72°, 90°.

(d) H2" - H3′ pattern indicates (72(a)) P = 72°, 90°.

(e) H3′-H4′ pattern indicates (72(a)) P = 72°, 90°, 324°.

For peaks below the diagonal (Fig. 5.5 (f)) we have :

(f) H1′ - H2′ pattern indicates (Fig. 5.10) P = 72°- 99°, 180°-225°.

(g) H1′ - H2" pattern indicates (Fig. 5.10) P = 90° - 225° (wide range).

(h) H2′ - H3′ pattern indicates (Fig. 5.10) P = 72°, 207 - 225°.

The observed results clearly depict the presence of a mixed sugar with predominant P_S either 72° - 99° or 207 - 225°. $\Sigma H1' \simeq$ 13.9 Hz (at 325 K) gives χ_S = 0.71 (± 0.05) and we assume that χ_S lies in the range 0.66 - 0.70. Comparing the cross peak patterns with those simulated for two interconverting N and S conformers for peaks above diagonal (Fig. 5.5 (d,e)) we have :

(i) H1′ - H2′ pattern indicates (Fig. 5.13) χ_S = 0.6 - 0.7.

(j) H1′ - H2" pattern indicates (Fig. 5.13) χ_S = 0.6 - 0.7 (more close to 0.7).

(k) H2′ - H3′ pattern indicates (72(a) deduced from COSY 45 peak) χ_S = 0.6 - 0.7.

(l) H2" - H3′ pattern indicates (72(a) deduced from COSY 45 peak) χ_S = 0.6 - 0.8.

For cross peaks below the diagonal (Fig. 5.5 (f)) we have :

(m) H1′ - H2′ pattern indicates (Fig. 5.13) χ_S = 0.5 - 0.7.

(n) H1′ - H2" pattern indicates (Fig. 5.13) χ_S = 0.5 - 0.8.

(o) H2′ - H3′ pattern indicates (Fig. 5.13) $\chi_S \simeq 0.7$.

From (i-o), it is seen that the patterns and χ_S = 0.7 generally fit into the observed results satisfactorily. Considering the value of χ_S in the range 0.70 - 0.75, a variation in P_S is explored. From (a) to (h) we find that major S conformer is either ~ 90° - 99° or ~ 207°- 225° whereas (i) or (o) fit in well for $P_S \simeq 162°$. In fact the simulated patterns obtained on mixing of P_S = 90° - 99° and P_S = 207 - 225° (that is presence of three conformer, third one being P_N = 18°, minor) could be similar to that obtained for P_S = 162° (that is two conformer second being P_N = 18°).

P_S = 207°- 225° however leads to low values of ΣH3′ as observed. Thus the C1 residue has predominant P_S as 207°- 225° with $\chi_S \simeq 0.75$. It is not possible to obtain these values to a greater accuracy due to limited data available. A mixture of three conformers P_N = 18°, P_S = 90°- 99°, P_S = 207°- 225° cannot be ruled out.

Schmitz et al. (114) have shown that the simulated patterns for a 85% S mixture with P_S = 144° using two state model are identical to that obtained by employing two different conformers in the S range of pseudorotation , with P_S = 162° and P_S = 126° in a pyrimidine residue of $d(GTATATAC)_2$. Therefore one cannot distinguish between a two state model employing a less

conventional P_S value or a three state model employing two S conformers, the dominant one of which has a conventional P_S. Indeed, molecular dynamics simulations carried out with the sequence $[d(CGCGAATTCGCG)]_2$ revealed recently (54(a)) that sugar puckers in the middle range of the pseudorotation phase cycle (P = 54°-126°) do occur and sometimes represent up to 30% of the observed sugar puckers. These results support the idea of involving a third conformer to describe dynamic sugar pucker and show that the energy barriers between conformers exhibiting puckers located in S and N pseudorotation half cycles are lower than commonly assumed. The low conformational barriers could mean that a three state model is more realistic. We made an attempt to fit the experimental data into three state model i.e. P_N = 9°/18°, P_S = 126°, P_S = 162°. We found that significantly low value of ΣH3′ observed (i.e. 8.3 Hz) cannot be satisfied using dominant P_S conformer as the conventional one i.e. P_S = 162° and it was necessary to use P_S with range 207°-225°.

C5

Considering the C5 residue, all the 2D cross peak patterns match exactly with those obtained for C1 residue. The only difference between the observed results of these two residues is that ΣH3′ for C5 is higher being ~ 12.6 Hz at 325 K as compared to a value of ~ 8.3 Hz at 325 K for C1 residue. This may be inferred in terms of a variation in relative fraction of P_S ~ 99° and P_S = 207°-225° conformer. The C5 residue may have more of P_S = 99° and

less of P_S = 207° - 225° as compared to the C1 residue. The simulated patterns for both residues match with those obtained for χ_S = 0.7 - 0.75, P_S = 162° and χ_N = 0.3 - 0.25, P_N = 9° (Fig. 5.13). Thus a mixture of three conformers with P_N = 18°, P_S = 90°-99°/117° and P_S = 207° - 225° may exist.

CONFORMATION OF DEOXYRIBOSE SUGAR FROM RELATIVE INTENSITIES OF NOE CROSS PEAKS AND DISTANCE CONSTRAINTS

In recent years, much use has been made of cross-relaxation rates measured by one-dimensional or two-dimensional NOE. These are translated into proton - proton distances. However there are difficulties in obtaining sugar conformation from these distances due to the very nature of pseudorotation phenomena and the conformational heterogeneity. It has since been shown (124(a),131) that unambiguous and precise determination of conformation of deoxyribose sugars in oligonucleotides is further complicated due to presence of S to N equilibrium with $\chi_S \simeq 0.65$ to 1.0 and P_S lying in the range 90° - 180°. The NOE data therefore needs to be supplemented by other data to arrive at a conclusion. We have therefore followed the strategy of using results obtained by coupling constant analysis and check if these are in confirmity with the observed interproton distances. The intra sugar proton-proton distances vary over a large range with pseudorotation as shown in Fig. 5.14. From the table of distances (Table 5.9) obtained for different standard sugar geometries in the pseudorotation cycle we find that all but two of the intra

Table 5.9 : Calculated intranucleotide distances (A°) between different hydrogen atoms in deoxyribose ring as a function of P (133).

P	1′-2′	1-2"	1′-3′	1′-4′	2′-3′	2"-3′	2′-4′	2"-4′	3′-4′
9°	2.52	2.18	3.64	3.15	2.29	2.91	3.54	2.31	2.84
18°	2.55	2.15	3.65	3.00	2.29	2.90	3.51	2.29	2.85
36°	2.65	2.11	3.69	2.73	2.25	2.91	3.48	2.36	2.84
90°	2.80	2.07	3.69	2.19	2.18	2.75	3.58	3.05	2.80
99°	2.83	2.11	3.65	2.20	2.18	2.71	3.58	3.19	2.77
108°	2.83	2.15	3.60	2.25	2.20	2.69	3.60	3.34	2.75
117°	2.84	2.18	3.60	2.36	2.20	2.64	3.60	3.48	2.73
126°	2.84	2.18	3.57	2.52	2.24	2.61	3.60	3.54	2.69
135°	2.84	2.20	3.54	2.58	2.25	2.58	3.58	3.66	2.64
144°	2.84	2.20	3.54	2.73	2.28	2.55	3.58	3.77	2.60
153°	2.84	2.20	3.54	2.84	2.30	2.55	3.57	3.79	2.55
162°	2.84	2.18	3.54	3.04	2.31	2.52	3.54	3.80	2.52
180°	2.84	2.16	3.58	3.28	2.33	2.52	3.51	3.90	2.45
189°	2.85	2.15	3.65	3.37	2.31	2.50	3.51	3.93	2.42
198°	2.83	2.11	3.69	3.48	2.30	2.50	3.51	3.93	2.42
207°	2.83	2.11	3.74	3.57	2.30	2.50	3.52	3.93	2.39
216°	2.80	2.07	3.82	3.65	2.29	2.80	3.57	3.93	2.39
225°	2.75	2.09	3.87	3.77	2.25	2.58	3.60	3.89	2.40

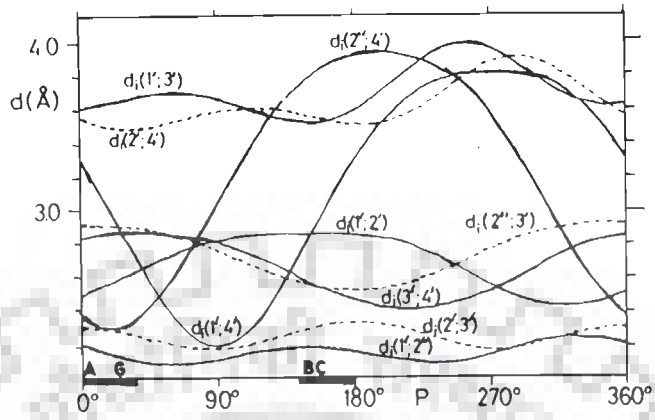

Fig. 5.14 Intranucleotide distances between different hydrogen atoms in the deoxyribose ring versus the pseudorotation phase angle *P*. The heavy lines below the *P* axis indicate the regions of the preferred ring puckers 3'C-*endo* near 20° and 2'C-*endo* near 160°. A, B, C, and G identify the *P*-values for A-DNA, B-DNA, and the nucleotides C and G in the Z form of $d(CGCGCG)_2$ **(133)**.

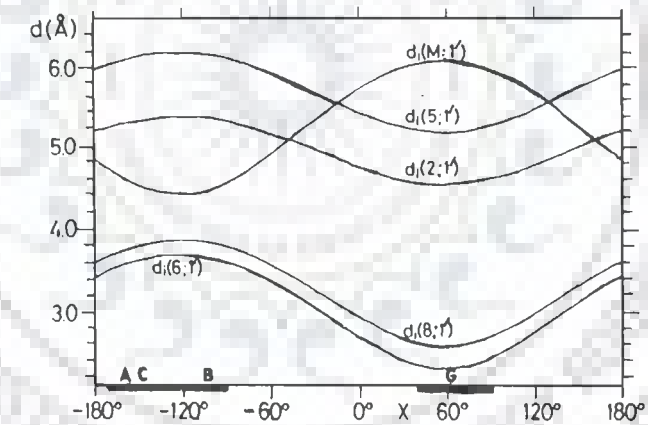

Fig. 5.15(a) Intranucleotide distances between base protons and 1'H versus the torsion angle χ. Preferred χ regions from -90 to $-170°$ (anti) and 40 to 90° (syn) are indicated with heavy lines at the bottom. A, B, C, and G identify the χ-values for A-DNA, B-DNA, and the nucleotides C and G in the Z form of $d(CGCGCG)_2$ **(133)**.

sugar ^1H - ^1H distances vary less than 0.25 A° relative to their average in going from N to S region of sugar conformational space and thus are not useful. The H1′ - H4′ distance varies by more than 1 A° but the minimum distance lies in the O1′ endo (P = 90°) region, thus this distance cannot discriminate between N and S conformers or their relative populations. The H2" - H4′ distance serves as a marker as it changes from approximate 2.3 A° in the N region to about 3.6 to 4.0 A° in S conformational space.

Table 5.4(a) gives a list of various intra sugar connectivities in NOESY spectra (Fig. 5.6 (a-j)) obtained for τ_m = 75, 150, 200 and 250 ms. The intensities of all observed peaks are graded into small ranges designated as w (weakly intense), ws (fairly intense), s (intense), ss (very intense) in order of increasing intensity by visual inspection at different τ_m values using data from Fig. 5.6 (a-j). Table 5.10(a) lists the relative intensities of various intra sugar NOE cross peaks. Further we have calculated the interproton distances from intensity of NOE cross peaks. Volume integrals are obtained for various NOE cross peaks. These are plotted as a function of τ_m for each cross peak to determine an acceptable value of τ_m for distance measurements. Fig. 5.7 shows the NOE build-up curves obtained for various pairs of protons. It is found that integrals obtained are in linear regime for τ_m = 75 as well as 150 ms and hence are used for distance measurements. The distance r(CH5-CH6) = 2.45 A° is used as an internal reference (103). Interproton distances calculated

at τ_m = 75 and 150 ms for various intrasugar connectivities are listed in Table 5.10(b).

The H1′ - H2" distance varies within a small range around 2.2 A° (Table 5.9 and Fig. 5.14) irrespective of the pseudorotation value. We obtained very intense H1′ - H2" NOE cross peaks (Table 5.10 (a)) in NOESY spectra obtained at all τ_m values, i.e. 75, 150, 200 and 250 ms. The distance obtained by integrating cross peaks (Table 5.10(b)) in NOESY spectra is 2.3 A° for all the residues and is in confirmity with the standard distances (Table 5.9). The distance H1′ - H2′ is $\simeq$ 2.84 A° for P lying in the range 99° to 207° (Fig. 5.14 and Table 5.9) and is lowest for P_N = 9°/18°, being ~ 2.55 A°. We have observed generally a mixture of two interconverting sugar conformers, N conformer with P_N = 9°/18° and predominant S conformer, with P_S = 99° - 207° for different residues. Therefore it is expected that distance will be minimum for the sugar having maximum population of N conformer and increases with percentage of S conformer. This is indeed observed and only G6 residue having 75% S conformer gives an intense H1′ - H2′ cross peak at 75 ms (Table 5.10(b) and Fig. 5.6(e,f)) yielding distance of 2.4 A° while G2, A3, T4 residues having 80% to 94% S conformer yield higher distance ~ 2.8 A° (Table 5.10(b)). Among different residues the distance increases in the order G6 < G2, A3, T4 < C1, C5 residue (Table 5.10(a,b)). However the C1 and C5 residues are found to be peculiar in the sense that although their χ_S ~ 0.80 they did not give a cross peak at 75 ms. Their cross peaks are significantly

Table 5.10(a) : The observed relative intensities of various intra sugar NOE connectivities in NOESY spectra recorded at τ_m = 75, 150, 200 and 250 ms of d-$(CGATCG)_2$ (Fig. 5.6 (a-j)).

Connectivity	τ_m (ms)	C1	G2	A3	T4	C5	G6
H1′-H2′	250	ws	ss	ss	ss	s	ss
	200	-	ss	ss	ss	ws	ss
	150	-	s	s	s	w	s
	75	-	w	w	w	-	s
H1′-H2"	250	ss	ss	ss	ss	ss	ss
	200	ss	ss	ss	ss	ss	ss
	150	ss	ss	ss	ss	ss	ss
	75	ss	ss	ss	ss	ss	ss
H2′-H3′	250	ss	ss	ss	ss	ss	ss
	200	ss	ss	ss	ss	ss	ss
	150	s	ss	ss	s(o)	s(o)	s
	75	w	s	s	s	ws	s
H2"-H3′	250	ss	ss	ss	ss	-	ss
	200	ss	ss	ss	ss	-	ss
	150	s(o)	ss	ss	s	-	s(o)
	75	w(o)	s	ws	ws	-	w(o)
H3′-H4′	250	ss(o)	ss	ss	ss(o)	ss(o)	s
	200	ss(o)	ss	ss	ss(o)	ss(o)	s
	150	ss(o)	ss	ss	ss(o)	ss(o)	s
	75	ws	s	ss	ws(o)	w	ws

H1'-H4'	250	-	s	s	ss	s	w
	200	w	s	s	ss	s	ws
	150	-	ws	s	ss	ws	w
	75	-	-	-	s	-	-
H1'-H3'	250	-	-	-	-	-	-
	200	-	ws	ws	-	-	w
	150	-	-	-	-	-	-
	75	-	-	-	-	-	-
H2'-H4'	250	-	s	s	s	s	-
	200	-	ws	ws	-	ws	w
	150	-	w	w	-	-	-
	75	-	-	-	-	-	-
H2"-H4'	250	s	s	s	s	s	s
	200	s	ws	ws	s	ws	ws
	150	-	-	w	ws	ws	-
	75	-	-	-	-	-	-

- : absence of peak. w : weak intensity of peak.

ws : fairly intense. s : intense. ss : very intense.

o : Overlap of peaks.

Table 5.10(b) : Interproton distances* calculated from observed intrasugar NOE cross peaks in spectra recorded at τ_m = 75 and 150 ms.

	C1		G2		A3		T4		C5		G6	
τ_m(ms)	75	150	75	150	75	150	75	150	75	150	75	150
Connectivity												
H2'-H2"	1.9	-	-	-	1.7	-	1.8	-	1.8	-	1.8	-
H1'-H2'	-	-	2.8°	-	3.3	2.8	-	2.8	-	3.0	2.4	-
H1'-H2"	2.3°	-	2.3°	-	2.4	2.3	2.3	-	2.3	-	2.3°	-
H2'-H3'	2.7	-	2.0°	-	2.0°	-	2.4°	-	2.4°	-	2.8	-
H2"-H3'	2.5°	-	2.0°	-	2.9	-	3.2	2.8	-	-	2.5°	-
H3'-H4'	-	2.5	2.8	-	2.6	-	-	2.6°	-	2.6°	3.0	-
H4'-H5'	2.2	-	-	2.0	2.0	-	-	-	-	-	-	-
H3'-H5'	2.7	-	3.0	-	2.6	-	-	-	-	-	2.9	-
H1'-H4'	-	-	-	3.1	-	2.9	2.8	-	-	3.4	-	3.3

o : overlap

- : Cross peak either absent or not integrated.

* r(CH5-CH6) = 2.45°, used as internal standard distance.

weaker than all other residues in NOESY spectra recorded at τ_m = 250 ms (Fig. 5.6(d)). The C1 residue does not show cross peak at τ_m = 200 and 150 ms (Table 5.10 (a), Fig. 5.6 (c,e)). This may be due to the fact that χ_N is actually less than even 0.06 (that observed for G2 residue) and it is mostly a mixture of two major S conformer with P_S anywhere in the range 90° to 225° i.e. a mixture of three sugar conformers. The values of χ_S are calculated from ΣH1′ assuming that minor conformer is P_N = 18° (having ΣH1′ = 9.4 Hz) and major is close to P_S = 117° - 180° (having ΣH1′ ≃ 15.7 Hz) (Table 5.5(b)). If two S conformers with P_S = 99° - 126° having (ΣH1′ = 15.5 - 15.7 Hz) and P_S = 207° - 225° (having ΣH1′ = 14.8 - 13.5 Hz) are present, the apparent χ_N calculated will be much lower to give an average value of ΣH1′ ≃ 14.1 Hz found for C1 and C5 residues, as shown below :

P_N	χ_N	$P_S^{(1)}$	$\chi_S^{(1)}$	$P_S^{(2)}$	$\chi_S^{(2)}$	ΣH1′	r(H1′-H2′)
9°/18°	0.25	117-180°	0.75	-	-	14.1 Hz	2.76 A°
9°/18°	0.04	-	-	216°	0.96	14.0 Hz	2.83 A°
18°	0.03	117°	0.20	207°	0.77	14.2 Hz	2.83 A°
18°	0.03	126°	0.27	225°	0.70	14.0 Hz	2.83 A°
18°	0.03	126°	0.37	225°	0.60	14.2 Hz	2.83 A°

A low value of χ_N < 0.04 will yield higher distance r(H1′ - H2′) ~ 2.83 A°.

Out of the two sugar protons H2′ and H2", the H2′ is close to H3′ proton, the distance being 2.2 - 2.3 A° over a wide range of pseudorotation values of sugar pucker (Table 5.9). We observed

intense cross peaks in NOESY spectra (Fig. 5.6 (c-f)) even for τ_m = 75 ms (Table 5.10(a)). The H2" - H3' distance on the other hand, decreases gradually from a distance of 2.9 A° to 2.5 A° as pseudorotation value is varied from 18° to 207°. We observed most intense peak corresponding to this connectivity in case of G2 residue for which the H2" - H3' distance is minimum (Table 5.10(a,b)). The same is understandable as G2 has least population of N conformer. Since the variation in H2' - H3' and H2" - H3' distances with P value are low, the distance information cannot be used to derive conclusions about sugar conformation. At τ_m = 150 ms the intensity of peak H1'-H4' decreases as T4 > A3> G2, C5, G6 > C1 (no cross peak seen) indicating that the distances are increasing in this order (Table 5.10(a)). The distances obtained by volume integration of NOE cross peaks (Table 5.10 (b)) confirm the same, i.e. T4 (H1' - H4') distance is least being 2.8 A°. We made an attempt to calculate the H1' - H4' distance for G2, A3, T4 and G6 residues by using results of sugar conformation obtained by analysis of spin-spin coupling constants (Table 5.8), that is P_S = 162°, χ_S = 0.94; P_S = 153°, χ_S = 0.82; P_S = 135 / 144°, χ_S = 0.77 and P_S = 189°, χ_S = 0.75, respectively. The calculated distances for G2, A3, T4 and G6 residues are 3.04, 2.87, 2.68-2.79, and 3.28 A° and are in accord with the corresponding observed distances of 3.1, 2.9, 2.8 and 3.3 A° (Table 5.10(b)). Among the C1 and C5 residues, which appear to have a mixture of three conformers, the C1 residue does not show a H1'-H4' NOE connectivity at τ_m = 150 ms while C5 residue gives relatively a weakly intense cross peak

(Fig. 5.6 (i), Table 5.10(a,b)). At τ_m = 200 ms, the intensity of peak for C5 residue is higher than that for C1 residue (Fig. 5.6(h)). Since the H1' - H4' distance for P_S = 117°-126° is much lower than that for P_S = 225°, the observed result may be interpreted in terms of difference in relative fractional population of P_S = 117°/126° and P_S = 225° in C1 and C5 residues. An increase of 10% in P_S = 225° conformer in a mixture of three conformers with P_N = 18° (χ_N = 0.03), P_S = 117°/126° (χ_S = 0.37), P_S = 225° (χ_S = 0.60) to P_N = 18° (χ_N = 0.03) P_S = 117°/126° (χ_S = 0.27), P_S = 225° (χ_S = 0.70) leads to increase in distance from 3.22 - 3.28 A° to 3.37 - 3.41 A°. The H3' - H4' distance decreases from 2.84 A° to 2.40 A° gradually as P value is increased from 18° to 225°. We observed intense cross peaks for G2 and A3 residues (Table 5.10 (a,b)) at τ_m = 75 ms as compared to T4, C5 and G6 residues. For G6 residue, the distance is found to be greater by 0.2 A° than that for G2 residue which is in confirmity with the fact that G6 has maximum content of N conformer. Among the C1 and C5 residues, the distance in C1 residue is shorter than that in C5 residue (Fig. 5.6 (g), Table 5.10 (a,b)). If both these residues have a mixture of two S conformer in the range 90° - 117° and 207°-225° besides having a very low fraction of N conformer (0.03-0.04), then a smaller H3' - H4' distance in C1 residue (Table 5.10 (b)) may be interpreted as due to the presence of greater fraction of S conformer having P_S = 207°- 225° than that in C5 residue.

The H1′ - H3′ distance varies over a small range with change in pseudorotation value of sugar, it being minimum for P = 135 - 162° (Table 5.9). We observed weakly intense NOE cross peak corresponding to this connectivity for G2 and A3 residue (Table 5.10 (a), Fig. 5.6 (h)). For other residues either the population of N conformer is high or the P_S value is less than 135° or higher than 162° resulting in a comparatively larger distance.

The H1′ - H4′ distance varies relatively to a greater extent with P value than other distances referred above. It shows a minima at P value of 90° (Table 5.9, Fig. 5.14) and increases on either increasing P value (towards P_S = 162°- 225°) or decreasing P value (towards P_N = 9°/18°). In NOESY spectra taken at τ_m = 75 ms we have observed intense peak for T4 residue (Table 5.10 (a,b)).

The NOE cross peak corresponding to H2′ - H4′ connectivity are observed for all residues except C1 residue (Fig. 5.6 (c-e)). Weak cross peaks(Fig. 5.6 (e)) are seen for G2 and A3 residue in spectra taken at τ_m = 150 ms for which the distance expected is ≃ 3.53 A°. The variation in H2′ - H4′ distance with P value is not large and does not permit any further elucidation of sugar conformation. However it is notable that H2′ - H4′ distance is largest ≃ 3.60 A° for P_S = 117°/126° and P_S = 225° (Table 5.9) and will therefore result in relatively larger distance for both C1 and C5 residues.

It has been shown in literature (131) that it is the H2" - H4′ distance which can be used to distinguish between various sugar conformations since it varies over a large range, from 2.29 A° to 3.93 A° on increasing P value from 18° to 225° (Table 5.9, Fig. 5.14). We observe NOE cross peaks corresponding to H2" - H4′ connectivity for all the residues in NOESY spectra at τ_m = 200 ms and 250 ms (Fig. 5.6 (c,d)). The most intense peak is observed for T4 residue and the least intense peak is observed for G2 residue (Table 5.10(a)). We attempted to calculate the distance using the standard values (Table 5.9) for G2, A3, T4 and G6 residues. The calculated distances are 3.71, 3.52, 3.52, 3.34 - 3.43 A° for G2, A3, G6 and T4 residues, respectively and are in accord with the observed relative intensities of peaks which decrease in the order T4 > A3, G6 > G2. Among C1 and C5 residues, the H2" - H4′ connectivity is observed only for C5 residue in NOESY spectra at τ_m = 150 ms (Table 5.10(a), Fig. 5.6(e)) indicating that the distance H2" - H4′ is smaller in C5 residue than that in C1 residue which is understandable if a lesser fraction of P_S = 225° conformer is present in C5 residue than that in C1 residue.

Thus we find that the observed results on relative intensities of NOE cross peaks (Table 5.10(a)) as well as distances (Table 5.10 (b)) obtained on integration of these cross peaks are in accord with the analysis of sugar conformation based on spin-spin coupling constants. In particular the results pertaining to H1′ -H4′ and H2" - H4′ connectivities which serve as

a marker in sugar conformational space, are qualitatively as well as quantitatively (in case of H1′ - H4′) in agreement with the corresponding distance values calculated by using P_S, χ_S, P_N, χ_N obtained independently by spin-spin coupling analysis in previous section. In case of C1 and C5 residues, it may be recalled that the observed results of cross peak patterns obtained in DQF COSY spectra could be fitted into existence of two or three sugar conformers. The spin-spin coupling constant analysis cannot clearly distinguish between presence of $P_S = 162^\circ$ conformer or instead of a mixture of $P_S = 117^\circ/126^\circ$ and $P_S = 225^\circ$ conformers, as also suggested in literature (114). However the variation in H1′ - H4′ and H2" - H4′ distances with P value (Fig. 5.14 and Table 5.9) can differentiate between the presence of two conformer or three conformers. Our results of NOE data indicate that C1 residue has a larger fraction of $P_S = 225^\circ$ conformer than that in C5 residue. Using this fact we made an attempt to evaluate J(H1′ - H2′), J(H1′ - H2"), ΣH1′ for different P_S and χ_S values. We find that presence of three conformer $P_N = 18^\circ$, $\chi_N = 0.03$, $P_S = 126^\circ$, $\chi_S = 0.27$ and $P_S = 225^\circ$, $\chi_S = 0.70$ gives J(H1′ - H2′) J(H1′ - H2") and ΣH1′ as 6.7 , 7.2 and 14.0 Hz respectively which fits into the observed results (Table 5.6(a,b)) for C1 residue. For C5 residue, $P_N = 18^\circ$, $\chi_N = 0.03$; $P_S = 126^\circ$, $\chi_S = 0.37$ and $P_S = 225^\circ$, $\chi_S = 0.60$ fits satisfactorily. Similar results have also been obtained for T1 and C5 residues in a study of conformation of d-TGATCA (unpublished). It may be emphasized that the values of P_S, χ_S for C1 and C5 residues are only suggestive estimates due to

limited data available. However it may inferred that C1 residue has relatively larger fraction of $P_S = 225^\circ$ conformer than that in C5 residue.

GLYCOSIDIC BOND ROTATION

The glycosidic bond rotation defined as O4' - C1' - N9 - C8 in case of purines and O4' - C1' - N1 - C6 in case of pyrimidines may be estimated from the knowledge of intranucleotide distances between the base protons AH8/GH8/CH6/TH6 and their corresponding sugar protons H1', H2', H2", H3' and H4'. Of these five distances, the base to H1' distance depends only upon the value of χ (Fig. 5.15(a)) while others (Fig. 5.15 (b,c)) depend upon both χ and pseudorotation angle P of the deoxyribose sugar. Table 5.11 (a-c) show these distances for some of the standard sugar geometries close to both A-DNA as well as B-DNA for χ values of -150°, -120°, -90° and -60° (133). The relative intensities of NOE cross peaks observed in NOESY spectra Fig. (5.6 c-f,h,j) at different τ_m values i.e. 250, 200, 150 and 75 ms are given in Table 5.12 (a). The corresponding distances obtained by integration of NOE cross peaks at 150 ms and 75 ms are given in Table 5.12(b).

Considering the base H8 - H1' distance it is noted (Table 5.11(a)) that it varies within a small range 3.58 - 3.92 A° on increasing χ from - 120 to -60°. In case of pyrimidines the distance H6 - H1' are shorter and lie in the range 3.30 - 3.68 A° for χ = -120 to -60°. We observed intense cross peak for all base

(b)

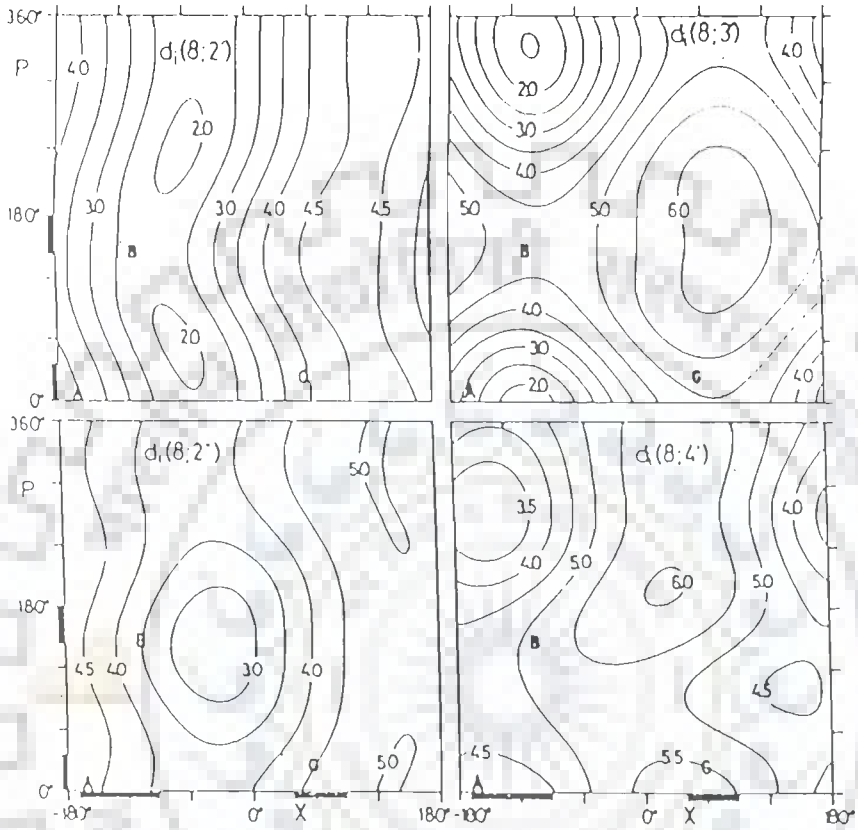

Fig. 5.15 (b) : P-χ plane with contour lines indicating the H8 to (i) H2′ (ii) H2" (iii) H3′ and (iv) H4′ distances. The preferred regions C3′-endo near 20° and C2′-endo near 160° for P and syn near 60° and anti near 130° for χ are indicated with heavy lines on the left and the bottom. A, B, and G identify the χ values for A DNA, B DNA and nucleotide G in the Z form of d-$(CGCGCG)_2$ (133).

(c)

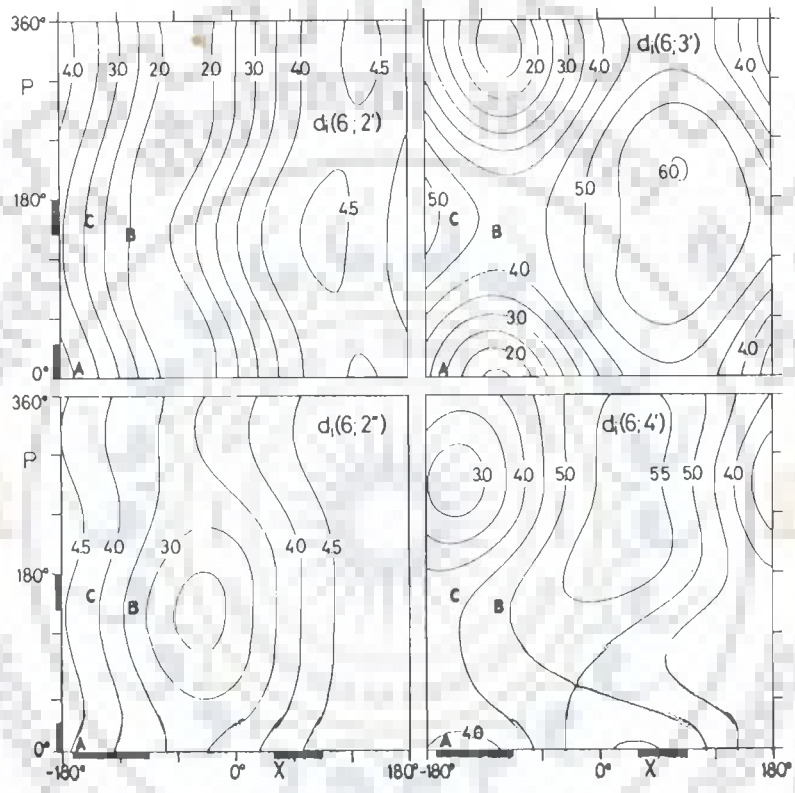

Fig. 5.15 (c) : P-χ plane with contour lines indicating the H6 to (i) H2′ (ii) H2" (iii) H3′ and (iv) H4′ distances. The preferred regions C3′-endo near 20° and C2′-endo near 160° for P and syn near 60° and anti near 130° for χ are indicated with heavy lines on the left and the bottom. A, B and C identify the χ values for A DNA, B DNA and nucleotide C in the Z form of d-$(CGCGCG)_2$ (133).

Table 5.11(a) : Intranucleotide distances (A°) between base protons H8, H6 and deoxyribose H1′ proton corresponding to different χ (in degrees) values (133).

χ	H8-H1′	H6-H1′
-150	3.72	3.50
-120	3.92	3.68
-105	3.88	3.66
-90	3.81	3.58
-60	3.58	3.33

Table 5.11(b) : Intranucleotide distances (A°) between base proton H8 and deoxyribose ring protons corresponding to different P and χ (in degrees) values (133).

	χ=-105			χ= - 150			χ= - 90			χ= - 60		
P	B-2′	B-2"	B-3′	B-2′	B-2"	B-3′	B-2′	B-2"	B-3′	B-2′	B-2"	B-3′
9°	2.8	4.1	1.8	4.0	4.7	2.7	2.5	3.9	2.0	2.1	>3.5	2.5
18°	4.0	4.1	3.0	2.7	4.7	3.0	2.5	3.9	2.3	2.0	>3.5	2.8
90°	2.2	3.7	4.0	3.4	4.7	4.5	2.2	3.5	4.1	2.1	3.1	4.4
117°	2.3	3.5	4.5	2.3	3.5	5.0	>2.0	3.4	4.5	>2.0	2.9	>4.5
126°	>2.0	3.5	>4.5	3.4	4.5	>5.0	>2.0	3.4	>4.5	>2.0	<3.0	>4.5
135°	2.3	3.5	>4.5	3.4	4.5	>5.0	>2.0	3.3	>4.5	2.4	<3.0	>4.5
144°	2.3	3.5	>4.5	3.4	4.5	>5.0	>2.0	3.3	>4.5	2.4	<3.0	4.5
153°	<2.5	3.5	4.5	3.4	4.5	5.0	>2.0	3.3	>4.5	-	-	-
162°	2.2	3.6	4.8	3.4	4.5	>5.0	>2.0	3.3	4.8	2.4	2.8	4.5
180°	>2.0	3.6	>4.5	3.4	>4.5	>5.0	>2.0	3.5	>4.5	>2.0	3.0	>4.5
189°	>2.0	3.7	4.5	3.5	>4.5	5.0	>2.0	3.5	4.5	-	3.2	-
198°	>2.0	3.7	4.5	3.5	>4.5	5.0	>2.0	3.6	4.4	-	3.3	-
207°	<2.5	3.8	4.3	3.5	>4.5	5.0	>2.0	3.7	4.3	-	-	-
225°	<2.5	4.0	4.0	3.6	>4.5	>4.5	>2.0	>3.5	4.0	-	-	-

B - Base proton

Table 5.11(c) : Intranucleotide distances (A°) between base proton H6 and deoxyribose ring protons corresponding to different P and χ values (133)(in degrees).

	χ=-105			χ= - 150			χ= - 90		
P	B-2′	B-2"	B-3′	B-2′	B-2"	B-3′	B-2′	B-2"	B-3′
9°	2.6	3.8	1.5	3.8	4.4	2.6	2.3	3.7	1.6
18°	2.5	3.8	1.8	3.7	4.5	2.8	2.3	3.7	1.8
90°	1.9	3.5	3.6	3.3	4.4	>4.0	<2.0	3.3	3.5
99°	<2.0	3.5	3.8	3.2	4.4	4.5	<2.0	3.3	3.9
117°	1.9	3.4	4.2	3.1	4.3	4.5	<2.0	3.0	>4.0
126°	1.9	3.4	4.2	3.1	4.3	4.5	<2.0	3.0	>4.0
135°	1.9	3.4	>4.0	3.1	4.3	4.7	<2.0	3.0	>4.0
144°	2.0	3.4	>4.0	3.1	4.3	4.8	<2.0	3.0	>4.0
153°	2.0	3.4	>4.0	3.2	4.3	5.0	<2.0	3.0	>4.0
162°	2.0	3.4	4.2	3.1	4.3	5.0	<2.0	3.1	>4.0
180°	2.0	3.5	>4.0	3.2	4.5	5.0	<2.0	3.3	>4.0
207°	2.0	3.7	3.8	3.4	>4.5	4.5	<2.0	3.5	3.8
225°	2.2	3.7	3.5	3.5	>4.5	>4.0	<2.0	3.6	3.5

	χ= - 60			χ = -120		
P	B-2′	B-2"	B-3′	B-2′	B-2"	B-3′
9°	<2.0	<3.5	2.5	3.0	4.0	1.6
18°	<2.0	<3.5	2.6	-	-	-
90°	<2.0	2.8	4.5	2.3	3.7	3.3
99°	<2.0	2.7	4.5	2.3	3.7	3.9
117°	2.0	2.5	4.5	-	-	-
126°	2.0	2.5	4.5	-	-	-
135°	2.1	2.5	4.5	2.3	3.6	4.2
144°	2.1	2.5	4.5	2.3	3.6	4.4
153°	2.1	2.5	4.5	2.3	3.6	4.4
162°	2.0	2.5	4.5	2.3	3.6	4.4
180°	<2.0	2.7	4.5	-	-	-
207°	<2.0	3.0	4.5	2.4	3.9	4.0
225°	<2.0	>3.0	3.7	2.5	4.0	3.5

B - Base proton

H8/H6-H1′ connectivities in NOESY spectra taken at τ_m = 200 ms (Fig. 5.6 (j)). In the spectra recorded at 150 ms, the cross peaks for A3, T4, G6 residues are found to be intense while the same for G2 and C1 residues are weak in intensity (Table 5.12(a)). No cross peak is seen for C5 residue. The relative distance among various residues, therefore, increases in the order A3, T4, G6 < G2, C1 < C5. The distance obtained by integration of cross peaks also show (Table 5.12 (b)) that the H8 - H1′ distance in G2 residue is higher (3.6 A°) by 0.1 A° than the corresponding distance in T4, G6 residues (3.5 A°). We observe mixtures of N and S conformer in all the deoxyribose sugars with the average fractional population of S conformer in G2, A3, G6 and T4 residues as 0.94, 0.82, 0.75 and 0.77 respectively. Since G2 residue has least population of N conformer, the H8 - H1′ distance is expected to be least (Table 5.11 (a)) among the purine residues i.e. G2, A3 and G6. Among the pyrimidines C1, C5 and T4, the cytosine residues have least fractional population of N conformer and therefore distance H6 - H1′ in T4 is expected to be lower than that in C1 and C5 residues, which is in accord with the relative intensities of their cross peaks (Table 5.12 (a)) in NOESY spectra recorded at τ_m = 150 ms. The maximum possible value of distance H6 - H1′ if 3% of N conformer having glycosidic rotation χ =- 150° (as generally found to occur in A-DNA) exists is 3.67 A° (Fig. 5.15 (a), Table 5.11(a)). The corresponding glycosidic rotation angle is - 120°. If χ is -105° for the major S conformer, the maximum distance H6 - H1′ for a mixture of 3% N conformer, and 97%

Table 5.12(a) : The observed relative intensities of intraresidue NOE cross peaks in NOESY spectra recorded at mixing time 75, 150, 200 and 250 ms of d-$(CGATCG)_2$ (Fig. 5.6(c-f)).

Connectivity	τ_m(ms)	C1	G2	A3	T4	C5	G6
B-H1′	250	s	ss	s	s	s	s
	200	s	s	s	s	s	s
	150	w	w	s	s	-	s
	75	-	-	-	-	-	-
B-H2′	250	ss	ss	ss	ss	ss	ss
	200	ss	ss	ss	ss	ss	ss
	150	ss	ss	ss	ss	ss	ss
	75	ss	ss	ss	ss	ss	ss
B-H2"	250	ws	ss	ss	ss	ss	ss
	200	-	ss	ss	ss	ss	ss
	150	-	s	s	s	s	s
	75	-	ws	ws	ws	-	s
B-H3′	250	-	s	ss	-	-	ss
	200	-	s	ss	-	-	ss
	150	-	s	ss	-	-	ss
	75	-	-	-	-	-	-

B : base proton. - : absence of peak.

w : weak intensity of peak. ws : fairly intense.

s : intense. ss : very intense.

Table 5.12(b) : Interproton distances* calculated from observed intraresidue NOE connectivities in NOESY spectra recorded at mixing time 75 and 150 ms for d-$(CGATCG)_2$.

	C1		G2		A3		T4		C5		G6	
τ_m(ms)	75	150	75	150	75	150	75	150	75	150	75	150
Connectivity												
B-H1′	-	-	-	3.6	-	3.3	-	3.5	-	-	-	3.5
B-H2′	2.5	-	2.2°	-	2.1°	-	2.2	-	2.2	-	2.2	-
B-H2"	-	-	2.4	-	3.2	-	3.4	-	-	2.9°	3.0°	-
B-H3′	-	-	-	3.5	-	3.3	-	-	-	-	-	3.3

B : base proton. o : overlap.

- : Cross peak either not integrated or absent.

* r(CH5-CH6) = 2.45 A°, used as internal standard distance.

of S conformer is ~ 3.66 A° irrespective of the pseudorotation angle P (Fig. 5.15 (a)). We did not observe NOE cross peak corresponding to H6 - H1′ connectivity for C5 and C1 residue at τ_m = 75 ms, while for C1 residue a weakly intense peak is seen at 150 ms (Table 5.12 (a)). It may be inferred that a cut off distance beyond which the NOE peak is not seen in NOESY spectra recorded at τ_m = 150 ms is 3.67 A° or perhaps lesser than this distance. If G2 residue has major S conformer (average χ_S = 0.94) with glycosidic rotation as -105°, the standard value in B-DNA structures, the distance may be calculated as 3.88 x 0.94 + 3.72 x 0.06 = 3.87 A°. Since a weak cross peak is observed for G2 residue (Table 5.12 (a)), the H8 - H1′ distance is certainly < 3.67 A°. The calculated distance for 94% S conformer for χ = -90° and -60° are 3.80 and 3.58 A°. Therefore the observed weakly intense cross peak in G2 residue corresponds to a glycosidic bond rotation in the range - 60 to -75°. It may be noted that the distance H8/H6 - H1′ obtained by integration of observed cross peak in NOESY spectra recorded τ_m = 150 ms are 3.6, 3.5, 3.5 and 3.3 A°, for G2, T4, G6 and A3 residues respectively (Table 5.12(b)). Although the absolute values of these distances appear to be on lower side, these distances may be used in a relative sense for comparison in different residues. We made an attempt to calculate these distances using average value of χ_S (to an accuracy of ± 0.05 to account for the resolution ~ 0.5 Hz in 1D NMR spectra used to measure ΣH1′ values). The calculated values for A3, G6, T4 residues having χ_S = 0.82, 0.75, 0.77 for

glycosidic bond rotation χ value as - 60°, - 60°, - 105° are 3.605, 3.615, 3.620 A°, respectively. Comparing calculated distances with those obtained by peak integration as well as consistent with relative intensities of observed cross peaks provides the following range of χ for C1, G2, A3, T4, C5, G6 residues as -105°, -75°, -60°, -90°, -120°, and -60° (to an accuracy of ± 15°) respectively.

The base to H2′ distance in B-DNA geometries are known to be the least out of all base to sugar proton distances (Table 5.11 (b,c)). We observed very intense cross peak corresponding to H8/H6 - H2′ distance in case of all residues. The distance obtained in T4, C5 and G6 residues is ~ 2.2 A° (Table 5.12 (b)). In C1 residue, the observed corresponding distance is somewhat higher being, 2.5 A°. It may be noted from the standard value of H6 - H2′ distance data (Table 5.11(c), Fig. 5.15 (c)) available in literature (133) that a larger H6 - H2′ distance ~ 2.5 A° is expected for the combination P - χ of the deoxyribose sugar as P_N = 18°, χ = -105° or P_S = 225°, χ = -120°. Since there is no evidence of major N conformer to be present in C1 residue of d-CGATCG, it may be inferred that a large fraction of P_S = 225° with χ =- 120° ± 15° exists in the present case. For other five residues, the distance H6/H8 - H2′ cannot be used to narrow down the range of χ values, it being ~ 2.2 A° in all cases resulting in very intense cross peaks.

Considering the distance of base H8/H6 proton to H2" sugar proton, we find that these vary with both P and χ. For a glycosidic bond rotation as anti, typically say χ = -105°, the distance is least for P = 153°/162° and increases on either decreasing it towards P = 9°/18° or on increasing it towards P = 207°/225°. Further by varying the glycosidic bond rotation from an anti conformation, say χ = -105°, to high anti conformation, that is χ = -90° or -60°, the distance H8/H6 - H2" decreases for a given pseudorotation value (Fig. 5.15 (b,c), Table 5.11 (b,c)). We observed intense cross peak corresponding to H8/H6-H2" connectivity in NOESY spectra recorded at τ_m = 150 ms for all residues except C1 residue, for which the corresponding cross peak is found to be missing (Fig. 5.6 (e)). At τ_m = 75 ms the corresponding cross peak for both C1 and C5 residues are not observed (Fig. 5.6 (f)). The cross peak for G6 residue is intense even in spectra recorded at 75 ms as compared to that for G2, A3, T4 residues (Table 5.12 (a)). These results indicate that the H8/H6 - H2" distance increases in the order G6 < G2, A3, T4 < C5 < C1. The distance obtained by peak integration are ~ 3.2 - 3.4 A° in case of A3 and T4 residues (Table 5.12 (b)). We made an attempt to calculate average distance for a mixture of N and S conformer with χ for N conformer (being minor component) to be -150° (i.e. that for A-DNA) and that for S conformer to vary in the range - 120° to -60°. Some of calculated values of distances in A° are as follows :

Residue	χ_S	P_S (in degrees)	χ (in degrees)			
			-120	-105	-90	-60
G2	0.94	162	-	3.67	3.38	2.91
A3	0.82	153	-	3.72	3.55	3.06
G6	0.75	189	-	3.95	3.80	3.57
T4	0.77	135	-	3.49	3.16	-
C1	0.70, 0.27	225, 117/126	3.89	3.62	3.44	3.01
C5	0.60, 0.37	225, 117/126	3.85	3.59	3.38	2.94

Comparing the calculated values with those observed (Table 5.12(b)) as well as with the observed relative intensities of cross peaks (Table 5.12 (a)), we find that the range of glycosidic bond rotation for G2, A3, G6, T4 residues is - 60°, -60°, -60°, and -90°, respectively. For C1 and C5 residues, the χ_S and P_S values are not obtained to a good accuracy due to overlapping of peaks. However we have used a particular mixture of P_S = 225° and P_S = 117/126° suggested by independent analysis discussed earlier to estimate χ. Since H6-H2" cross peak is not observed for C1 residue in NOESY spectra recorded at τ_m = 150 ms (Table 5.12(a)) for which cut off distance beyond which cross peak is not observed is ~ 3.67 A°, it may be inferred that χ for C1 residue is

less than χ = - 105°. For C1 and C5, it may be in the range -105° to -120° and -90° to -105°, respectively.

Considering base H8 to H3' sugar proton distance we find that the cross peak of A3 and G6 residues are more intense than the corresponding cross peak for G2 residue (Fig. 5.6 (h,i), Table 5.12(a)). The H8 - H3' distance for N conformer with P_N = 18°, χ =- 150° (typical value for A-DNA) is ~ 3.0 A° while that for S conformer lies in the range 4.5 - 4.8 A°. Since G2 has least population of N conformer, it is expected to yield less intense cross peak than A3 and G6 residues. Typical value of anti conformation i.e. χ = -105° yield distance H8 - H3' as 4.1, 4.5 and 4.7 A° for G6, A3 and G2 residues respectively using the standard tables (Table 5.11 (b)). In order to make these peaks observable NOESY spectra particularly at τ_m = 150 (Fig. 5.6 (i)) distances are required to be lowered and close to the observed value ~ 3.5 A° which can be possible only by increasing χ from anti to high anti conformation such as χ = -60° in purines.

Thus we find that it is possible to narrow down the range of glycosidic bond rotation by using the data on base - H1', base - H2'/H2", base - H3' NOE connectivities. Combining these results we conclude that the glycosidic bond rotation for C1, G2, A3, T4, C5 and G6 residues are - 105°, -75°, -60°, -90°, -105° and -60° (to an accuracy of ± 15°) respectively.

INTERACTION OF ADRIAMYCIN WITH DEOXYHEXANUCLEOTIDE d-$(CGATCG)_2$

Interaction of adriamycin with d-$(CGATCG)_2$ has been studied by 1D and 2D NMR techniques. Titration studies are carried out on adriamycin-d-$(CGATCG)_2$ complex by addition of adriamycin (26.46 mM) to 0.4 ml of d-$(CGATCG)_2$ (duplex concentration = 2.98 mM) in steps of 10 μl. 90 μl of adriamycin is added in the final step in order to achieve 2:1 ratio of adriamycin to hexamer duplex concentration. 1D NMR spectra recorded at various drug to hexamer concentration ratios are shown in Fig. 6.1 (a-g). The chemical shifts of adriamycin and hexamer protons as a function of drug to DNA ratio are shown in Fig. 6.2 (a, b). One-dimensional NMR spectra are recorded on 2:1 adriamycin + d-$(CGATCG)_2$ complex at different temperatures in the range 295 - 325 K (Fig. 6.3(a-c)). The chemical shift of adriamycin and hexamer protons as a function of temperature are shown in Fig. 6.4 (a, b). Two-dimensional phase-sensitive NOESY spectra of 2:1 adriamycin-hexamer complex are recorded at different mixing times (τ_m = 250, 200, 150, 75 and 50 ms). Phase-sensitive NOESY spectra recorded at τ_m = 250 ms is shown in Fig. 6.5 (a-i).

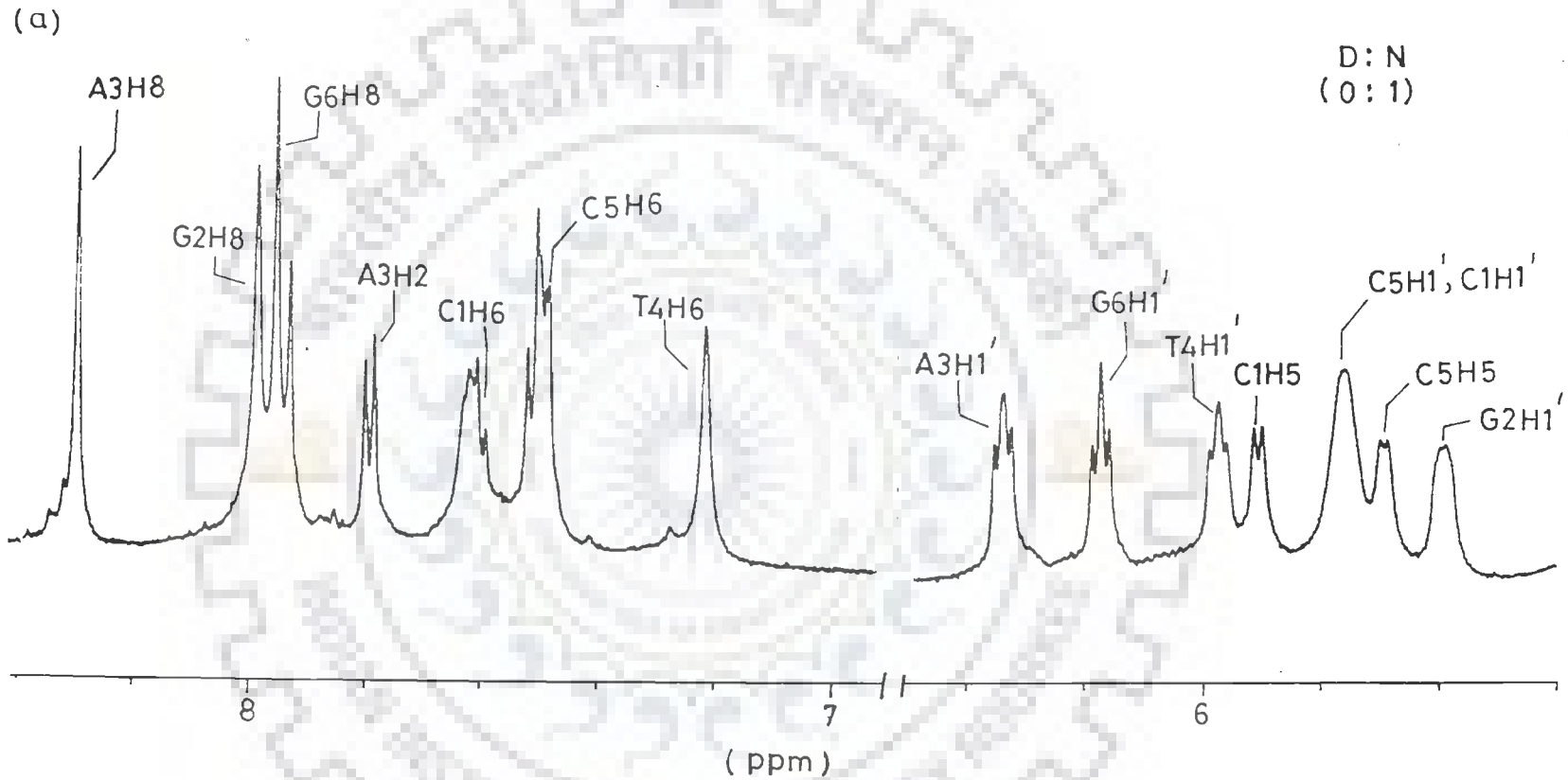

Fig. 6.1(a-g) : 1D proton NMR spectra of d-$(CGATCG)_2$ + adriamycin complex in D_2O at various drug/ DNA (D/N) ratios (295 K).

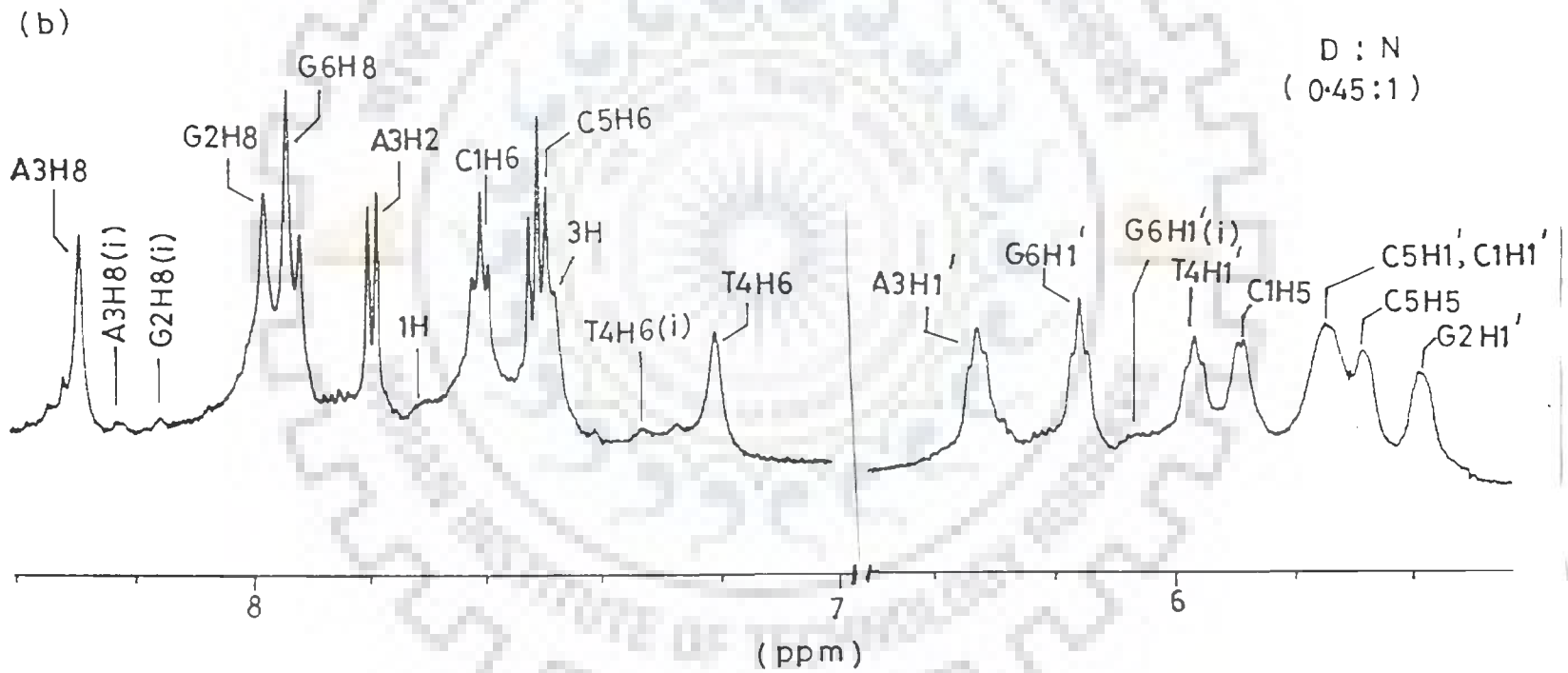
(b)
D : N
(0·45 : 1)
A3H8
A3H8(i)
G2H8(i)
G2H8
G6H8
A3H2
1H
C1H6
C5H6
3H
T4H6(i)
T4H6
A3H1'
G6H1'
G6H1'(i)
T4H1'
C1H5
C5H1', C1H1'
C5H5
G2H1'
8
7
6
(ppm)

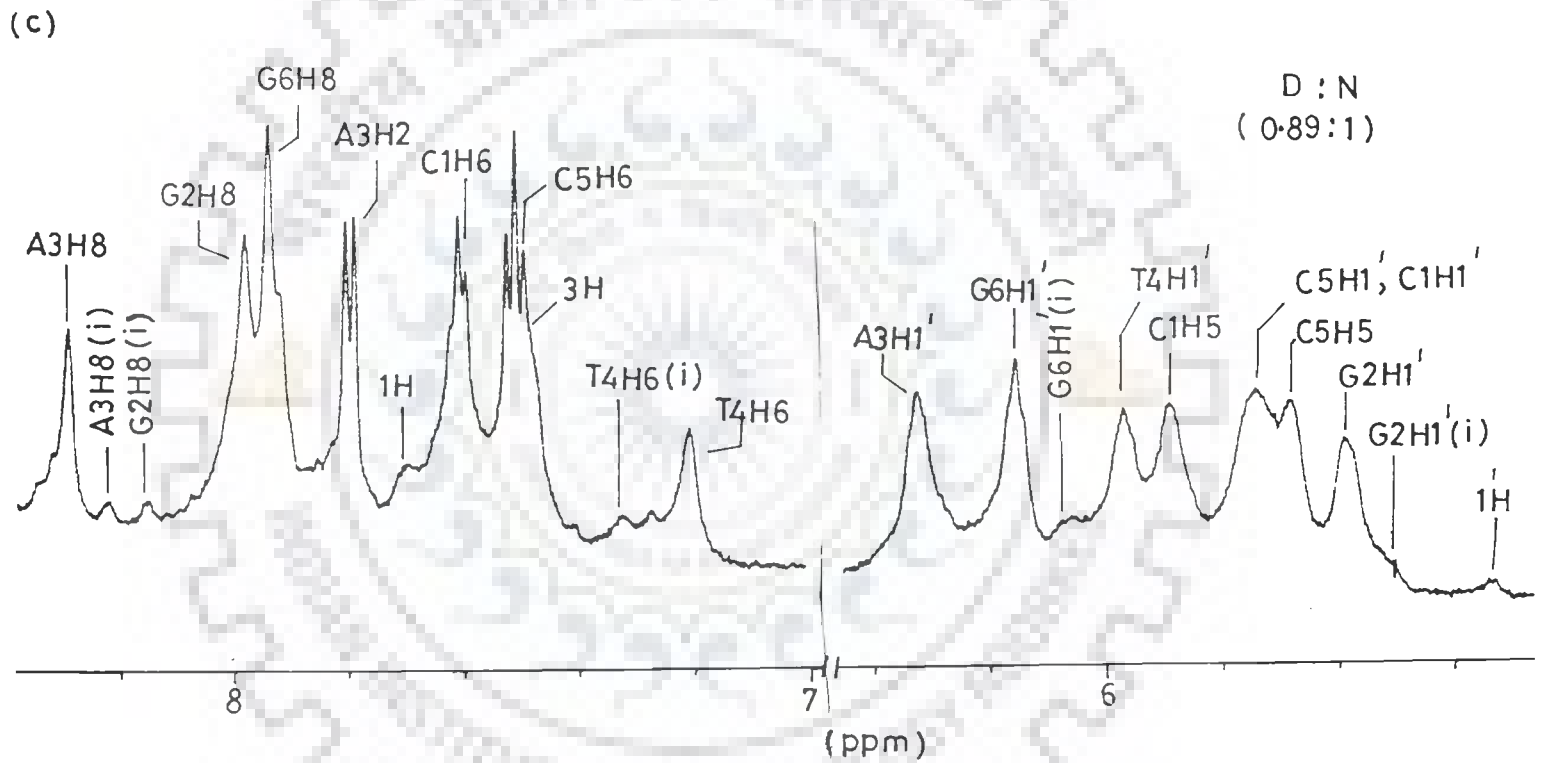
(c)
D : N
(0·89 : 1)
A3H8
A3H8(i)
G2H8(i)
G2H8
G6H8
A3H2
C1H6
C5H6
3H
1H
T4H6(i)
T4H6
A3H1'
G6H1'
G6H1'(i)
T4H1'
C1H5
C5H1', C1H1'
C5H5
G2H1'
G2H1'(i)
1H
8
7
6
(ppm)

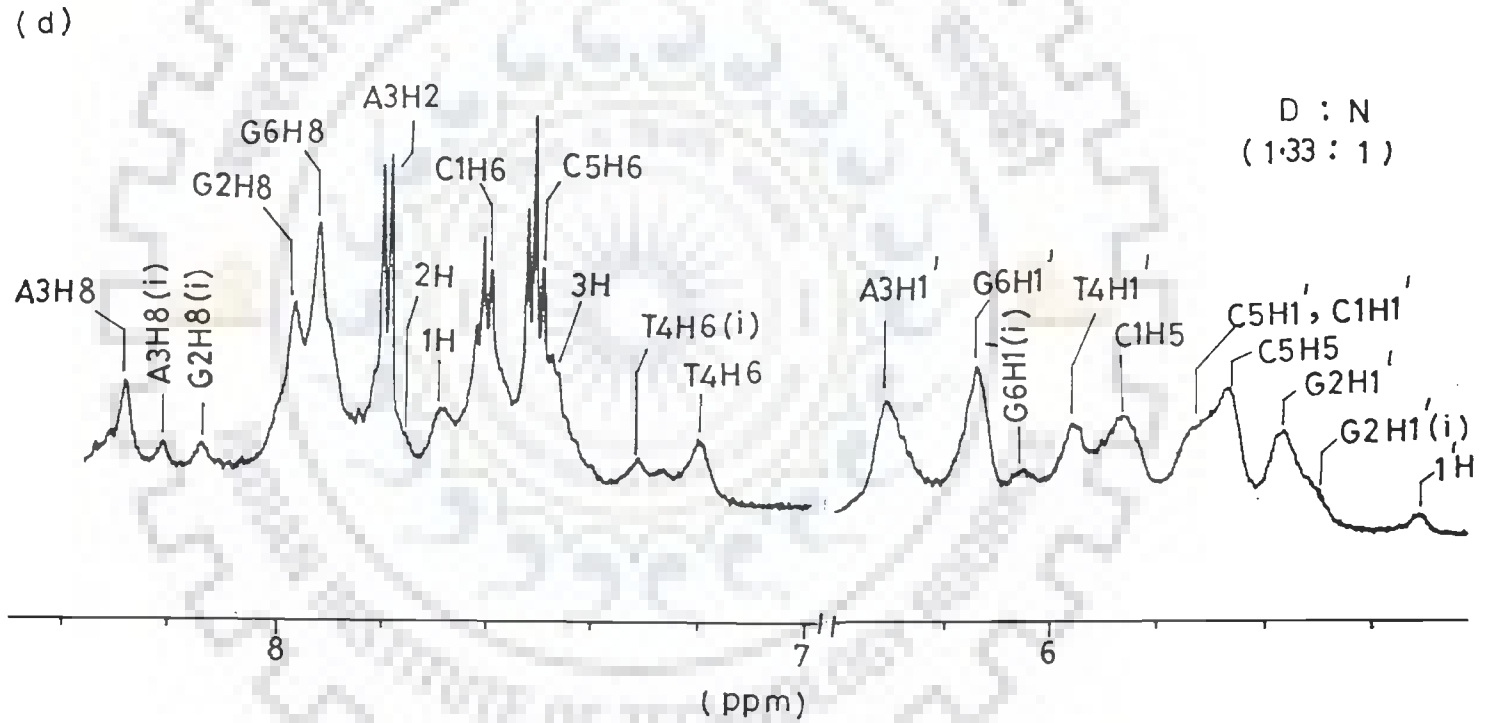
(d)
A3H8
A3H8(i)
G2H8(i)
G2H8
G6H8
A3H2
C1H6
C5H6
2H
1H
3H
T4H6(i)
T4H6
A3H1'
G6H1'
G6H1(i)'
T4H1'
C1H5
C5H1', C1H1'
C5H5
G2H1'
G2H1'(i)
1'H
D : N
(1·33 : 1)
8
7
6
(ppm)

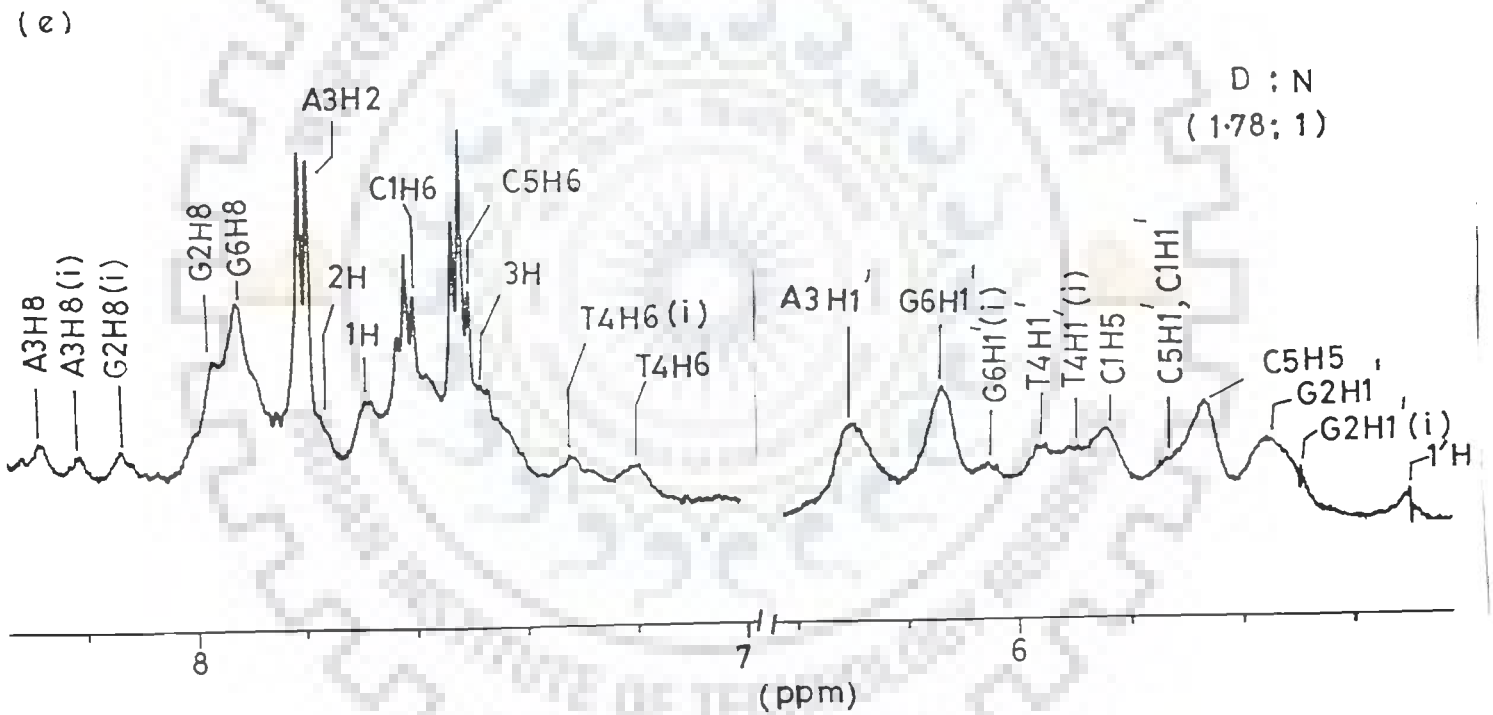
(e)
D : N
(1·78; 1)
A3H8
A3H8(i)
G2H8(i)
G2H8
G6H8
A3H2
2H
1H
C1H6
C5H6
3H
T4H6(i)
T4H6
A3H1'
G6H1'
G6H1'(i)
T4H1'
T4H1'(i)
C1H5
C5H1', C1H1'
C5H5'
G2H1'
G2H1'(i)
1'H
8
7
6
(ppm)

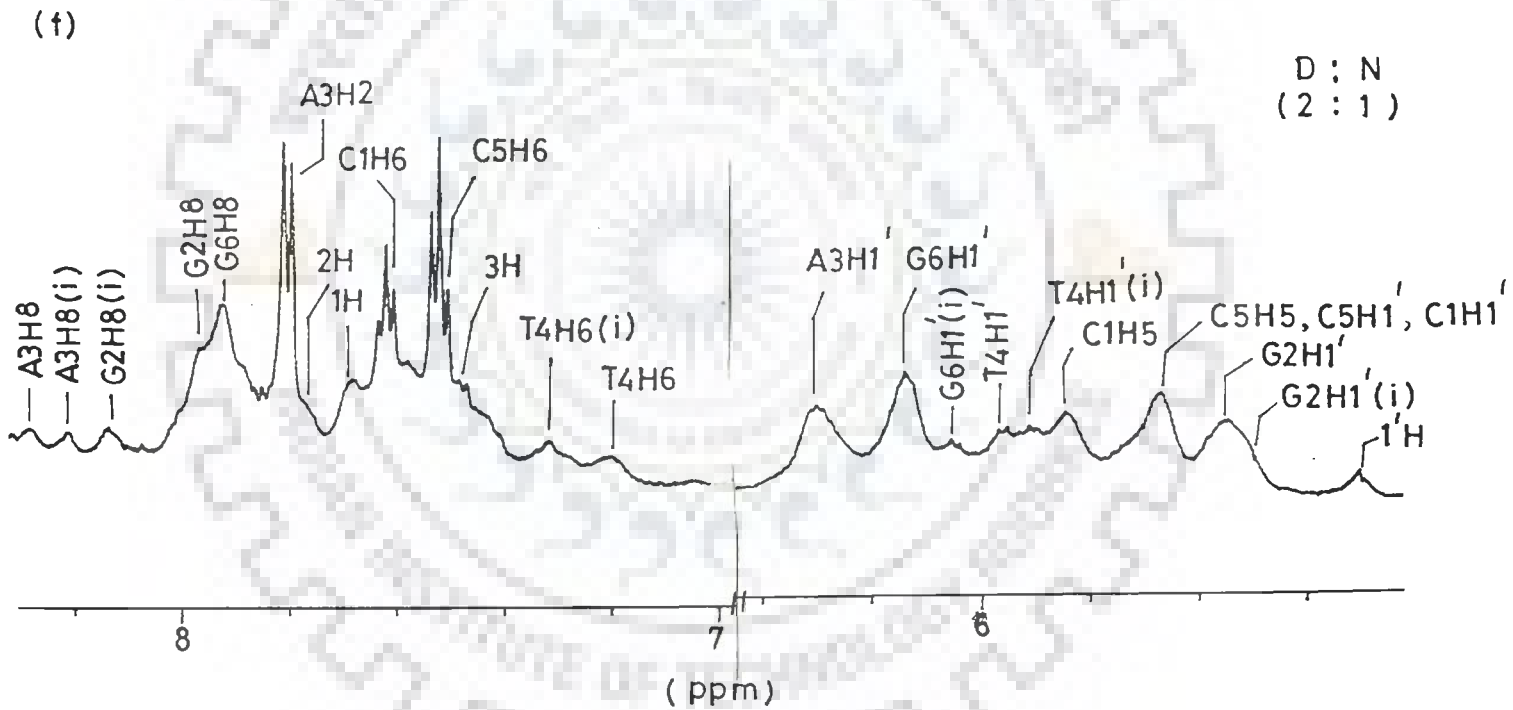
(f)
D : N
(2 : 1)
A3H8
A3H8(i)
G2H8(i)
G2H8
G6H8
A3H2
C1H6
2H
1H
C5H6
3H
T4H6(i)
T4H6
A3H1'
G6H1'
G6H1'(i)
T4H1'
T4H1'(i)
C1H5
C5H5, C5H1', C1H1'
G2H1'
G2H1'(i)
1'H
8
7
6
(ppm)

(g)
D : N
(2 : 1)
A3H3′
G2H3′
7H, G6H3′, C1H3′
A3H4′
G2H4′
A3H5′, 5′H
4′H
C1H4′, 3′H
G2H5′, 3′H
40 CH3
C1H5′
G2H2″, G6H2″(B), 10 eq H, A3H2″
G2H2′ A3H2′ G6H2″(A)
T4H2″, G6H2′(B), 10axH
C1H2″, C5H2″, G6H2′(A), 8eq H
2′eq H
C1H2′, 2′axH, 8axH
5′CH3
T4CH3
5·0
4·0
2·4
1·2
(ppm)

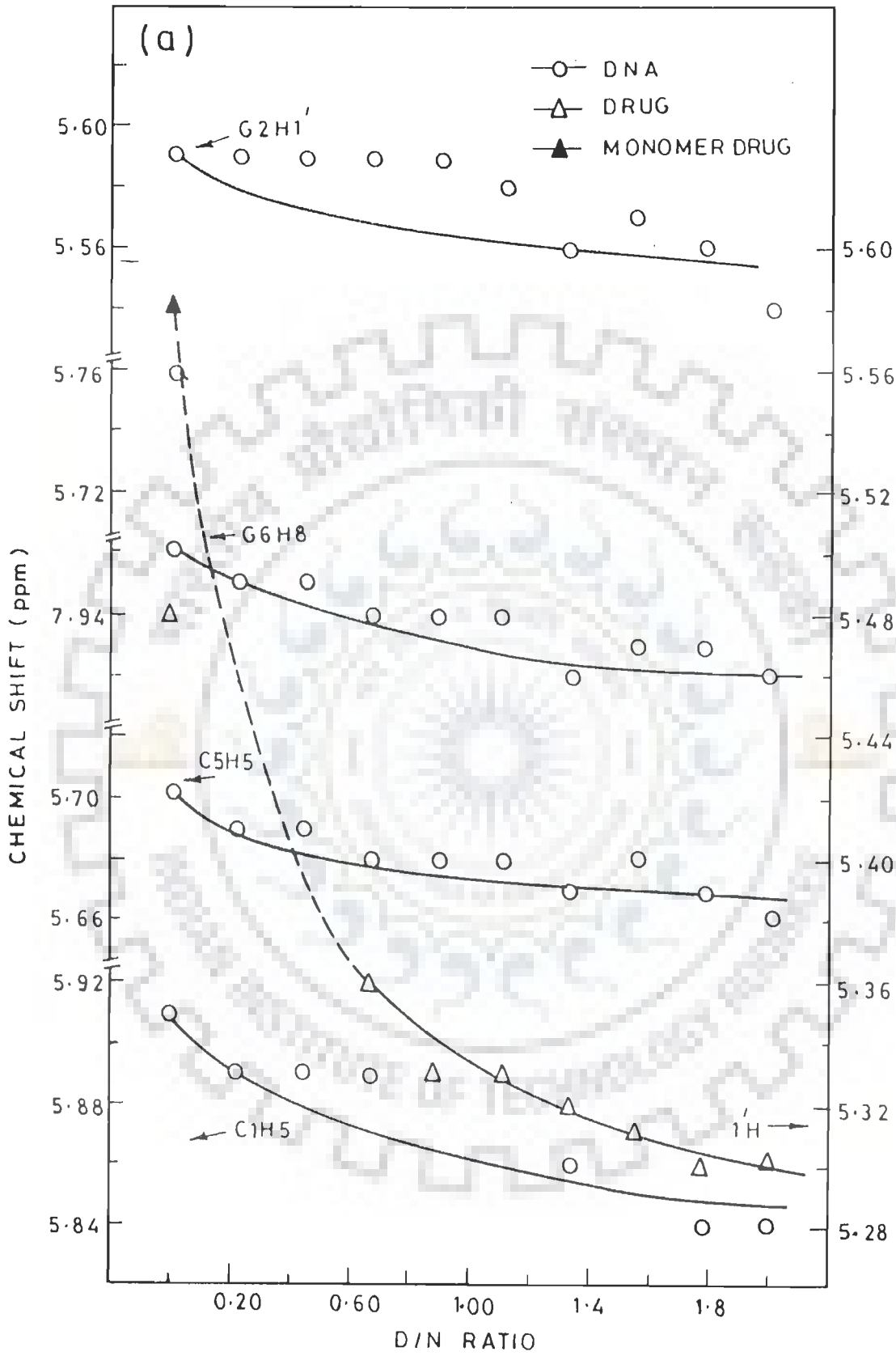

Fig. 6.2(a,b) : Chemical shift of various protons of d-$(CGATCG)_2$ and adriamycin at various drug/DNA (D/N) ratios.

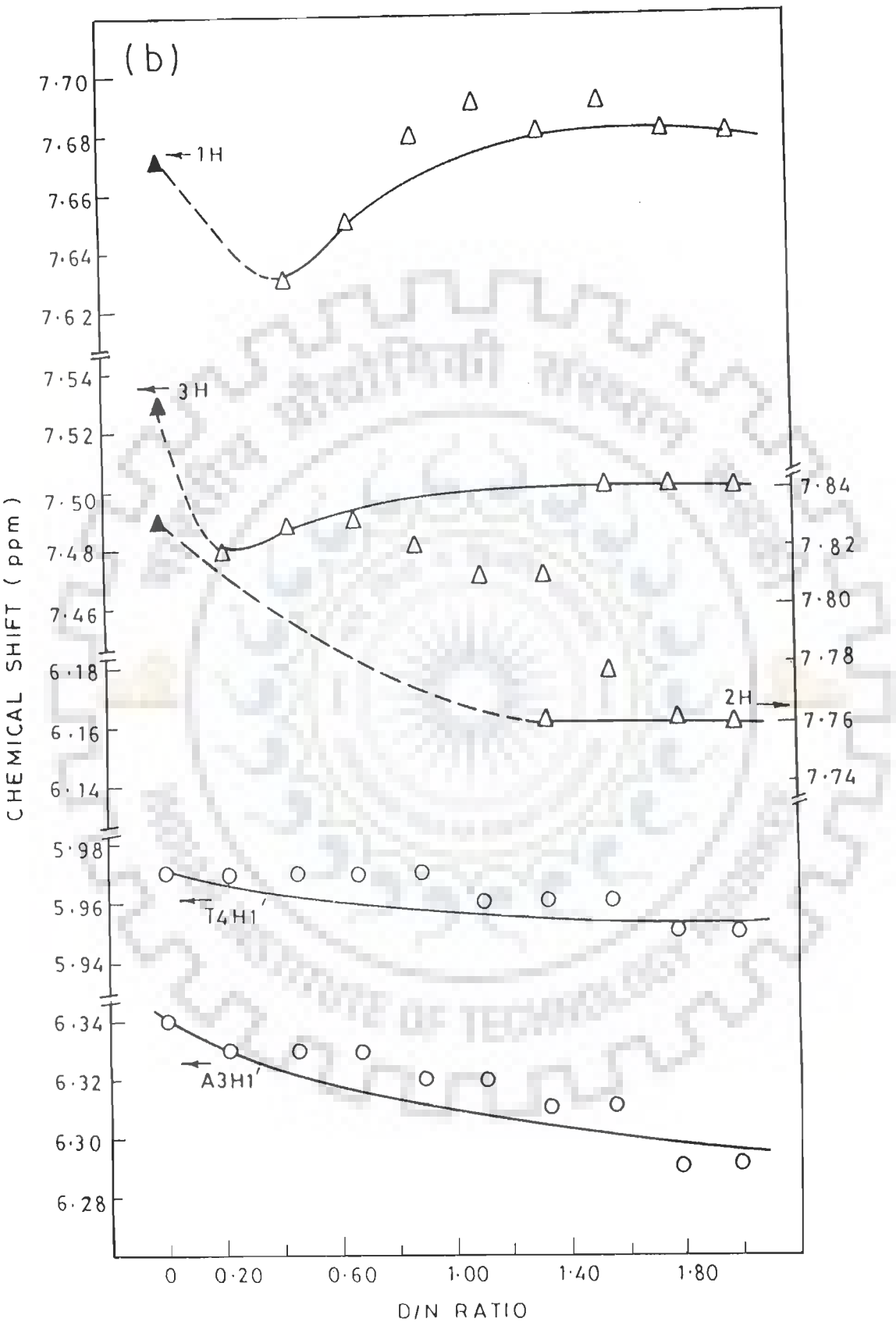
(b)
7·70
7·68
7·66
7·64
7·62
7·54
7·52
7·50
7·48
7·46
6·18
6·16
6·14
5·98
5·96
5·94
6·34
6·32
6·30
6·28
1H
3H
2H
T4H1′
A3H1′
7·84
7·82
7·80
7·78
7·76
7·74
0
0·20
0·60
1·00
1·40
1·80
D/N RATIO
CHEMICAL SHIFT (ppm)

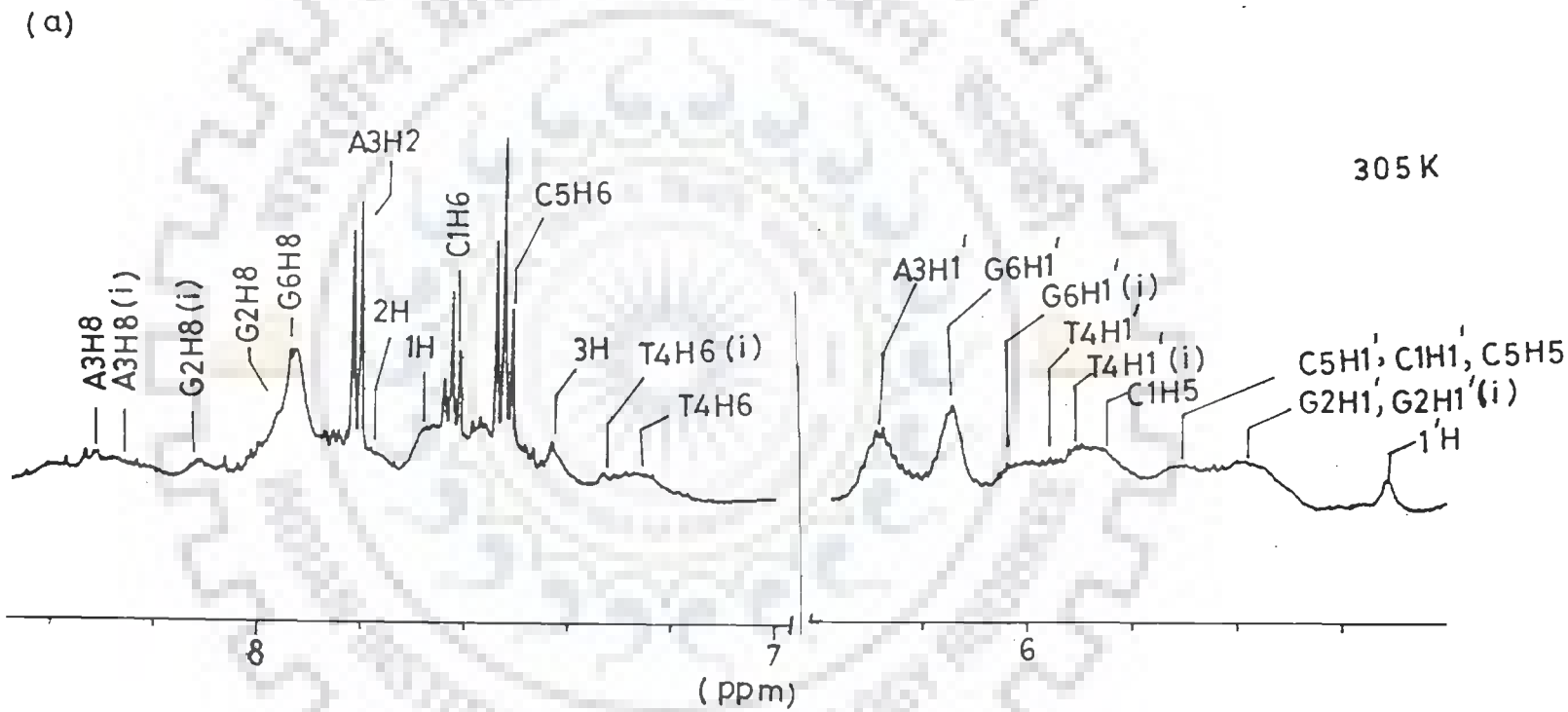

Fig. 6.3 (a-c) : 1D proton NMR spectra of d-$(CGATCG)_2$ + adriamycin complex (2:1) in D_2O at different temperatures.

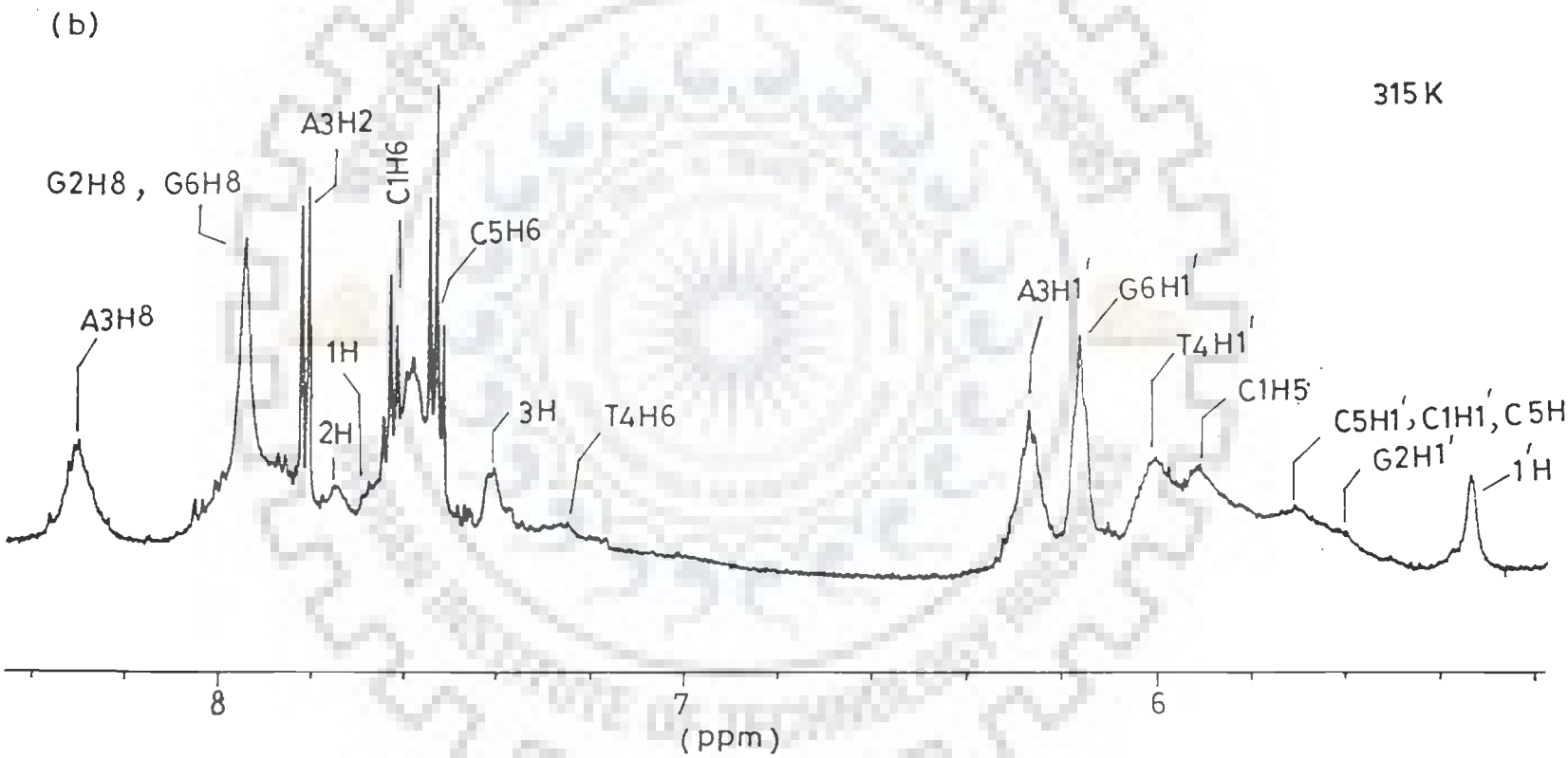
(b)
315 K
A3H2
G2H8 , G6H8
C1H6
C5H6
A3H8
1H
2H
3H
T4H6
A3H1'
G6H1'
T4H1'
C1H5'
C5H1', C1H1', C5H5
G2H1'
1'H
8
7
6
(ppm)

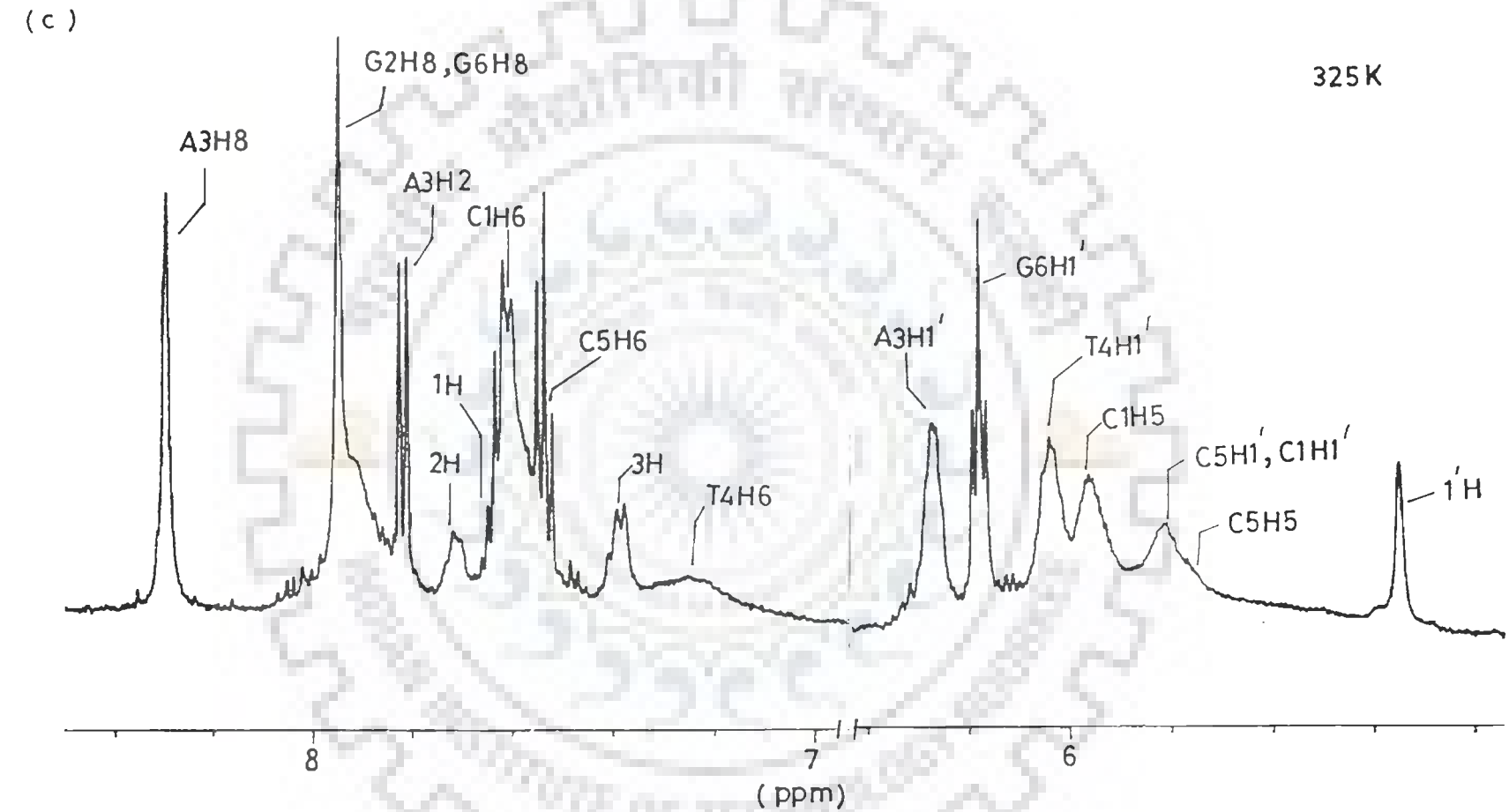
(c)
325K
A3H8
G2H8,G6H8
A3H2
C1H6
C5H6
1H
2H
3H
T4H6
A3H1'
G6H1'
T4H1'
C1H5
C5H1', C1H1'
C5H5
1'H
8
7
6
(ppm)

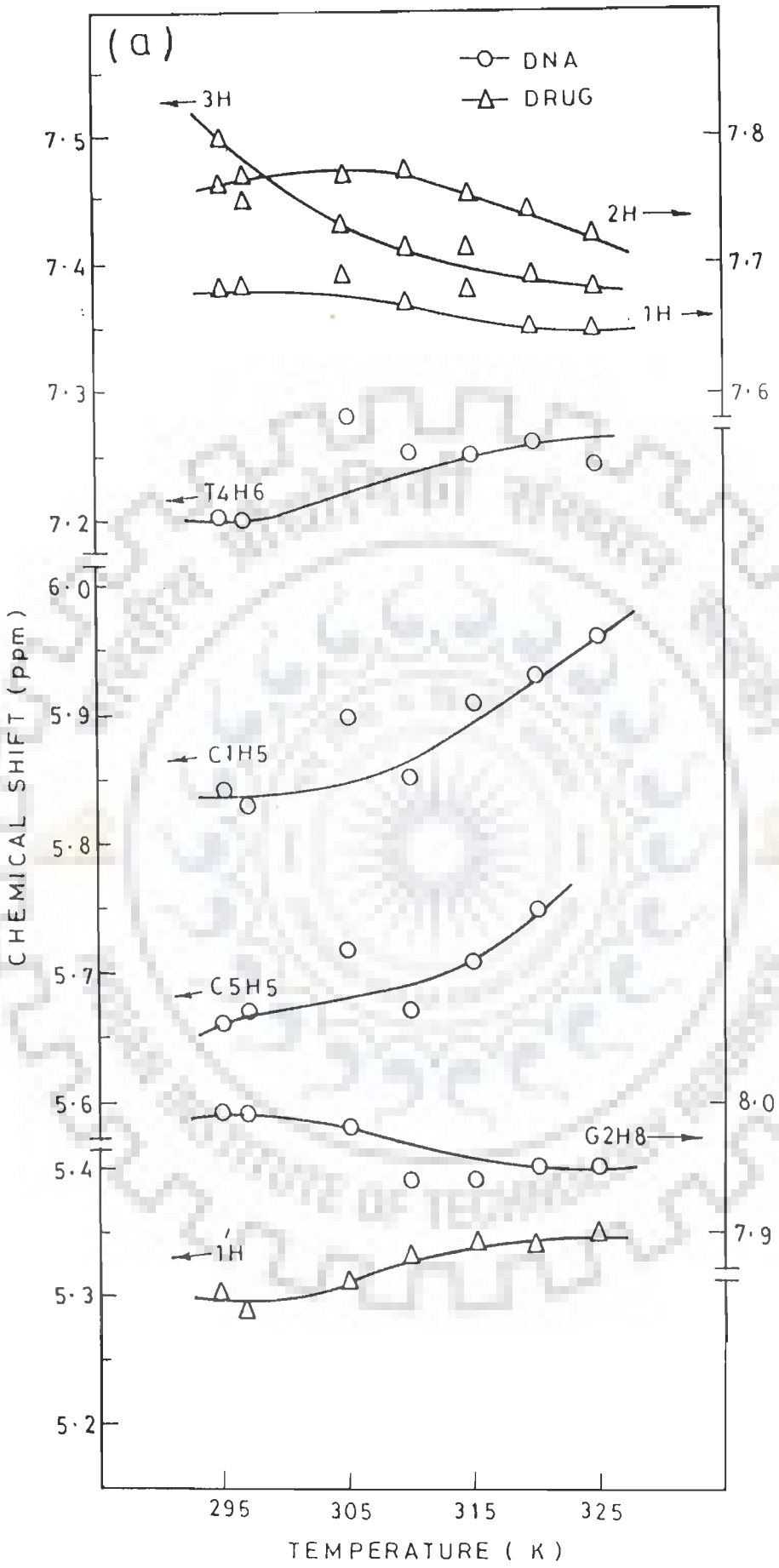

Fig. 6.4(a,b) : Chemical shift of various protons of d-$(CGATCG)_2$ and adriamycin at different temperatures in the range (295 K-325 K).

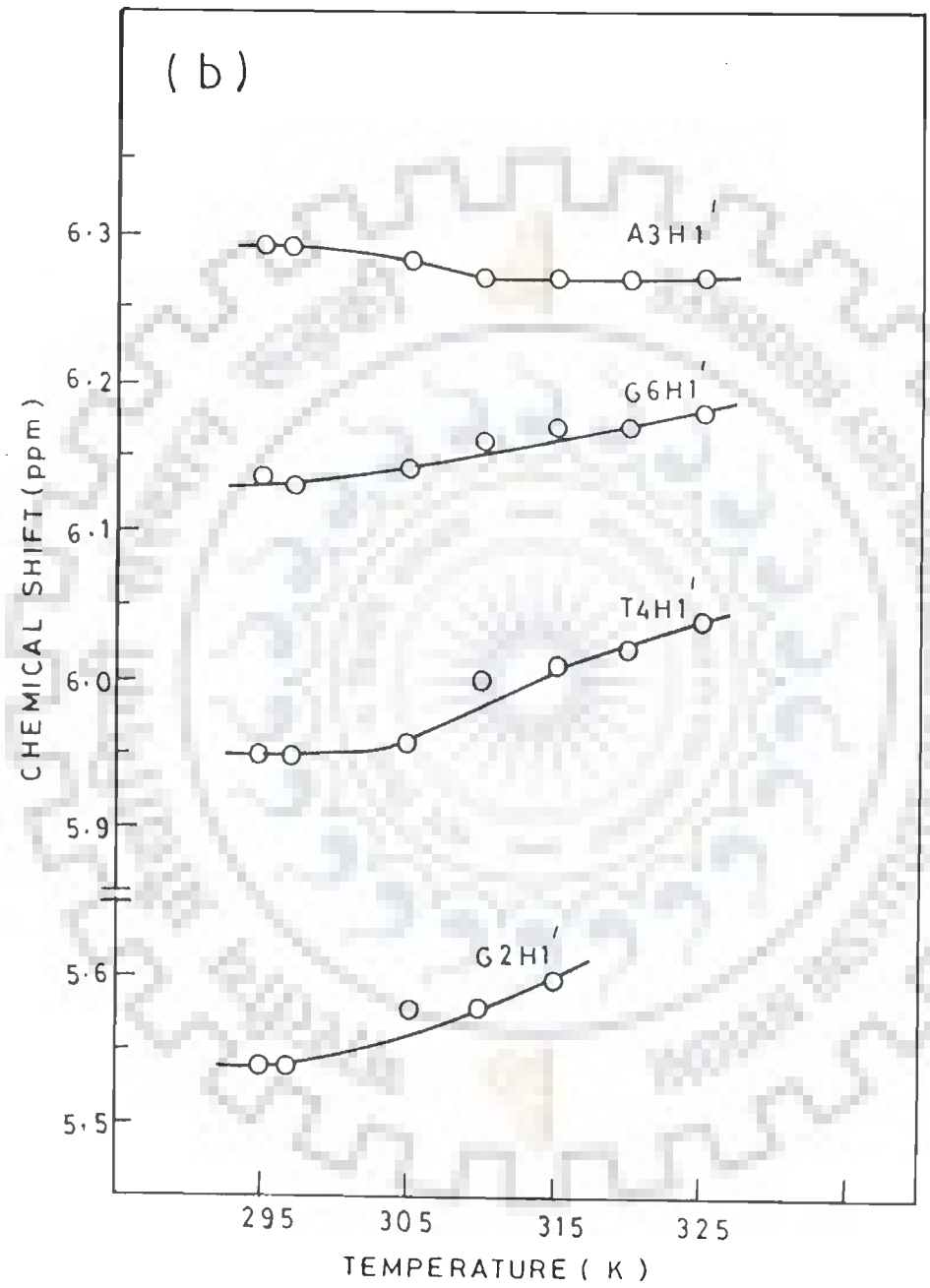
(b)
A3H1'
G6H1'
T4H1'
G2H1'
6·3
6·2
6·1
6·0
5·9
5·6
5·5
CHEMICAL SHIFT (ppm)
295
305
315
325
TEMPERATURE (K)

SEQUENTIAL ASSIGNMENT

The H8, H2 and H6 resonances appear in the region of aromatic protons in the range of 7.30 - 8.30 ppm (Fig. 6.1(f)). The deoxyribose sugar H1′ protons resonate between 5.50 - 6.30 ppm and the sugar H3′, H4′, H5′, H5", H2′ and H2" resonate between 1.80 - 5.10 ppm. The thymine CH_3 protons are observed around ~ 1.20 ppm (Fig. 6.1 (f,g)).

The resonances of adriamycin and hexanucleotide d-$(CGATCG)_2$ are assigned on the basis of 2D phase-sensitive NOESY spectrum recorded at τ_m = 250 ms (Fig. 6.5 (a-i)). The 2D double quantum filter COSY spectra recorded on this complex is not helpful for spectral assignment due to broad signals of all protons being observed at drug to DNA (D/N) ratio of 2:1.

Resonance assignment of d-$(CGATCG)_2$

The resonance assignment of d-$(CGATCG)_2$ in its complex with adriamycin is carried out by following the standard strategies available in literature for assignment of B-DNA (30,31,42,45,113). Fig. 6.5 (b) shows all the six sets of H2′-H2" connectivities. These sets of H2′-H2" connectivities are coupled to their corresponding H1′ and H3′ protons (Fig. 6.5(c,d)). The H3′ of all residues are coupled to their H4′ proton which are further coupled to their respective H5′, H5" protons (Fig. 6.5(e)). The six sets of deoxyribose sugar protons thus recognised are assigned to their corresponding residues on the basis of base - H2′, H2" connectivities (Fig. 6.5(c)).

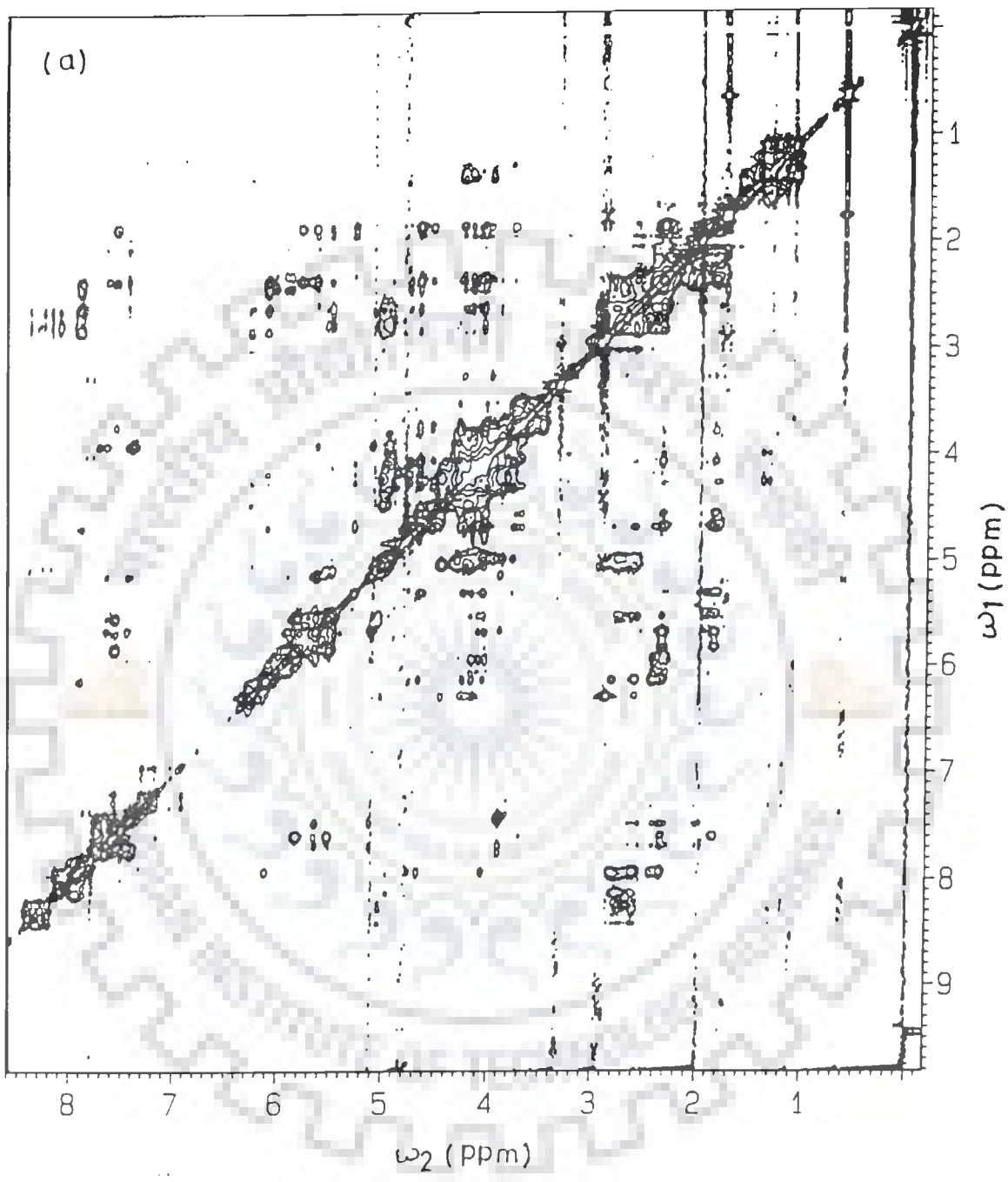

Fig. 6.5(a-i) : Phase-sensitive NOESY spectrum (at τ_m 250 ms) of d-$(CGATCG)_2$ + adriamycin complex highlighting specific NOE connectivities in D_2O at 295 K.

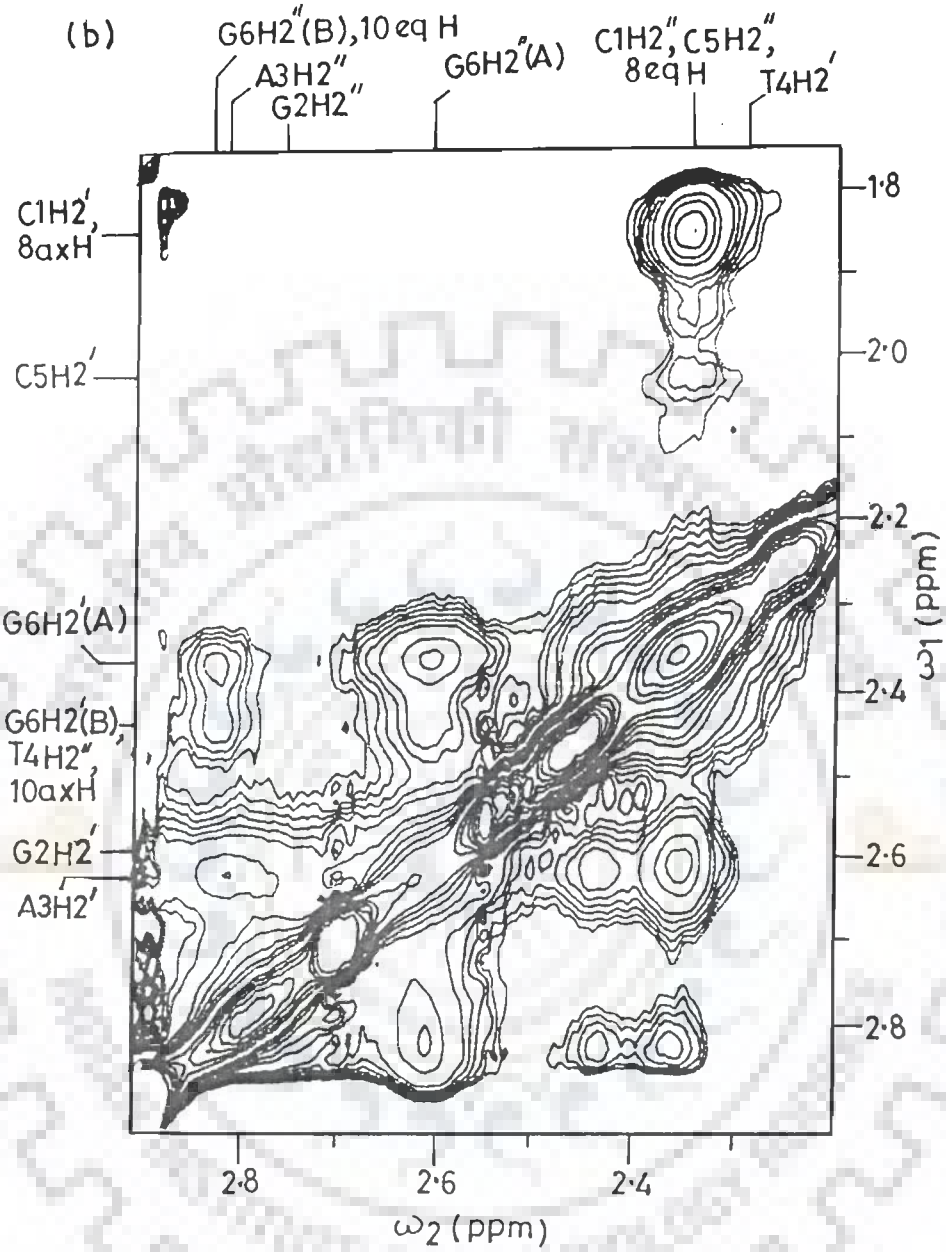
(b)
G6H2''(B),10eq H
A3H2''
G2H2''
G6H2''(A)
C1H2'', C5H2'',
8eq H
T4H2'
C1H2',
8axH
C5H2'
G6H2'(A)
G6H2'(B),
T4H2'',
10axH
G2H2'
A3H2'
1·8
2·0
2·2
2·4
2·6
2·8
ω1 (ppm)
2·8
2·6
2·4
ω2 (ppm)

(c)
A3H8
A3H8(i)
G2H8(i)
G2H8
G6H8
1H
C1H6
C5H6
T4H6(i)
A3H1'
G6H1'
G6H1'(i)
T4H1'
T4H1'(i)
C1H5
C1H1'
C5H5, C5H1'
G2H1''
G2H1''(i)
1'H
T4CH3
5'CH3
8axH,
2'axH,
C1H2'
2'eqH
C5H2'
8eqH, T4H2'
C1H2'',
C5H2'',
G6H2'(A)
G6H2'(B), T4H2''
G2H2', G6H2''(A)
A3 H2'
G2H2''
G6H2''(B),
A3H2''
8·0
7·5
7·0
6·5
6·0
5·5
ω2 (ppm)
1·5
2·0
2·5
ω1 (ppm)

(d)

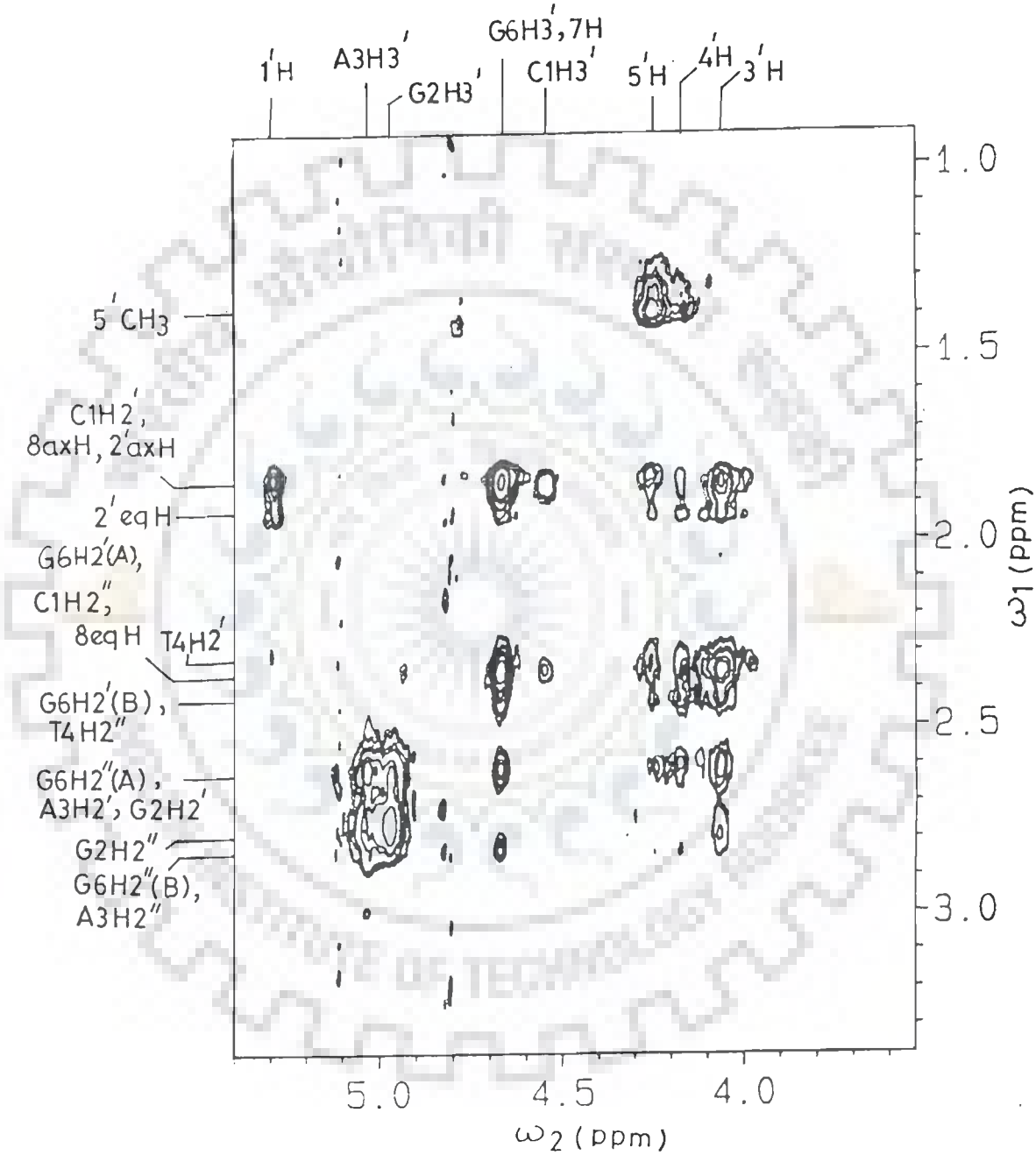
1'H
A3H3'
G2H3'
G6H3',7H
C1H3'
5'H
4'H
3'H
5'CH3
C1H2', 8axH, 2'axH
2'eqH
G6H2'(A), C1H2'', 8eqH
T4H2'
G6H2'(B), T4H2''
G6H2''(A), A3H2', G2H2'
G2H2''
G6H2''(B), A3H2''
1.0
1.5
2.0
2.5
3.0
ω1 (ppm)
5.0
4.5
4.0
ω2 (ppm)

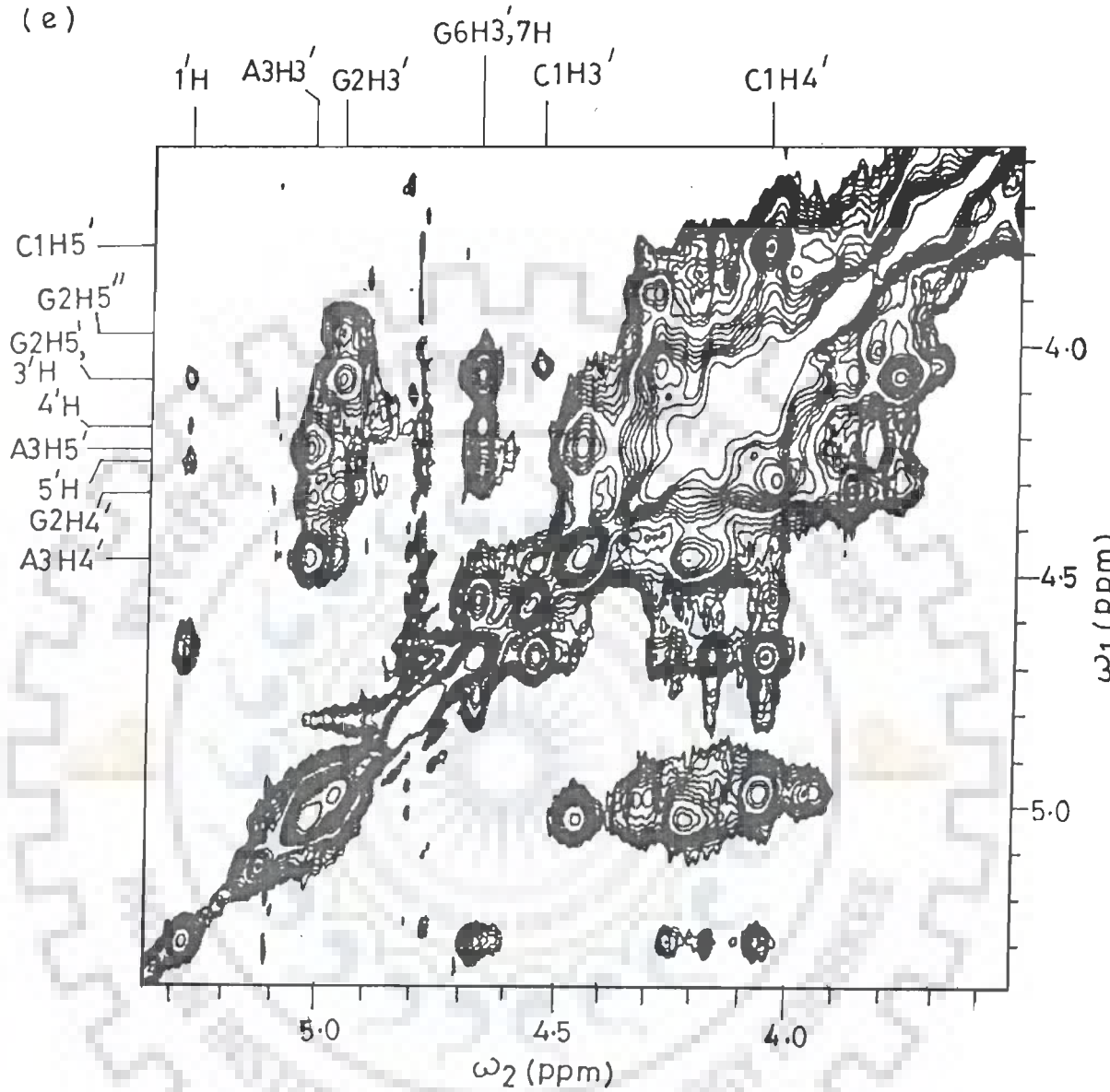
(e)
1′H
A3H3′
G2H3′
G6H3′,7H
C1H3′
C1H4′
C1H5′
G2H5″
G2H5′,
3′H
4′H
A3H5′
5′H
G2H4′
A3H4′
4·0
4·5
5·0
ω1 (ppm)
5·0
4·5
4·0
ω2 (ppm)

The base resonances at 7.57 and 7.46 ppm give intense NOE cross peaks with protons resonating at 5.82 and 5.66 ppm, respectively and are therefore assigned to pairs of cytosine H6 and H5 protons (Fig. 6.5 (g)). The methyl resonance at 1.20 ppm give NOE cross peak with base proton at 7.32 ppm. This connectivity refers to $T4CH_3$ and T4H6 base protons (Fig. 6.5 (c)).

Each residue is expected to give two intranucleotide connectivities with H2′ and H2" protons and two internucleotide connectivities with H2′ and H2" protons of the preceeding residue in the sequence. It is evident from Fig. 6.5 (c) that one of the cytosine H6 proton resonating at 7.57 ppm gives only two intranucleotide connectivities with H2′, H2" protons and hence is assigned as the terminal residue at 5′-end. Therefore the other H6 proton resonating at 7.46 ppm gets assigned to C5H6 base proton.

We did not observe the internucleotide connectivity of T4H6 base proton with H2′/H2" proton of A3 residue in the NOESY spectra recorded at τ_m = 250 ms (Fig. 6.5(c)). Similarly, in NOESY spectra recorded at τ_m = 250 ms, G6H8 - C5H2" inter residue connectivity is observed while G6H8-C5H2′ NOE cross peak is not observed. Table 6.1 lists various inter residue NOE cross peaks of $d\text{-}(CGATCG)_2$ observed on complexation.

The adenine base proton, A3H8 in the sequence also gives NOE with $T4CH_3$ proton showing their proximity (Fig. 6.5(c)), Table 6.1). Fig. 6.5(g) shows internucleotide connectivity between C5H6-T4H1′ which confirms the sequential assignment. Several

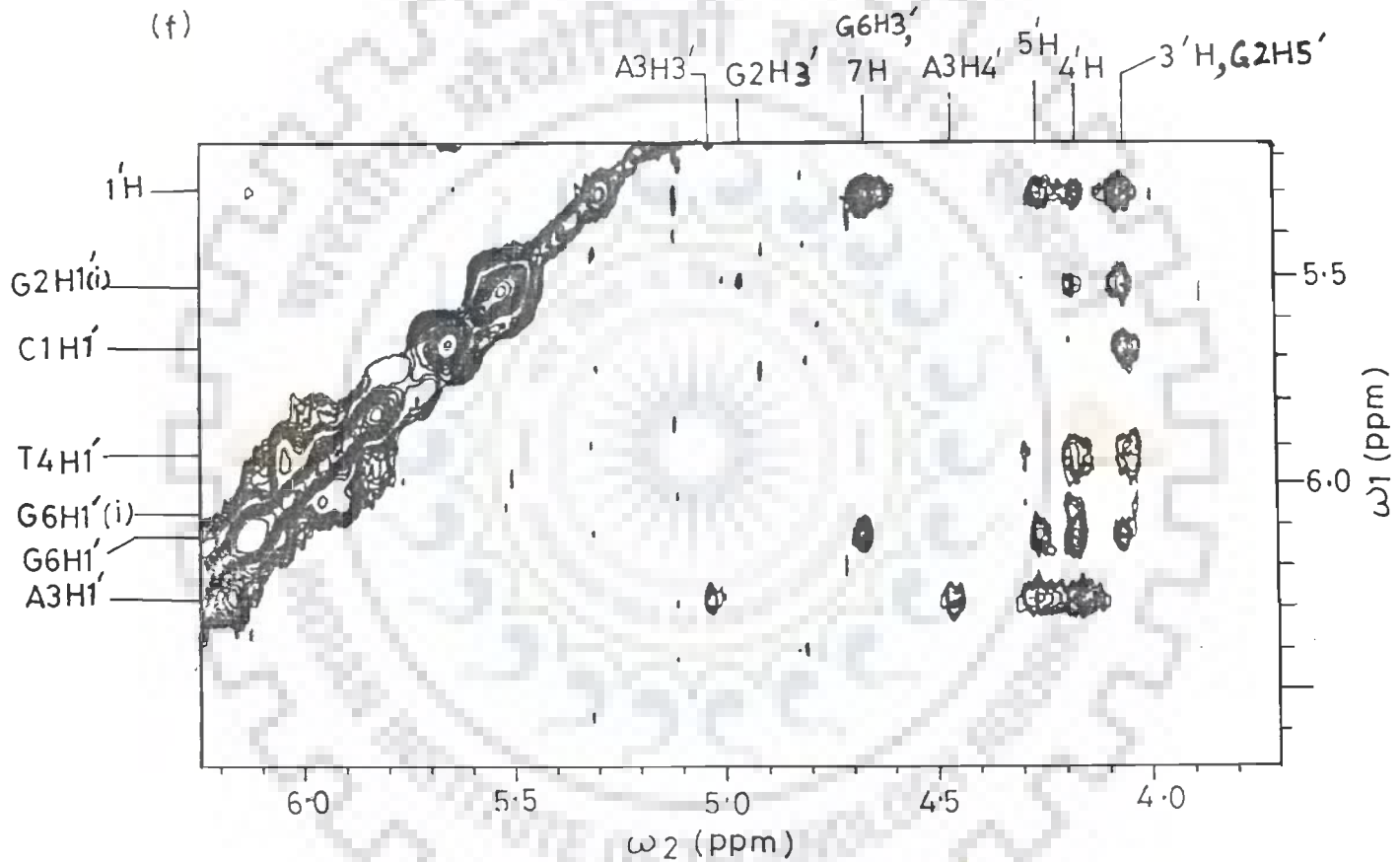
(f)
A3H3′
G2H3′
G6H3′, 7H
A3H4′
5′H
4′H
3′H, G2H5′
1′H
G2H1′(i)
C1H1′
T4H1′
G6H1′(i)
G6H1′
A3H1′
5·5
6·0
ω1 (ppm)
6·0
5·5
5·0
4·5
4·0
ω2 (ppm)

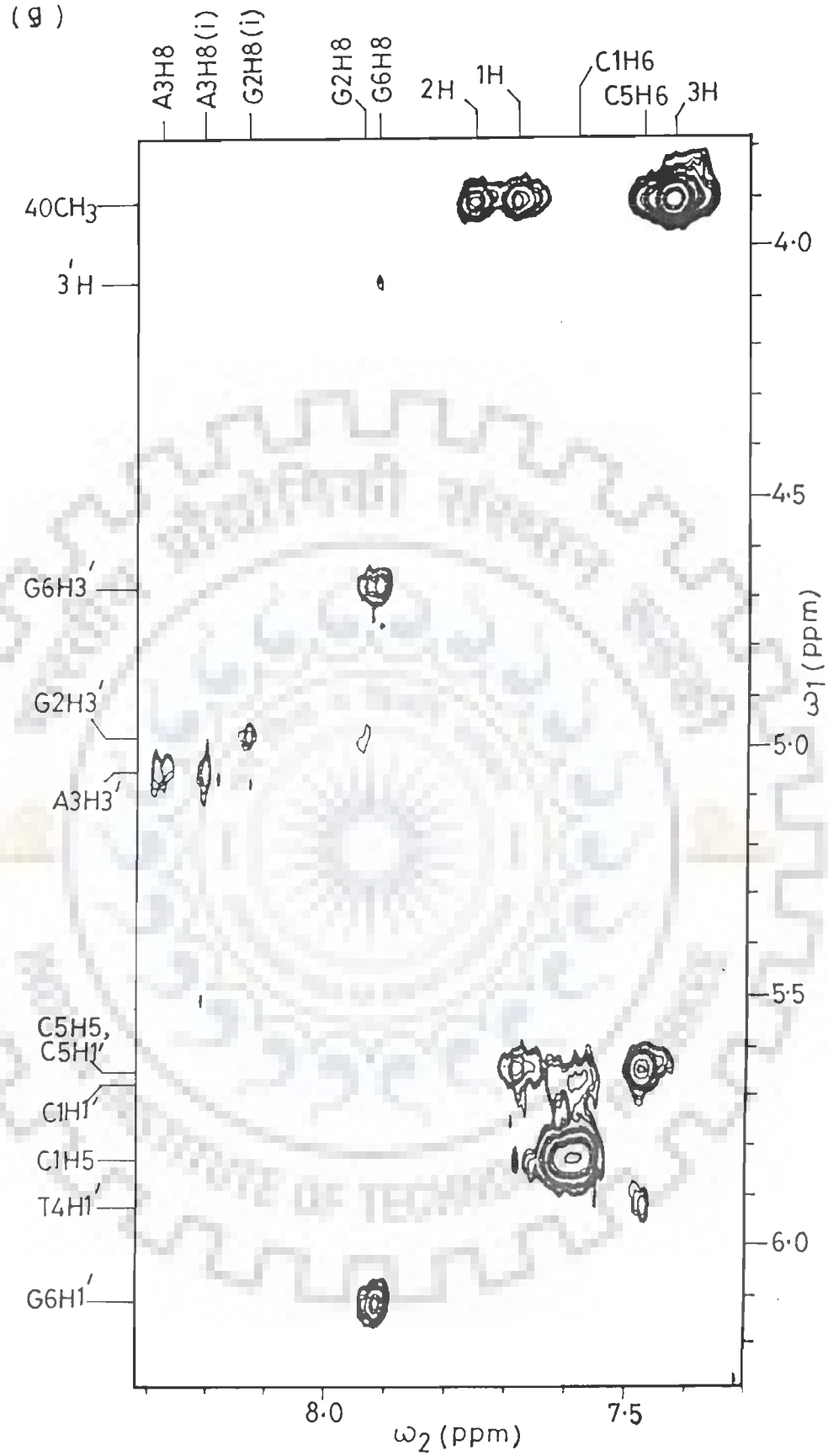
(g)
A3H8
A3H8(i)
G2H8(i)
G2H8
G6H8
2H
1H
C1H6
C5H6
3H
40CH3
3'H
G6H3'
G2H3'
A3H3'
C5H5,
C5H1'
C1H1'
C1H5
T4H1'
G6H1'
4·0
4·5
5·0
5·5
6·0
ω1 (ppm)
8·0
7·5
ω2 (ppm)

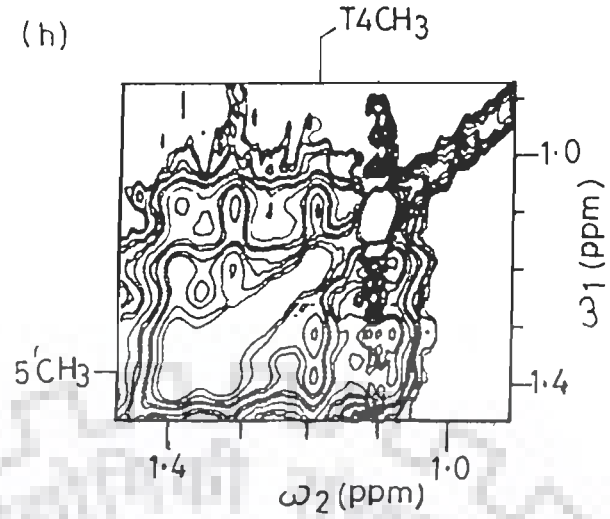
(h)
T4CH3
5'CH3
1·0
1·4
ω1 (ppm)
1·4
1·0
ω2 (ppm)

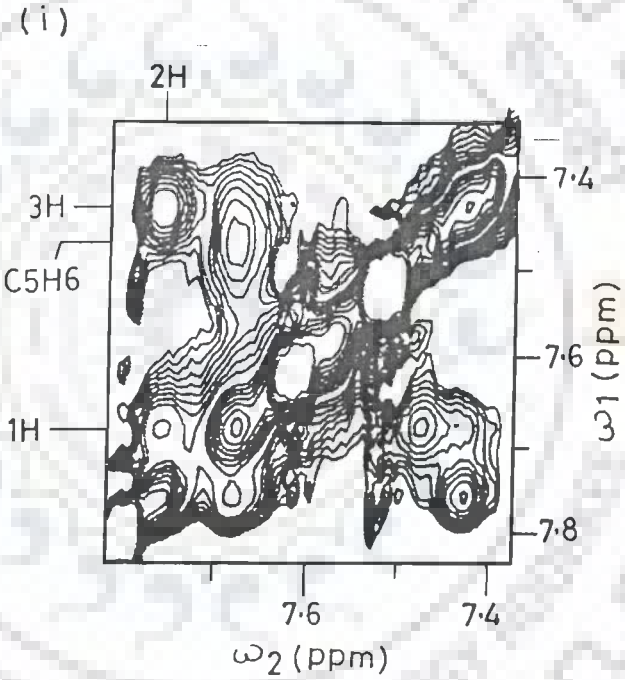
(i)
2H
3H
C5H6
1H
7·4
7·6
7·8
ω1 (ppm)
7·6
7·4
ω2 (ppm)

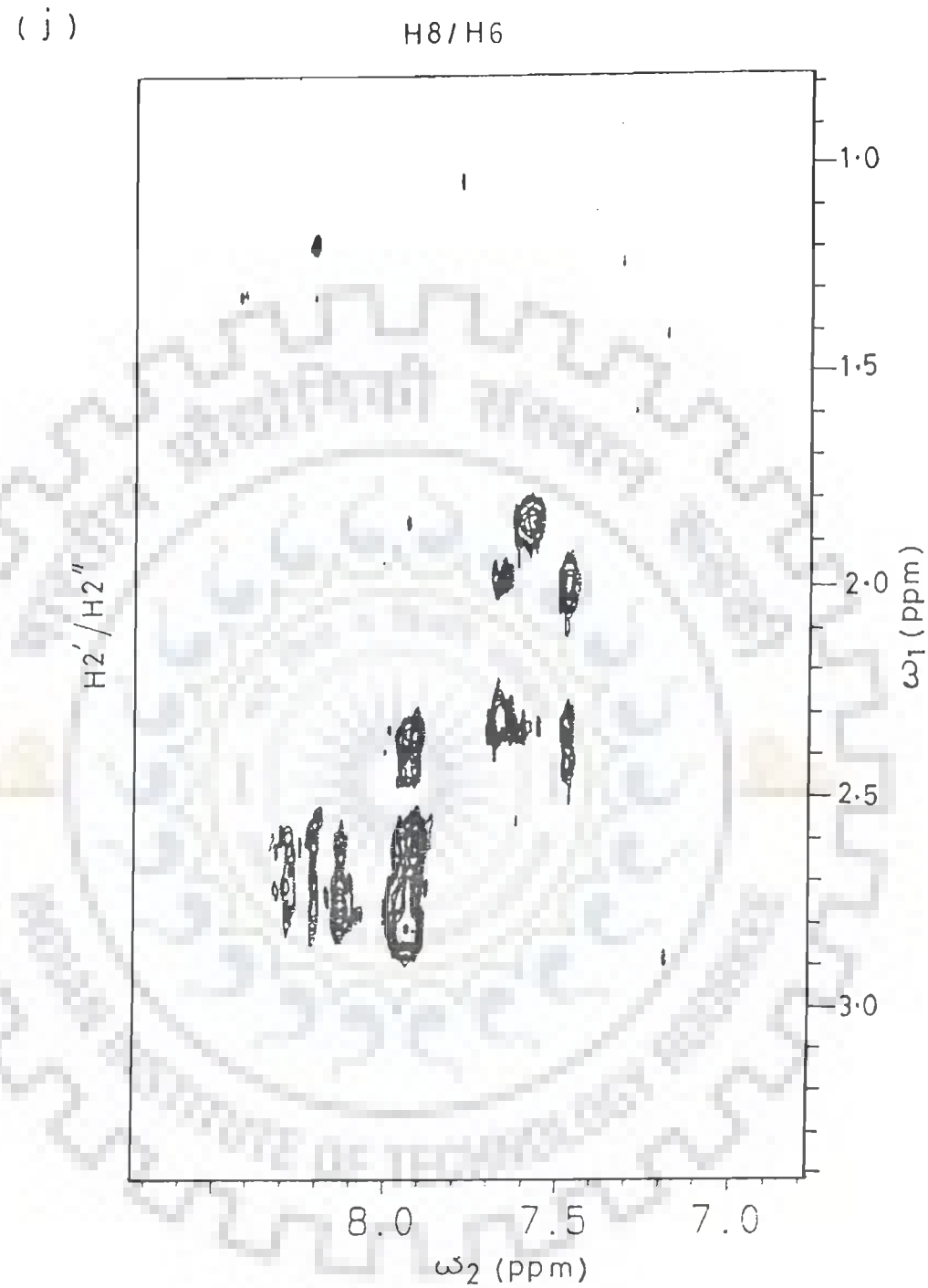

Fig. 6.5 (j) : Phase-sensitive NOESY spectrum (at τ_m 75 ms) of d-$(CGATCG)_2$ + adriamycin complex showing intra and inter-residue base -H2′/H2" NOE connectivites.

Table 6.1 : Presence of inter-residue (sequential) NOE cross peaks of d-$(CGATCG)_2$ on complex formation as observed in phase-sensitive NOESY spectra (τ_m = 250 ms).

G2H8	- C1H2′
G2H8	- C1H2"
A3H8	- G2H2′
A3H8	- G2H2"
A3H8(i)	- T4CH_3
C5H6	- T4H2′
C5H6	- T4H2"
C5H6	- T4H1′
G6H8	- C5H2"

additional NOEs between pairs of protons H1′-H3′ and base - H1′, H3′ are also observed (Fig. 6.5(f,g)) which are used further in analysis of glycosidic bond rotation (χ) and pseudorotation angles of deoxyribose sugars. The unambiguous assignment of all protons of d-$(CGATCG)_2$ in complex is thus made.

Fig. 6.5(c) shows that G6H1′ gives NOE connectivities with four H2′/H2" resonances i.e. at 2.36, 2.60 and 2.43, 2.83 ppm. Fig. 6.5(b) shows that the resonances of 2.36 and 2.60 as well as 2.43 and 2.83 ppm form pairs of H2′-H2" proton which are here after referred to as A and B pair of protons. Another H1′ resonance at 6.05 ppm gives NOE connectivity with H2′ proton of each set A and B. This H1′ proton is tentatively assigned to G6 residue (referred to as G6H1′(i), and is discussed later). It is notable that the H1′(G6H1′(i)) proton shows NOE connectivity with H2′ proton of set A and B and not with H2" proton as expected for right-handed B-DNA. Thus perhaps more than one complex may be present in solution. We also observe that four AH8/GH8 resonances at 8.29, 8.21, 8.13 and 7.95 ppm give NOE connectivity with the pair of H2′-H2" protons resonating at 2.62, 2.81 and 2.60, 2.75 ppm. Two of these base protons (at 8.29 and 8.21 ppm) show NOE connectivity with A3H3′ while the other two base protons (at 8.13 and 7.95 ppm) show NOE connectivity with G2H3′ (Fig. 6.5(g)). Hence the H8 resonances at 8.29 and 8.21 ppm are assigned to A3H8 (referred to as A3H8 and A3H8(i), respectively) while the resonances at 8.13 and 7.95 ppm are assigned to G2H8 (referred as G2H8(i) and G2H8, respectively).

In case of G2 residue, two H1′ resonances are observed resonating at 5.55 and 5.52 ppm (referred as G2H1′ and G2H1′(i), respectively) which gives NOE connectivity with its H2′-H2" pair (Fig. 6.5(c)). However, the resonance at 5.52 ppm i.e. G2H1′(i) gives NOE connectivity with G2H3′ (Fig. 6.5(f)). Similarly, two H1′ resonances at 5.96 and 5.91 ppm are observed for T4 residue which gives NOE connectivity with its corresponding H2′-H2" pair of protons. Table 6.2 gives the list of chemical shifts of various protons of d-$(CGATCG)_2$ on complex formation.

Spectral assignment of adriamycin

The ring D 1H, 2H and 3H protons are expected in the range of chemical shift, 7.40 - 7.70 ppm. The resonance at 7.76 ppm gives NOE connectivity with protons resonating at 7.68 and 7.43 ppm. This assigns the resonance at 7.76 ppm to 2H proton while the resonance at 7.68 and 7.43 ppm are assigned to 1H and 3H protons, respectively (Fig. 6.5(i)). Further, 1H, 2H and 3H protons give NOE connectivity with the resonance at 3.91 ppm, which assigns this resonance to $4OCH_3$ protons of ring D (Fig. 6.5(g)).

The intense signal at 1.39 ppm gives NOE cross peak with the resonance at 4.25 ppm and therefore are assigned to $5'CH_3$ and 5′H protons of daunosamine sugar, respectively (Fig. 6.5(c)). The 5′H proton gives NOE with the resonance at 4.18 ppm which is assigned to 4′H proton. Further 4′H proton is coupled to 3′H proton resonating at 4.07 ppm. 3′H proton of sugar shows NOE with protons at 1.83 and 1.91 ppm which are assigned to 2′axH and 2′eqH

Table 6.2 : Chemical shift of various protons of d-$(CGATCG)_2$ (in ppm) on complex formation with adriamycin in D_2O at 295 K.

Protons	C1	G2	A3	T4	C5	G6
H8/H6	7.57	7.95	8.29	7.32	7.46	7.92
		(i)8.13	(i)8.21			
H1′	5.68	5.55	6.29	5.96	5.66	6.13
		(i)5.52		(i)5.91		(i)6.05
H2′	1.84	2.60	2.62	2.29	2.03	(A)2.36
						(B)2.43
H2"	2.36	2.75	2.81	2.43	2.36	(A)2.60
						(B)2.83
H3′	4.56	4.97	5.04	-	-	4.68
H4′	4.04	4.31	4.46	-	-	-
H5′	3.79	4.07	4.22	-	-	-
H5"	-	3.97	-	-	-	-
H5/H2/CH_3	5.82	-	-	1.20	5.66	-

protons, respectively. These 2'axH-2'eqH protons further give NOE to a resonance at 5.30 ppm which is assigned to 1'H proton of daunosamine sugar (Fig. 6.5 (c-e)).

Thus, all protons of daunosamine sugar are assigned following the interconnected network of coupled protons. The resonance at 4.68 ppm gives NOE with protons at 1.84 and 2.36 ppm (Fig. 6.5(d)) which are coupled to each other and give intense cross peak as shown in Fig. 6.5(b). These are assigned to 7H, 8axH and 8eqH protons of ring A, respectively. Fig. 6.5(b) shows 10eqH-8eqH NOE connectivity which assigns the resonances at 2.44 and 2.83 ppm to 10axH and 10eqH protons of ring A.

The assignments of specific adriamycin protons are further confirmed from titration studies as adriamycin is gradually added to hexamer. Table 6.3 lists the chemical shifts of various protons of adriamycin in D_2O at 295 K on formation of complex with d-$(CGATCG)_2$.

TITRATION STUDIES

Expansions of one - dimensional proton NMR spectra of d-$(CGATCG)_2$ + adriamycin complex at various drug/DNA (D/N) ratios showing base H8, H6, H5, sugar H1' and drug resonances are presented in Fig. 6.1 (a-g).

On addition of 10 μl of adriamycin to DNA hexamer in the first step, i.e. at drug/DNA duplex concentration ratio of 0.22:1, new signals (here after referred to as (i)) are found to grow in the base as well as H1' region (spectra not shown here). These are

Table 6.3 : The chemical shift δ (in ppm) of adriamycin protons in d-$(CGATCG)_2$ - adriamycin complex at 295 K in D_2O and changes in chemical shift $\Delta\delta$ (in ppm) on complex formation in adriamycin protons with respect to its monomer position (δ at 355 K)*.

Proton	δ	$\Delta\delta$
1H	7.68	0.01
2H	7.76	0.07
3H	7.43	0.10
$4OCH_3$	3.91	0.15
8axH	1.84°	0.37
8eqH	2.36	0.09
7H	4.68	0.23
10axH	2.44	0.47
10eqH	2.83	0.30
1'H	5.30	0.28
2'axH	1.83°	0.31
2'eqH	1.91	0.24
3'H	4.07	-0.22
4'H	4.18	-0.19
5'H	4.25	0.11
$5'CH_3$	1.39	0.06

-ve : refers to downfield shift of protons.

+ve : refers to upfield shift of protons.

o : Overlapping of peaks.

* Monomer position (δ at 355 K, refer to Table 4.2).

assigned to specific protons, A3H8(i), G2H8(i), T4H6(i), G6H1'(i) on the basis of 2D phase-sensitive NOESY spectrum. A new signal at 7.48 ppm due to 3H proton of adriamycin appears in this complex. In aromatic protons region, the resonances are sharp. However, in H1' region the splitting patterns of all H1' protons disappear and the resonances are broadened.

In the complex containing drug to DNA concentration ratio 0.45:1 (Fig. 6.1 (b)), the effect of line broadening in several resonances is more pronounced. The base protons become less intense and the signals A3H8(i), G2H8(i), T4H6(i) further increase in intensity. Adriamycin ring D 1H proton at 7.63 ppm is also evident in this complex along with 3H proton. In H1' region, the G6H1'(i) resonance further increases in intensity and all other H1' resonances along with C1H5 and C5H5, broaden considerably. However, A3H1' and G6H1' are relatively sharp than other H1' signals.

At 0.67 :1 drug to DNA concentration ratio, the base protons of all residues become less intense and adriamycin 1H and 3H protons further increase in intensity (spectra not shown here). T4H6 base proton is relatively the most affected resonance in this complex. The multiplet structure of all H1' protons including that of A3 and G6 residues disappear. A new signal corresponding to adriamycin 1'H proton emerges at 5.36 ppm.

The signals A3H8(i), G2H8(i), T4H6(i) gradually increase in intensity with drug : DNA ratio while A3H8 and T4H6 resonances become less intense and broad. In the complex of drug/DNA ratio of 1.78:1 the intensity of A3H8, T4H6 and A3H8(i), G2H8(i), T4H6(i) are almost equal (Fig. 6.1(e)). All the base resonances are broadened further. Adriamycin 1H proton is clearly seen at 7.70 ppm while 2H proton appears to emerge at 7.78 ppm as a shoulder of A3H2 resonance (Fig. 6.1(e)). G2H8 and G6H8 signals are broadened and C1H6, C5H6 protons also become less intense.

In H1′ region, the G2H1′(i) resonance appears at D/N ratio of 0.89:1 (Fig. 6.1(c)) while T4H1′(i) resonance appears at D/N ratio of 1.55:1 (spectra not shown here). The adriamycin 1′H resonance which appears at D/N ratio of 0.67:1, gradually becomes intense and resonates at 5.30 ppm (Fig. 6.1(e)). The H1′ resonances of all residues are relatively more broadened than the base H8/H6 protons. However, among all H1′ protons, C5H1′ and C1H1′ are broadened beyond recognition at D/N ratio of 1.78:1 (Fig. 6.1(e)).

Fig. 6.1 (f,g) shows 1D spectra of 2:1 drug to DNA complex. In this complex the intensity of A3H8, A3H8(i), G2H8(i) and T4H6, T4H6(i) are equal. The signals of G2H8, G6H8, C1H6 and C5H6 are broadened and are less intense. The ring D protons 1H, 2H, 3H and daunosamine 1′H proton of adriamycin are evident in this complex. Among base protons, C1H5, C1H6 and G2H8 protons are upfield shifted by 0.11, 0.09 and 0.07 ppm, respectively. The C5H6, C5H5 and G6H8 protons also exhibit upfield shifts of $\simeq$ 0.06 ppm (Table

6.4). The changes in C1H6, C1H5, G2H8, C5H6, C5H5 and G6H8 resonances are attributed to the destacking of the adjacent base pairs in order to permit opening of the DNA helix followed by stacking with adriamycin chromophore between 5'-CpG-3' step of d-$(CGATCG)_2$.

Deoxyribose sugar H1' protons of d-$(CGATCG)_2$ are shifted upfield by 0.05-0.15 ppm (Table 6.4). Such changes in chemical shifts of DNA protons due to interaction of daunomycin (an analogue of adriamycin) are also reported in literature (82,88,89,92).

2D phase-sensitive NOESY spectra recorded on this 2:1 (D/N) complex are shown in Fig. 6.5 (a-i) in which all protons have been assigned, as discussed earlier. It is noted that several new resonances are found to grow on gradual addition of drug such as, 1H, 2H, 3H, 1'H, G2H1'(i), T4H1'(i), A3H8(i) etc. These are assigned independently on the basis of NOE connectivities observed, as discussed earlier.

At 2:1 drug/DNA ratio, all signals are found to be broadened. This could be due to presence of protons corresponding to multiple complexes. There may be slow exchange between them on NMR time scale which results in broadening of signals. The DQF-COSY spectra recorded on this complex is not helpful due to broad signals observed in this complex. Therefore, 2D phase-sensitive NOESY spectra have been used to characterize the complexes present and are discussed later. The resonances of DNA and drug protons

Table 6.4 : Changes in chemical shift ($\Delta\delta$) in ppm, of various protons of d-$(CGATCG)_2$ on complex formation.

Proton	C1	G2	A3	T4	C5	G6
H8/H6	0.09	0.07	0.06	-0.09	0.06	0.05
H1′	0.10	0.07	0.08	0.05	0.15	0.08
H2′	0.10	0.19	0.13	-0.21	0.01	(A) 0.31
						(B) 0.24
H2"	0.08	0.14	0.20	0.06	0.07	(A)-0.18
						(B)-0.41
H3′	0.18	0.08	0.04	-	-	0.05
H4′	0.07	0.07	0.08	-	-	-
H5′	-0.04	0.06	0.07	-	-	-
H5"	-	0.06	-	-	-	-
H5/H2/CH_3	0.11	-	-	0.24	0.05	-

-ve : sign refers to downfield shift of protons.

+ve : sign refers to upfield shift of protons.

corresponding to these complexes and assigned on the basis of NOESY spectra are followed at various D/N ratios. The chemical shifts of various protons are plotted as a function of D/N ratios and are shown in Fig. 6.2 (a-b).

Considering protons of adriamycin, it is found that ring D protons 2H and 3H are shifted upfield by 0.07 and 0.10 ppm, respectively while 1H does not exhibit any change on complexation. The daunosamine sugar 1'H proton shows upfield shift of 0.28 ppm with respect to its chemical shift position at 355 K (i.e. the chemical shift of monomer adriamycin, Table 4.2 of chapter IV). Similar changes in chemical shift of ring D protons 1H, 2H and 3H on complex formation have been reported in literature (82,88,89,92). The $4OCH_3$ protons of ring D of adriamycin also exhibit upfield shift of 0.15 ppm.

Among ring A protons, 8axH and 10axH show significant upfield shifts of 0.37 and 0.47 ppm, respectively. Since these protons are in axial position, they experience large upfield shift in comparison to 8eqH and 10eqH protons. 7H exhibits upfield shift of 0.23 ppm due to change in conformation of adriamycin on complex formation.

The changes in chemical shift of daunosamine sugar protons 2'axH, 2'eqH, 4'H, 3'H, 5'H and $5'CH_3$ are in the range of 0.06 - 0.31 ppm which could be due to conformational adjustment of sugar on binding of adriamycin with d-$(CGATCG)_2$. Table 6.3 lists the

observed changes in chemical shift of adriamycin on complex formation.

CHANGES WITH TEMPERATURE

The 1D NMR spectra of 2:1 drug/DNA complex obtained as a result of last titration is monitored as a function of temperature. The chemical shift of drug and DNA protons are plotted as a function of temperature and are shown in Fig. 6.4(a-b). It is observed that 3H proton of adriamycin in 2:1 complex resonating at 7.43 ppm at 295 K shifts upfield with increase in temperature to 7.38 ppm at 325 K. The chemical shift of this proton in self associated and monomer adriamycin (i.e. chemical shift of adriamycin at 297 and 355 K, refer to Table 4.2 of chapter IV) are 7.34 and 7.53 ppm, respectively.

It has been shown by Patel et al. (88) that an increase in temperature results in downfield shift of 1H, 2H, 3H, and $4OCH_3$ protons due to dissociation of complex. However our results are contrary to that obtained by Patel et al. (88) since, 3H is found to shift upfield with increase in temperature. Further it may be noted that chemical shift of 3H in complex at 295 K is shifted upfield by 0.10 ppm with respect to the corresponding proton of monomer adriamycin and is shifted downfield by 0.09 ppm with respect to that for self associated adriamycin. The above results suggest that increase in temperature in the range 295 - 325 K does not result in dissociation of complex.

An upfield shift of about ≃ 0.03-0.05 ppm is observed for 1H and 2H protons of adriamycin with increase in temperature, while 1'H of daunosamine sugar shifts downfield by ≃ 0.06 ppm. The resonating position of 1H, 2H, 3H and 1'H of adriamycin in 2:1 complex at 325 K therefore refers to that of complex (and not of drug alone) which may have structure different from that at 295 K resulting in altered chemical shift positions.

The base proton G2H8 exhibits an upfield shift with temperature. However, the resonating position of G2H8 at 325 K is different from the corresponding position of unbound DNA at 295 K (i.e. duplex DNA) as well as unbound DNA at 325 K (i.e. single stranded DNA). Further no significant change in the chemical shift of C1H6, A3H8, G6H8 and A3H2 protons are observed with increase in temperature. The C1H5, T4H6, C5H6 and C5H5 base protons shift downfield with temperature. Thus DNA as well as drug are in complexed state at 295 and 325 K.

INTERACTIONS OF DRUG WITH DNA

The conformational features of the drug-DNA complex are investigated primarily on the basis of 2D NOESY spectra. Since the signals in 1D NMR are quite broadened and DQF-COSY could not be used, it was not possible to carry out rigorous analysis of the conformation of deoxyribose sugar of the complexed DNA on the basis of spin-spin coupling constants. The ΣH1' and spin-spin coupling constants could only be ascertained for G6 residue at 325 K. We observe several NOEs corresponding to intra sugar and base

to sugar proton connectivities which are listed in Tables 6.5 and 6.6, respectively. Some of the NOEs have been used to analyse the C3′-endo ⇆ C2′-endo equilibrium in sugar pucker as well as the glycosidic bond rotation (Table 6.6). The intramolecular NOEs of adriamycin show changes in conformation of drug (Table 6.7). Several intermolecular NOEs are also observed which are used to analyse the interaction of drug with DNA to arrive at a specific geometry of the complex.

The research group of Alexander Rich and Olga Kennard have extensively studied the structure of complexes of daunomycin and adriamycin with d-CGATCG, d-CGTACG, d-TGATCA and d-TGTACA (32,71,81,98,128) by X-ray crystallography technique. We have used the structure obtained by them as a reference to start with, in order to understand the conformation of drug-DNA complex. Fig. 6.6 shows the schematic drawing of the intercalation geometry of adriamycin chromophore within base pairs of DNA hexamer. Two adriamycin molecules intercalate their aglycone chromophores between the 5′-3′ (pyr-pur) i.e. CpG sites at both ends of the hexamer duplex. The DNA unwinds to accommodate the drug chromophore resulting in change in the orientations of adjacent base pairs. The ring D hangs out in the solvent region while the daunosamine sugar occupies the space in minor groove with its hydrophilic (hydroxyl and amino) functional groups pointing away from the DNA molecule and projects into the solvent region. We have analysed the observed results regarding structural details of

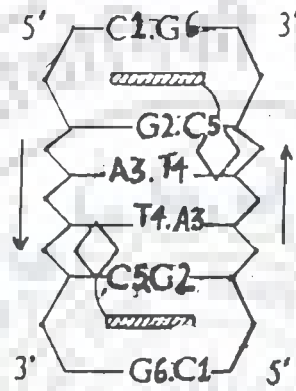

Fig. 6.6 : Schematic drawing of the adriamycin-d-$(CGATCG)_2$ complex. The aglycone chromophores of the adriamycin are shown as hatched bars, which are intercalated between the CpG sequences. The nucleotides are numbered C1 to G6 along each 5'-3' strand.

drug-DNA complex in the following way :

(i) Change in conformation of d-$(CGATCG)_2$ in order to allow intercalation due to alterations in backbone torsional angles, sugar pucker, etc. which will be reflected as change in C3′-endo ⇆ C2′-endo equilibrium, pseudorotation (P) of major conformer and glycosidic bond rotation (χ) :

The deoxyribose sugar protons are broadened at 295 K and hence could not be used to estimate J(H1′-H2′), J(H1′-H2") or, sums of couplings. At 325 K, only G6H1′ resonance is sharp and its splitting patterns are clear. A3H1′ and T4H1′ resonances are considerably sharp but, their splitting patterns are not resolved. The ΣH1′ calculated for G6 residue is 13.5 Hz and J(H1′-H2′), J(H1′-H2") are 6.8 and 6.7 Hz, respectively. G2H1′ is unusually broadened beyond recognition even at 325 K (Fig. 6.3 (c)) which may be due to the implication of this residue in binding, as discussed later.

The mole fraction of major S conformer is calculated for G6 residue as 0.65, using the analysis of Wijk et al.(131). It has been observed that the mole fraction of major S conformer decreases (~ 0.05) with temperature in unbound d-$(CGATCG)_2$. The G6 residue therefore may have χ_S somewhat higher than 0.65 at 295 K; however an average value of ~ 0.65 ± 0.05 is considered reasonable. The χ_S for G6 residue in unbound state is 0.75, thus the percentage of N conformer has increased on complex formation. The observed values of J(H1′-H2′) and J(H1′-H2") couplings in G6

residue show that the pseudorotation of the S conformer is either $\simeq 108^{\circ}$ or, $\simeq 180^{\circ}$. A mixture of two S conformer with $P \simeq 108^{\circ}$ and $P \simeq 180^{\circ}$ may be present but it is not possible to confirm the same and obtain mole fraction of each of the S conformer from the limited data available.

Table 6.5 shows the relative intensities of cross peaks for intra sugar protons observed in the NOESY spectra of the complex recorded at τ_m = 250 ms (Figs. 6.5 (a-i)). The intensities of H1'-H2' NOE cross peak is observed to decrease in the order : C1, G6 > G2, A3, T4 > C5. It is evident from Table 5.9 and Fig. 5.14 that the distance H1'-H2' increases from 2.52 A° to 2.85 A° as P is increased from 9° to 189°. The variation in distance H1'-H2' reflects the percentage of S conformer as it does not vary significantly with P_S in the range 108° - 207°. This implies that C1 and G6 residues have maximum fraction of N conformer while C5 residue has least fraction of N conformer. The relative intensities of H1'-H2' cross peak for G2, A3 and T4 residues show that the fraction of N conformer present in these residues is less than that for C1 and G6 residues (Table 6.5).

The H1'-H2" distance is not expected to differentiate between different pseudorotation values as they vary over a narrow range (Table 5.9, Fig. 5.14). Table 5.9 shows that H2'-H3' distance is lowest, being $\simeq$ 2.18 - 2.20 A° in the P_S range 90° - 117° and it is $\simeq$ 2.29 - 2.30 A° for $P_N = 18^{\circ}$ as well as for $P_S = 144^{\circ}$ - 225°. Thus, this distance does not establish the C3'-endo $\leftrightarrows$ C2'-endo

Table 6.5 : Observed relative intensities of various intrasugar NOE connectivities of d-$(CGATCG)_2$ on complex formation in phase-sensitive NOESY spectra (τ_m = 250 ms).

Connectivities	C1	G2	A3	T4	C5	G6
H1'-H2'	ss	s	s	s	w	(A) ss
						(B) ss
H1'-H2"	ss(O)	s	ss	s	ss(O)	(A) ss
						(B) ss
H2'-H3'	s	ss	ss	-	-	(A) s
						(B) ws
H2"-H3'	ws	ss	ss	-	-	(A) s
						(B) ws
H3'-H4'	ws	ss	ss	-	-	O
H1'-H4'	-	-	ws	-	-	-
H1'-H3'	-	-	ws	-	-	s

ss : very intense. s : intense. ws : fairly intense.

w : weakly intense. O : overlap. (-) : absence of peak.

equilibrium. However, the presence of P_S in the range 90° - 117° will significantly decrease this distance. The H2'-H3' NOE connectivity is found to be most intense for G2 and A3 residues as compared to C1 and G6 residues. We may therefore infer that P_S for G2 and A3 residues is low, $\simeq 90^\circ$ - 117°.

The H2"-H3' and H3'-H4' standard distances are largest for $P_N = 9^\circ/18^\circ$ and decrease with increase in P_S value implying that these distances depend on both P_S as well as χ_S. Thus, these distances cannot be used to estimate P_S and χ_S of deoxyribose sugars.

It is the H1'-H4' distance which can be used as a marker since it varies with P_S over a large range, 2.20 - 3.65 A°. But, the H1'-H4' distance does not distinguish between C3'-endo $\leftrightarrows$ C2'-endo equilibrium since for both $P_N = 18^\circ$ and $P_S = 162^\circ$, the distance is $\simeq$ 3.0 A°. The H1'-H4' distance for all residues increases in the order A3 < C1, G2, T4, C5 and G6 (Table 6.5). This distance is least for $P_S = 90^\circ$ - 117° (Table 5.9, Fig. 5.14). Hence, the lowest distance of A3 residue indicates that A3 has lowest P_S value as compared to all other residues.

The variation in H1'-H3' distance is rather low and it cannot be used to obtain P values. Thus the relative intensities corresponding to intrasugar distances show that :

(i) C1 and G6 residues have maximum percentage of N conformer.

(ii) The P_S value of all residues increase in the order, A3 < G2 < C1, G6.

(iii) G2 and A3 residues have less percentage of N conformer as compared to C1 and G6 residues and their P_S is $\simeq 90^\circ$ - 117°.

(iv) C5 residue has least extent of mixing with N conformer.

In the X-ray crystal structure of adriamycin + d-(CGATCG) complex (32), it has been observed that P_S values in residues from 5′ to 3′ end are 158°, 141°, 129°, 124°, 151° and 161°. Similar results were obtained for the crystal structure of daunomycin-hexamer complexes (71,81,128). These are not really comparable with the present solution structure. In our case the P_S value refers to that of major S conformer with a C3′-endo $\leftrightarrows$ C2′-endo equilibrium existing while in X-ray structures either there is a single S conformer with the P_S value indicated or else it may be the average P_S value if C3′-endo $\leftrightarrows$ C2′-endo equilibrium were to exist.

The relative intensities of NOE cross peaks corresponding to base - H1′ connectivities (Fig. 6.5 (g), Table 6.6) are used to get a range of values of glycosidic bond rotation using the data of interproton distances available for standard A-DNA and B-DNA geometries (Table 5.11(a), Fig. 5.15(a)). We observe intense H6/H8 - H1′ cross peak in NOESY spectra recorded at τ_m = 250 ms, for C1 and G6 residues which becomes weak at τ_m = 75 ms. The

Table 6.6 : Relative intensities of intra-residue NOE cross peaks as observed in 2D phase-sensitive NOESY spectra (τ_m = 250 and 75 ms).

	B-H2′		B-H2"		B-H1′	
τ_m	250	75	250	75	250	75
C1	ss	ss	s	w	s	w
G2	ss	ws	ss	ws	-	-
A3	ws	ws	ws	-	-	-
T4	-	-	w	-	-	-
C5	ws	w	ws	ws	-	-
G6	ws	w	ss	s	s	w

B : base proton. (-) : absence of peak. ss : very intense.

s : intense. ws : fairly intense. w : weakly intense.

H6/H8 - H1′ cross peak is not observed for G2, A3, T4 and C5 residues (Table 6.6).

Among pyrimidines, the distance for C1 residue is lesser than that for T4 and C5 residues. This may be interpreted as due to presence of either a larger fraction of N conformer and/or a value of χ as -60° to -70° or -150° for C1 residue. The glycosidic bond angle for T4 and C5 residue may be in the range -90° to -120°. The base - H1′ distance in standard B-DNA are lower for pyrimidines than that for purines (Table 5.11(a)). The H8 - H1′ NOE connectivity observed for G6 residue indicates its χ to be $\simeq -60^{\circ}$ ($\pm 15^{\circ}$).

Since the distance of base - H2′ is low and varies over P - χ values in a narrow range (Fig. 5.15 (b,c), Table 5.11(b,c)), it cannot be used to deduce inference about χ. Table 6.6 shows that intense H6-H2′ cross peak is observed for C1 residue even at τ_m = 75 ms (Fig. 6.5(j)). Thus, this excludes $\chi = -150^{\circ}$ for C1 residue as this distance is $\simeq$ 3.7 A° in standard A-DNA (Table 5.11 (c)).

The relative intensities of base - H2" NOE connectivities for C1, C5, G2 and G6 residues indicate that their χ cannot be -150° as this distance is $\simeq$ 4.5 - 4.7 A° in standard A-DNA (Table 5.11(b,c)). Among pyrimidine residues the increasing order of distance of base - H2" is C5 < C1 < T4. In the NOESY spectra recorded at τ_m = 250 ms, C1 residue shows intense cross peak, whereas fairly intense and weak cross peaks are observed for C5 and T4 residues, respectively. However, at τ_m = 75 ms, fairly

intense cross peak is observed for C5 residue whereas weakly intense cross peak is observed for C1 residue and for T4 residue the base - H2" cross peak is not observed at τ_m = 75 ms. The fairly intense peak at τ_m = 75 ms (Fig. 6.5(j), Table 6.6) for C5 residue reflects the base - H2" distance to be in the range 2.4 - 2.8 A°. If $\chi = -105^\circ$ for major S conformer in C5 residue then base - H2" distance is expected to be in the range 3.4 - 3.7 A° (Fig. 5.15 (c), Table 5.11 (c)). Therefore the χ value is likely to be higher and lie in the range - $60^\circ \pm 15^\circ$ for C5 residue. For C1 residue the base - H2" NOE connectivity at τ_m = 75 ms corresponds to a distance $\simeq$ 3.0 A° which indicates the glycosidic bond rotation for C1 residue to be $\simeq -90^\circ$ ($\pm 15^\circ$). The NOE connectivity of base - H2" is not observed for T4 residue at τ_m = 75 ms which indicates its χ to be lower i.e. $\simeq -105^\circ$.

Among purines the base - H2" distance increases in the order G6 < G2 < A3. An intense and fairly intense NOE cross peaks are observed for G6 and G2 residues, respectively in the NOESY spectra recorded at τ_m = 75 ms (Fig. 6.5 (j), Table 6.6). However, the base - H2" NOE cross peak is not observed for A3 residue at τ_m = 75 ms. For χ value of -105°, P_S in the range 90° - 198° and χ_S = 0.65 - 0.80, the calculated distances of base - H2" would be $\simeq$ 3.9 A° (Table 5.11(b)). Since relatively intense cross peaks are seen for G6 and G2 residues, this indicates their χ to be $\simeq -60^\circ$ and $\simeq -90^\circ$, respectively (to an accuracy of $\pm 15^\circ$). Since the NOE connectivity of base - H2" is not observed for A3 residue at τ_m = 75 ms, the glycosidic bond rotation (χ) is $\simeq -105^\circ$ ($\pm 15^\circ$). Thus,

we conclude that χ for C1, G2, A3, T4, C5 and G6 residues are -90°, -90°, -105°, -105°, -60° and -60° (to an accuracy of $\pm 15^{\circ}$), respectively.

We observe that glycosidic bond rotation (χ) changes from anti for C1, C5 and high anti for G2, A3, T4 and G6 residues (in unbound form) to high anti for C1 and C5 residues; anti for A3 and T4 residues on complex formation. In crystal structure of adriamycin - d-$(CGATCG)_2$ complex it has been observed that the χ values for residues from 5'-3' end are -148°, -91°, -130°, -113°, -88° and -88° (32). Similar trend of glycosidic bond angle (χ) was observed for residues from 5'-3' end in daunomycin + d-$(CGATCG)_2$ (71) and daunomycin + d-$(CGTACG)_2$ complexes (128). Thus, our results are consistent with those reported in literature (32).

(ii) Changes in conformation of adriamycin due to binding which would be reflected in interproton distances and changes in chemical shifts :

We observe changes in chemical shifts of various protons of adriamycin (Table 6.3) as well as in relative intensities of various NOE connectivities within adriamycin molecule on complexation (Fig. 6.5(a-i), Table 6.7). The observed upfield shifts for ring A, ring D and 1'H protons are in the range 0.07-0.47 ppm (Table 6.3). These are best understood in terms of stacking with base pairs and are discussed later. The changes in chemical shift ($\Delta\delta$) of daunosamine sugar protons, in the range

-0.19 to +0.31 ppm (-ve refers to downfield shift while + ve sign refers to upfield shifts), could be due to alterations in sugar conformation as well as its proximity to DNA. Some of the interproton distances, the range of which is inferred from relative intensities of cross peaks in NOESY spectra in bound adriamycin are found to be different from the corresponding distances in unbound adriamycin. Within the sugar moiety, the interproton distance, 1'H-3'H is different from the corresponding value obtained in unbound drug. The 1'H-3'H distance in unbound adriamycin is 3.3 A°, while the intensity of 1'H-3'H in bound adriamycin reflects a distance of about $\simeq$ 2.8 - 3.0 A°. An additional weakly intense cross peak is observed between 5'H-2'eqH protons of daunosamine sugar on complex formation.

Within ring A, the NOE cross peaks 10axH-8axH, 10axH-8eqH and 10eqH-8axH are not observed (Fig. 6.5(b), Table 6.7) which implies that the corresponding interproton distances are more than 4.0 A° while these distances in unbound state are observed as 2.82, 2.78 and 3.01 A°, respectively. Intense cross peaks are observed for 7H-8axH and 7H-8eqH spin-spin coupled protons, which correspond to a distance of 2.4-2.8 A° whereas in unbound adriamycin the corresponding distances were 3.3 and > 4.0 A°, respectively. Among the NOE connectivities of ring A protons with daunosamine sugar protons, the interproton distance of 7H with daunosamine 1'H, 3'H, 4'H, 5'H and 5'CH_3 protons are altered on binding (Table 6.7). The 7H-5'CH_3, 8axH-5'CH_3 and 8eqH-5'CH_3 cross peaks are not observed on complexation which reflects this distance to be more

Table 6.7 : Observed relative intensities of intra molecular NOE cross peaks of adriamycin in phase - sensitive NOESY spectra (τ_m = 250 ms).

Connectivities		Connectivities	
1H'-2'axH	s(o)	3'H-5'H	o
1H'-2'eqH	ws	3'H-5'CH_3	-
2'axH-2'eqH	o	4'H-2'axH	ws(o)
3'H-2'axH	s(o)	4'H-2'eqH	ws
3'H-2'eqH	ws	10axH-8axH	-
3'H-4'H	o	10axH-8eqH	-
4'H-5'H	o	10eqH-8axH	-
5'H-5'CH_3	ss	7H-1'H	ss
4'H-5'CH_3	s	7H-3'H	ss
1H-2H	s	7H-4'H	ss
2H-3H	ss	7H-5'H	ss
1H-4OCH_3	s	7H-5'CH_3	-
2H-4OCH_3	s	7H-2'eqH	ws
3H-4OCH_3	ss	8axH-1'H	s(o)
7H-8axH	ss	8axH-3'H	s(o)
7H-8eqH	s(o)	8axH-4'H	ws(o)
8axH-8eqH	ss(o)	8axH-5'H	ws
10axH-10eqH	s(o)	8axH-5'CH_3	-
10eqH-8eqH	s	8eqH-1'H	-

1'H-3'H	s	8eqH-3'H	ss
1'H-4'H	ws	8eqH-4'H	ws
1'H-5'H	ws	8eqH-5'H	ws
1'H-5'CH_3	-	8eqH-5'CH_3	-
5'H-2'eqH	w		

o : overlap. ss : very intense. s : intense. ws : fairly intense

w : weakly intense. (-) : absence of peak

than 4.0 A° as compared to distance ≃ 2.6 - 3.9 A° in unbound adriamycin. Intense cross peaks are observed for 7H-1'H, 7H-3'H and 7H-5'H connectivities which correspond to a distance of the order of 2.4 - 2.6 A°, which is lesser than the corresponding distance ≃ 3.0 - 3.3 A° in unbound adriamycin (Table 4.4 of chapter IV). NOE connectivity is also observed between 7H and 2'eqH proton of daunosamine sugar. Fairly intense cross peaks are observed for 8axH-5'H and 8eqH-5'H connectivity corresponding to a distance of ≃ 3.0 A° which is larger than the distances 2.50 and 2.40 A° observed in unbound adriamycin, respectively. The 8eqH - 1'H NOE cross peak is not observed on complexation which reflects this distance to be more than 4.0 A° as compared to a distance of 3.16 A° in unbound adriamycin.

The above results show that within ring A, 8axH and 8eqH protons are close to 7H proton while their relative orientation with respect to 10axH and 10eqH protons have altered on binding. The ring A proton 7H is close to daunosamine 1'H, 2'eqH, 3'H, 4'H and 5'H protons while it is away from 5'CH_3 protons. Further 5'CH_3 and 5'H protons of daunosamine sugar are also found to be away from ring A 8axH and 8eqH protons on binding, resulting in change in conformation of adriamycin. Within daunosamine sugar 5'H proton is also close to 2'eqH proton.

In crystal structures of adriamycin and daunomycin with DNA hexamers (32,71,81,128) it has been shown that conformation of ring A changes on binding. Particularly the change in relative

positions of C8 and C9 atoms were observed. We observe a significant change in 8axH-10axH, 10axH-8eqH and 10eqH-8axH distances which are increased from the value of ≃ 2.8 - 3.0 A° in unbound state to > 4.0 A° on interaction with DNA. The relative orientation of daunosamine sugar with respect to ring A also changes considerably on complexation.

(iii) Structure of drug-DNA complex reflecting the interaction between drug and DNA molecule :

(a) Stacking interactions between base protons and drug chromophore due to intercalation of aglycone chromophore in the 5'-CpG-3' step (C1pG2) i.e. between base pairs C1.G6 and G2.C5 :

Several workers have earlier reported stacking of drug chromophore between base pairs on the basis of upfield shifts (0.16-0.45 ppm) in 1H, 2H, 3H and $4OCH_3$ protons on interaction of drug with DNA (5,82,86,88,89,92). In the present investigation the changes in chemical shifts ($\Delta\delta$) of ring D protons, 1H, 2H, 3H and $4OCH_3$ are 0.01, 0.07, 0.10 and 0.15 ppm, respectively (Table 6.3). Besides these we observe intermolecular NOEs between non-exchangeable base protons of C1 and C5 residues with ring D protons (Table 6.8). The C1H5 proton gives a weakly intense NOE with 1H proton while intense cross peak is observed between C5H6 and $4OCH_3$ protons of ring D (Table 6.8, Fig. 6.5 (g)). These NOEs are a direct proof of intercalation of drug chromophore and suggests specific positioning of ring D protons with respect to C1.G6 and G2.C5 base pairs.

Table 6.8 : Inter molecular NOE connectivities observed on complexation of d-$(CGATCG)_2$ with adriamycin using phase-sensitive NOESY spectra (τ_m = 250 ms).

1.	C1H5 - 1H	w	19.	C5H5 - 1H	s(o)
2.	C5H6 - 4OCH_3	s	20.	C5H6 - 1H	ss
3.	G2H1'(i) - 8eqH	s	21.	C5H2' - 1H	w
4.	G2H1'(i) - 8axH	ws(o)	22.	C5H2" - 1H	s
5.	*A3H1' - 5'CH_3	w	23.	C1H3' - 7H	ss
6.	A3H1' - 5'H	s	24.	C1H5' - 4'H	ws
7.	#A3H1' - 4'H	s	25.	C1H1' - 3'H	s
8.	A3H2' - 5'H	ws	26.	G2H1'(i)-4'H	ws
9.	#A3H2' - 4'H	ws	27.	G2H1'(i)-2'eqH	ws
10.	A3H2' - 3'H	s	28.	G2H2" - 3'H	s
11.	T4CH_3 - 5'CH_3	ws	29.	G6H8 - 3'H	w
12.	*T4H1' - 4'H	s	30.	G6H2"(A)-10axH	s
13.	*T4H1' - 3'H	s	31.	G6H1' - 5'H	s
14.	T4H2' - 1'H	w	32.	G6H1' - 4'H	s
15.	T4H2" - 5'H	w	33.	G6H1' - 3'H	s
16.	T4H2" - 4'H	ws	34.	G6H1' - 1'H	w
17.	T4H2" - 3'H	ws	35.	G6H1'(i) - 4'H	ws
18.	#C5H2' - 1'H	w			

#These NOE connectivities are comparable to daunomycin + d-$(CGTACG)_2$ complex (128).

*NOE connectivities also observed in daunomycin + d-$(TGATCA)_2$ complex in solution.

ss : very intense s : intense ws : fairly intense

w : weakly intense o : overlap.

In order to have an idea of geometry of intercalation of adriamycin, we consider intercalation of adriamycin between first two base pairs with aglycone chromophore oriented perpendicular to the base pairs in a geometry of d-$(CGATCG)_2$ + adriamycin complex obtained by X-ray crystallography (32). It is evident that C1H6/C1H5 base protons are close to 1H and C5H6/C5H5 protons are close to $4OCH_3$ protons of ring D (Fig. 6.7(a)) (32). This geometry is likely to result in NOEs observed by us. Ring B and C overlap to a greater extent with base pairs, however there are no non-exchangeable protons to monitor this. It is observed that ring A protons are close to G2 residue. The G2H1'(i) proton gives NOE connectivity with 8eqH and 8axH protons of ring A showing their proximity (Fig. 6.5 (c)).

This geometry would lead to upfield shifts in ring D and ring A protons due to anisotropic ring current effects from the adjacent base pairs. We have tried to assess the effect of ring currents due to C1.G6 and G2.C5 base pairs using the standard upfield shifts ($\Delta\delta$) due to anisotropic ring currents of C.G and G.C base pairs available in literature (35(a)), on ring A and D protons in the geometry of d-$(CGATCG)_2$ + adriamycin complex obtained by Frederick et al. (32) (Fig. 6.7(a)). The changes in chemical shifts ($\Delta\delta$) obtained for 1H, 2H, 3H and $4OCH_3$ protons are lesser than 0.05 ppm. However, the experimentally observed values for changes in chemical shifts for the corresponding protons are in the range 0.07-0.15 ppm (Table 6.3). This suggests that ring D protrudes less towards solvent and shows more overlap with C1.G6

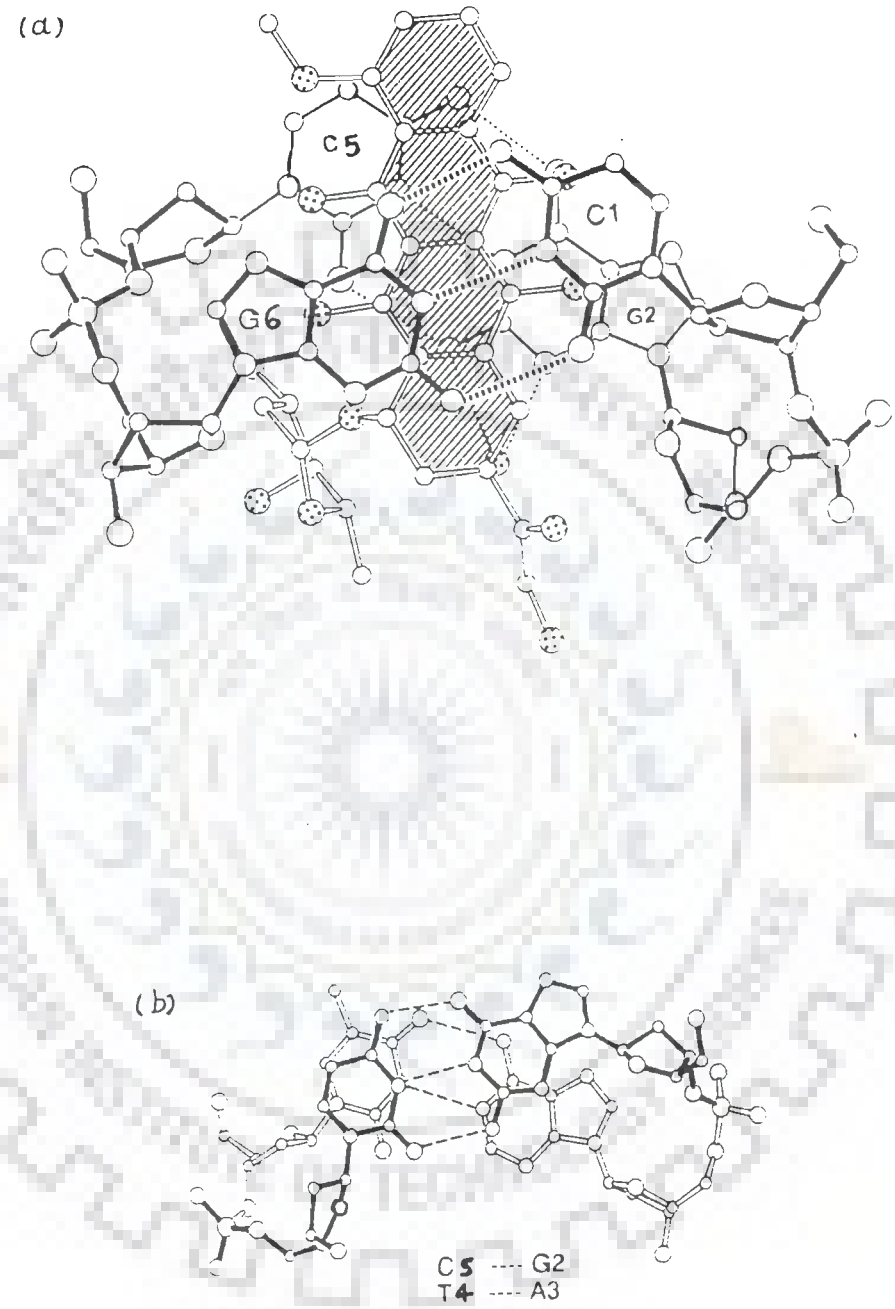

Fig. 6.7:(a) Intercalation of adriamycin chromophore between 5'-3' d-CpG base pair. (b) Overlap geometry of G2.C5 and A3.T4 base pairs in adriamycin + d-$(CGATCG)_2$ complex (32).

and G2.C5 base pairs. The ring A will then move further away from base pairs and will result in lesser overlap of ring A protons with adjacent base pairs resulting in lower upfield shifts on complexation. Since we observe large upfield shifts for both ring D (~ 0.07 - 0.15 ppm) as well as ring A protons (~ 0.09 - 0.47 ppm), it is possible that in present case the aglycone chromophore is somewhat tilted and is not perpendicular to the base pairs.

The changes in chemical shifts of base protons of C1.G6 and G2.C5 base pairs due to binding are a result of destacking of adjacent base pairs as they move apart to a distance of 6.8 A° followed by stacking of aglycone chromophore with each base pair. Destacking of base pairs are expected to induce downfield shifts while stacking of drug chromophore is expected to induce upfield shifts in base protons. The net effect will be an upfield or downfield shift of base protons. We observe $\Delta\delta$ = 0.05 to 0.11 ppm in base protons of C1, G2, C5 and G6 residues (Table 6.4).

(b) Stacking interaction in G2pA3 step, that is, between G2.C5 and A3.T4 base pairs due to alterations in base to base overlap on binding of drug to DNA :

Due to interaction of drug with DNA, the base pairs of DNA have to move apart in order to accommodate the drug molecule. It has been shown in literature that on complexation of adriamycin with d-$(CGATCG)_2$ (32), the helix axis of the DNA is not in the same position in two base pairs as is expected for a perfect B-DNA conformation, and the G2.C5 base pair is translated towards the

major groove relative to A3.T4 base pair by about 1.3 A°. This results in reduced overlap between G2.C5 and A3.T4 base pairs (Fig. 6.7 (b)) (32). Such changes in overlap geometry get reflected as changes in chemical shifts of corresponding protons. We do observe changes in chemical shifts of third base pair protons on complexation, $\simeq$ 0.24 ppm in $T4CH_3$, - 0.09 ppm in T4H6 and 0.08 ppm in A3H1' protons (Table 6.4).

(c) Stacking interaction in A3pT4 step, that is, between A3.T4 and T4.A3 base pairs due to alterations, if any, in base to base overlap on binding of drug to DNA :

It has been shown in literature that A3.T4 and T4.A3 base pairs show typical stacking of pyrimidine-purine sequences like B-DNA, in complexes of adriamycin + $d-(CGATCG)_2$ (32), daunomycin + $d-(CGATCG)_2$ (71) and daunomycin + $d-(TGATCA)_2$ (81). Assuming the stacking of A3.T4 and T4.A3 base pairs to be similar in solution, we do not expect any change in chemical shift of corresponding protons. Therefore the observed upfield shifts in T4H6, A3H1' and $T4CH_3$ protons on binding, may be attributed to relative change in overlap geometry of G2.C5 with respect to A3.T4 base pair on complexation.

(d) Proximity of daunosamine sugar to DNA protons :

Several intermolecular NOEs are observed between protons of adriamycin and $d-(CGATCG)_2$ on complexation. Table 6.8 gives a list of intermolecular contacts observed. The first two contacts (serial no. 1, 2 of Table 6.8) correspond to NOE connectivity

between base proton and ring D protons (discussed earlier) indicating stacking of drug chromophore with the base pairs. The NOE contacts (serial no. 3-18 of Table 6.8) suggest the proximity of the daunosamine sugar with A3, T4 and C5 residues. Wang et al. (128) have studied the complex of daunomycin + d-$(CGTACG)_2$ and have reported some of the van der Waals contacts as well as NOEs expected in solution phase for the geometry of the complex. The NOE connectivity A3H1'-4'H and A3H2'-4'H (serial no. 7, 9, Table 6.8) are comparable to van der waal contact T3O2-4'H having a distance of 2.61 A° in X-ray crystal structure of daunomycin + d-$(CGTACG)_2$ complex (128). Since in the present investigation adenine is present in place of thymine, it is likely that positioning of H8, H1' protons etc. of A3 residue are close to 4'H and 5'CH_3 daunosamine sugar protons. Weakly intense cross peak is observed for C5H2'-1'H proton (Fig. 6.5(c)) of daunosamine sugar which is comparable to C5H1'-2'eqH van der Waal contact observed in crystal structure (128). We observe several additional NOEs between deoxyribose sugar protons H1', H2', H2" of A3 and T4 residues and daunosamine sugar protons 1'H, 3'H, 4'H, 5'H and 5'CH_3 (Fig. 6.5 (c,d,f,h), Table 6.8). These NOEs are not listed for the X-ray crystal structure of adriamycin + d-$(CGATCG)_2$ (32) or, in daunomycin + d-$(CGTACG)_2$ complex (128) although they are feasible in the crystallographic structures with slight alterations in the geometry of adriamycin. In a separate study carried out by us on complex of daunomycin with d-$(TGATCA)_2$ (unpublished) in solution phase, the NOE connectivities, A3H1' -

5'CH_3, T4H1'-4'H, T4H1'-3'H were also observed indicating the proximity of daunosamine sugar with A3.T4 base pair.

In the X-ray structures, it has also been seen that C2', C3' and C4' atoms of daunosamine sugar are at a distance of 2.30 - 2.47 A° from adjacent C5 residue and A3.T4 base pair resulting in a more tight fit in daunomycin + d-$(CGATCG)_2$ complex (71) as compared to daunomycin + d-$(CGTACG)_2$ (128) complex. These contacts are comparable to the NOEs observed with C5 and A3.T4 base pairs listed in Table 6.8.

Hence we find that the amino sugar of adriamycin molecule is positioned in a similar way to that in X-ray crystal structures i.e. in minor groove of hexamer duplex (32,71,81,98,128). In order to allow van der Waals contacts due to daunosamine sugar placed in the minor groove, its conformation is likely to change. This change in conformation of daunosamine sugar is reflected as a significant change in 7H-5'CH_3, 8axH-5'CH_3 and 8eqH-5'CH_3 distances which increase from a distance of $\simeq$ 2.6-3.9 A° (in unbound adriamycin, Table 4.4) to about $>$ 4.0 A° in bound state (Table 6.7). The resonance G2H1' is broadened to a greater extent (Fig. 6.3 (c)) than the corresponding H1' resonances of other residues at 325 K which perhaps implies immobilization of G2 residue in the complex.

Besides these NOE connectivities which show proximity of daunosamine sugar to A3.T4 base pair, several other NOE contacts are also observed (serial no. 19-35, Table 6.8). The C5H5 and

C5H6 base protons exhibit NOE connectivity with 1H proton of ring D. Further 1H proton also gives NOE connectivity with H2′, H2" protons of C5 residue (Fig. 6.5 (c,g,i)). The daunosamine sugar 1′H, 2′eqH, 3′H, 4′H and 5′H protons give NOE connectivities with C1, G2 and G6 residues. These NOE connectivities are not feasible in the geometry of adriamycin + d-$(CGATCG)_2$ complex (32) (Fig. 6.7(a)). This indicates that another complex may be existing in solution phase. We observe several additional signals e.g. G2H1′(i), A3H8(i), G2H8(i) etc. (Fig. 6.5(c)) which may pertain to the other complex. In the absence of a reference structure (as is available by X-ray crystallography for A3H8, G2H8, G2H1′ etc.) it is difficult to work out further details of this complex. A 2D phase-sensitive NOESY spectra recorded at high temperature is likely to resolve the signals and provide further guidelines to characterize these complexes independently. Additional experiments in water solvent may help in specifying the hydrogen bonds stabilising the complex. Hence there is further scope to spell out the geometrical differences in these complexes.

The significance of the present study on adriamycin + d-$(CGATCG)_2$ complex is that it augments the observation that a right-handed segment of DNA can have significant variations both in backbone geometry and sugar puckering associated with the accommodation of a large intercalator molecule with an amino sugar. However, we observe greater flexibility in backbone geometry and sugar puckering than that observed in X-ray crystal structures obtained by the research group of Alexander Rich and

Olga Kennard (32,71,81,128). The previously studied X-ray crystal structures of dinucleoside monophosphate complex with simple intercalators raise a question about end effects of such short nucleic acid fragments. Simple C3'-endo-(3'-5')-C2'-endo mixed sugar pucker pattern around intercalator site were reported (111,126).

However, the present investigations show that in solution phase even in uncomplexed DNA fragments the deoxyribose sugars are a mixture of both north and south conformers. It has been further observed that percentage of north conformer (χ_N) has increased on complexation for C1 and G6 residues.

We have carried out an independent study on the complex of d-$(TGATCA)_2$ with a similar drug, daunomycin (unpublished) and observed variation in terms of backbone geometry, sugar puckering etc. on complexation. The variation in χ_S, P_S and glycosidic bond angle due to complexation are different for the corresponding values in the present study. This suggests that there are no general rules which can be applied to intercalators. Apparently these subtle variations are specific to the type of drug and specific intercalating base pair (CpG/TpG) selected. Since, the anticancerous activity is related to structure of the drug. Hence the differences observed in adriamycin + d-$(CGATCG)_2$ and daunomycin + d-$(TGATCA)_2$ complexes are related to the differences in anticancerous activity of adriamycin and daunomycin.

CONCLUSIONS

The spin-spin coupling constants, torsional angles and interproton distances are used to reveal the structural details of adriamycin in solution state. There are major differences in some of the interproton distances in the present case as compared to the corresponding distances of daunomycin obtained by X-ray crystallography techniques (78). These interproton distances are 7H-8axH, 1'H-4'H, 7H-1'H, 7H-3'H, 7H-4'H and 5'H-8axH. The interproton distances different from the solution structure of n-acetyl daunomycin are 4'H-5'H, 7H-8axH, 7H-1'H and 5'H-8axH (70). The molecular model obtained on the basis of these structural constraints suggest that various torsional angles in solution structure of adriamycin are different from the corresponding crystal structure of daunomycin by $\pm$ 15°. The position of C, N and O atoms is likely to be same but the position of hydrogen atoms are quite different in solution.

The analysis of the structure of deoxyhexanucleotide d-$(CGATCG)_2$ indicates that DNA molecule does not have a rigid structure with motions of the sugar ring restricted to a small region of pseudorotation angle. There appears to be time averaging of two different conformers, one N conformer (observed in A-DNA), one S conformer (close to standard B-DNA) existing in a fast equilibrium in solution. Presence of two S conformer and one N conformer is also suggested by some of the results. The pseudorotation angle of sugar pucker of major S conformer varies

in the range 117° - 225° while the mole fraction of major S conformer varies between 0.75 - 0.94. Considerable flexibility at the 3'- end of hexamer leads to maximum percentage of N-conformer for G6 residue, χ_S = 0.75, χ_N = 0.25. Glycosidic angle for purines and pyrimidines lie in the range -60° to -105° (to an accuracy of ± 15°).

Multiple complexes of d-$(CGATCG)_2$ + adriamycin are formed on titration, with adriamycin aglycone chromophore intercalating at 5'-CpG-3' step at both ends of DNA hexamer. The pseudorotation angle of several residues changes due to interaction with the drug while the glycosidic bond rotation (χ) is in high anti conformation for most of the residues. Several NOEs between base protons of C1.G6 and G2.C5 base pairs with 1H, 2H and 3H proton of adriamycin confirm the intercalation of aglycone chromophohre of adriamycin between terminal base pairs resulting in upfield shifts of ring A and D protons of adriamycin. The relative overlap between G2.C5 and A3.T4 base pairs is also altered on interaction. The intermolecular NOEs between daunosamine sugar protons and A3.T4 base pair exhibit the proximity of daunosamine sugar to the third base pair in sequence. The geometry of complex is somewhat different from that obtained by X-ray crystallography (32,71,81,98,128).

REFERENCES

1. Altona C. and Sundaralingam M. Conformational analysis of the sugar ring in nucleosides and nucleotides. Improved method of interpretation of proton magnetic resonance coupling constants. J. Amer. Chem. Soc., 1973, 95, 2333.

1(a). Altona C. and Sundaralingam M. Conformational analysis of the sugar ring in nucleosides and nucleotides. A new description using the concept of pseudorotation. J. Amer. Chem. Soc., 1972, 94, 8205.

2. Angiulli R., Foresti E., Rivi di S.L., Isaacs N.W., Kennard O., Motherwell W.D.S., Wampler D.L. and Arcamone F. Structure of daunomycin; X-ray analysis of N-Br-Acetyl daunomycin solvate. Nature (London) New Biol., 1971, 234, 78.

3. Arora S. K. Molecular structure, absolute stereochemistry, and interactions of nogalamycin, a DNA-binding anthracycline antitumor antibiotic. J. Amer. Chem. Soc., 1983, 105, 1328.

4. Aue W. P., Bartholdi E. and Ernst R. R. Two-dimensional spectroscopy : application to nuclear magnetic resonance. J. Chem. Phys., 1976, 64, 2229.

5. Barthwal R.B., Mujeeb A. and Govil G. Interaction of daunomycin with deoxydinucleotide d-CpG by two dimensional

proton magnetic resonance techniques. Archives Biochem. Biophys., 1994, 313, 189.

6. Beraldo H., Suillerot A. G., Tosi L. and Lavelle F. Iron (III)-adriamycin and Iron (III)-daunorubicin complexes : Physicochemical characteristics, interaction with DNA, and antitumour activity. Biochemistry, 1985, 24, 284.

7. Bodenhausen G., Freeman R. and Turner D. L. Supression of artifacts in two-dimensional spectroscopy . J. Magn. Reson., 1977, 27, 511.

8. Brown D.R., Kurz M., Kearns D.R. and Hsu V.L. Formation of multiple complexes between actinomycin D and a DNA hairpin: Structural characterization by multinuclear NMR. Biochemistry, 1994, 33, 651.

9. Calendi E., Di Marco A., Reggiani M., Scarpinato B. and Valentini L. On physico-chemical interactions between daunomycin and nucleic acids. Biochim. Biophys. Acta, 1965, 103, 25.

10. Celda B., Widmer H., Leupin W., Chazin W., Denny A. and Wuthrich K. Conformational studies of d-$(AAAAATTTTT)_2$ using constraints from nuclear overhauser effects and from quantitative analysis of the cross peak fine structures in two-dimensional ^1H nuclear magnetic resonance spectra. Biochemistry, 1989, 28, 1462.

10(a). Chary K.V.R., Hosur R.V. and Govil G. Sequence specific solution structure of d-GGTACGCGTACC. Biochemistry, 1988, 27, 3858.

10(b). Chary K.V.R., Modi S., Hosur R.V., Govil G., Chen C. and Miles H.T. Quantification of DNA structure from NMR data : conformation of d-ACATCGATGT. Biochemistry, 1989, 28, 5240.

11. Chaires J.B. Daunomycin inhibits the B $\longrightarrow$ Z transition in poly d(G-C). Nucleic Acids Res., 1983, 11, 8485.

12. Chaires J.B. Thermodynamics of the daunomycin-DNA interaction: Ionic strength dependence of the enthalpy and entropy. Biopolymers, 1985, 24, 403.

13. Chaires J.B., Dattagupta N. and Crothers D.M. Self-association of daunomycin. Biochemistry, 1982, 21, 3927.

14. Chaires J.B., Dattagupta N. and Crothers D.M. Studies on interaction of anthracycline antibiotics and deoxyribonucleic acid : Equilibrium binding studies on interaction of daunomycin with deoxyribonucleic acid. Biochemistry, 1982, 21, 3933.

15. Chaires J.B., Dattagupta N. and Crothers D.M. Kinetics of the daunomycin-DNA interaction. Biochemistry, 1985, 24, 260.

16. Chaires J.B., Fox K.R., Herrera J.E., Britt M. and Waring M.J. Site and sequence specificity of the daunomycin-DNA interaction. Biochemistry, 1987, 26, 8227.

17. Chaires J.B., Herrera J.E. and Waring M.J. Preferential binding of daunomycin to 5′ $\begin{matrix}A\\T\end{matrix}$CG and 5′ $\begin{matrix}A\\T\end{matrix}$GC sequences revealed by footprinting titration experiments. Biochemistry, 1990, 29, 6145.

18. Chen K.X., Gresh N. and Pullman B. A theoretical investigation on the sequence selective binding of daunomycin to double-stranded polynucleotides. J. Biomol. St. Dyn., 1985, 3, 445.

19. Chen K.X., Gresh N. and Pullman B. A theoretical investigation on the sequence selective binding of adriamycin to double-stranded polynucleotides. Nucleic Acids Res., 1986, 14, 2251.

20. Chen C.W., Knop R.H. and Cohen J.S. Adriamycin inhibits the B to Z transition of poly (dGm^5dC). poly (dGm^5dC). Biochemistry, 1983, 22, 5468.

21. Choudhury K., Chakraborty R., Dhar T. and Neogy R.K. DNA base sequence preference for adriamycin and nogalamycin binding. Indian J. Biochem. Biophys., 1985, 22, 166.

22. Cieplak P., Rao S.N., Grootenhuis P.D.J. and Kollman P.A. Free energy calculation on base specificity of drug-DNA

interactions : Application to daunomycin and acridine intercalation into DNA. Biopolymers, 1990, 29, 717.

23. Cirilli M., Giomini M., Giuliani A.M. and Trotta E. A truncated driven overhauser effect study of adriamycin in water : conformation of the glycosidic linkage. Biochimica Acta, 1991, 47 A, 759.

24. Courseille C., Busetta B., Geoffre S. and Hospital M. Complex daunomycin-butanol. Acta Cryst., 1979, B 35, 764.

25. Dalgleish D.G., Fey G. and Kersten W. Circular dichroism studies of complexes of the antibiotics daunomycin, nogalamycin, chromomycin and mithramycin with DNA. Biopolymers, 1974, 13, 1757.

25(a). Davies B.D. Prog. in NMR spectroscopy, 1978, 12, 135.

26. Delepierre M., Dinh T.H. and Roques B.P. Bisintercalation of ditercalinium into a d-$(CpGpApTpCpG)_2$ minihelix : A ^1H and ^{31}P- NMR study. Biopolymers, 1989, 28, 2115.

27. Derome A.E. In 'Modern NMR techniques for chemistry research'. Volume 6, Pergamon Press, Oxford U.K. (1987).

28. Dhananjaya K.V.R. and Antony A. Inhibition of avian myeloblastosis virus reverse transcriptase and its associated activities by daunomycin and adriamycin. Indian J. Biochem. Biophys., 1987, 24, 265.

29. Ernst R.R. and Anderson W.A. Rev. Sci. Instrum., 1966, 37, 93 .

30. Feigon J., Wright J.M., Leupin W., Denny W.A. and Kearns D.R. Use of two-dimensional NMR in the study of a double-stranded decamer. J. Amer. Chem. Soc., 1982, 104, 5540.

31. Frechet D., Chen D.M., Kan L.S. and Tso P.O.P. Nuclear overhauser effect as a tool for the complete assignment of non-exchangeable proton resonances in short deoxyribonucleic acid helices. Biochemistry, 1983, 22, 5194.

32. Frederick C.A., Williams L.D., Ughetto G., Van der Marel G.A., Van Boom J.H., Rich A. and wang A.H.J. Structural comparison of anticancer drug-DNA complexes : Adriamycin and daunomycin. Biochemistry, 1990, 29, 2538.

33. Fritzsche H., Triebel H., Chaires J.B., Dattagupta N. and Crothers D.M. Studies on interaction of anthracycline antibiotics and deoxyribonucleic acid : geometry of intercalation of iremycin and daunomycin. Biochemistry, 1982, 21, 3940.

34. Gabbay E.J., Grier D., Fingerle R.E., Reimer R., Levy R., Pearce S.W. and Wilson W.D. Interaction specificity of the anthracyclines with deoxyribonucleic acid. Biochemistry, 1976, 15, 2062.

35. Geierstanger B.H., Jacobsen J.P., Mrksich M., Dervan P.B. and Wemmer D.E. Structural and dynamic characterization of the heterodimeric and homodimeric complexes of distamycin

and 1-methylimidazole 2-carboxamide - netropsin bound to the minor groove of DNA. Biochemistry, 1994, 33, 3055.

35(a) Giessner-Prettre C. and Pullman B. On the atomic or local contributions to chemical shifts due to the anisotropy of the diamagnetic susceptibility of the aromatic side chain of amino acids and of the porphyrin ring. Biochem. Biophys. Res. Commun., 1981, 101, 921.

36. Gilbert D.E., Van der Marel G.A., Van Boom J.H. and Feigon J. Unstable Hoogsteen base pairs adjacent to echinomycin binding sites within a DNA duplex. Proc. Natl. Acad. Sci. USA., 1989, 86, 3006.

37. Gochin M., Zon G. and James T.L. Two-dimensional COSY and two-dimensional NOE spectroscopy of $d(AC)_4$. $d(GT)_4$: Extraction of structural constraints. Biochemistry, 1990, 29, 11161.

38. Govil G. and Hosur R.V. In 'Conformation of biological molecules : New results from NMR'. Springer Verlag, Heidelberg.

39. Graves D.E. and Krugh T.R. Adriamycin and daunorubicin bind in a cooperative manner to deoxyribonucleic acid. Biochemistry, 1983, 22, 3941.

40. Gresh N. and Kahn P.H. Theoretical design of novel, 4 base pair selective derivatives of mitoxantrone. J. Biomol. St. Dyn., 1990, 7, 1141.

41. Gronenborn A.M. and Clore G.M. Investigation of the solution structure of short nucleic acid fragments by means of nuclear overhauser enhancement measurements. Progress in NMR spectroscopy, 1985, 17, 1.

42. Hare D.H., Wemmer D.E., Chou S.H., Drobny G. and Reid B.R. Assignment of the non-exchangeable proton resonances of d-$(CGCGAATTCGCG)_2$ using two-dimensional methods. J. Mol. Biol., 1983, 171, 319.

43. Henry D.W. Structure-activity relationship among daunorubicin and adriamycin analogs. Cancer Treat. Rep., 1979, 63, 845.

44. Holbrook S.R., Wang A.H.J., Rich A. and Kim S.H. Local mobility of nucleic acids as determined from crystallographic data. III. A daunomycin - DNA complex. J. Mol. Biol., 1988, 199, 349.

45. Hosur R.V., Govil G. and Miles H.T. Application of two-dimensional NMR spectroscopy in the determination of solution conformation of nucleic acids. Magn. Reson. Chem., 1988, 26, 927.

46. Hosur R.V., Ravikumar M., Chary K.V.R., Sheth A., Govil G., Tan-Zu-Kunn and Miles H.T. Solution structure of d-GAA TTCGAATTC by 2D NMR : a new approach to determination of sugar geometries in DNA segments. FEBS Letts., 1986, 205, 71.

47. Hosur R.V., Ravikumar M., Roy K.B., Tan-Zu-Kun, Miles H.T. and Govil G. In 'Magnetic resonance in biology and medicine'. (Eds. Govil G., Khetrapal C.L.and Saran A.) Tata McGraw Hill, New Delhi (1985), pp 305.

48. Islam S.A., Neidle S., Gandecha B.M., Partridge M., Patterson L.H. and Brown J.R. Comparative computer graphics and solution studies of the DNA interaction of substituted anthraquinones based on doxorubicin and mitoxantrone. J. Med.Chem., 1985, 28, 857.

49. Iwamoto R.H., Lim P. and Bhacca N.S. The structure of daunomycin. Tetrahedron Letts., 1968, 36, 3891.

50. Jeener J. Paper presented at the AMPERE international summer school, Borsko, Polje, Yugoslavia. 1971.

51. Jones M.B., Hollstein U. and Allen F.S. Site specificity of binding of antitumor antibiotics to DNA. Biopolymers, 1987, 26, 121.

52. Karplus M. Contact electron-spin coupling of nuclear magnetic moments. J. Chem. Phys., 1959, 30, 11.

53. Karplus M. Vicinal proton coupling in nuclear magnetic resonance. J. Amer. Chem. Soc., 1963, 85, 2870.

54. Keeler J. and Neuhaus D. Comparison and evaluation of methods for two-dimensional NMR spectra with absorption mode line shape. J. Magn. Reson., 1985, 63, 454.

54(a). Kollman P.A. and Rao S.N. Biopolymers, 1989 (in press).

55. Kriebardis T., Meng D. and Aktipis S. On the inhibition of the RNA polymerase - catalysed synthesis of RNA by daunomycin. Interference of the inhibitor with elongation and pre-longation steps. Biochem. Biophys. Res. Commun., 1984, 123, 914.

56. Langlois d'Estaintot B., Gallois B., Brown T. and Hunter W.N. The molecular structure of a 4'-epiadriamycin complex with d(TGATCA) at 1.7 A° resolution : Comparison with the structure of 4'-epiadriamycin d(TGTACA) and d(CGATCG) Complexes. Nucleic Acids Res., 1992, 20, 3561.

57. Leonard G.A., Hambley T.W., Mc Auley Hecht K., Brown T. and Hunter W.N. Anthracycline-DNA interactions at unfavourable base pair triplet binding sites : Structures of d(CGGCCG)/daunomycin and d(TGGCCA)/adriamycin complexes. Acta Cryst., 1993, D49, 458.

58. Lerman L.S. Structural considerations in the interaction of DNA with acridines. J. Mol. Biol., 1961, 3, 18.

59. Liaw Y.C., Gao Y.G., Robinson H., Van der Marel G.A., Van Boom J.H. and Wang A.H.J. Antitumor drug nogalamycin binds DNA in both grooves simultaneously : Molecular structure of nogalamycin - DNA complex. Biochemistry, 1989, 28, 9913.

60. Lipscomb L.A., Peek M.E., Zhou F.X., Bertrand J.A., Van Derveer D. and Williams L.D. Water ring structure at DNA

interfaces : Hydration and dynamics of DNA-anthracycline complexes. Biochemistry, 1994, 33, 3649.

61. Lown J.W., Hanstock C.C., Bleackley R.C., Imbach J.L., Rayner B. and Vasseur J.J. Synthesis, Complete ^{1}H assignment and conformations of the self-complementary hexadeoxynucleotide $d(CpGpApTpCpG)_2$ and its fragment by high field NMR. Nucleic Acids Res., 1984, 12, 2519.

62. Lown J.W., Morgan A.R., Yen S.F., Wang Y.H. and Wilson W.D. Characteristics of the binding of the anticancer agents mitoxantrone and ametantrone and related structures to deoxyribonucleic acids. Biochemistry, 1985, 24, 4028.

63. Lown J.W., Sim S.K., Majumdar K.C. and Chang R.Y. Strand scission of DNA by bound adriamycin and daunorubicin in the presence of reducing agents. Biochem. Biophys. Res. Commun., 1977, 76, 705.

64. Manfait M., Alix A.J.P., Jeannesson P., Jardillier J.C. and Theophanides T. Interaction of adriamycin with DNA as studied by resonance raman spectroscopy. Nucleic Acids Res., 1982, 10, 3803.

65. Marion D. and Wuthrich K. Application of phase-sensitive two-dimensional correlated spectroscopy (COSY) for measurements of ^{1}H-^{1}H spin coupling constants in proteins. Biochem. Biophys. Res. Commun., 1983, 113, 967.

66. McLennan I.J., Lenkinski R.E. and Yanuka Y. A nuclear magnetic study of the self-association of adriamycin and daunomycin in aqueous solution. Can. J. Chem., 1985, 63, 1233.

67. Miller K.J. and Newlin D.D. Interactions of molecules with nucleic acids. VI. Computer design of chromophoric intercalating agents. Biopolymers, 1982, 21, 633.

68. Momparler R.L., Karon M., Siegel S.E. and Avila F. Effect of adriamycin on DNA, RNA, and protein synthesis in cell-free systems and intact cells. Cancer Res., 1976, 36, 2891.

69. Mondelli R., Ragg E., Fronza G. and Arnone A. Nuclear magnetic resonance conformational study of daunomycin and related antitumour antibiotics in solution. The conformation of ring A. J. Chem. Soc. Perkin Trans., 1987, II, 15.

70. Mondelli R., Ragg E. and Fronza G. Conformational analysis of N-acetyl daunomycin in solution. A transient ^{1}H nuclear overhauser effect study of the glycosidic linkage geometry. J. Chem. Soc. Perkin Trans., 1987, II, 27.

71. Moore M.H., Hunter W.N., Langlois d'Estaintot B. and Kennard O. DNA-drug interactions. The crystal structure of d(CGATCG) complexed with daunomycin. J. Mol. Biol., 1989, 206, 693.

72. Mujeeb A., Kerwin S.M., Egan W., Kenyan G.L. and James

T.L. A potential gene target in HIV-1 : rationale, selection of a conserved sequence, and determination of NMR distance and torsional angle constraints. Biochemistry, 1992, 31, 9325.

72(a). Majumdar A. and Hosur R.V. Simulation of 2D NMR spectra for determination of solution conformation of nucleic acids. Prog. in NMR Spectroscopy, 1992, 24, 109.

73. Munt N.A. and Kearns D.R. Poly (dA-dT) has a right-handed B conformation in solution : A two-dimensional NMR study. Biochemistry, 1984, 23, 791.

74. Nakata Y. and Hopfinger A.J. Predicted mode of intercalation of doxorubicin with dinucleotide dimers. Biochem. Biophys. Res. Commun., 1980, 95, 583.

75. Nakata Y. and Hopfinger A.J. An extended conformational analysis of doxorubicin. FEBS Letts., 1980, 117, 259.

76. Neidle S., Achari A., Taylor G.L., Berman H.M., Carrell H.L., Glusker J.P. and Stallings W.C. Structure of a dinucleoside phosphate - drug complex as model for nucleic acid-drug interaction. Nature, 1977, 269, 304.

77. Neidle S. and Sanderson M.R. In 'Molecular aspects of anti-cancer drug action'. Volume 3, (Eds. Neidle S. and Waring M.J.) Macmillan Press Ltd. (1983), pp 35.

78. Neidle S. and Taylor G.L. Nucleic acid binding drugs : Part IV. The crystal structure of the anti cancer agent daunomycin. Biochim. Biophys. Acta, 1977, 479, 450.

79. Neidle S. and Taylor G. L. Nucleic acid binding drugs . Some conformational properties of the anti-cancer drug daunomycin and several of its derivatives. FEBS Letts., 1979, 107, 348.

80. Neumann J.M., Cavailles J.A., Herve M., Dinh S.T., Langlois d'Estaintot B., Huynh Dinh T. and Igolen J. 500 MHz ^{1}H-NMR study of the interaction of daunomycin with B and Z helices of d(CGm^{5}CGCG). FEBS Letts., 1985, 182, 360.

81. Nunn C.M., Meervelt L.V., Zhang S., Moore M.H. and Kennard O. DNA-drug interactions. The crystal structures of d(TGTACA) and d(TGATCA) complexed with daunomycin. J. Mol. Biol., 1991, 222, 167.

82. Nuss M.E., James T.L., Apple M.A. and Kollman P.A. An NMR study of the interaction of daunomycin with dinucleotides and dinucleoside phosphates. Biochim. Biophys. Acta, 1980, 609, 136.

83. Pachter J.A., Huang C.H., Du Vernay V.H., Prestayko A.W. and Crooke S.T. Viscometric and fluorometric studies of deoxyribonucleic acid interactions of several new anthracyclines. Biochemistry, 1982, 21, 1541.

84. Paoletti J. and Le Pecq J.B. The change of the torsion of the DNA helix caused by intercalation. Biochimie, 1971, 53, 969.

85. Paoletti J. and Le Pecq J.B. Resonance energy transfer between ethidium bromide molecules bound to nucleic acids. J.Mol.Biol., 1971, 59, 43.

86. Patel D.J. and Canuel L.L. Anthracycline antitumor antibiotic. Nucleic acid interactions. Structural aspects of the daunomycin.poly(dA-dT) complex in solution. Eur. J. Biochem., 1978, 90, 247.

87. Patel D.J. Mutagen-Nucleic acid complexes at the polynucleotide duplex level in solution : Intercalation of proflavine into poly(dA-dT) and the melting transition of the complex. Biopolymers, 1977, 16, 2739.

88. Patel D.J. Helix-coil transition of the dG-dC-dG-dC self-complementary duplex and complex formation with daunomycin in solution. Biopolymers, 1979, 18, 553.

89. Patel D.J., Kozlowski S.A. and Rice J.A. Hydrogen bonding, overlap geometry, and sequence specificity in anthracycline antitumor antibiotic. DNA complexes in solution. Proc. Natl. Acad. Sci., 1981, 78, 3333.

90. Pearlman L.F. and Simpkins H. The differential effects produced by daunomycin and adriamycin on RNA, polynucleotides, single stranded, supercoiled DNA and nucleosomes. Biochem. Biophys. Res. Commun., 1985, 131, 1033.

91. Pettit G.R., Einck J.J., Herald C.L., Ode R.H., Von Dreele R.B., Brown P., Brazhnikova M.G. and Gause G.F. The structure of carminomycin I. J. Amer. Chem. Soc., 1975, 97, 7387.

92. Phillips D.R. and Roberts G.C.K. Proton nuclear magnetic resonance study of the self-complementary hexanucleotide $d(pTpA)_3$ and its interaction with daunomycin. Biochemistry, 1980, 19, 4795.

93. Piantini U., Sorensen O.W. and Ernst R.R. J.Amer. Chem. Soc., 1982, 104, 6800.

94. Pigram W.J., Fuller W. and Hamilton L.D. Stereochemistry of intercalation : Interaction of daunomycin with DNA. Nature New Biol., 1972, 235, 17.

95. Plumbridge T.W. and Brown, J.R. Spectrophotometric and fluorescence polarization studies of the binding of ethidium, daunomycin and mepacrine to DNA and to poly (I.C). Biochim. Biophys. Acta, 1977, 479, 441.

96. Pohle W., Flemming J. and Bohl M. Adriamycin binding to DNA phosphate as evidenced by spectroscopic and quantum - chemical results. Studia biophysica, 1987, 122, 223.

97. Pohle W., Bohl M., Flemming J. and Bohlig H. Subsidiary hydrogen bonding of intercalated anthraquinonic anticancer drugs to DNA phosphate. Biophysical Chem., 1990, 35, 213.

98. Quigley G.J., Wang A.H.J., Ughetto G., Van der Marel G., Van Boom J.H. and Rich A. Molecular structure of an anticancer drug - DNA complex : Daunomycin plus d(CpGpTpApCpG). Proc. Natl. Acad. Sci., 1980, 77, 7204.

99. Ragg E., Mondelli R., Battistini C., Garbesi A. and Colonna F.P. ^{31}P NMR study of daunorubicin - d(CGTACG) complex in solution. FEBS Lett., 1988, 236, 231.

100. Rameta D.P., Mudd C.P., Berger R.L. and Breslauer K.J. Thermodynamic characterization of daunomycin - DNA interactions : Microcalorimetric measurements of daunomycin - DNA binding enthalpies. Biochemistry, 1991, 30, 9799.

101. Ravikumar M., Hosur R.V., Roy K.B., Miles H.T. and Govil G. Resonance assignment of the 500 MHz proton NMR spectrum of self complementary dodecanucleotide d-GGATCCGGATCC: Altered conformation at Bam HI cleavage sites. Biochemistry, 1985, 24, 7703.

102. Redfield A.G., Kunj S. and Ralph E.K. Quadrature fourier NMR detection, simple multiplex for dual detection and discussion. J. Magn. Reson., 1975, 19, 116.

103. Reid B.R., Banks K., Flynn P. and Nerdal W. NMR distance measurements in DNA duplexes : Sugars and bases have the same correlation times. Biochemistry, 1989, 28, 10001.

104. Reuben J., Baker B.M. and Kallenbach N.R. Structure of mutagen nucleic acid complexes in solution. Proton chemical shifts in 9-aminoacridine complexes with dG-dC, dC-dG, and dA-dT-dG-dC-dA-dT. Biochemistry, 1978, 17, 2915.

105. Rinkel L.J. and Altona C. Conformational analysis of the deoxyribofuranose ring in DNA by means of sums of proton-proton coupling constants : A graphical method. J. Biomol. St. Dyn., 1987, 4, 621.

106. Robinson H., Liaw Y.C., Van der Marel G.A., Van Boom J.H. and Wang A.H.J. NMR studies on the binding of antitumor drug nogalamycin to DNA hexamer d(CGTACG). Nucleic Acids Res., 1990, 18, 4851.

107. Roche C.J., Berkowitz D., Sulikowski G.A., Danishefsky S.J. and Crothers D.M. Binding affinity and site selectivity of daunomycin analogues. Biochemistry, 1994, 33, 936.

108. Roche C.J., Thomson J.A. and Crothers D.M. Site selectivity of daunomycin. Biochemistry, 1994, 33, 926.

109. Ryser H.J.P. Science, 1968, 159, 390.

110. Saenger W. In 'Principles of nucleic acid structure'. (Ed. Cantor C.R.). Springer Verlag, New York Inc. (1984).

111. Sakore T.D., Jain S.C., Tsai C.C. and Sobell H.M. Mutagen-nucleic acid intercalative binding : Structure of

a 9-aminoacridine : 5-iodocytidylyl (3′-5′) guanosine crystalline complex. Proc. Natl. Acad. Sci., USA, 1977, 74, 188.

112. Saucier J.M., Festy B. and Le Pecq J.B. The change of the torsion of the DNA helix caused by intercalation. Biochimie, 1971, 53, 973.

113. Scheek R.M., Russo N., Boelens R., Kaptein R. and Van Boom J.H. Sequential resonance assignments in DNA ^{1}H NMR spectra by two-dimensional NOE spectroscopy. J. Amer. Chem. Soc., 1983, 105 2914.

114. Schmitz U., Zon G. and James T.L. Deoxyribose conformation in $[d(GTATATAC)]_2$: evaluation of sugar pucker by simulation of double-quantum filtered COSY cross peaks. Biochemistry, 1990, 29, 2357.

114(a). Schmitz U., Sethson I., Egan W.M. and James T.L. Solution sructure of a DNA octamer containing the Pribnow box via restrained molecular dynamics simulation with distance and torsion angle constraints derived from two-dimensional nuclear magnetic resonance spectral fitting. J. Mol. Biol., 1992, 227, 510.

115. Shafer R.H. Spectroscopic studies of the interaction of daunomycin with transfer RNA. Biochem. Pharmacol., 1977, 26, 1729.

116. Simpkins H. and Pearlman L.F. The binding of actinomycin D and adriamycin to supercoiled DNA, single-stranded DNA

and polynucleotides. Biochim. Biophys. Acta., 1984, 783, 293.

117. Sinha B.K. and Sik. R.H. Binding of [^{14}C]- adriamycin to cellular macromolecules in vivo. Biochem. Pharmacol., 1980, 29, 1867.

118. Sobell H.M. and Jain S.C. Stereochemistry of actinomycin binding to DNA. II. Detailed molecular model of actinomycin-DNA Complex and its implications. J. Mol. Biol., 1972, 68, 21.

119. States D.J., Haberkorn R.A. and Reuben D.J. A two-dimensional nuclear overhauser experiment with pure absorption phase in four quadrants. J. Magn. Reson., 1982, 48, 286.

120. Sundaralingam M. Biopolymers, 1969, 7, 821.

121. Trist H. and Phillips D.R. In vitro transcription analysis of the role of flanking sequence on the DNA sequence specificity of adriamycin. Nucleic Acids Res., 1989, 17, 3673.

122. Tsai C.C., Jain S.C. and Sobell H.M. Visualization of drug-nucleic acid interactions at atomic resolution. I. Structure of an ethidium/dinucleoside monophosphate crystalline Complex, ethidium : 5-iodouridylyl (3'-5') adenosine. J. Mol. Biol., 1977, 114, 301.

123. Tsou K.C. and Yip K.F. Cancer Res., 1976, 36, 3367.

124. Ughetto G., Wang A.H.J., Quigley G.J., Van der Marel G.A., Van Boom J.H. and Rich A. A comparison of the structure of echinomycin and triostin A complexed to a DNA fragment. Nucleic Acids Res., 1985, 13, 2305.

124(a). Van de Van F.J.M. and Hilbers C.W. Nucleic acids and nuclear magnetic resonance. Eur. J. Biochem.,1988, 178,1.

125. Wang A.H.J., Gao Y.G., Liaw Y.C. and Li Y. K. Formaldehyde cross-links daunorubicin and DNA efficiently : HPLC and X-ray diffraction studies. Biochemistry, 1991, 30, 3812.

126. Wang A.H.J., Nathans J., Van der Marel G., Van Boom J.H. and Rich A. Molecular structure of a double helical DNA fragment intercalator complex between deoxy CpG and a terpyridine platinum compound. Nature, 1978, 276, 471.

127. Wang A.H.J., Ughetto G., Quigley G.J., Hakoshima T., Van der Marel G.A., Van Boom J.H. and Rich A. The molecular structure of a DNA-triostin A complex. Science, 1984, 225, 1115.

128. Wang A.H.J., Ughetto G., Quigley G.J. and Rich A. Interactions between an anthracycline antibiotic and DNA : Molecular structure of daunomycin complexed to d(CpGpTpApCpG) at 1.2 A° resolution. Biochemistry, 1987, 26, 1152.

129. Waring M. Variation of the supercoils in closed circular DNA by binding of antibiotics and drugs : Evidence for molecular models involving intercalation. J. Mol. Biol., 1970, 54, 247.

130. Widmer H. and Wuthrich K. Simulated two-dimensional NMR cross-peak fine structures for ^{1}H spin systems in polypeptides and polydeoxynucleotides. J. Magn. Reson., 1987, 74, 316.

130(a). Widmer H. and Wuthrich K. J. Magn. Reson., 1986, 70, 270.

131. Wijk J.V., Huckriede B.D., Ippel J.H. and Altona C. Furanose sugar conformations in DNA from NMR coupling constants. Methods in Enzymology, 1992, 211, 286.

132. Williams L.D., Frederick C.A., Ughetto G. and Rich A. Ternary interactions of spermine with DNA : 4'-epiadriamycin and other DNA : anthracycline complexes. Nucleic Acids Res., 1990, 18, 5533.

133. Wuthrich K. In 'NMR of proteins and nucleic acids'. John wiley, New York (1986).

134. Xodo L.E., Manzini G., Ruggiero J. and Quadrifoglio F. On the interaction of daunomycin with synthetic alternating DNAs: sequence specificity and polyelectrolyte effects on the intercalation equilibrium. Biopolymers, 1988, 27, 1839.

135. Yang D. and Wang A. H. J. Structure by NMR of antitumor drugs aclacinomycin A and B complexed to d(CGTACG). Biochemistry, 1994, 33, 6595.

136. Yu C. and Tseng Y.Y. NMR study of the solution conformation of actinomycin D. Eur. J. Biochem., 1992, 209, 181.

137. Zhang X. and Patel D.J. Solution structure of the nogalamycin-DNA complex. Biochemistry, 1990, 29, 9451.

138. Zunino F., Gambetta R., Di Marco A. and Zaccara A. Interaction of daunomycin and its derivatives with DNA. Biochim. Biophys. Acta, 1972, 277, 489.

139. Zunino F., Gambetta R. and Di Marco A. Effects of the stereochemical configuration on the interaction of some daunomycin derivatives with DNA. Biochem. Biophys. Res. Commun., 1976, 69, 744.